CRANFIELD UNIVERSITY

SCHOOL OF MECHANICAL ENGINEERING

DEPARTMENT OF PROPULSION, POWER AND AUTOMOTIVE ENGINEERING

PhD THESIS

E. GEOFFREY ENGELBRECHT

Modelling of Premixed Combustion in a Gas Turbine

Supervisor: J.B. Moss Ph.D.

July 1998

This thesis is submitted in partial fulfilment for the degree of
DOCTOR OF PHILOSOPHY

Abstract

Three steady state combustion models, two turbulence models and a model for the prediction of NO_x were implemented and investigated on a simple backward facing step experiment as well as an experimental lean prevaporised premixed (LPP) combustor. The three combustion models included the simple Eddy Break-up model as well as a presumed probability density function (pdf) model and a form of the BML crossing frequency flamelet model. These models were adapted to consider a variable mixture fraction to account for a non-homogeneous fuel air mixture. The two turbulence models used were the k-ε and second moment models.

Despite being unable to capture the flame front spreading in the case of the backward facing step, these predictions provided insight into the performance and implementation of the models. All three of the combustion models, after appropriate tuning, worked well for the LPP test combustor. This illustrates that such time averaged models are useful for flows which do not contain large transient coherent structures, such as that of the LPP test combustor and most practical engine combustors designed today. The second moment closure turbulence model was found to have the greatest impact on the flame front through the flow field predictions rather than through counter gradient diffusion. The Eddy Break-up and BML crossing frequency models both performed very well, qualitatively predicting the correct trends. The additional consideration of flame front straining in the BML crossing frequency model did not appear to significantly influence the flame front. This is because the type of model adopted to predict this effect had a relatively uniform influence everywhere in the flow. The presumed pdf model also performed well and was additionally found to self ignite without the existence of hot products when the inlet temperature was high enough. The NO_x model faired well for a simple experimental geometry. However, it considerably over predicted the NO_x formed within the LPP test combustor, which was most probably due to poor boundary conditions. Despite this overprediction, the results give insight into how to improve the NO_x emissions for the experimental combustor.

Acknowledgements

I would like to acknowledge the assistance and encouragement of my supervisor Professor J.B. Moss without which this thesis would not be possible. I would also like to thank Phil Rubini, Murat Aksit, Patrick Escher, Steve Harding, Cecil Stewart, Khawar Syed, Ian Bennet and Mike Lewis for their assistance and helpful advise.

As well I would like to thank Rolls-Royce Aeroengines PLC and the British Government Overseas Research Scholarship for their financial assistance.

List of Contents

List of Figures

List of Tables

Notation

c	heat release reaction progress variable
c_{NO}	NO reaction progress variable
f	mixture fraction
k	reaction rate coefficient, turbulent kinetic energy
ℓ	integral length scale of turbulence
m_T	total molecular mass
p	static pressure
pdf	probability density function
t	time
u	velocity
v	velocity
w	rate of reaction
w_{CO_2}	molecular weight of CO_2
A	area
AFR	air to fuel ratio
C_{ebu}	Eddy Break-up model constant
E	Arrhenius activation energy
K	strain
K_q	strain rate at which the flame quenches
Le	Lewis number
$\hat{L}_y$	integral length scale
P	probability density function
PDF	probability density function
Pr	Prandtl number
R	universal gas constant
Re	Reynolds number
RSTM	second moment turbulence model
Sc	Schmidt number
S_L	laminar burning velocity
T	temperature
$Y_{CO_2}^{c=1}$	equilibrium mass fraction of CO_2
$Y_{NO}^{c=1}$	equilibrium mass fraction of NO
α	presumed probability density function parameter
β	presumed probability density function parameter
δ	presumed probability density function parameter

δ_L laminar flame thickness

ε turbulent kinetic energy dissipation rate

ϕ equivalence ratio

γ presumed probability density function parameter

λ_T Taylor microscale

μ dynamic viscosity

ν kinematic viscosity

ρ density

σ variance

$\overline{|\sigma_y|}$ factor describing the mean angle of the flamelet crossing to the unit line in space

τ heat release parameter, time scale

Σ flame front surface area per unit volume

1 Introduction

By the mid 1970's, although the Concorde did not sell very well, it was expected that a second-generation supersonic transport would eventually be designed. Such an aircraft would have to be much more commercially viable than the Concorde, and in particular much larger numbers of these aircraft would need to be sold and operated. The potential environmental impact would therefore be greater and pollutant emissions would become a primary concern in the combustor design.

Supersonic transports fly in the stratosphere, which places them near to the ozone layer (Figure 1.1). This makes the reduction of emissions, which react to deplete the ozone layer, critical. NO is one such emission, which reacts with ozone to produce oxygen and then is replenished in the following set of reactions (cf. Jones, 1978).

$$NO + O_3 \rightarrow NO_2 + O_2 \qquad (1\text{-}1)$$

$$NO_2 + O \rightarrow NO + O_2 \qquad (1\text{-}2)$$

Therefore, these types of aircraft must demonstrate very low NO_x emissions if they are to operate without significantly damaging the ozone layer.

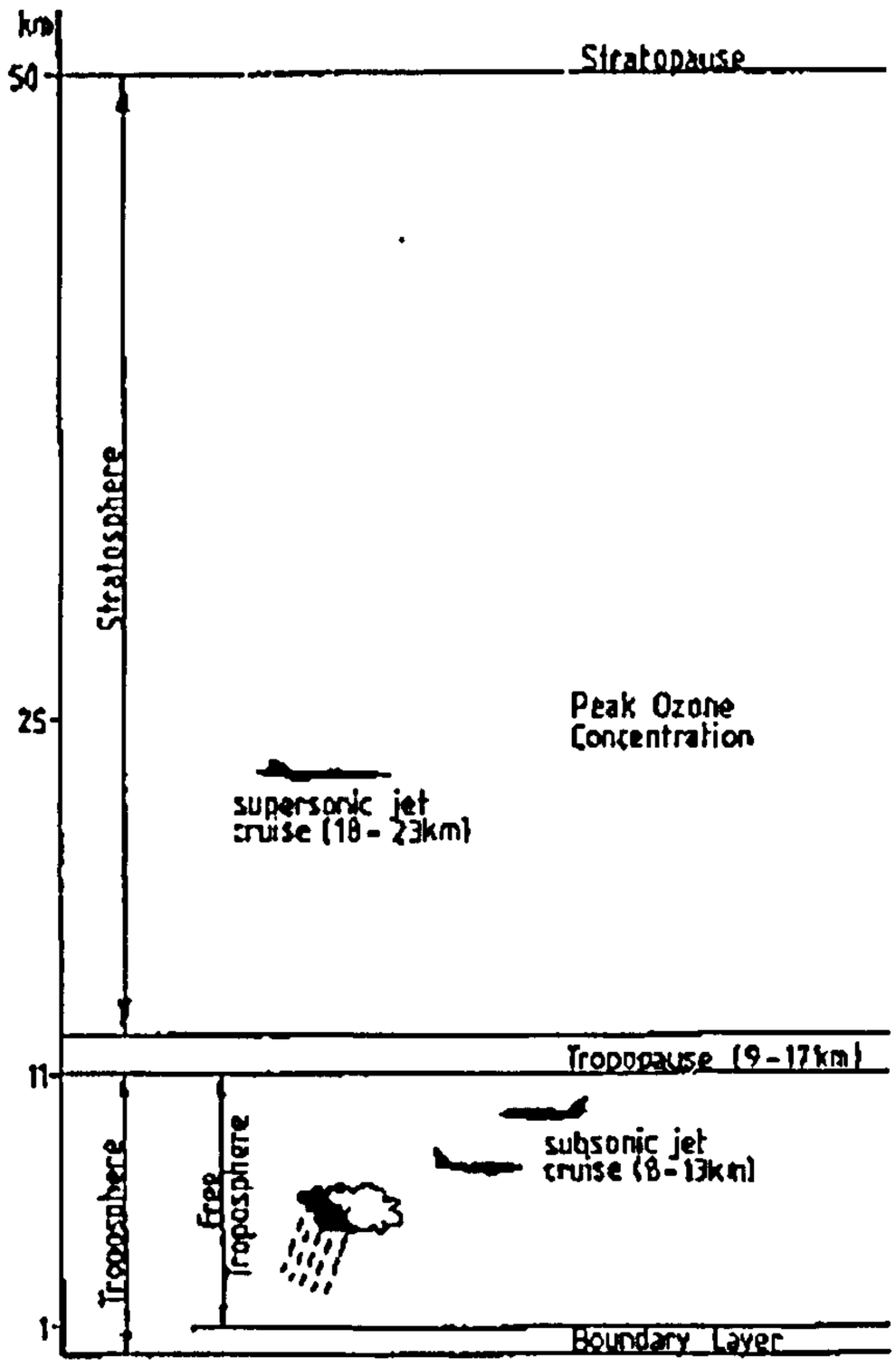

Figure 1.1 Normal Aircraft Cruise Altitudes

More generally, subsonic aircraft fly in the upper troposphere. NO_x produced here reacts to create ozone which then acts as a global warming gas (Gardner, 1995). NO_x also contributes to acid rain and urban smog (Price, 1995).

Although aircraft currently contribute only about 3% of the total global production of NO_x, because they fly in regions of the atmosphere which are sensitive to NO_x, the effect of these emissions is expected to be many times that of NO_x produced nearer the ground (Gardner, 1995). Additionally, ground level NO_x is removed from the air within a few days of its production by rain whereas high altitude NO_x can persist for long periods of time (Price, 1995).

It is this impetus which has driven the combustor research of the last three decades into finding a means of dramatically reducing NO_x emissions from aircraft gas turbine engines.

One of the more promising techniques currently being proposed to reduce these emissions is Lean Prevaporised Premixed (LPP) combustion. This involves prevaporising and premixing the fuel and air in a lean mixture prior to burning it. The oxidation rate of nitrogen is a strong exponential function of the temperature and by operating with a very homogeneous lean fuel air mixture, one can ensure a very low flame temperature which will minimise the amount of thermal NO_x produced. A number of distinctive design problems accompany this strategy, however.

Clearly, since the fuel and air are mixed before combustion there is a risk of the flame flashing back from the combustor and stabilising at the fuel injector or autoigniting within the premixing duct. Additionally, since it is most desirable to have the minimum NOx at the design point, this means that at full load the engine will be operating very close to its lean extinction limit. This, in turn, implies problems for part load operation and potential problems for flame stability at full load.

In order to inform and accelerate the design of such a combustor it is necessary to develop a computational tool, which can model lean premixed combustion. This tool should be able to both predict the fuel air mixing and predict combustion with a non-uniform equivalence ratio. It should also be able to predict NO_x emissions and be computationally efficient so that it can produce answers in a reasonable time scale within a development environment.

The purpose of this study is to investigate CFD combustion modelling techniques which can be used to model this type of combustor within a design environment. Given the intended practical application of this tool, it is considered unreasonable at

this time to consider transient calculations, employing for example Large-Eddy Simulation techniques. This makes the computation of combustion-flowfield instabilities, flashback and autoignition particularly difficult, however design information can often be drawn from steady state solutions to help gauge the risk of their occurrence in some designs.

We shall first describe the background to low NO_x combustor technology to identify the framework in which this work sits and provide a better understanding of the problems faced by LPP combustors. Then we will discuss how lean premixed combustion can be modelled and which modelling approaches are considered here. Preliminary calculations conducted on simple two-dimensional geometries which seek to evaluate the differences in the models and their implementation will then be described. Finally we will discuss calculations which were performed on an experimental LPP combustor which was tested at Cranfield (Harding, 1996).

2 Literature Review

2.0 Introduction

The design of a combustor is a complicated process drawing on experience and a large array of computational and experimental tools. The aim of this project is to investigate combustion models, in the context of CFD analysis, which can be used to assist the development engineer in the task of designing a low NO_x combustor.

As a means of setting the stage, a brief description of the current status of low NO_x combustion technology will be provided. First a brief discussion of emissions and how they interrelate in a gas turbine engine will be presented. This is important since it is desirable to keep all emissions low whilst reducing NO_x. Then several current proposals for low NO_x combustors, including LPP, will be introduced, and an analysis of the benefits and problems of these proposals will be reviewed. Finally, practical geometries for LPP will be discussed.

After this introduction to the technological challenges, the problems posed in relation to numerical simulation will be discussed. The status of premixed turbulent combustion modelling will be assessed and CFD issues will be discussed in the context of this exercise.

2.1 Gas Turbine Emissions

2.1.0 Introduction

Although NO_x emissions are particularly important for high altitude aircraft, there are essentially four types of emissions which have received the attention of the regulatory authorities for gas turbine engines. These consist of NO_x, CO, unburnt hydrocarbons (UHC), and smoke. We will first examine these emissions in detail and then review current proposals for low NO_x combustors.

2.1.1 NO_x

Oxides of Nitrogen or NO_x consist of NO and NO_2. Within a gas turbine there are two possible sources of nitrogen which can be oxidised to form NO_x. The primary one is from the N_2 in the air, although some low grade fuels have nitrogen bound to the fuel. Currently, this latter source is not a significant problem for aeroengines, however it may become more important in the future as the world oil supply drops and lower fuel grades are introduced more widely.

NO is formed by three main routes: the thermal NO mechanism, the prompt NO mechanism, and the nitrous oxide route.

The thermal NO mechanism, which was first suggested by Zeldovich and is the dominant route in current engines, is strongly temperature dependent: the larger the temperature the greater the formation rate of NO.

It is considered to be comprised of three principal reactions (Lavoie *et al*, 1979):

$$O + N_2 \overset{1}{\Leftrightarrow} NO + N \qquad (2\text{-}1)$$

$$N + O_2 \overset{2}{\Leftrightarrow} NO + O \qquad (2\text{-}2)$$

$$N + OH \overset{3}{\Leftrightarrow} NO + H \qquad (2\text{-}3)$$

where the rate coefficients as given by Baulch *et al* (1973) in $cm^3/(g\ mole\ s)$ are:

$$\text{for (2-1) } k_1 = 7.6 \times 10^{13} \exp\left(\frac{-38000}{T}\right) \qquad (2\text{-}4)$$

$$\text{for (2-2) } k_2 = 1.5 \times 10^{9} T \exp\left(\frac{-19500}{T}\right) \qquad (2\text{-}5)$$

$$\text{for (2-3) } k_3 = 4.1 \times 10^{13} \qquad (2\text{-}6)$$

and where k_i denotes the respective forward rate coefficient.

Since these reactions are very slow in comparison with the fuel oxidation rate and typically NO concentrations are small, it is generally assumed that this mechanism is de-coupled from the combustion heat release.

Unlike thermal NO production, the prompt mechanism forms NO rapidly near the reaction zone. It was first identified by Fenimore (1971) and is prevalent in fuel rich conditions. Fenimore (1971) found a peak in prompt NO at an equivalence ratio of 1.4. However it is also thought to be important for very lean flames where the flame temperature is no longer high enough for the thermal mechanism to completely dominate (Dupont, 1993a, 1993b, Hayhurst, 1980). It has also been reported that the NO formation rate by this mechanism increases proportional to the square root of pressure (Fenimore, 1971).

The main reactions associated with the prompt NO mechanism are (cf. Miller *et al*, 1989):

$$CH + N_2 \Leftrightarrow HCN + N \qquad (2\text{-}7)$$

$$CH_2 + N_2 \Leftrightarrow HCN + NH \qquad (2\text{-}8)$$

$$CH_2 + N_2 \Leftrightarrow H_2CN + N \qquad (2\text{-}9)$$

$$C + N_2 \Leftrightarrow CN + N \qquad (2\text{-}10)$$

where the rate coefficients given by Miller *et al* (1989) in $cm^3/(mole\ s)$ are:

$$\text{for (2-7)}\ k_f = (3.00 \times 10^{11}) \exp\left(\frac{13600}{RT}\right) \qquad (2\text{-}11)$$

$$\text{for (2-8)}\ k_f = (1.00 \times 10^{13}) \exp\left(\frac{74000}{RT}\right) \qquad (2\text{-}12)$$

$$\text{for (2-9)}\ k_r = (2.00 \times 10^{13}) \qquad (2\text{-}13)$$

$$\text{for (2-10)}\ k_r = (1.04 \times 10^{15}) T^{-0.5} \qquad (2\text{-}14)$$

In these equations R is the universal gas constant in calories/(mole K), k_r is the rate coefficient of the reverse reaction and k_f is the rate coefficient of the forward reaction.

In very lean flames the nitrous oxide mechanism, first pointed out by Malte and Pratt (1974), may also become important. The main reactions for this mechanism are:

$$N_2 + O + M \Leftrightarrow N_2O + M \qquad (2\text{-}15)$$

$$N_2O + H \Leftrightarrow N_2 + OH \qquad (2\text{-}16)$$

$$N_2O + O \Leftrightarrow N_2 + O_2 \qquad (2\text{-}17)$$

$$N_2O + O \Leftrightarrow NO + NO \qquad (2\text{-}18)$$

There is considerable debate in the literature over the role of this mechanism. More recently, Corr *et al* (1992) found from their experiments on lean premixed combustion in a jet stirred reactor at atmospheric conditions that this mechanism was not important.

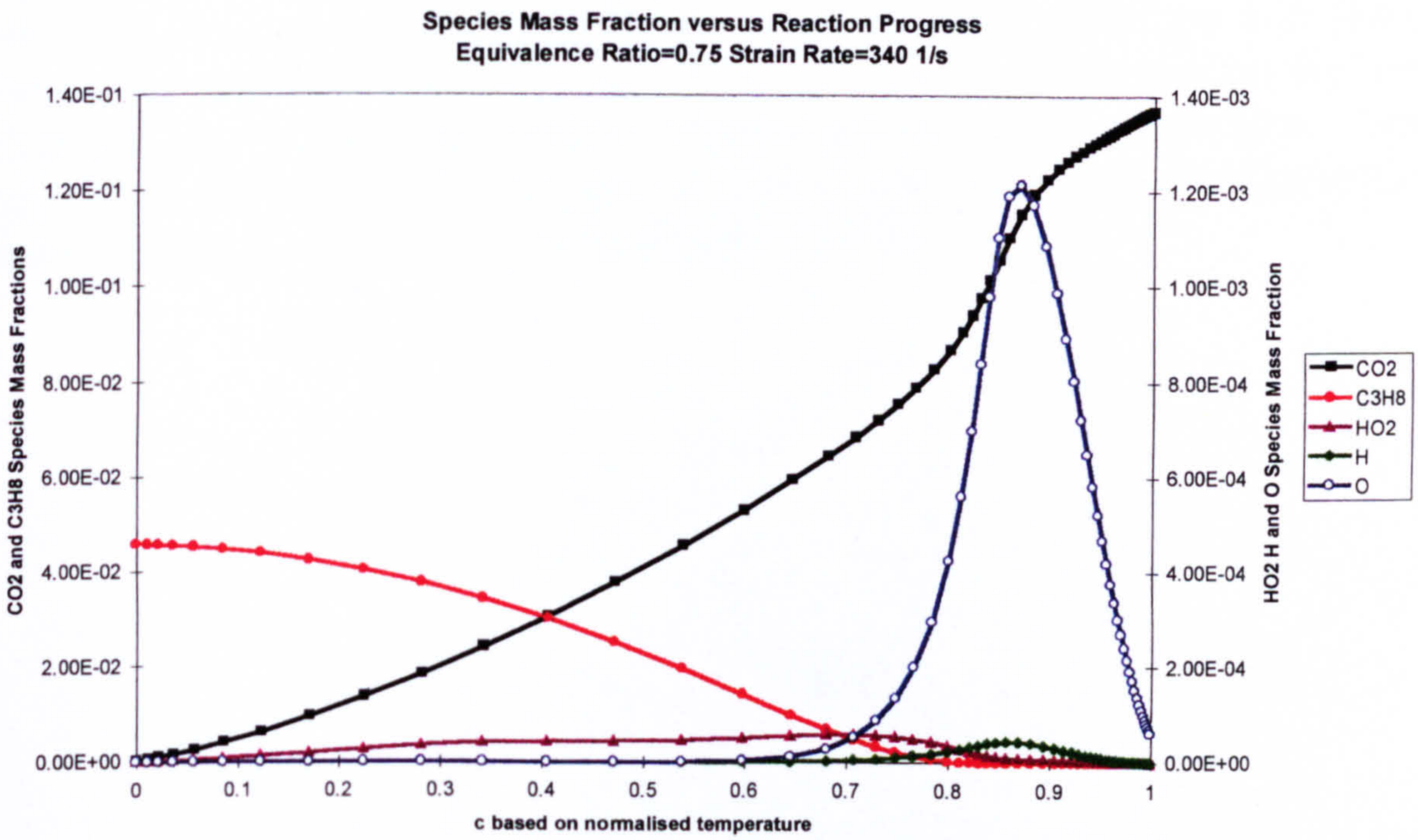

Figure 2.1.1.1 profile of C_3H_8, CO_2, HO_2, H and O across the flame front

NO_2 forms from NO and is generally believed to constitute no more than 5% of exhaust NO_x. Under atmospheric conditions NO has a half life of several days before conversion into NO_2. However levels of NO_2 of up to 80% of NO_x have been measured from gas turbine exhausts (Schefer *et al*, 1977, Cernansky *et al*, 1975, Laurendeau, 1975). Measurements in the flame region have also suggested that there are relatively high concentrations of NO_2 as a fraction of NO_x near the flame front (Merryman *et al*, 1975, Fenimore, 1975). While some of this is attributed to probe reactions (Cernansky, 1976, Drake *et al*, 1987, Duterque *et al*, 1981, Allen, 1975, Johnson *et al*, 1979), Sano (1985, 1984, 1982) suggests the following scheme for the production and destruction of NO_2 within the flame:

$$NO + HO_2 \Leftrightarrow NO_2 + OH \qquad (2\text{-}19)$$

$$NO_2 + H \Leftrightarrow NO + OH \qquad (2\text{-}20)$$

$$NO_2 + O \Leftrightarrow NO + O_2 \qquad (2\text{-}21)$$

In the low temperature regions of the flame there are significant concentrations of HO_2. Sano believes that some NO, formed in the high temperature regions, is transported to the low temperature regions and reacts to form NO_2. The removal reactions of Equations (2-20) and (2-21) are very rapid in the presence of high radical concentrations and so the NO_2 which is formed is rapidly converted back to NO in the high temperature regions of the flame. The location of the peaks of HO_2, H and O are illustrated in Figure 2.1.1.1 for a calculated laminar atmospheric pressure propane air flame at an equivalence ratio of 0.75. The position in the flame front is defined by a scalar c, which is based on normalised temperature such that it takes on the value 0 in the unburnt and 1 in the fully burnt. Clearly one can see that HO_2 peaks early in the flame, however not long after that both O and H peak. The peak of O is much higher than the peak of HO_2 thus one would expect all of the NO_2 formed in this flame to be converted rapidly back to NO.

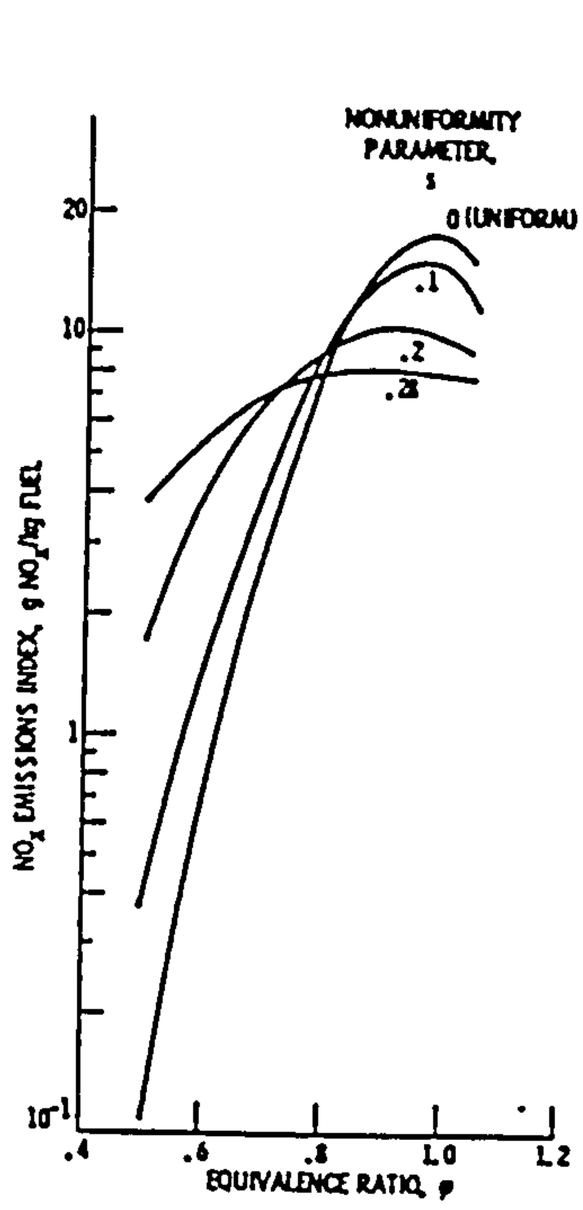

Figure 2.1.1.2 NO_x versus Equivalence Ratio for Various degrees of Mixture Uniformity (Lyons, 1981)

Based on this analysis NO_2 which is formed at flame temperatures can only exist as a transient species. For NO_2 to persist into the exhaust there must be quenching of the NO_2 formed in the flame. This quenching might occur by rapid mixing of hot and cold fluid elements in a highly turbulent flame which acts to reduce the radical concentrations (Sano, 1984, McLean, 1979, Hori, 1986, Leung *et al*, 1987). Since the concentration of NO_2 is expected to be low at the combustor exit it will not be considered further here.

Reducing NO_x emissions in gas turbine combustors to date has been accomplished by concentrating on the Zeldovich mechanism. This mechanism is highly temperature dependent and relatively slow compared to the heat release, thus techniques for reducing NO formed by this route have focused on reducing the flame temperature and residence time.

Flame temperature is a function of the equivalence ratio, with the peak temperature occurring at an equivalence ratio of approximately unity. Thus burning lean or rich of this ratio will reduce NO_x production. Mixture homogeneity then plays an important part in the NO_x production rate. Mixtures that are poorly mixed and have a large distribution of equivalence ratios will produce more or less NO_x than a perfectly premixed mixture, depending on their mean equivalence ratio. For a mean equivalence ratio near one a poor mixture quality will mean that at any instant in time a high proportion of the flow will burn at equivalence ratios leaner or richer than stoichiometric. Thus the mean level of NO_x produced will be less than that of a perfectly premixed mixture. However, more importantly for the low emissions combustor if the target mixture is much leaner than stoichiometric, the opposite will occur. A poor mixture quality will imply that a proportion of the flow is burning near the stoichiometric equivalence ratio which will produce more NO_x. Figure 2.1.1.2 illustrates a comparison of the concentration of NO_x produced against the mean equivalence ratio for various levels of mixture quality based on a theoretical investigation by Lyons (1981). This figure indicates that the crossover point between these two trends occurs at an equivalence ratio of about 0.7 for a propane air mixture.

2.1.2 CO, UHC and Smoke

Since we are primarily concerned with NO_x emissions, we will only touch briefly on the subject of CO, UHC and smoke emissions and how reducing them affects NO_x production and vice versa.

Both CO and unburnt hydrocarbons (UHC) are formed as an intermediate stage of combustion. If they are present in the exhaust it implies that the combustion is incomplete. Increasing flame temperature and residence time tends to reduce both

of these emissions, by increasing reaction rates and giving them more time to complete.

Smoke consists of soot particles which tend to form in rich fuel air mixtures. The formation mechanism of soot is comprehensively reviewed by Haynes *et al* (1981). It can be a large problem for diffusion flames, particularly burning liquid fuels at elevated pressure, but is generally not thought to be a problem for lean premixed flames.

Increasing the flame temperature and residence time to reduce CO and UHC emissions typically conflicts with strategies for reduced NO_x emissions by speeding up N_2 oxidation rates and giving more time for them to occur. In contrast, reducing flame temperature and residence time which is good for reducing Zeldovich NO_x generally produces more CO and UHC. Thus a balance needs to be struck between NO_x, CO and UHC. Generally speaking, engines tend to be optimised at idle conditions for CO and UHC, since this is where their emission is worst and at full power for NO_x.

2.1.3 Current Proposals for Low NO_x Combustors

Three basic approaches are currently proposed in the literature for future generation low NO_x combustors for aeroengines. The first of these is lean premixed prevaporised (LPP) combustion. This technique was first promoted in the early 1970's by Wade *et al* (1973) and others (Nagey *et al*, 1973, White *et al*, 1973) in the automotive industry. It involves premixing and prevaporising fuel with air such that the mixture is lean, and then burning it in the primary zone of the combustor. By premixing and prevaporising the mixture should be very homogeneous, and it could potentially give reductions in emissions of the order of 80 to 90% (Burbank, 1992) over current commercial aircraft engines. Problems which plague this device are that it operates close to the weak extinction limit (Lefebvre, 1974), and flashback and auto-ignition could potentially occur in the premixing duct (Bahr, 1978, Jones, 1978, Lefebvre, 1974, Burbank, 1992). Considerable effort has gone into ironing out these problems during the late 1970's and 1980's (Mosier *et al*, 1974a, 1974b, 1973, Sattelmayer *et al*, 1992, Proctor II *et al*, 1987a, 1987b, Smith *et al*, 1987, Sotheran *et al*, 1985, Ross *et al*, 1983, Fiorentino *et al*, 1980, Lefebvre, 1977, Mularz, 1979, Buchheim, 1978, Marek *et al*, 1976, Anderson, 1976, and Roffe *et al*, 1975) which will be discussed later.

Another technique proposed is catalytic combustion. This involves the lean Prevaporised premixed technique of fuel air preparation, however the fuel air mixture is not burned in a conventional manner. It is introduced into a catalyst bed where the oxidation of the fuel can occur at a much lower temperature than that required to

produce oxides of nitrogen. The bed can also be designed to give extremely high combustion efficiency removing most CO and UHC emissions (Bahr, 1978, Mularz *et al*, 1979). This device appears to be the ultimate in emission reduction. A ceramic substrate, similar to that employed in exhaust gas clean-up, has been proposed, however a robust catalyst substrate combination, effective over the complete operating range, has yet to be discovered (Correa, 1991).

The third solution lies in the rich-lean (RQL) combustion method. Fuel is burnt in the primary zone in a rich diffusion flame, it is then quenched quickly with additional air, and finally burnt in a lean mixture. This makes use of both the rich and lean sides of stoichiometric. It also avoids the need to premix and prevaporise the fuel. The rich burning section has the added advantage of having a very small quantity of oxygen available for NO_x production as well as a low flame temperature. In the rich zone, any fuel droplets that are unburnt are vaporised and mixed with the remaining air and combustion products before entering the lean combustion zone (Burbank, 1992). The temperatures of the rich zone and the lack of oxygen make an ideal area for fuel bound nitrogen to be converted to N_2 and thus this technique deserves further investigation as fuel quality gradually declines.

At the present time opinions are divided over which of these is the best approach. MTU in Germany have argued that RQL is the best technique to reduce all emissions, despite a potential problem of smoke emissions from the rich burning zone (Burbank, 1992). On the other hand Correa (1991) at General Electric in the U.S. and Sasaki *et al* (1991) at Nissan in Japan have argued that RQL will never achieve the emission reduction levels of LPP. In particular they suggest it is limited by the rate at which the hot rich gases can be mixed with the remaining air to produce the lean conditions for the second combustion zone.

Catalytic combustion clearly offers the best of all of these solutions as far as minimising emissions is concerned, however the technology to make this work efficiently and reliably is not yet established. LPP therefore appears to be the most promising near term solution. It also has the added advantage that the same fuel air preparation technology is required for catalytic combustion and so might be considered a stepping stone to this technology. Thus we shall now concentrate on LPP configurations.

2.2 Background on Lean Prevaporised Premixed Combustion

2.2.0 Introduction

As mentioned earlier LPP combustion involves burning a prevaporised and premixed fuel air mixture at a lean equivalence ratio. Given the control of peak temperature which it introduces, this form of combustion has a great potential for reducing NO_x emissions and thus has received considerable attention over the last two decades in terms of both fundamental and applied research.

There are essentially three types of gas turbines which have been considered for the application of LPP combustion. These are aircraft, automotive and industrial engines. NO_x produced by ground based engines such as those for automotive and industrial applications, although much more significant in quantity to aircraft, remains in the atmosphere for only a short time and is not considered to have the same strong effect that NO_x produced at aircraft cruising altitude has (Price, 1995, Gardner, 1995). This is especially true of supersonic aircraft which fly very near to the ozone layer. Thus larger total emissions of NO_x are tolerated from ground based engines over aircraft engines. In a large number of countries in the developed world 25 ppm NO_x (15% O_2) is the accepted limit for stationary gas turbines operating with natural gas. In some places such as California this limit is only 9 ppm NO_x (15% O_2). Higher limits usually exist for liquid fuels.

For aeroengines, with which we are mainly concerned here, LPP is presently being considered primarily for the next supersonic transport. An engine of this sort is expected, at cruise conditions, to have a combustor inlet temperature of around 800 to 1000 K and pressure of about four atmospheres (Roffe, 1976). At take off conditions the pressure and temperature will be much higher however NO_x will not be as large a concern given the short time scales and low altitude of the engines.

The automotive industry was one of the earliest groups to investigate LPP combustion, starting in the early 1970's (Wade *et al*, 1973). Automotive gas turbines have similar combustor inlet conditions at full load to a supersonic aero engine at cruise with around a 1000 K and four atmospheres temperature and pressure respectively (Ross *et al*, 1983). As in all transport applications, such engines should be compact and light to minimise drag and fuel consumption but they also need to be able to accelerate and decelerate quickly. Given that LPP combustion implies that the combustor is operating near its lean extinction limit then a reliable mechanism needs to be devised such that the power can be reduced quickly without the flame extinguishing. Similar to the experience with aero engines, a large amount of research has been conducted and experimental combustors have been tested but to date no commercial engine with LPP exists.

More progress has been made by industrial gas turbine companies and a number have successfully applied commercial variants of LPP combustor (Sattelmayer *et al*, 1992) since the mid 1980's. Industrial engines do not have the size and weight constraints of vehicular engines, nor do they have the requirement for rapid deceleration that the automotive engines have. They do have a higher pressure ratio over automotive engines, however, with typical combustor inlet pressures between 10 and 30 atmospheres. Combustor inlet temperatures vary between 500 to 1000 K. The major difficulty facing these engines is that they are required to burn a wide variety of fuels. Most of the success for LPP thus far in this industry has been with engines fuelled by natural gas, however, ABB claim to be able to burn oil distillate number 2 as well in their second generation LPP burner (Sattelmayer *et al*, 1992) with a small deterioration in NO_x emissions.

We now examine some of the more fundamental investigations which have been carried out into fuel and air mixture preparation, flame stability, autoignition and flashback. This research underpins most practical LPP configurations.

2.2.1 Fundamental Research

The primary problems associated with this type of combustor relate to the potential for flashback or autoignition in the premixing duct and operation near to the lean extinction limit.

Many studies of LPP have concentrated on the idea of using a flameholder to stabilise the flame. Bosque Fernández (1983), Al Dabbagh and Andrews (1984), Stwalley and Lefebvre (1987a, 1987b) and Sjunnesson *et al* (1991a, 1991b) investigated the influence of flameholder shape and pressure drop on the stability of a flame. They found that the simpler the geometry, the more stable the flame. Flame stability was found to improve with increasing pressure drop, however, the characteristic blow off velocity decreased with an increase in flameholder blockage, and hence local velocities around the flame holder.

Concerns for the reliability and durability of a flameholder, which would be very difficult to cool, have prompted other researchers to investigate techniques of aerodynamically stabilising the flame. Stabilisation of the flame in the recirculation downstream from a sudden expansion was investigated by Parker *et al* (1979), Pitz and Daily (1983, 1981, Ganji *et al*, 1980), Proctor *et al* (1985) and Ahmed and Nejad (1992). Additionally, stabilisation in the recirculation bubble created by a vortex breakdown has been studied by Anand and Gouldin (1985), Proctor II and Mellor (1987b), Hillemanns and Lenze (1988) and Philipp *et al* (1992). These researchers found similar trends related to flame stability and pressure drop to those for flame

holder stabilised flames. Investigations of the impact of different radial distributions of swirl were carried out by Anand and Gouldin (1985). Their experiment consisted of a swirl stabilised flame with an annular jet of swirling air around the flame. They observed that the greater the difference in the tangential velocity of the outer jet and that of the inner fuel air mixture the shorter the flame. This they argued was due to a greater degree of mixing between the two streams which resulted in lower NO_x emissions and higher CO emissions.

A large number of investigations have sought to identify the possible causes of flashback within a typical LPP combustor. Wierzba and Kar (1992) have investigated flashback limits for various fuels, including propane, in lean homogeneous turbulent flames for high Reynolds number flows. Proctor *et al* (1985), Nein and Mellor (1983), Coats (1980) and Marek *et al* (1977) experimentally studied flashback in practical LPP test combustors. Generally, these researchers confirmed that the tendency for flashback increased as the equivalence ratio increased towards the stoichiometric value and as the inlet temperature was increased. Proctor *et al* (1985) found that the conditions for flashback were independent of the mean velocity and wall temperature of their rig and suspected that instabilities, causing local regions of reverse flow or velocities below the turbulent burning velocity, were responsible for flashback. Nein and Mellor (1983) established that their fuel air mixture was not homogeneous and contained regions which were closer to the stoichiometric equivalence ratio. Flashback then occurred along these so called stoichiometric contours. Plee and Mellor (1980, 1978b) suggested four possible mechanisms by which flashback could occur in an LPP combustor. These include autoignition, "classical" flashback (i.e. the turbulent burning velocity is greater than the mean velocity of the premixing duct), flame propagation through reversed flow fields, and preignition of a separated flow region. Thus to avoid flashback one needs to ensure that the velocity is always positive and greater than the turbulent burning velocity, that there are no stoichiometric contours and that there are no large reverse flow zones in the premixing duct which could potentially stabilise a flame. The influence of autoignition is more profound but also needs to be avoided.

Rather less fundamental research related to LPP has been undertaken on autoignition. Following the approach adopted in reciprocating engines, Marek *et al* (1977) tried to characterise the ignition delay time as a function of temperature T and pressure p in an Arrhenius type equation:

$$t = \frac{k e^{\frac{E}{RT}}}{p^n} \qquad (2\text{-}22)$$

where E is the Arrhenius activation energy (around 41 840 joules per mole for Jet A fuel), R is the universal gas constant, and k and n are empirical constants. Marek *et al* (1977) cite other studies which found that the activation energy for kerosene depended on temperature and pressure levels. They also noted that near the point where Jet A fuel is first injected evaporative cooling, and preflame reactions occur which would cause a change in the fuel-air temperature prior to the main combustion. This temperature rise is very critical when designing the flame holder open area. If the temperature rise is high, the pressure drop across the flame holder will change and the flow split between the combustor premixing tube and all other air inlets to the combustor will change. As the pressure drop increases, less air will flow through the premixing tube causing the mixture equivalence ratio to increase. The resulting situation is unstable and may lead to ignition in the premixing tube. Thus care needs to be taken that both the preflame temperature rise is not too high and that the time between fuel injection and arrival at the flame front is less than the ignition delay time.

From an operational perspective, the other problem which plagues LPP combustion is the fact that the combustor is operating close to its lean extinction limit. This severely limits the load range over which the combustor can operate. Most researchers have tackled this problem through staging. Either incorporating diffusion flame burners at lower power or through variable burning, with some burners operating above their lean extinction limit and some below, piloted by the former (Sattelmayer *et al*, 1992, Smith *et al*, 1987, Sotheran *et al*, 1985). Other researchers have proposed solutions involving variable geometry (Sasaki *et al*, 1991, Goyal *et al*, 1983, Ross *et al*, 1983, Fiorentino *et al*, 1980) which would control the airflow split between the premixing duct and the secondary zone of the combustor. The problem with this technique is that any mechanism is required to operate in extreme conditions of temperature and pressure and may not be very reliable mechanically in practical engines.

2.2.2 Practical LPP Configurations

Lean premixed Prevaporised (LPP) combustors have been designed, built, and tested for both research as well as commercial engines with some success. To date the aerospace engine field has only built these combustors on a research basis. Most of the literature on these, appears as a result of the Stratospheric Cruise Emission Reduction Program (SCERP) (Fiorentino *et al*, 1980, Mularz, 1979, Goyal *et al*, 1983) of the early 1980's. Rolls-Royce, which was not involved in this American funded program, also designed their own research combustor at this time. The automotive engine manufacturers have also worked on research engines, however their present efforts have been to design specific combustors for application to commercially available engines of the near future. Only industrial

engine manufacturers have already applied this technology commercially.

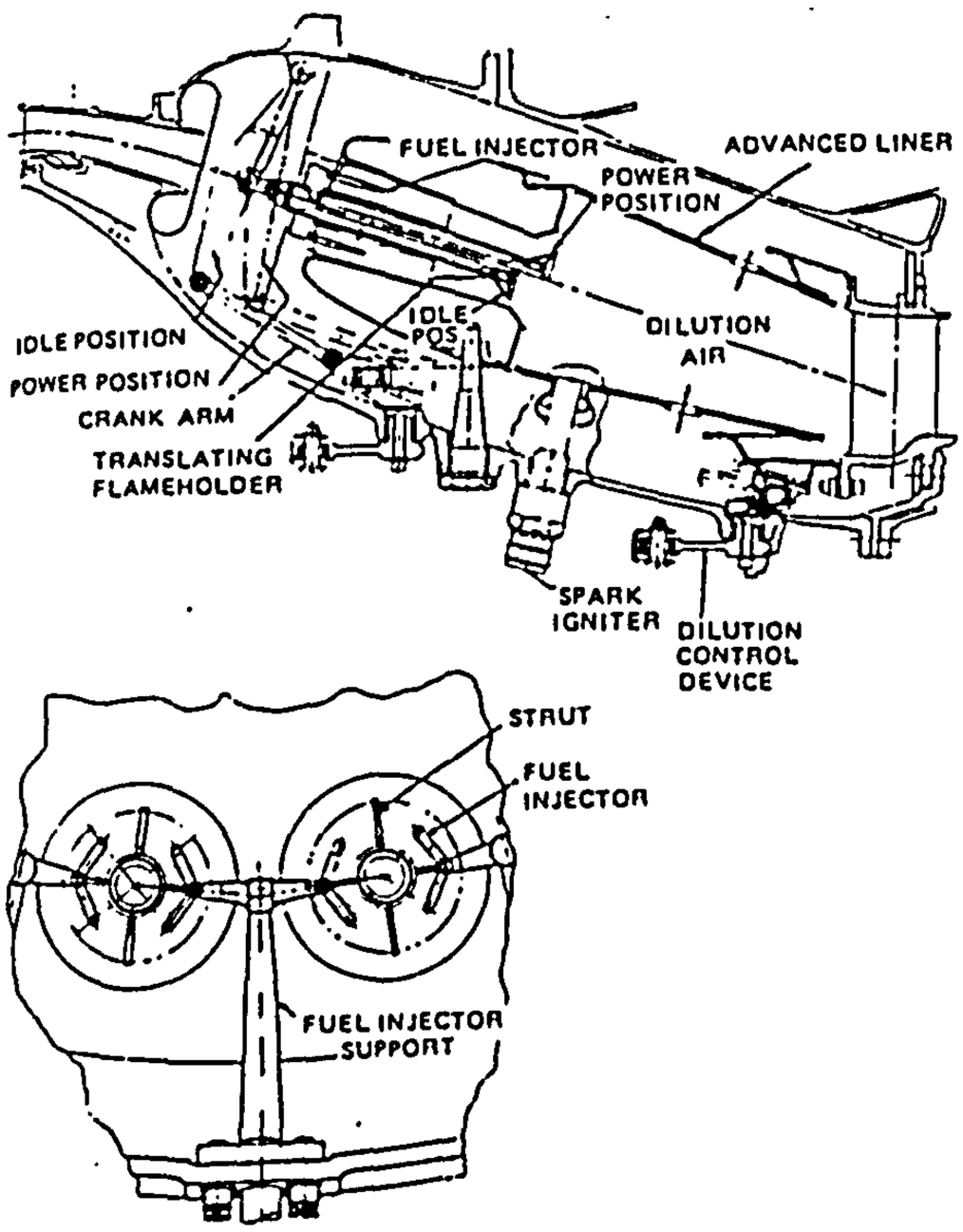

Variable geometry LPP combustor—concept 1

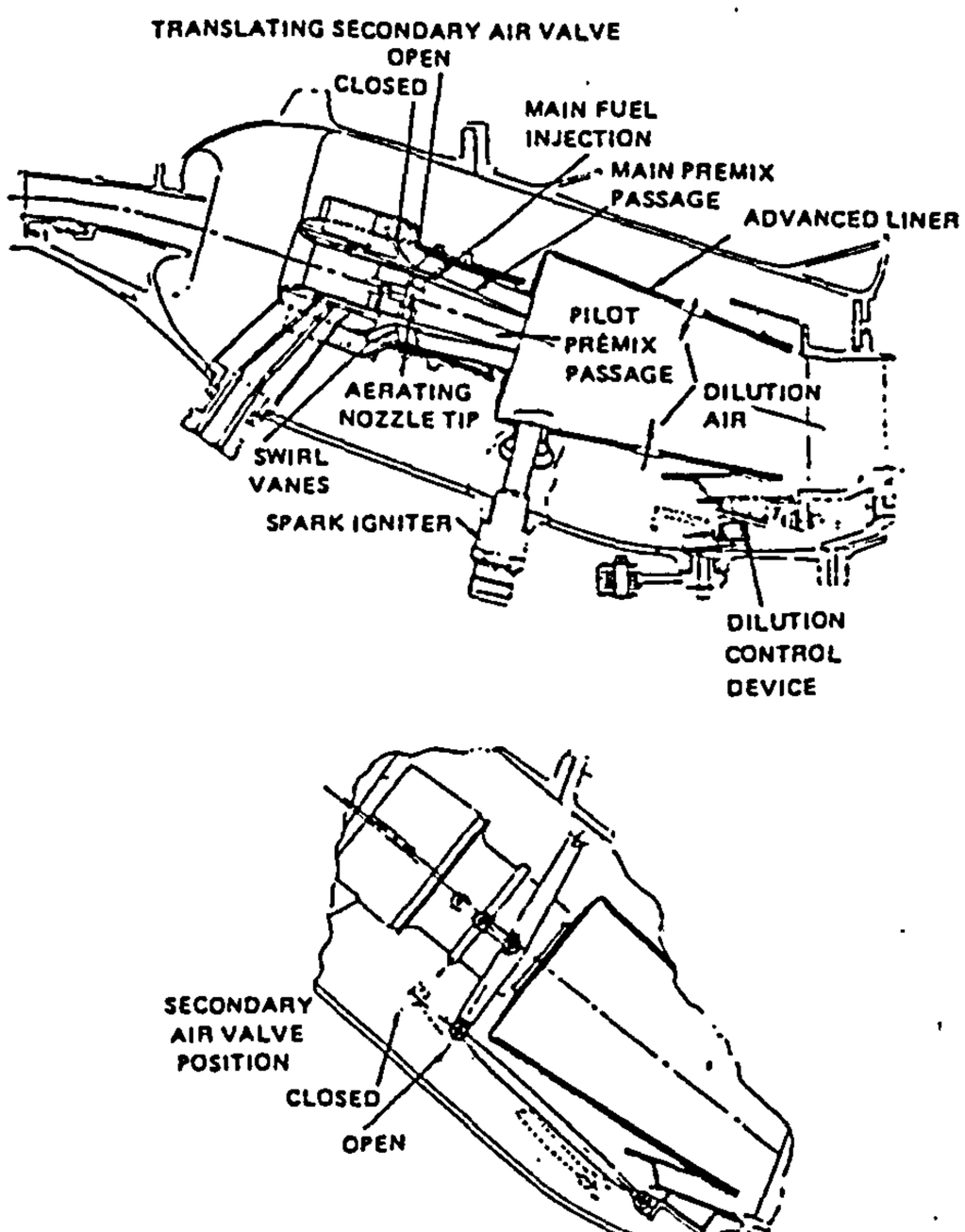

Variable geometry LPP combustor—concept 2

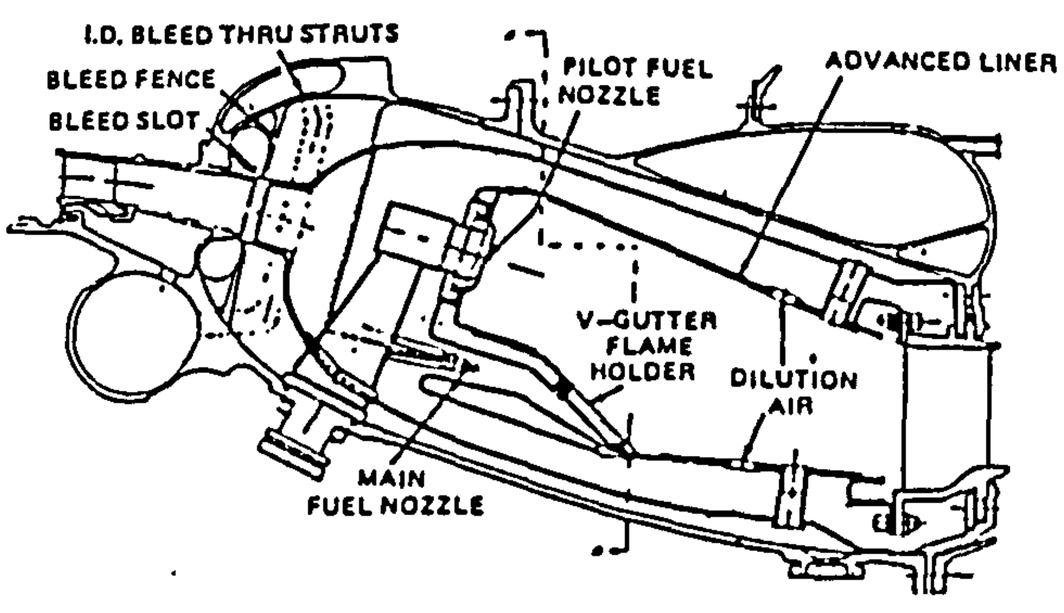

Variable geometry LPP combustor—concept 3

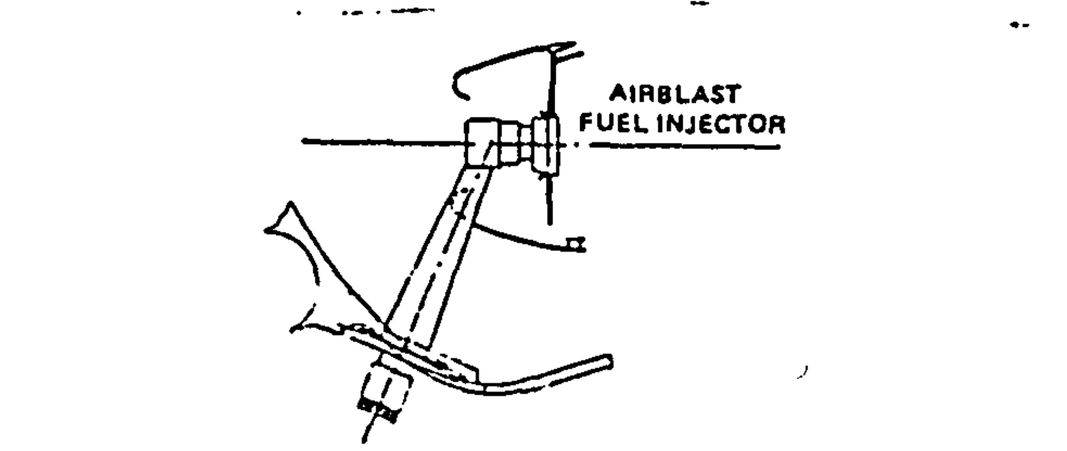

Variable geometry LPP combustor—concept 4

Figure 2.2.2.1 Pratt and Whitney LPP Test Combustors (Fiorentino *et al*, 1980)

As described earlier ultra-low emission combustors were deemed absolutely necessary for supersonic aircraft because of their high altitude cruise. Because LPP was seen to be more feasible in the shorter term than catalytic combustion, and was expected to offer superior performance to rich-lean (RQL) combustion, NASA established SCERP to investigate this type of combustor for application to supersonic aircraft. Both Pratt & Whitney and General Electric were involved in this program. Variable geometry was used by both companies to maintain the correct amount of air flowing through the premixing duct and into the primary zone at all power conditions.

The four designs proposed by Pratt & Whitney are illustrated in Figure 2.2.2.1 (Fiorentino *et al*, 1980). The first two concepts control the amount of dilution air and maintain a constant combustor pressure loss through an air bypass valve. The first concept also controls front end air using a movable flame holder. When the flame holder is in the "in" position, it produces a large blockage and accelerates the mixture in an attempt to prevent flashback. This is the idle position, which operates at an equivalence ratio of 1.0 to maintain high combustion efficiency and hence low CO and UHC emissions. At high power the equivalence ratio is reduced to 0.55 to minimise NO_x production, and the flame holder is in the "out" position. The "out" position reduces blockage, encouraging more air through the premixing duct, and introduces less acceleration. This is acceptable due to the reduced threat of flashback at a lower equivalence ratio. The second concept uses fuel staging to improve transient stability. The premixing duct consists of two concentric premixing passages. The inner passage has fixed geometry and acts as a pilot stage. The outer passage has a variable geometry sleeve and acts as the main stage. Once again an equivalence ratio of unity is used for high combustion efficiency at idle conditions while lean conditions (equivalence ratio of 0.55) are used for high power, to minimise NO_x production. At idle, only the pilot stage is used. A small amount of purge air is sent through the outer passage. At approach conditions both the outer and inner passages are used with the majority of fuel being supplied through the inner passage. The outer passage is kept richer than full power conditions to maintain high combustion efficiency. At high power conditions most of the fuel is supplied through the outer passage. The pilot passage equivalence ratio is kept richer than the main stage to protect against lean blow-outs during snap decelerations. The third concept is much simpler than the first two. It is a variation on a combustor proposed for an earlier research program run by NASA, the Experimental Clean Combustor Program (ECCP) (Jones, 1978), which uses diffuser wall bleed to vary the inlet air velocity profile. Inner and outer bleeds are used to divert airflow for the combustor front end at the approach condition. The fourth concept does not use LPP. It uses an airblast atomiser and variable geometry to control the exact position along the length of the combustor where combustion and dilution air is admitted. More detail on this concept is reported by Fiorentino *et al*

(1980). Emission estimates for each concept are given in Table 2.2.2.1. Both concepts 1 and 2 were believed to offer the best chance of reaching the emission goals. Concept 3 lacks sufficient bleed capability, and concept 4 has too poor fuel air mixing to be able to meet the NO_x goals at cruise. Concept 2 was judged slightly superior to concept 1 due to its improved stability, re-light capability, and transient operation.

		Concept			
	Goal	1	2	3	4
CO EPAP (g/kN)	≤ 25	12	34	21	12
UHC EPAP (g/kN)	≤ 3.3	1.7	0.5	2.9	1.7
NO_x EPAP (g/kN)	≤ 33	< 33	< 33	> 33[1] < 33[2]	< 33
NO_x EI at cruise (g/kg)	≤ 3.0	3.1 to 3.9	2.4	30[1] 4.8[2]	7.5
Smoke number	≤ 20	< 10	< 10	< 10	< 15

[1] with 25% front end flow diversion
[2] with 50% front end flow diversion

Table 2.2.2.1 Emission estimates for Pratt and Whitney's LPP Test Combustors (EPAP is an integration of the emission production over a standard flight pattern of taxi, take-off, cruise, and landing for specific time intervals) (Fiorentino *et al*, 1980)

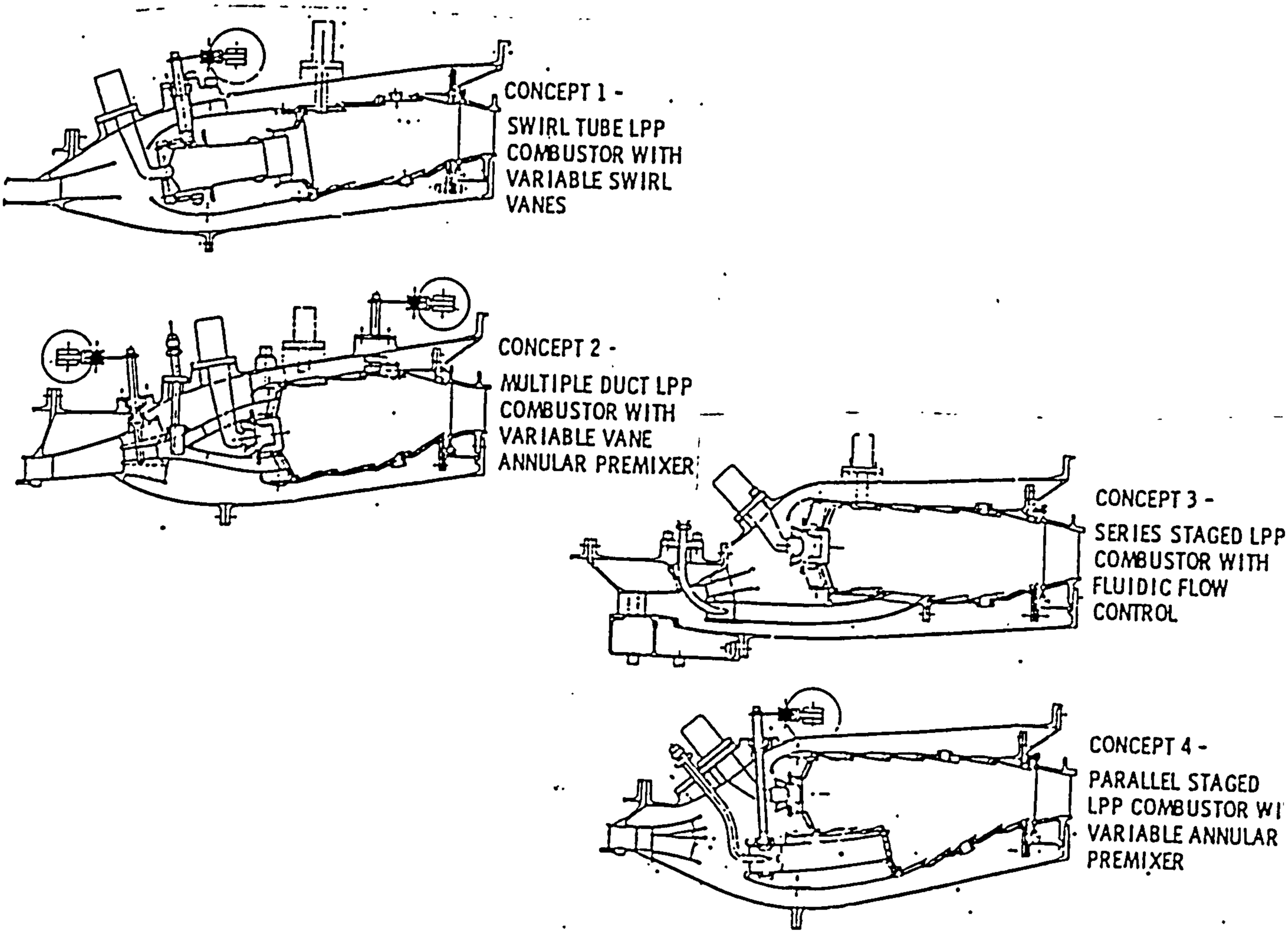

Figure 2.2.2.2 General Electric LPP Test Combustors (Goyal *et al*, 1983)

All four of the General Electric proposals, shown in Figure 2.2.2.2, except the first, use staging of LPP with a standard airblast atomiser combustor section (Goyal *et al*, 1983). The first proposal, the swirl tube combustor, consists simply of a single stage premixing duct. The series staged combustor uses a pilot stage to stabilise the combustion of the main premixed stage which is further downstream. In the parallel staged combustors both the pilot and main premixed stages operate in parallel and the pilot stage does not act as a flame holder for the main stage. Each combustor uses airflow modulation from variable geometry. In Goyal *et al* (1983) testing had only been conducted on the first three combustors with the series staged combustor appearing to be the most promising. We were not able to find any subsequent reports on this work. The variable-tube parallel-staged combustor, which had yet to be tested, was also expected to be promising. The residence time in the premixing duct was kept to 1.3 ms for each design which was well below the 3 ms autoignition delay time expected for takeoff conditions. Despite this, autoignition occurred due to mechanical design problems, which required modification. None of these combustors was tested at the full takeoff pressure, and it would be necessary to do this to verify that autoignition would never occur.

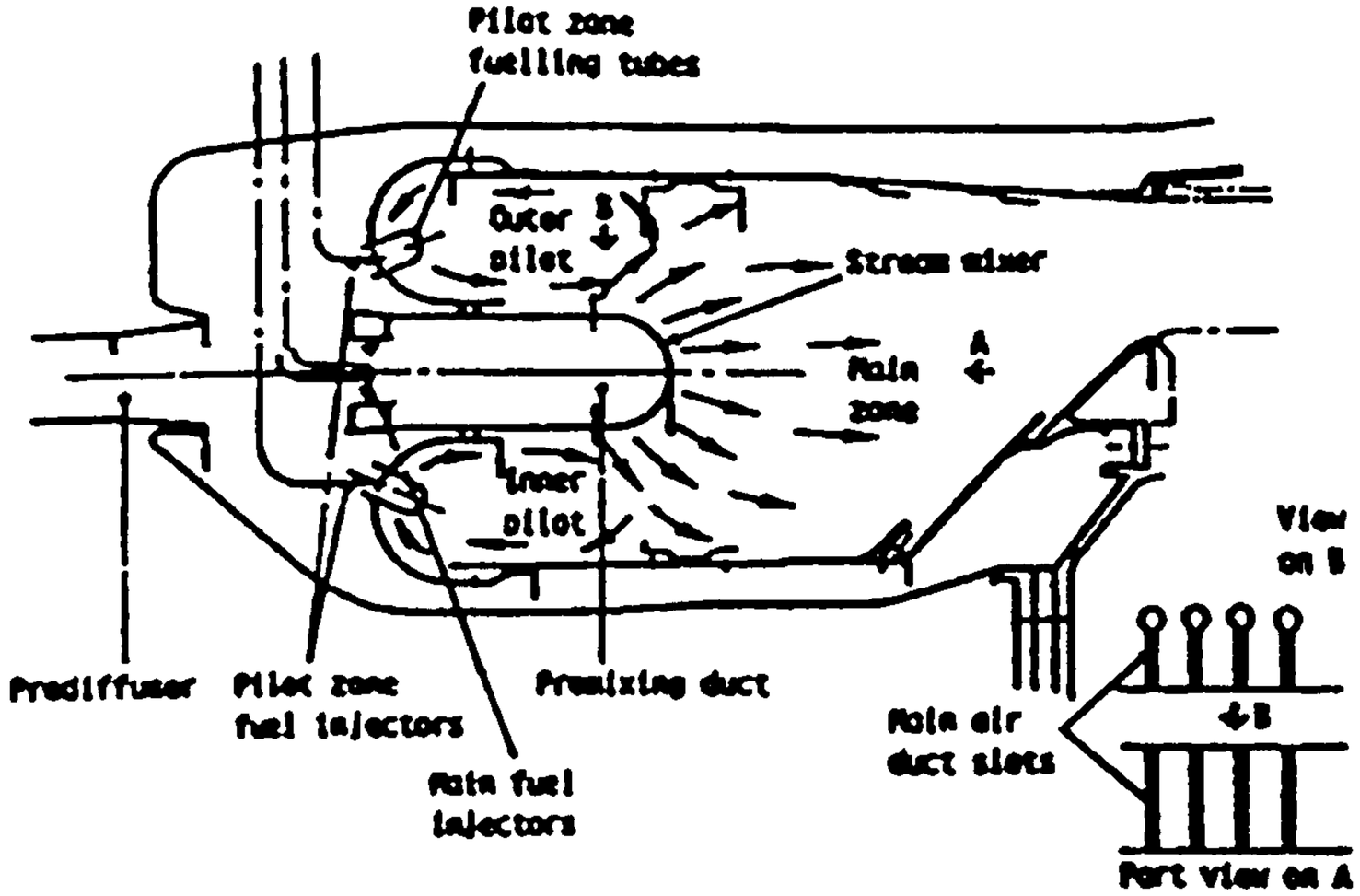

Figure 2.2.2.3 Early Rolls-Royce Radially Staged LPP Test Combustor (Sotheran *et al*, 1985)

In this same period Rolls-Royce also investigated LPP combustion (Sotheran *et al*, 1985). The configuration they designed and tested is illustrated in Figure 2.2.2.3. Their design was similar to that of General Electric, and consisted of a centrally

located premix duct between two standard non-premixed pilot stages. Flashback was avoided by making the holes in the flame holder so small that it would also act as a flame trap. The advantage of placing the premix duct between the two pilot stages was that heat from these stages would help to speed up fuel evaporation. The pilot stages were used at idle conditions only. The main stage was engaged as power was increased and dominated at full power. Emission levels were reduced over conventional combustor designs. It was decided that to reduce emissions even further both the primary and main stages would have to be lengthened. Problems related to flame holder durability, part load emissions, and control over outlet temperature pattern factor still required more research.

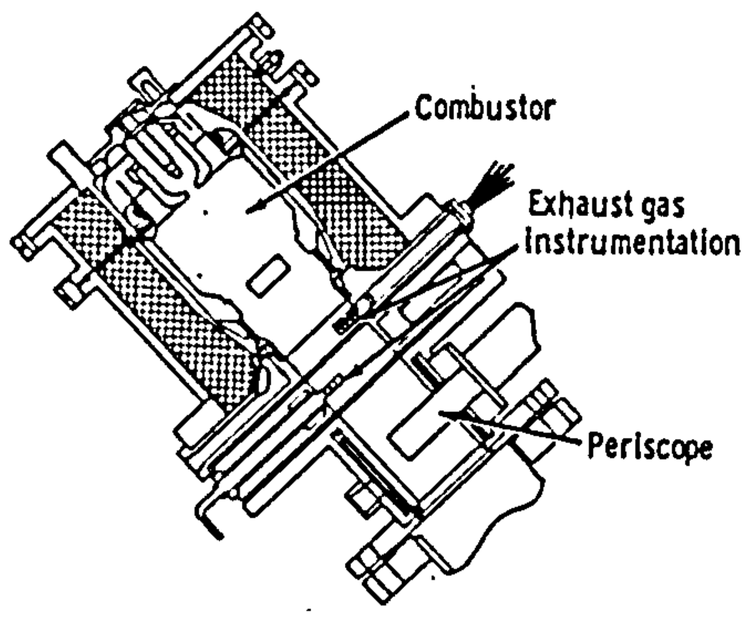

Figure 2.2.2.4 Allison LPP Combustor (Ross *et al*, 1983)

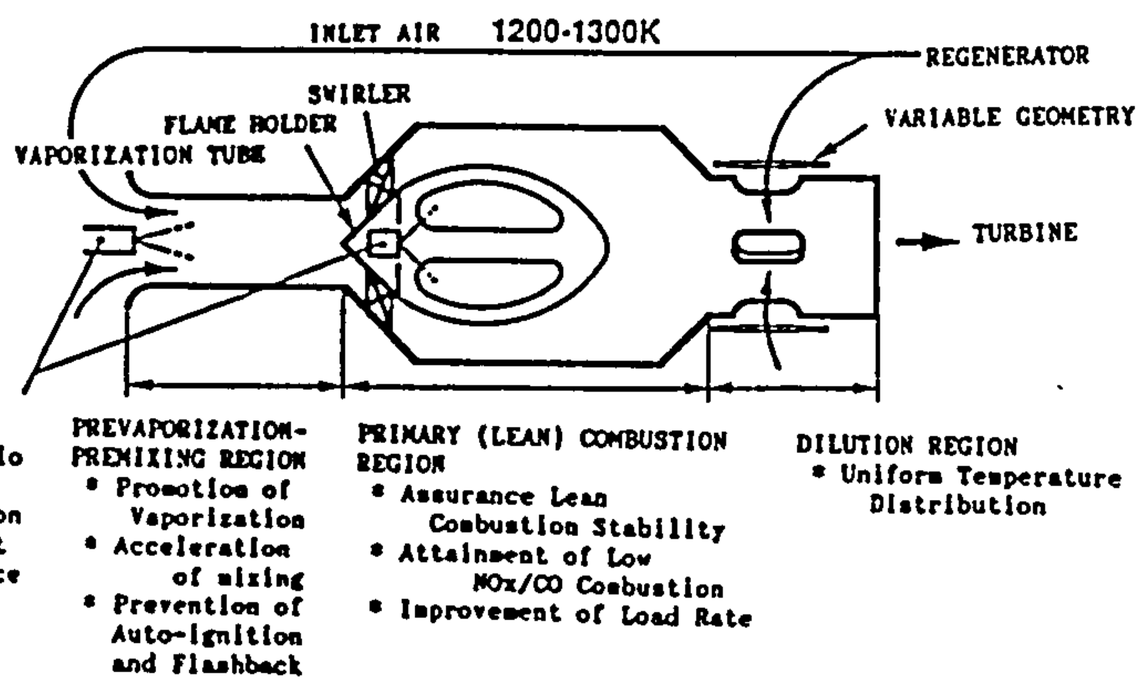

Figure 2.2.2.5 Nissan LPP Combustor (Sasaki *et al*, 1991)

In the early and mid 1980's Detroit Diesel Allison developed an LPP combustor for its AGT 100 automotive gas turbine (Ross *et al*, 1983). This combustor is illustrated in Figure 2.2.2.4. It has a small pilot chamber at the side of the main combustor which is ignited first and burns continuously. Fuel enters the premix duct just downstream of an air swirler. Variable geometry is used to control the amount of air entering the primary zone and the dilution zone. At idle conditions the dilution air flow is at a maximum and the primary air is at a minimum. As power increases more air is admitted into the primary zone and less into the dilution zone. The variable geometry works to uncover a swirler that allows more air to feed into the premixing duct. This combustor worked exceptionally well. Emissions were found to be a function of inlet temperature but with the lowest emissions at the highest inlet temperatures. NO_x emissions were 2 orders of magnitude below program goals, and CO emissions were 30 times below program goals. Both flashback and autoignition were never encountered at any of the engine operating conditions.

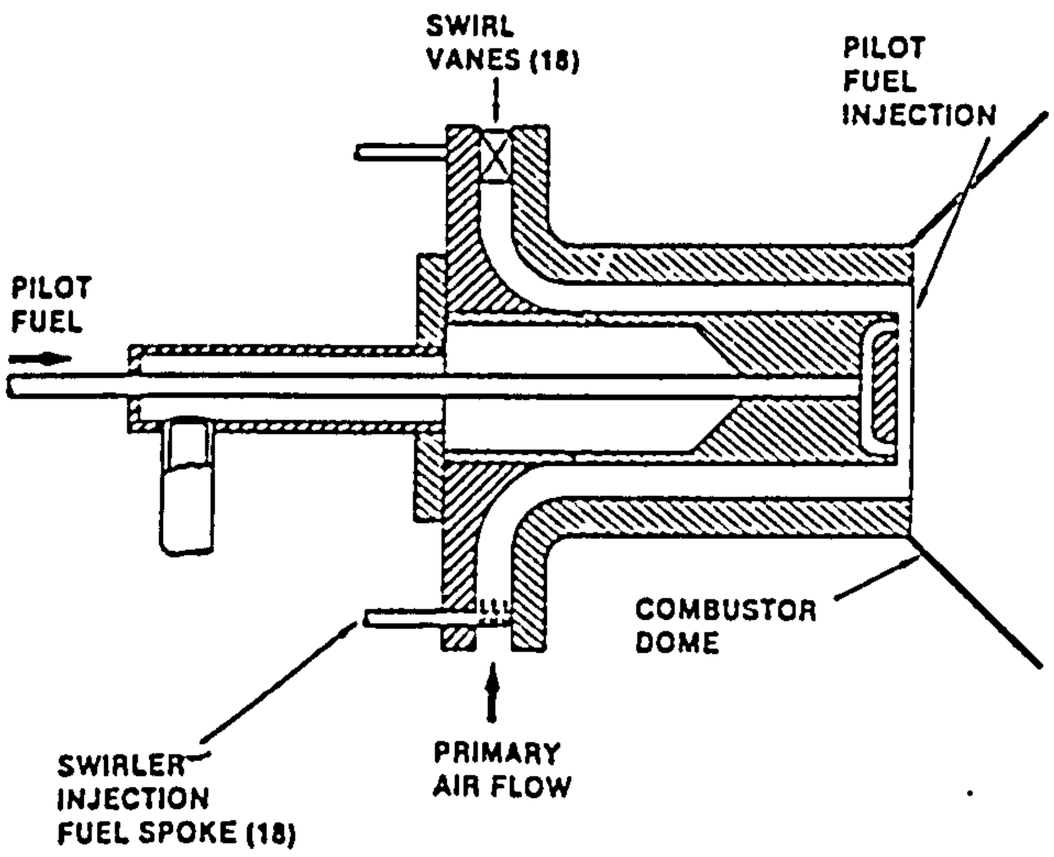

Figure 2.2.2.6 Solar Turbine LPP Combustor (Smith *et al*, 1987)

Nissan (Sasaki *et al*, 1991) also reported work on a gasoline fuelled LPP combustor for an automotive gas turbine to meet Japanese Mode 10 regulation. Their conceptual design is illustrated in Figure 2.2.2.5. Basically, it operates in the same fashion as the AGT 100 combustor. A pilot is used which is located in the middle of the combustion zone, and variable geometry is employed over the dilution holes to control the airflow split between the premixing duct and the dilution zone.

Solar Turbines investigated a natural gas powered LPP swirl-stabilised combustor for their Mars and Centaur Type H industrial engines (Smith *et al*, 1987). The combustor head is illustrated in Figure 2.2.2.6. A pilot fuel supply is injected through the centre of the head. On the outside, a centrifugal swirler supplies swirling air into an annular premixing duct. Fuel is injected with the air as it enters the swirler. The swirling mixture leaves the premixing duct as a vortex, which breaks down to form a recirculation bubble and which in turn stabilises the flame. This combustor worked well, achieving its design goals. It was found to be very sensitive to variations in fuel flow turndown with only a 7% margin to lean blow out. Smith *et al* (1987) point out that normal combustors have a 60-70% margin.

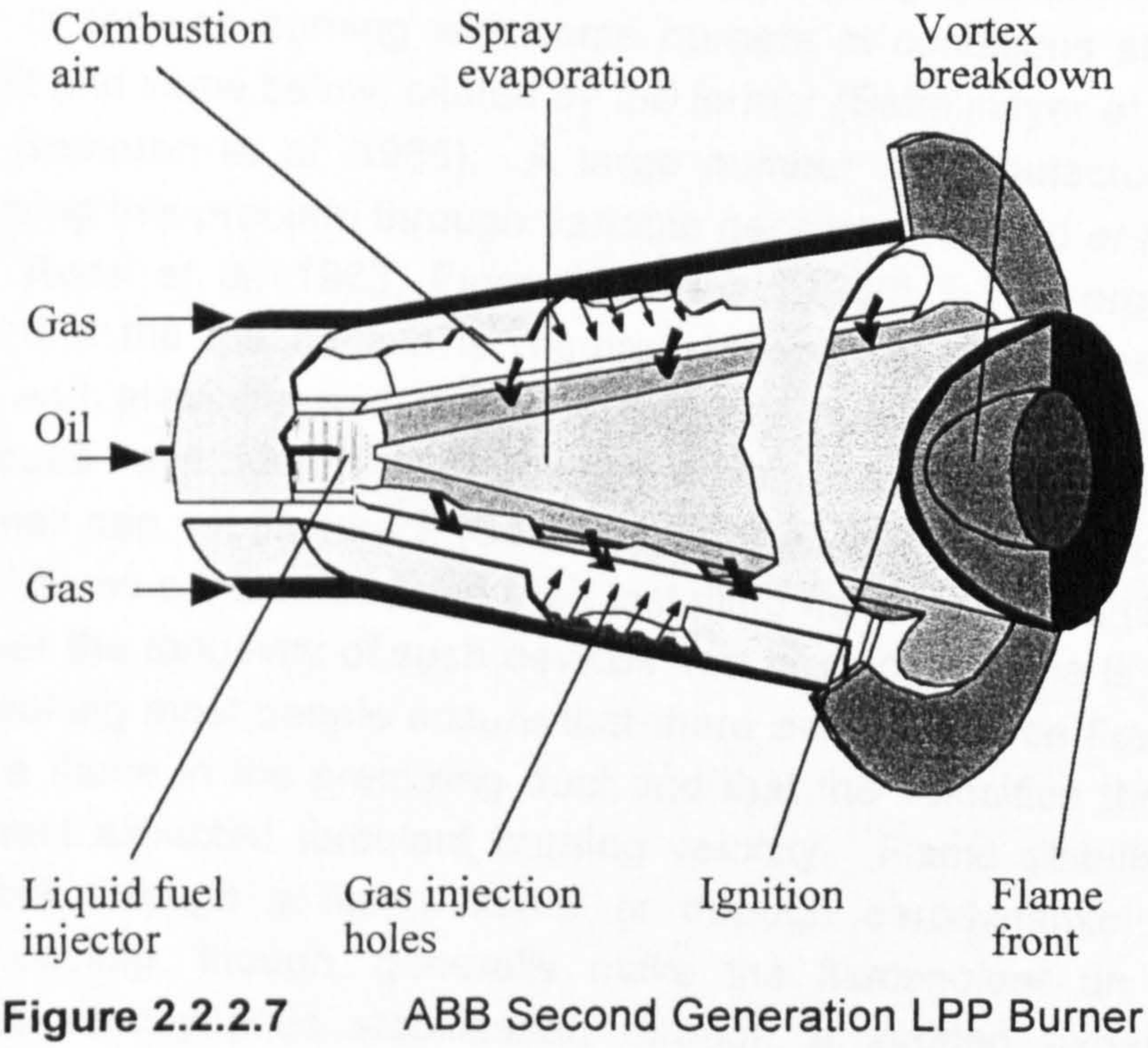

Figure 2.2.2.7 ABB Second Generation LPP Burner

ABB has also conducted work on applying industrial LPP combustors to commercial gas turbines (Sattelmayer *et al*, 1992). In 1984, they introduced their first generation LPP combustor, and by the beginning of 1992, they had designed an improved version. An illustration of one of the combustor heads or burners of their second generation LPP combustor can be found in Figure 2.2.2.7. This combustor works

under the same principles as the Solar Turbines combustor. It is swirl stabilised, employing a vortex breakdown to stabilise the flame. It can use both gaseous and liquid fuels, however, in common with other systems lower emissions are gained from gaseous fuels. It is also proposed to introduce fuel staging for axial combustor applications. Smaller combustor heads with the same direction of swirl are placed between larger ones and act as pilots. The fuel flow is split to obtain the desired equivalence ratio for the pilot burner always to be in a self-stabilising mode. At idle this means that there is not enough fuel in the main burners to sustain a flame. The flame from the pilot burners ignites this fuel. At full power the main burners are in self-stabilising mode. The temperature profile from this configuration has been found to be very good, with little change from low power to high. Sattelmayer *et al* (1992) point out that this burner also has the added advantage that it can never flashback due to the technique of stabilisation.

In general, a large variety of companies in the aerospace, automotive, and industrial fields have successfully designed research and, in some cases, even commercially available LPP combustors. Most have tackled the problem of operating near the lean extinction limit through staging. Either incorporating diffusion flame burners at lower power or through burning with some burners at conditions above their lean extinction limit and some below, piloted by the former (Sattelmayer *et al*, 1992, Smith *et al*, 1987, Sotheran *et al*, 1985). A large number of manufacturers have also proposed solving this problem through variable geometry (Sasaki *et al*, 1991, Goyal *et al*, 1983, Ross *et al*, 1983, Fiorentino *et al*, 1980). The problem with this technique is that the mechanism is required to operate in extreme conditions of temperature and pressure and may not be very reliable in practical engines. Flashback issues have been tackled in many ways. Some state that swirl stabilised premixed flames can not flashback (Sattelmayer *et al*, 1992) although this point may be arguable. Some companies have tried installing flame arrestors (Sotheran *et al*, 1985), however the longevity of such devices in a practical engine is questionable. Generally speaking most people ensure that there are no reverse flow zones which can stabilise a flame in the premixing duct and that the velocities there are higher than the highest expected turbulent burning velocity. Flame stabilisation itself is generally either through a flame holder or through aerodynamic stabilisation. Problems of cooling, though, generally make the flameholder an unacceptable option. Thus aerodynamic stabilisation through a sudden expansion usually accompanied with a swirl induced vortex breakdown was the preferred option of most companies.

At Cranfield, an experimental LPP combustor was investigated by Harding (1996). The modelling of this combustor, and the necessary methods development, will be the main focus of this work. The combustor incorporates many of the features discussed earlier. The layout of this combustor can be seen in Figure 5.1. Air is

admitted through radial inflow swirlers and through an opening on the axis of the burner. Fuel is injected into the swirling flow towards splash plates which allow any fuel which hits them to be reatomised prior to entering the premixing duct. The premixing duct is shaped like a convergent divergent nozzle which causes the flow to reach a maximum velocity at its throat. This is designed to prevent flashback. In addition, the positive non swirling air along the axis helps to ensure that the vortex breakdown occurs outside of the premixing duct, again reducing the risk of flashback. The magnitude of the swirl plus the sudden expansion at the end of the premixing duct help to induce the vortex breakdown which generates a reverse flow bubble along the axis. The sudden expansion itself should induce a reverse flow zone in the corner of the expansion step similar to a backward facing step. These two reverse flow zones help to stabilise the flame.

2.3 Status of Premixed Combustion Modelling

2.3.0 Introduction

So far we have only discussed the current status of gas turbine combustor development related to LPP. Concept development can be accelerated by careful numerical simulation and now we shall concentrate on modelling options for this type of combustor.

The discussion so far has raised a number of issues which are important to the designer of an LPP combustor: rates of heat release, pollutant emissions, fuel air mixing, lean extinction, thermo-acoustic instabilities, flashback and autoignition. From a steady-state modelling perspective focus on the first two issues, addressing the third to a lesser degree. Most practical aircraft engines operate on liquid fuel and a comprehensive model requires a treatment of multiple phase processes such as droplet formation, evaporation and agglomeration, breakup and wall interactions. These processes introduce many additional modelling uncertainties and therefore we limit consideration of mixture preparation to the single phase influence of non-uniformities of fuel air mixing on flame front development and emission production. In relation to emissions we concentrate on oxides of nitrogen as this is most relevant to this type of combustor and provides much of the motivation for its development. We shall avoid the direct prediction of flame instabilities, flashback and autoignition, since these are essentially transient phenomena, and it is our goal here to produce a practical tool for combustor design and development. However, useful information can be inferred from steady-state predictions which assist in assessing the risks of these phenomena occurring.

In the literature there is very little work concerning the modelling of premixed combustion in gas turbines and the few papers which are available concentrate on relatively simple steady-state models. Most work to date has concentrated on diffusion flame modelling which is much more commonly applied to current aircraft gas turbines. A recent example of which can be found in the work of Tolpadi *et al* (1997, 1996) at General Electric. Correa (1995) and Correa *et al* (1996) at General Electric report premixed calculations made in the context of perfectly stirred reactors but not of practical gas turbine combustors. Sharifi *et al* (1995) report the use of CFD to help improve fuel air mixing and pressure loss in a Westinghouse LPP combustor however they do not use CFD to predict combustion. ABB's Corporate Research Division (Polifke *et al*, 1995, 1996) present limited findings of NO_x and CO emission predictions made for their EV burner using a simple two step Eddy Dissipation model which will be described in more detail in Section 2.3.3.1. They made the assumption that the fuel and air were perfectly premixed prior to the inlet of the domain and their predictions of NOx compared reasonably well with

experiments. However, their predictions of CO were an order of magnitude lower than that measured. More recently Hsu *et al* (1997) at Allison reported results of a pdf (probability density function) transport model with two step methane chemistry of a type which will be discussed in Section 2.3.3.2. They were forced to use a very coarse grid because of the high computational demand of this technique however their results compared well with the experimental measurements. They managed to accurately predict the burning velocity of the flame front however over predicted the flame temperature by about 300 C° which will be important for NO_x predictions. They made comparisons with a prediction made with the Eddy Dissipation model however they did not account for heat and radical loss in the vicinity near the wall and the flame stabilised in the wall boundary layer near the inlet of their domain. To date there is not a comprehensive comparison of various models in the context of a practical gas turbine combustor geometry available in the literature.

Firstly we will briefly review the fundamentals of turbulent premixed combustion and then discuss specific models applicable to this type of combustion.

2.3.1 Fundamentals of Turbulent Premixed Combustion

The structure of a laminar premixed flame is better understood and, in principle, more easily modelled than a turbulent one. Laminar flames comprise very thin reaction zones in which reactants are converted to products by comparatively well-established chemical mechanisms and transport processes which can be modelled mathematically. Unfortunately, steady laminar flames rarely occur in practical combustors. However, turbulent flames have been successfully modelled by considering them to be made up locally of disturbed laminar flames, or flamelets, which define, as an ensemble, the turbulent flame brush.

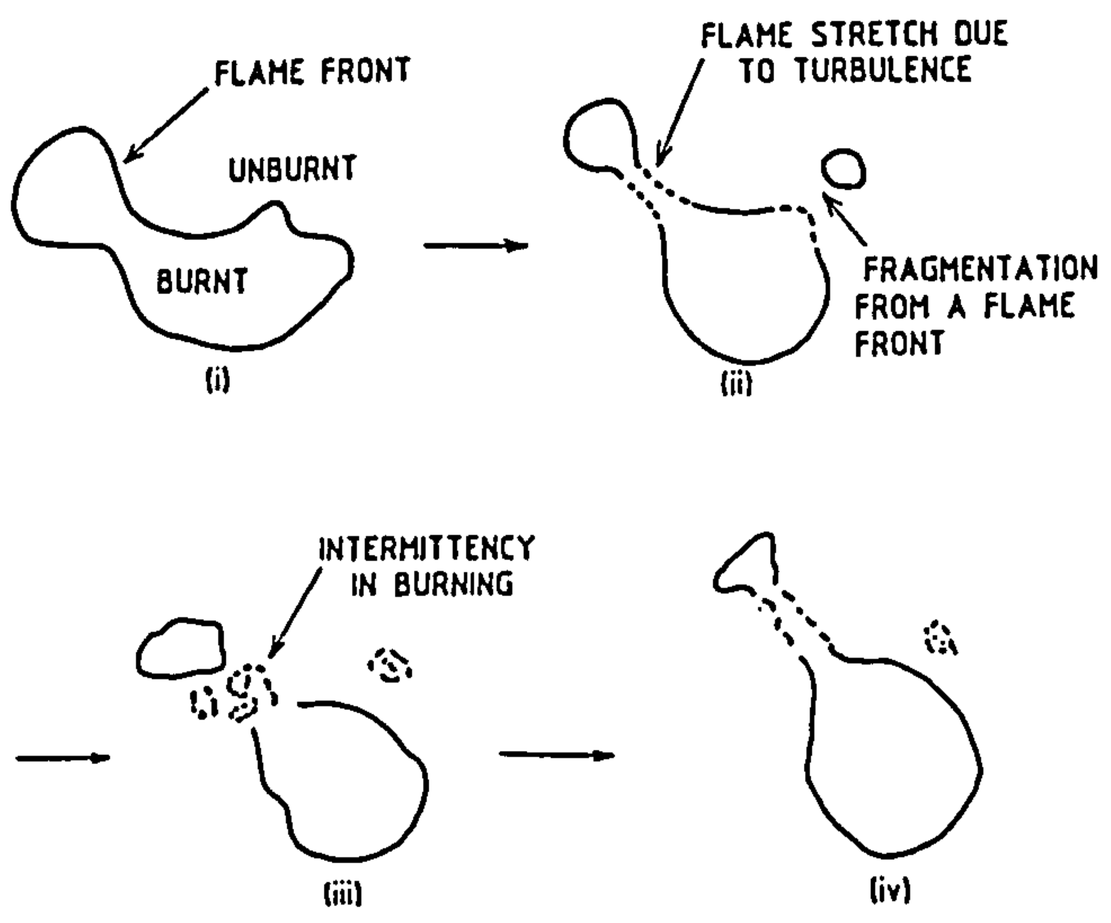

Figure 2.3.1.1 Island Creation within the Flame Front

An important property of premixed burning is the burning velocity, defined as the speed of the flow of reactants into, and perpendicular to, the flame front. In laminar flames this is easily visualised. By adding turbulence to the approach flow the flame front becomes wrinkled, increasing its area over the same patch of the flow. Generally speaking, this increases the quantity of reactants consumed per unit volume and thus the effective burning velocity. However, adding turbulence also has some adverse effects on the flame front. Increases in the component of the velocity parallel to the flame front causes the flame front to be stretched (or strained) which reduces the production of radicals and heat per unit area. The strain rate (K) is defined as:

$$K = \frac{1}{A}\frac{dA}{dt} \qquad (2\text{-}23)$$

where A is the flame front area. Too much positive stretch can cause a local extinction of the flame front, and if strong enough across the whole of the flame front, can cause the entire flame to be quenched. Therefore, as turbulence increases, the concept of a single uniform flame front also becomes invalid. High local stretch causes the formation of islands of burning reactant, separated from the main flame front. The process of island creation is illustrated schematically in Figure 2.3.1.1 (cf. Abdel-Gayed *et al*, 1989) and Schlieren pictures of flame fronts at various levels of turbulence are shown in Figure 2.3.1.2 (cf. Abdel-Gayed *et al*, 1989).

For the purposes of mathematical modelling, turbulent combustion has been subdivided into a number of different regimes, and models have been developed for each regime. The principal ones are the reaction-sheet regime and the distributed-reaction regime. The first of these arises when the chemistry occurs very rapidly compared to the time scales of the fluid flow. The flow can then be considered to comprise entirely reactants or products, with the combustion reaction occurring in a thin sheet dividing the two. This type of flame will arise when turbulence intensity is not too high and the dissipating eddy-scale is generally larger than the laminar flame thickness. The second regime, the distributed-reaction regime, exists when the combustion chemistry takes place more slowly, on time scales comparable with those of the fluid flow. A thin flame sheet no longer divides pure reactants and pure products. Now islands of reactants exist together with thickened reaction zones. This type of flame will arise when the dissipating eddy-scale is smaller than the laminar flame thickness and turbulent fluctuations interact directly with the chemical reactions.

Several indices have been proposed to classify the regime in which the flame is burning. Kovasznay (1956) suggested:

$$K_a = \frac{\delta_L / S_L}{u' / \lambda_T} \qquad (2\text{-}24)$$

which is the ratio of a characteristic time for the chemical reaction to that of the turbulent mixing. δ_L is the laminar flame thickness, S_L is the laminar burning velocity, λ_T is the Taylor microscale and u' is the turbulence intensity. This index is also known as the Karlovitz stretch factor and is the inverse of Damköhler number. When K_a«1 the flame is in the reaction sheet regime, and when K_a»1 then it is considered to lie in the distributed-reaction regime.

Andrews *et al* (1975) defined the reaction sheet regime in terms of a turbulent Reynolds number:

$$Re_\lambda = \frac{u' \lambda_T}{\nu} \qquad (2\text{-}25)$$

When Re_λ<100 then the flame may be considered to be in the reaction sheet regime.

Ballal *et al* (1975) and Ballal (1979a, 1979b, 1979c, 1979d) further divided the flame regimes into three zones that included a transition region between the reaction sheet and the distributed-reaction regimes. The reaction sheet regime was defined by $u'<2S_L$ and $\eta_K>\delta_L$ where η_K is the Kolmogorov length scale.

$$\eta_K = \left(\frac{\nu^3}{\varepsilon}\right)^{\frac{1}{4}} = \frac{15 \nu u'^2}{\lambda_T^2} \qquad (2\text{-}26)$$

where ε is the dissipation rate of turbulent energy. The distributed-reaction regime was characterised by $u'>2S_L$ and $\eta_K<\delta_L$, and the transition regime was defined by $u'»2S_L$ and $\eta_K»\delta_L$.

Katsuki *et al* (1990) experimentally characterised the fine flame structure of a turbulent premixed flame, observing that Re_λ, based on the Taylor microscale, was not a good indicator of the regimes. They argued that the best indicator was the Kolmogorov scale, and modified the approach of Ballal and Lefebvre to create a new index K_t,

$$K_t = \frac{u'/2S_L}{\eta_K/\delta_L} \qquad (2\text{-}27)$$

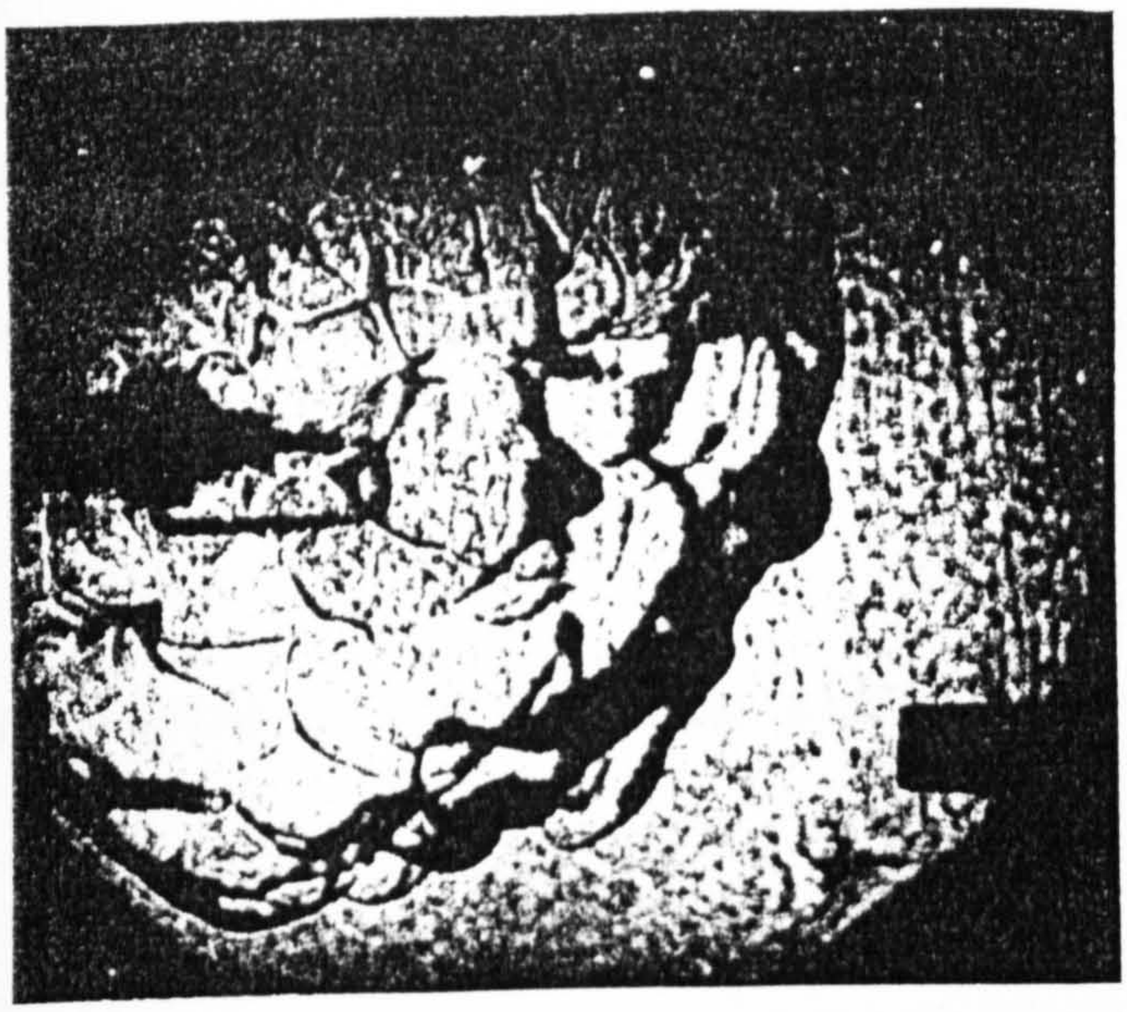

KLe = 0.003 Continuous laminar flame sheet.

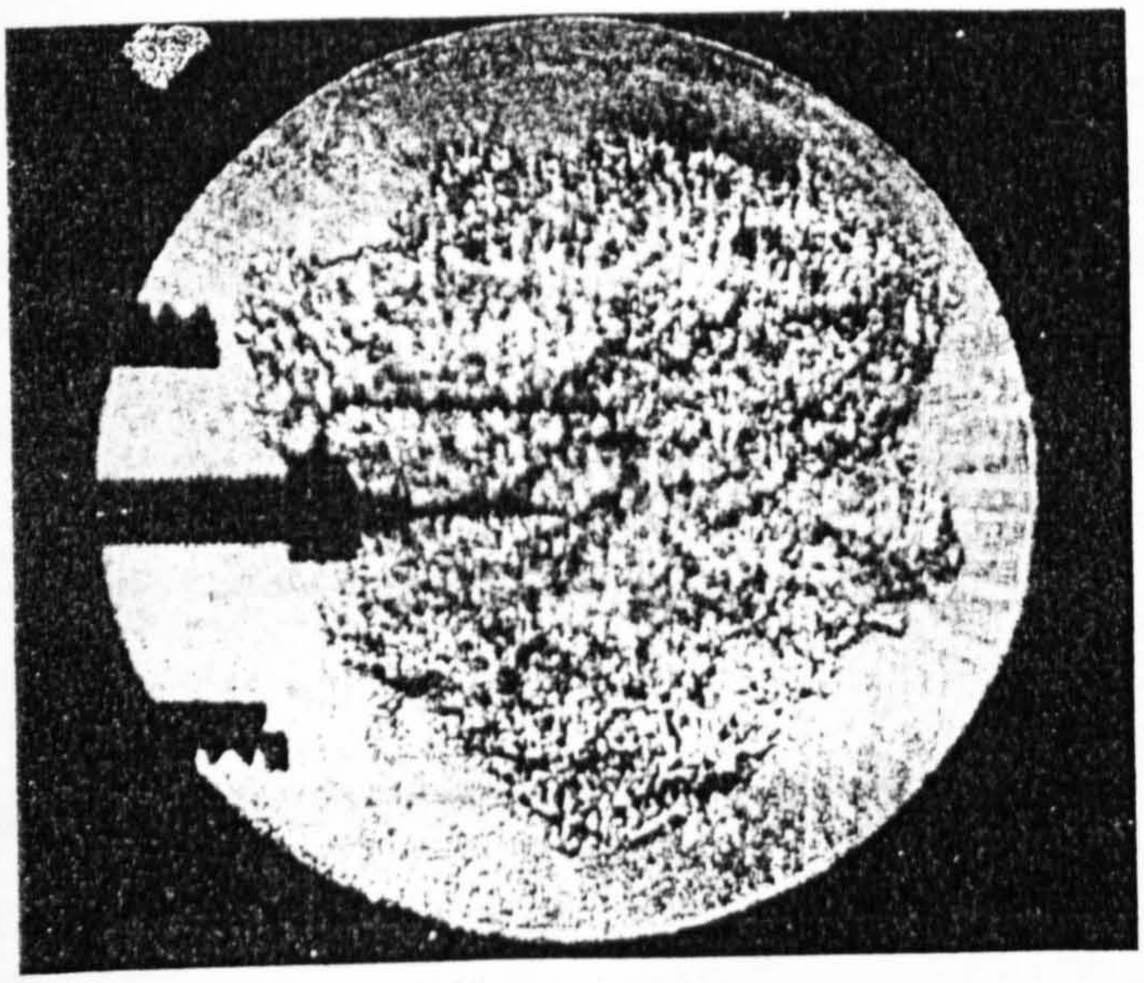

KLe = 0.238 Break-up of continuous flame sheet

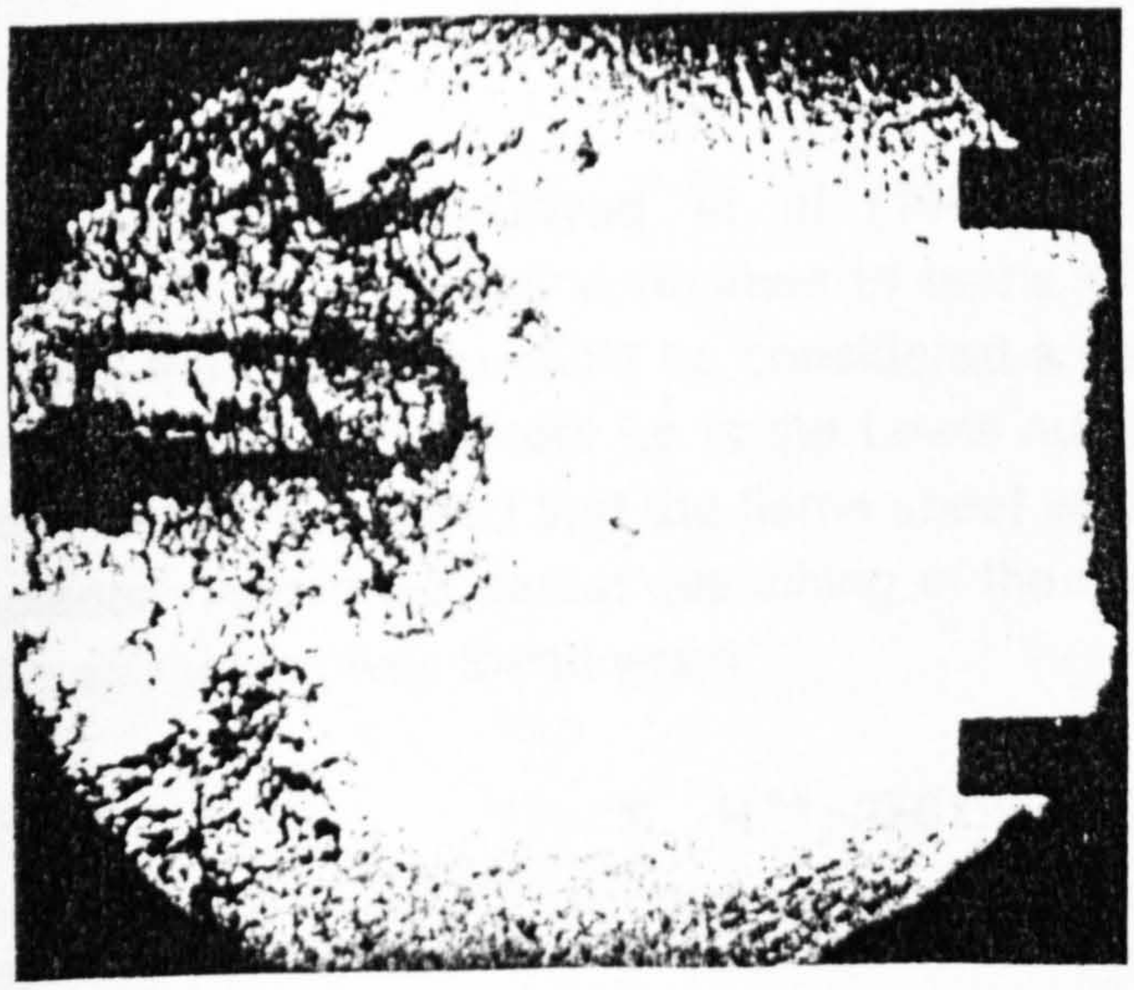

KLe = 0.651 Development of quenching in fragmented reaction zone.

Figure 2.3.1.2 Schlieren Photographs of a Flame Front at Various Levels of Turbulence

When $K_t<1$ then the flame is considered to be in the reaction sheet regime, otherwise it is in the distributed-reaction regime.

Williams (1976) also proposed a criterion based on a Reynolds number Re_η:

$$Re_\eta = \frac{u' \eta_K}{\nu} \qquad (2\text{-}28)$$

assuming that the Prandtl number is unity, such that for the reaction sheet zone:

$$Re_\eta > \frac{u'}{S_L} \qquad (2\text{-}29)$$

This again is based on the argument that the flame is in the reaction sheet regime when the laminar flame thickness δ_L is smaller than the Kolmogorov length scale η_K. Yoshida and Günther (1980b) sought to define precise limits between each regime on the basis of premixed flame measurements. For the reaction sheet regime they found that:

$$Re_\eta > 1.6 \frac{u'}{S_L} \qquad (2\text{-}30)$$

and for the distributed-reaction regime:

$$Re_\eta < 0.9 \frac{u'}{S_L} \qquad (2\text{-}31)$$

More recently Abdel-Gayed *et al* (1989) have correlated a wide range of experimental data on flame regimes in terms of Karlovitz stretch factor K_a. They reported that the flame could be considered a continuous wrinkled sheet for values of $K_a \cdot Le$ below 0.15 (where Le is the Lewis number). For values of $K_a \cdot Le$ between 0.15 and 0.3 they found that the flame sheet would break up into islands of burning reactants. Above 0.3 partial quenching of the flame front was observed. Complete flame quenching was found when:

$$K_a \cdot R_\ell^{-0.5} > 0.079 \text{ for } R_\ell < 300$$
$$K_a \cdot Le > 1.5 \text{ for } R_\ell > 300$$

0where R_ℓ is the turbulent Reynolds number based on the root mean square of the velocity fluctuation u' and the integral length scale ℓ of the turbulence. The data of

Abdel-Gayed *et al* (1989) is illustrated in Figure 2.3.1.3. Borghi (1985) also plotted combustion regimes in terms of K_a which is shown in Figure 2.3.1.4.

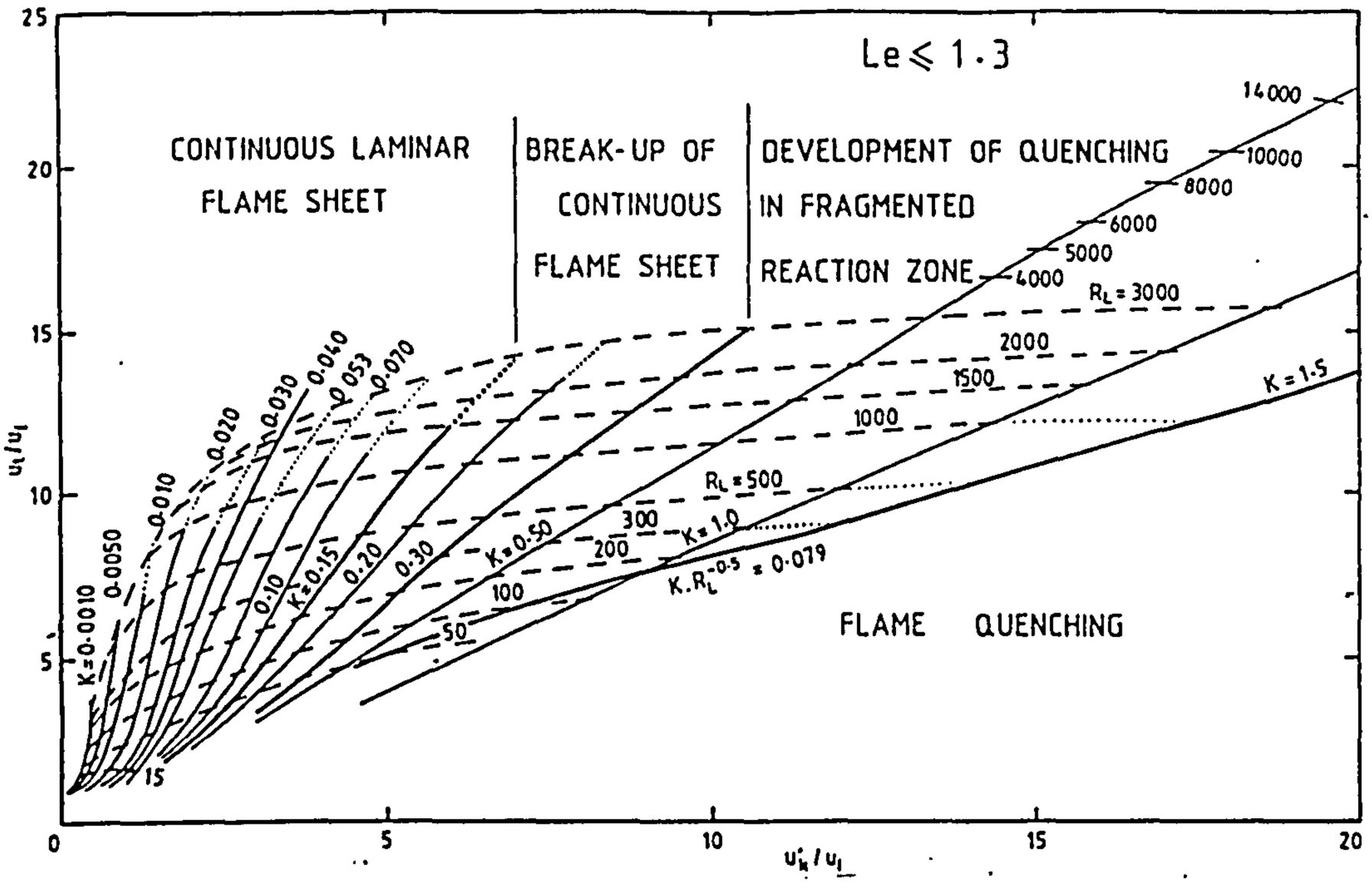

Figure 2.3.1.3 Combustion Regimes defined by Abdel-Gayed *et al* (1989)

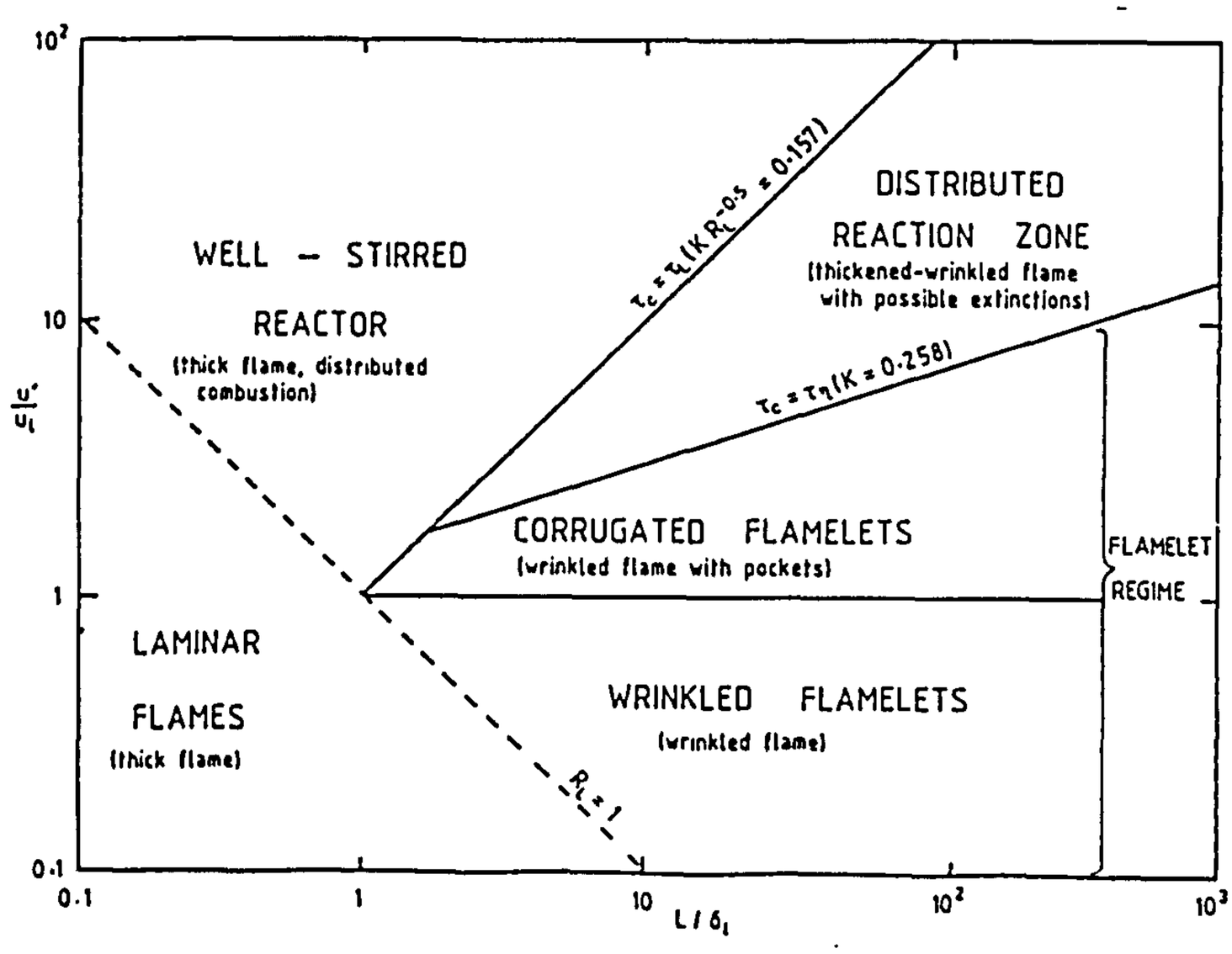

Figure 2.3.1.4 Borghi (1985) Combustion Regimes

Despite the generally accepted division between the two regimes, the distributed reaction regime has not been widely explored reflecting both its greater modelling complexity and inaccessibility to experimental measurement.

2.3.2 Turbulent Combustion Modelling

The delineation of these combustion regimes has influenced the mathematical approaches to premixed turbulent combustion modelling within the framework of CFD computation.

A direct solution of the Navier Stokes equations for fluid motion along with transport equations for the enthalpy and each of the species involved in a reaction mechanism is possible, however, extremely time consuming making it impractical except for the simplest of geometries. This is especially true of highly turbulent flow where an extremely fine grid would be required to resolve the smallest length scales of turbulence. To reduce the computational effort, time averaged equations for continuity, momentum, energy and scalars defining the state of the chemical reaction are solved introducing closure problems which are tackled by turbulence models.

Combusting flow fields frequently employ density weighted averaging (Favre averaging). This simplifies the equations, over conventional Reynolds averaging, by removing correlations with density fluctuations (Favre, 1969,1965). As an example, the Favre weighted mean velocity is defined as:

$$\tilde{u} = \frac{\overline{\rho u}}{\overline{\rho}} \qquad (2\text{-}32)$$

where the tilde represents Favre averaging and the overbar represents time or Reynolds averaging; ρ is the density and u is the velocity. When a Favre average is taken of two or more variables an overbar covering all of the variables with a tilde above it will be used in this text. The Favre fluctuation of the velocity is defined as:

$$u'' = u - \tilde{u} \qquad (2\text{-}33)$$

with a double prime in order to distinguish it from the Reynolds fluctuation.

The Favre mean continuity equation in tensor notation (cf. Anderson *et al*, 1984) is:

$$\frac{\partial \overline{\rho}}{\partial t} + \frac{\partial\left(\overline{\rho}\tilde{u}_j\right)}{\partial x_j} = 0$$

whilst the Favre mean momentum equation is:

$$\frac{\partial(\overline{\rho u_i})}{\partial t} + \frac{\partial(\bar{\rho}\tilde{u}_i\tilde{u}_j)}{\partial x_j} = -\frac{\partial \bar{p}}{\partial x_i} + \frac{\partial}{\partial x_j}\left(\bar{\tau}_{ij} - \overline{\rho u_i'' u_j''}\right)$$

where, neglecting viscosity fluctuations, $\bar{\tau}_{ij}$ is:

$$\bar{\tau}_{ij} = \mu\left[\left(\frac{\partial \tilde{u}_i}{\partial x_j} + \frac{\partial \tilde{u}_j}{\partial x_i}\right) - \frac{2}{3}\delta_{ij}\frac{\partial \tilde{u}_k}{\partial x_k}\right] + \mu\left[\left(\frac{\partial \overline{u_i''}}{\partial x_j} + \frac{\partial \overline{u_j''}}{\partial x_i}\right) - \frac{2}{3}\delta_{ij}\frac{\partial \overline{u_k''}}{\partial x_k}\right]$$

However, given that molecular diffusion is small compared to turbulent diffusion for high Reynolds number flows, this term is usually neglected. The dominant stress $\overline{\rho u_i'' u_j''}$, the Reynolds stresses, arise from turbulent velocity fluctuations and are mathematically closed by a turbulence model as discussed in a little more detail later. We shall focus here on the reacting scalars.

Most premixed combustion models characterise the progress of the chemical reaction through a normalised scalar which is known as the reaction progress variable (c). This is a variable which takes on values between zero and unity, such that c=0 corresponds to the unburnt state and c=1 corresponds to the fully burnt state. Typically, it is defined from the normalised temperature or the normalised mass concentration of some species which is created or destroyed by the combustion reaction.

The reaction progress variable is not then a conserved scalar and is described by a Favre averaged transport equation of the form:

$$\frac{\partial \overline{\rho c}}{\partial t} + \frac{\partial(\bar{\rho}\tilde{u}_j\tilde{c})}{\partial x_j} = \frac{\partial\left(-\overline{\rho u_j'' c''}\right)}{\partial x_j} + \overline{\rho w_c} \qquad (2\text{-}34)$$

where $\overline{\rho w_c}$ is the mean rate of chemical production of the reaction progress variable. w_c is the rate of reaction, typically a strong function of temperature, and thus this source term must accommodate the interaction of the chemical reaction with turbulent property fluctuations. The form of this chemical source term depends on the combustion model being implemented.

In addition to this chemistry, the turbulent scalar flux $\overline{\rho u_j'' c''}$ also requires modelling.

This term is closed by the turbulence model which will be described later.

If the flow can be considered to be adiabatic then the equation for the reaction progress variable is equivalent to an energy equation.

In particular, making the assumption that the flow is both adiabatic and at a low Mach number, the temperature can be considered a linear function of the reaction progress variable (Bray, 1985).

$$\frac{T}{T_r} = 1 + \tau c \qquad (2\text{-}35)$$

where T_r is the temperature of the unburnt reactants and τ is a heat release parameter defined such that:

$$\tau = \frac{T_p}{T_r} - 1 \qquad (2\text{-}36)$$

where T_p is the temperature of the fully burnt product. In this study the temperature of the products has been taken to be the adiabatic flame temperature, determined using the NASA equilibrium code developed by Gordon and Mc Bride (1971).

On averaging, the Favre mean temperature and progress variable are related by:

$$\frac{\tilde{T}}{T_r} = 1 + \tau \tilde{c} \qquad (2\text{-}37)$$

whilst density is obtained through the ideal gas law:

$$\frac{\bar{\rho}}{\rho_r} = \frac{1}{1 + \tau \tilde{c}} \qquad (2\text{-}38)$$

where ρ_r is the density of the unburnt reactants.

If the flow is not adiabatic but subject to significant heat loss then an additional balance equation for the enthalpy would need to be solved. Temperature would then be determined as a function of the enthalpy from the equation of state.

The fundamental investigations into the characteristics of premixed turbulent combustion outlined earlier have divided the turbulent flame front into two different regimes, depending on the ratio of the time scale of the chemistry to that of the

turbulent mixing. If the chemical time scale is small compared to that for the turbulent mixing then the reaction zone forms a thin, largely coherent sheet (Figure 2.3.3.3.1). Given the high pressures and temperatures the reactions associated with the primary heat release in practical combustors can be expected to fall into the same range as those demonstrated in laboratory flames (cf. Katsuki *et al*, 1990, Heitor *et al*, 1985, Yoshida *et al*, 1982, Moss, 1980). Fast chemistry models have therefore been developed most extensively to close the chemical source term for the reaction progress variable of the primary heat release mechanism.

If the chemical time scale is larger than that of the turbulent mixing then the reaction zone is thicker than the smaller scales of turbulence. This regime is known as the distributed reaction regime and is often associated with the formation of pollutants such as oxides of nitrogen. Finite rate chemistry models have been developed to model the oxidation rate of such reactions.

2.3.3 Fast Chemistry Models

If the chemistry is fast, relative to turbulent mixing, then one can assume that the effective reaction rate is determined by the rate at which chemical species and heat are mixed with unburnt product. This simplifies the task of modelling the combustion process.

In general, three basic combustion models of this nature are described in the literature. The first of these, mixing controlled models, completely neglects the reaction chemistry. They make the assumption that the reaction rate is dependent only on the rate of turbulent mixing, and account for the difference in fuel chemistry through constants in the model. Generally these models assume that the reaction occurs through a single step which establishes the stoichiometry (Mason and Spalding, 1973, Magnussen and Hjertager, 1976). Models do exist which consider the chemistry to consist of several reactions, each requiring the solution of a separate reaction progress variable (Polifke *et al*, 1995).

A second set of models is an extension of the mixing based models, which includes some influence of the chemistry through a simplified chemical scheme. Usually one or two step chemistry is assumed and the instantaneous rate of reaction is determined from an empirically defined Arrhenius expression for each reaction. Statistical averaging, typically embodying a pdf for reaction progress, is performed to establish the mean rate.

Finally, there are models which account for detailed chemistry. These models are based around the assumption that the flame front is a thin, largely continuous, surface which has the instantaneous properties of a strained laminar flamelet. The

reaction rate can be obtained through experimental measurements or detailed calculations of strained laminar flames defining the composition in terms of a progress variable. The mean rate is then computed through statistical averaging of the instantaneous term.

2.3.3.1 Mixing Controlled Models

These models are the simplest and most popular premixed combustion models. Most commercial CFD codes available today incorporate one of these types of combustion models.

Mason and Spalding (1973) proposed the earliest variant of these models known as the Eddy Break-up model. The rate of reaction is assumed to be proportional to the product of a time scale characteristic of the turbulent mixing process and the square root of the variance of the mass fraction of one of the reactants. Most of the reported applications of this model for continuous combustion systems involve only simple flame geometries. Mason and Spalding (1973) predicted the bluff-body stabilised flame experiment of Howe *et al* (1963). They initiated their calculation downstream of the flameholder at the first measurement point and obtained a reasonable agreement with the measurements. More recent studies (Bailly *et al*, 1995, Fureby *et al*, 1995) on similar flames, where steady state predictions have been initiated upstream of the flameholder, have not agreed as well with measurements. This has been blamed primarily on the large transient structures of such flows not being properly predicted by the steady state calculations rather than the combustion model. Fureby *et al* (1995) additionally modelled this flow field with Large Eddy Simulation (LES) and obtained much improved results. The main problem with the Eddy Break-up model lies in the fact that finite rate chemistry is ignored. It has been found in a number of practical applications of this model that it must be calibrated for every condition modelled (Borghi *et al*, 1986, Argueyrolles *et al*, 1986, Cant *et al*, 1988). Additionally the non-linear behaviour of the turbulent burning velocity with respect to the turbulence intensity is not captured by this model, which does not account for the affects of flame front straining (Choi *et al*, 1998, Duclos *et al*, 1993).

Magnussen and Hjertager (1976) extended the basic Eddy Break-up model, to create what is often termed the Eddy Dissipation Model, by adding an extra term to account for the possibility of slow chemistry. This term introduced a chemical time scale through an Arrhenius expression, which depended on the chemical equations being considered. The chemical source term was then selected to be the slower of the Eddy Break-up or Arrhenius terms. The Arrhenius expression was averaged at first order, neglecting all scalar correlations. In other words, the instantaneous values of the expression were simply replaced with mean ones and the turbulence

interaction was entirely neglected. This can be highly misleading since the Arrhenius expression is strongly non-linear. Similar sorts of applications of the Eddy Dissipation model as the Eddy Break-up model, with similar results, can be found in the literature (for example Olovsson, 1992). An example of a recent practical application of this model comes from the work of Polifke *et al* (1995, 1996), who have applied this model with good results to ABB's LPP combustor.

Given the simplifications introduced when averaging the additional chemical term of the Eddy Dissipation model, we have implemented here only the current version of the original Eddy Break-up model. This implementation will be discussed in detail in Section 3.1.

2.3.3.2 Reduced Chemistry Models

Reduced chemistry models assume that reaction occurs in one or two steps. The fuel oxidation to stable products is always one of the steps and, often, carbon monoxide oxidation is considered as the second step. For this type of model an Arrhenius expression is usually established from plug flow reactor measurements. The computation of mean heat release rate, employing statistical averaging, distinguishes the various proposals in the literature for this type of model. Essentially if the Arrhenius expression is defined as a function of a single reaction progress variable c, then the Favre mean reaction rate at any point in the flow may be determined by integrating the instantaneous reaction rate, weighted by the probability density function at that point, over the range of this reaction progress variable. Specifically,

$$\tilde{w}(\vec{x}) = \int_0^1 w(c;\vec{x})\tilde{P}(c;\vec{x})dc \qquad (2\text{-}39)$$

where $\vec{x}$ is a position vector, $\tilde{P}(c;\vec{x})$ is the Favre probability density function of the reaction progress variable c, and w is the instantaneous reaction rate.

Some of the earliest attempts to establish a framework for averaging the chemical source term are reported Toor *et al* (1962) and by Lin and O'Brien (1971). Rather than introduce a pdf they simply expanded the mean chemical source term in terms of moments of the species concentrations and temperature. They then neglected high order moments to simplify the equation. Due to the extremely non-linear nature of the instantaneous reaction rate, a large number of moments are required in order for a sufficiently high degree of accuracy to be computed. In some situations the radius of convergence of the series becomes infinite. Thus this approach is either very expensive computationally, given that transport equations are required for each

of the moments, or erroneous if not enough moments are considered.

Mao and Toor (1970) proposed that the general shape of the pdf be prescribed. The first several moments of the reaction progress variable could then be used as parameters to describe the nature of the pdf at any particular point in the flow. Transport equations would then only be needed for the moments that are required to define the pdf. This strategy has become known as the presumed pdf combustion model.

A more general method of modelling the pdf of the reaction progress variable was proposed by O'Brien (cf. Borghi, 1988), based on the work of Hopf (1952) and that of Lundgren (1969) for velocity pdfs (O'Brien, 1980). Subsequently others, notably Pope (1979, 1981a, 1981b, 1985) have worked on this method which involves solving transport equations for the pdf. This technique has the advantage that pdfs which are a function of more than one variable can be computed comparatively easily and there are no constraints on the general shape of the pdf. However, it also has the disadvantage of being computationally very expensive, typically employing a Monte Carlo simulation.

The presumed pdf model is sufficiently soundly based to give reasonable results whilst requiring the solution of a limited number of additional transport equations. This makes it the least computationally expensive of the models. Three simple presumed pdf functions have been proposed in the literature which only require computation of the first two moments of the reaction progress variable. Since the chemistry could be considered to be fast, Bray and Moss (1974) proposed that the pdf of the reaction progress variable was primarily bimodal (i.e. with delta functions at zero and unity). This approach was extended in the work of Borghi *et al* (1977, 1986, 1988) and Argueyrolles *et al* (1986). Figure 2.3.3.2.1 illustrates the shapes of these pdf.

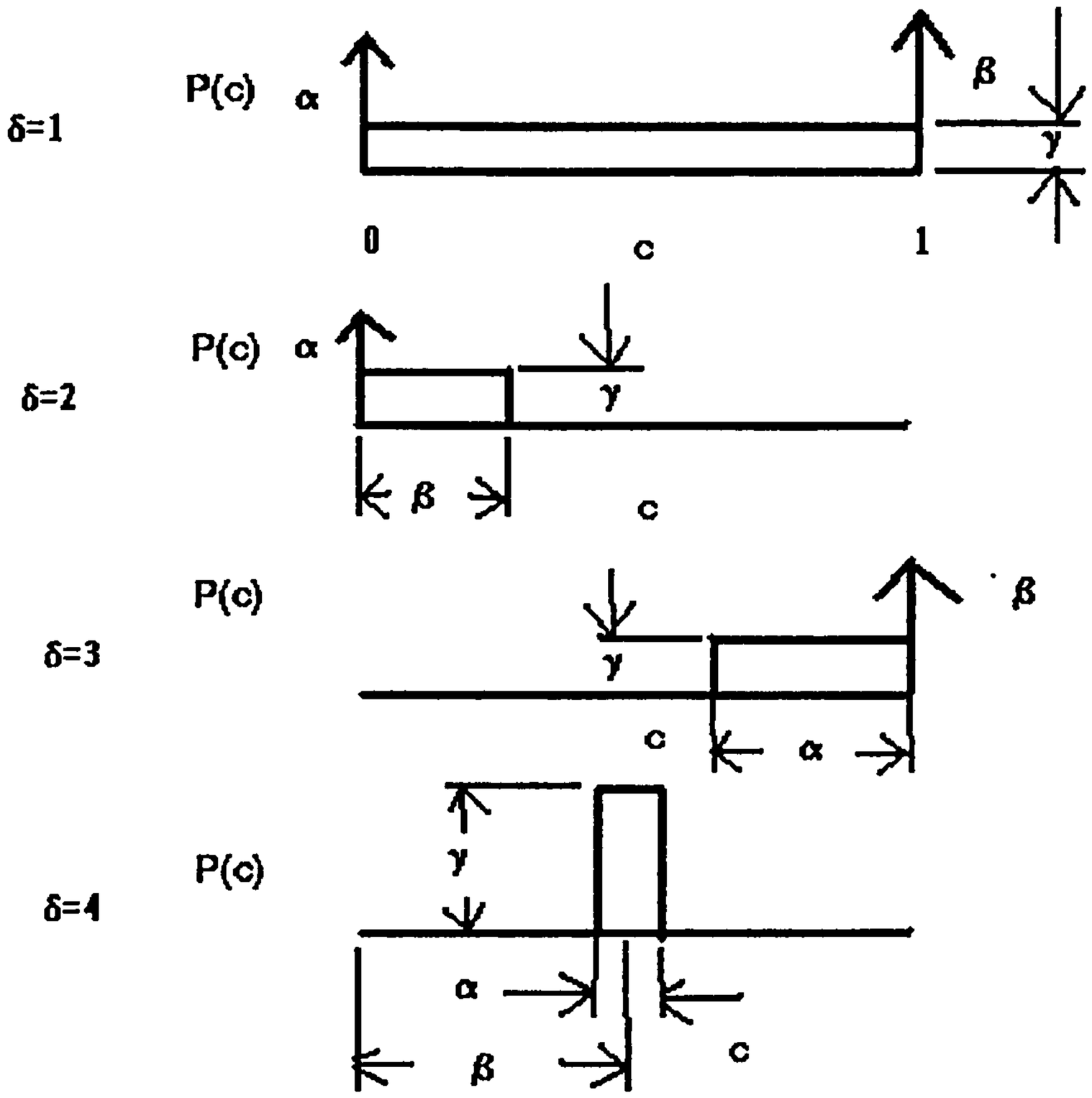

Figure 2.3.3.2.1 Simplified Presumed pdf Shapes

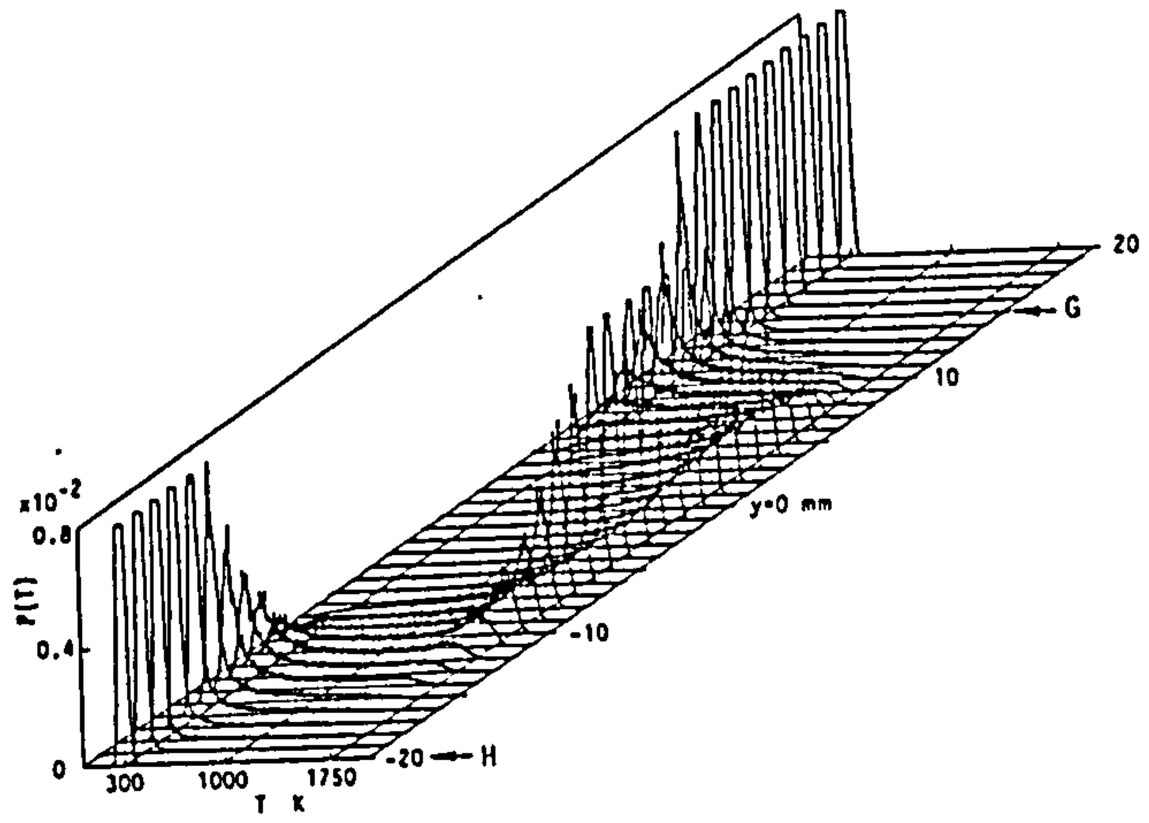

Figure 2.3.3.2.1b Typical pdf of Temperature Measured through a Laboratory Flame (Katsuki *et al*, 1990)

The three parameters α, $\beta$and γ and the shape δ can be determined from the fact that the pdf is defined only between zero and unity and by the three equations:

$$1 = \int_0^1 \widetilde{P}(c;\alpha,\beta,\gamma,\delta)dc \qquad (2\text{-}40)$$

$$\widetilde{c} = \int_0^1 c\widetilde{P}(c;\alpha,\beta,\gamma,\delta)dc \qquad (2\text{-}41)$$

$$\widetilde{c}^2 + \widetilde{c''^2} = \int_0^1 c^2\widetilde{P}(c;\alpha,\beta,\gamma,\delta)dc \qquad (2\text{-}42)$$

Such pdf shapes compare well with those measured in laboratory flames and based on temperature (Katsuki *et al,* 1990, Heitor *et al*, 1985, Yoshida *et al*, 1982, Moss, 1980). A typical measured pdf is illustrated in Figure 2.3.3.2.1b.

Peters (1982) and Bradley and co-workers (Bradley *et al*, 1994, Abd Al-Masseeh *et al*, 1990) also introduced a pdf based on the β-function for the reaction progress variable for premixed combustion, namely:

$$\widetilde{P}(c) = c^{\alpha-1}(1-c)^{\beta-1}\frac{\Gamma(\gamma)}{\Gamma(\alpha)\Gamma(\beta)} \qquad (2\text{-}43)$$

where:

$$\alpha = \widetilde{c}\gamma \qquad (2\text{-}44)$$

$$\beta = (1-\widetilde{c})\gamma \qquad (2\text{-}45)$$

$$\gamma = \frac{\widetilde{c}(1-\widetilde{c})}{\widetilde{c''^2}} - 1 \qquad (2\text{-}46)$$

This pdf has the advantage, provided the rate of reaction can be approximated by a polynomial, that the moments can be integrated semi-analytically. However, given the exponential nature of the reaction rate it is very difficult to find a suitable polynomial fit. If numerical integration is required and the variance is large such that the pdf is essentially bimodal then it becomes very difficult to integrate. Another advantage of this pdf is that it provides a continuous function, however the shape is constrained and the question arises as to how physically representative it is of the actual probability density function. No one, to the knowledge of this author, has compared this pdf with experimental measurements of the pdf of reaction progress variable in practical flames. A typical sketch of such a pdf is illustrated in Figure 2.3.3.2.2.

The third pdf type resolves the disadvantage of the β-function pdf when the reaction progress variable is bimodal (unbounded at c=0 and c=1). The truncated and renormalised Gaussian (or Clipped Gaussian) introduces two delta functions at zero and one together with a Gaussian curve, truncated below zero and above unity and renormalised such that the integral is unity.

The form of the pdf suggested by Lockwood and Naguib (1977) is:

$$\tilde{P}(c) = \frac{1}{\sigma\sqrt{2\pi}} \exp\left[-\frac{1}{2}\left(\frac{c-\mu}{\sigma}\right)^2\right][H(c) - H(c-1)] + \alpha\delta(0) + \beta\delta(1) \qquad (2\text{-}47)$$

where:

$$\alpha = \int_{-\infty}^{0} \frac{1}{\sigma\sqrt{2\pi}} \exp\left[-\frac{1}{2}\left(\frac{c-\mu}{\sigma}\right)^2\right] dc \qquad (2\text{-}48)$$

$$\beta = \int_{1}^{\infty} \frac{1}{\sigma\sqrt{2\pi}} \exp\left[-\frac{1}{2}\left(\frac{c-\mu}{\sigma}\right)^2\right] dc \qquad (2\text{-}49)$$

μ is the value of c with the highest probability, σ is the variance of the Gaussian curve, and H(c) is the Heaviside function such that $[H(c) - H(c-1)]$ has a value of unity in the range $0 \le c \le 1$ and zero elsewhere.

The mean reaction progress variable for this pdf is then given by:

$$\tilde{c} = \beta + \int_{0}^{1} \frac{c}{\sigma\sqrt{2\pi}} \exp\left[-\frac{1}{2}\left(\frac{c-\mu}{\sigma}\right)^2\right] dc \qquad (2\text{-}50)$$

$$\tilde{c} = 1 + (\mu - 1)F(z_1) - \mu F(z_0) + \frac{\sigma}{2\pi}\left[\exp\left(-\frac{1}{2}z_0^{\,2}\right) - \exp\left(-\frac{1}{2}z_1^{\,2}\right)\right] \qquad (2\text{-}51)$$

where:

$$z = \frac{c-\mu}{\sigma}, \quad z_0 = -\frac{\mu}{\sigma}, \quad z_1 = \frac{1-\mu}{\sigma}$$

and

$$F(z) = \frac{1}{\sqrt{2\pi}} \int_{-\infty}^{z} \exp\left(-\frac{s^2}{2}\right) ds$$

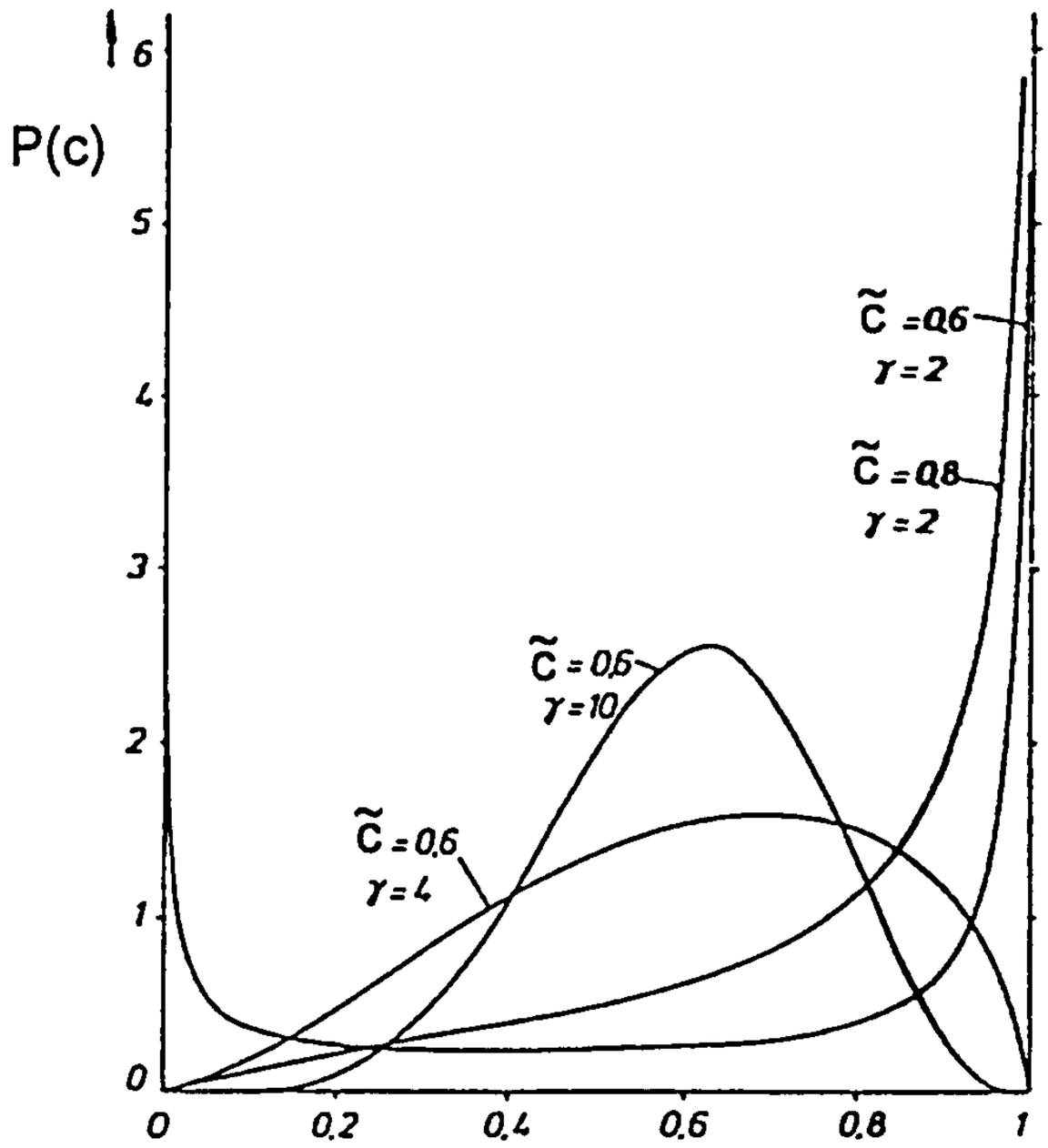

Figure 2.3.3.2.2 Typical β function PDF for various values of $\tilde{c}$ and γ

The variance of the reaction progress variable is given by:

$$\widetilde{c''^2} = \beta + \int_0^1 \left[\frac{c^2}{\sigma\sqrt{2\pi}} \exp\left(-\frac{1}{2}\left(\frac{c-\mu}{\sigma}\right)^2\right)\right] dc - \tilde{c}^2 \qquad (2\text{-}52)$$

$$\widetilde{c''^2} = 1 + (\sigma^2 + \mu^2 - 1)F(z_1) - (\sigma^2 + \mu^2)F(z_0) + \frac{\sigma^2}{\sqrt{2\pi}}\left[z_0 \exp\left(-\frac{1}{2}z_0{}^2\right) - z_1 \exp\left(-\frac{1}{2}z_1{}^2\right)\right]$$
$$+ \frac{2\sigma\mu}{\sqrt{2\pi}}\left[\exp\left(-\frac{1}{2}z_0{}^2\right) - \exp\left(-\frac{1}{2}z_1{}^2\right)\right] - \tilde{c}^2 \qquad (2\text{-}53)$$

Williams (1985) pointed out that this type of pdf compares well to experimentally measured pdfs for the degree of mixedness between the fuel and oxidant in mixing layers, jets, wakes, boundary layers and stirred reactors. It nonetheless introduces some unphysical features and it is perhaps the most computationally expensive of the three proposed pdfs, requiring a look-up table or an iterative solver in order to determine μ and σ from the mean and variance of the reaction progress variable

(Equations (2-51) and (2-53)).

Unlike pdf shapes for mixture fraction in non-premixed flames, the highly non-linear nature of the Arrhenius expression emphasises that the shape of the pdf is extremely important.

Borghi and co-workers (Borghi *et al*, 1977b, Moreau and Borghi, 1980) successfully applied the Presumed pdf model, using the simple block style pdf of Figure 2.3.3.2.1, to a co-flowing premixed flame experiment of Moreau (Moreau, 1974, Moreau *et al*, 1976, 1980). They made comparisons between their model, which agreed well with measurements, and a model similar to the chemical rate of the Eddy Dissipation model, which ignored the fluctuations in the reaction progress variable. The latter model was found to produce a much thinner flame front than that measured. Borghi and co-workers (Borghi *et al*, 1986, Argueyrolles *et al*, 1986) have also applied this model to a spark ignition engine obtaining very realistic results, although no comparisons with measurements were made.

2.3.3.3 Detailed Chemistry Models

As mentioned earlier, if the chemistry is assumed to be fast relative to the turbulent mixing then the flame front forms a thin, largely continuous sheet strained by the turbulence (Figure 2.3.3.3.1). The instantaneous reaction rate can then be computed or measured from the known structure of strained laminar flames.

There are essentially two applications of this concept. The first is based around a pdf approach similar to that of the reduced chemistry models. For this type of model, data for the consumption or production rate of species or the production rate of heat is obtained from either experimental measurements or calculations of strained laminar flames and related to a reaction progress variable. These data are then averaged by a joint pdf of the reaction progress variable and the strain rate (K).

$$\tilde{w} = \iint w(c,K)\tilde{P}(c,K)dcdK$$

Examples of such a model are those of Benim and Syed (1997), Bradley *et al* (1994) and Abd Al Masseeh *et al* (1990) which use the volumetric heat release rate, determined from flamelet calculations, with a reaction progress variable based on the normalised flame temperature.

The second type of model is based on the assumption that the instantaneous chemical source term is equal to the product of consumption rate of the reactants and the flame front surface area per unit volume, Σ:

$$\rho w = \rho_r S_L \Sigma$$

where ρ_r is the density of the reactants, and S_L is the laminar burning velocity. The laminar burning velocity is a function of the strain rate and so a pdf closure is usually introduced to average this term in order to determine the mean chemical source term:

$$\overline{\tilde{\rho w}} = \rho_r \Sigma \int S_L(K)\tilde{P}(K)dK$$

Abdel-Gayed *et al* (1988), Cant *et al* (1988), Rogg *et al* (1986) and others have used a log-normal probability distribution for the strain rate. Abdel-Gayed *et al* (1988) also proposed a quasi-Gaussian pdf and compared the predicted strain rate at which the flame would quench for both distributions with measured values for a propane-air flame in a fan-stirred reactor at several lean equivalence ratios. From these comparisons they concluded that the log-normal distribution provided slightly better agreement. Rather than compute the variance of the strain rate they propose a constant value for it, in line with most of the literature written to date, and parameterised their pdf with only the mean of the strain rate.

Their log-normal pdf is defined as:

$$\begin{aligned} P(K) &= \frac{1}{\sqrt{2\pi}\sigma K}\exp\left(-\frac{(\ln K-\mu)^2}{2\sigma^2}\right) \\ \sigma^2 &= 0.34 \\ \mu &= \frac{1}{2}\left(\ln\frac{\varepsilon}{3\upsilon}-2\sigma^2\right)-\ln 2 \\ \overline{K} &= \overline{\frac{1}{A}\frac{dA}{dt}} = 0.422\sqrt{\frac{\varepsilon}{3\upsilon}} = 0.94\frac{u'}{\lambda} \end{aligned} \qquad (2\text{-}54)$$

where K is the strain rate, ε is the dissipation rate of the turbulence kinetic energy, ν is the kinematic viscosity, A is the flame front area, and λ is the Taylor length scale of turbulence. This definition of the strain is based around the work of Batchelor (1952) which assumes that flame front straining occurs at the Kolmogorov scales in isotropic homogeneous turbulence. This is consistent with the original proposal for the definition of strain rate for the Crossing Frequency model (Cant *et al*, 1988). Other authors have also proposed that the rate of strain should be related to the larger time scale of the turbulence ε/k however neither of these methods have been shown to reproduce entirely satisfactorily the effects of turbulence length scales and chemistry on the turbulent burning velocity (Duclos *et al*, 1993).

Closures for $\sum$ have been developed from several different approaches. A large number of researchers have proposed solving a transport equation for $\sum$. The Coherent Flame model (Candel *et al*, 1990, Maistret *et al*, 1989, Veynante *et al*, 1988, Boudier *et al*, 1992) and the Cheng and Diringer model (Cheng *et al*, 1991a, 1991b, Lai *et al*, 1991, Wu *et al*, 1997) have both generated a transport equation for $\sum$ from the work of Marble and Broadwell (1977) for diffusion flames. These models are based on the equation for the evolution of material surfaces and are closed with additional source and sink terms accounting for the effects of chemistry and turbulent straining. Cant *et al* (1990) proposed a similar model based on the equation for the transport of the flame front surface area per unit volume developed by Pope (1988). Additionally, Mantel and Borghi (Mantel *et al*, 1991, 1994) developed a model for the flame front surface area from an equation for the scalar dissipation of the fuel mass fraction in a constant density flow. These models, which are often referred to as flame sheet models, have been primarily applied in the automotive industry for modelling spark ignition engines. A recent example of this comes from the work of Choi *et al* (1998) who investigated two variants of the Coherent Flame model and the Eddy Break-up model incorporated in the KIVA-II program. The results of their work indicate that the Coherent Flame model does a better job of capturing the non-linear behaviour of the turbulent burning velocity as the turbulence intensity is increased. The Eddy Break-up model, on the other hand, predicts a linear increase with turbulence intensity. Duclos *et al* (1993) also looked at the influence of the turbulence intensity on the turbulent burning velocity which was predicted by a wide variety of flame sheet models. They found that the Coherent Flame model which included a modification, inspired by the work of Mantel *et al* (1991), to account for flame annihilation in the fresh and burnt regions gave the best predictions.

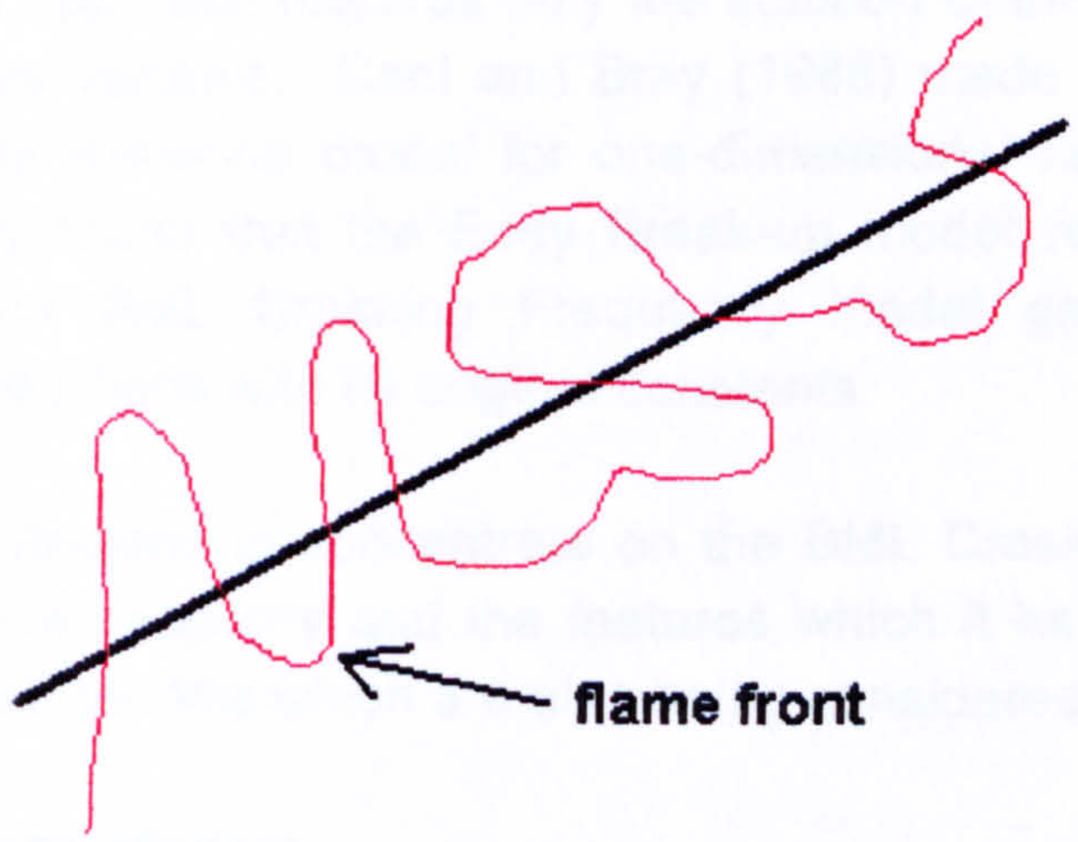

Figure 2.3.3.3.1

Other investigators approach the closure of $\sum$ based on the assumption that $\sum$ can be related to the integral length scale of the turbulence. Bray *et al* (1984b) introduce the BML Crossing Frequency model based on the frequency of flame front crossing (Figure 2.3.3.3.1). The number of times the flame front crosses the line per unit length, ν_y, is related to the flame front surface area per unit volume through the expression:

$$\Sigma = \frac{\upsilon_y}{\overline{|\sigma_y|}} = \frac{g\bar{c}(1-\bar{c})}{\overline{|\sigma_y|}\hat{L}_y} \qquad (2\text{-}55)$$

where g is a constant between 1 and 2 depending on the details of the crossing frequency probability density function (Bray *et al*, 1984a,1986). $\hat{L}_y$ is the integral length scale of the spatial random flamelet crossing process, $\bar{c}$ is the Reynolds averaged reaction progress variable and $\overline{|\sigma_y|}$ is a factor describing the mean angle of the flamelet crossing, relative to the unit line in space. Based on experimental measurements for a Bunsen type flame Cant and Bray (1988) suggest that $\hat{L}_y$ is nearly equal to the local turbulence length scale which can estimated from the turbulence model. This will be discussed in more detail later, however, for the present study L_y was assumed to be:

$$\hat{L}_y = C_\mu^{3/4} \frac{k^{3/2}}{\varepsilon} \qquad (2\text{-}56)$$

where k is the turbulence kinetic energy, ε is its dissipation rate and C_μ is a constant equal to 0.09. This approach requires only the solution of the transport equation of the reaction progress variable. Cant and Bray (1988) made comparisons with this model and the Eddy Break-up model for one-dimensional flame propagation in a stirred bomb. They found that the Eddy Break-up model required calibration for every run while the BML Crossing Frequency model gave reasonably good predictions for all conditions with its original constants.

In this study it was decided to concentrate on the BML Crossing Frequency model because of its relative simplicity and the features which it has in common with the reduced chemistry pdf models which are also being considered.

2.3.4 Slow Chemistry Models

For the case of slow chemistry the chemical time scale rather than the turbulent mixing limits the rate of the reaction. In addition to the Eddy Dissipation concept

introduced by Magnussen and Hjertager (1976) which incorporated both fast and slow chemistry, Zimont *et al* (1997) also proposed a model which is based on the G equation model for a laminar flame (Peters, 1992, Wirth *et al*, 1992). G is essentially a scalar which defines the location of the flame front where G takes on the value G_0. $G<G_0$ in the unburnt fluid and $G>G_0$ in the fully burnt fluid. Consider a thin wrinkled flame, whose mean position lies in the plane x=0, then G is specifically defined such that:

$$G(\vec{x},t) - G_0 = x + F(y,z,t)$$

where F(y,z,t) is the displacement of the flame front from its mean position towards the unburnt gas. Thus $G-G_0$ is simply the displacement in the x direction between the flame and the given level surface. G can be related to Σ, which was described earlier in Section 2.3.3.3, through the expression (Kerstein *et al*, 1988):

$$\Sigma = \frac{1}{(c_2 - c_1)(y_2 - y_1)(z_2 - z_1)} \int_{z_1}^{z_2}\int_{y_1}^{y_2}\int_{(c_1<G(x,y,z,t)<c_2)} |\nabla G| \, dx\, dy\, dz$$

for the plane G=c which initially lies normal to the x direction and in the absence of convection remains with this orientation. Peters (1992) proposed that the reaction rate could be simply represented by the product of the laminar burning velocity and the absolute value of the gradient of G. Extending this to turbulent flow one obtains the expression for the chemical source term in the form:

$$\tilde{w} = S_L \overline{\left|\frac{\partial G}{\partial x}\right|}^{\sim} \qquad (2\text{-}57)$$

where S_L is the laminar burning velocity. To close this term Peters and co-workers (Peters 1992, Wirth *et al*, 1992) have formulated an Eddy Break-up style expression. Zimont *et al* (1997) on the other hand, making the assumption of slow chemistry and a thin flame front, have closed this model by replacing the laminar burning velocity with a turbulent one (S_T) and replacing G with its mean.

$$\tilde{w} = S_T \left|\frac{\partial \tilde{G}}{\partial x}\right| \qquad (2\text{-}58)$$

The Zeldovich mechanism for NO formation is an example of a reaction mechanism which is slow relative to the turbulent mixing time scale in a practical engine. Far from chemical equilibrium, the progress of the Zeldovich mechanism can be related

to a single scalar c_{NO} in a similar fashion to the reaction progress variable for the primary heat release. The instantaneous rate of reaction is then a function of both the reaction progress variable and the progress variable of the Zeldovich mechanism. Thus the mean rate of formation of NO is given by:

$$\overline{\rho w_{c_{NO}}} = \int\int w_{c_{NO}}(c, c_{NO})\tilde{P}(c, c_{NO})dcdc_{NO} \quad (2\text{-}59)$$

However, since this mechanism is slow relative to the principal heat release, Moss and Bray (1975) proposed that:

$$\tilde{P}(c, c_{NO}) = \tilde{P}(c_{NO}|c = 1) \quad (2\text{-}60)$$

The scalar c_{NO} can be defined simply to be the mass fraction of NO. Here we have normalised this by its equilibrium value, on the assumption that this is not exceeded within the calculation domain. This gives us a convenient progress variable of the same type as that for the heat release.

2.3.5 Turbulence Closure

We shall briefly review turbulent closure more generally to identify its interaction with the foregoing combustion models. The time averaged Navier Stokes and energy equations introduce a number of correlations, Reynolds stress and scalar flux terms, which need to be closed and for which a range of turbulence models have been developed.

The simplest models available have evolved from the approximation proposed by Boussinesq (1877) more than a century ago. He suggested that turbulent shearing stresses might be related to the rate of mean strain through an apparent scalar or eddy viscosity by analogy with laminar Newtonian flow. This assumption yields a constitutive relationship for the Reynolds stress tensor in its Reynolds averaged form (cf. Anderson *et al*, 1984):

$$-\overline{\rho u_i' u_j'} = \mu_T\left(\frac{\partial \bar{u}_i}{\partial x_j} + \frac{\partial \bar{u}_j}{\partial x_i}\right) - \frac{2}{3}\delta_{ij}\left(\mu_T \frac{\partial \bar{u}_k}{\partial x_k} + \rho k\right) \quad (2\text{-}61)$$

where μ_T is the turbulent eddy viscosity and $k = \overline{u_i' u_i'}/2$ is the kinetic energy of the turbulence.

By analogy with the molecular viscosity for gases, derived from kinetic theory, the turbulent viscosity may be modelled as:

$$\mu_T = \rho v_T \ell \qquad (2\text{-}62)$$

where v_T and ℓ are characteristic velocity and length scales of the turbulence respectively.

One of the most robust turbulence models based on the Boussinesq approach is the two equation, k-ε turbulence model first proposed by Harlow and Nakayama (1968) and later developed by Jones and Launder (1972) and Launder and Spalding (1974). This model introduces transport equations for the turbulence kinetic energy and its dissipation rate ε, admitting the determination of an integral length scale ℓ of the form:

$$\ell = \frac{\rho C k^{3/2}}{\varepsilon} \qquad (2\text{-}63)$$

where C is a constant. The eddy viscosity is then related to k and ε through Equation (2-62) such that:

$$\mu_T = c' \rho k^{1/2} \ell = \frac{\rho C_\mu k^2}{\varepsilon} \qquad (2\text{-}64)$$

where c' and C_μ are constants. The latter is usually assigned the value 0.09.

The turbulent scalar fluxes are modelled in a similar fashion to the Reynolds stresses using a gradient closure expression:

$$-\overline{\rho u_i' c'} = \frac{\mu_T}{Sc_T} \frac{\partial \bar{c}}{\partial x_i} \qquad (2\text{-}65)$$

where Sc_T is a turbulent Prandtl-Schmidt number, usually assigned values of O(1). For our work we have normally assumed a value of unity.

This standard closure has been shown to work well in a wide range of simple flows. However flows containing strong swirl, where the turbulence stresses are highly non-isotropic, pose difficulties for such models (Launder, 1989, Hogg *et al*, 1989, Gibson *et al*, 1986). Additionally, for combusting flows where density differences promote alternative transport mechanisms and, in particular counter gradient diffusion for the scalar flux of the reaction progress variable, then the gradient assumption fails. This behaviour has been widely demonstrated experimentally and, of particular relevance to combustors, Shepherd *et al* (1982), found a significant contribution from counter

gradient diffusion in an experiment with a bluff body stabilised flame confined in a duct and therefore subject to a significant streamwise pressure gradient.

Both *ad hoc* and generalised solutions have been proposed to model counter gradient diffusion. One approach is to add a buoyancy-like correction term to the Reynolds flux assumption (Chomiak *et al*, 1995, Nisbet *et al*, 1994, 1993a, 1993b, 1992). Alternatively, a more complete second moment turbulence model can be adopted which is not based on the Boussinesq assumption but solves additional balance equations for the Reynolds stresses and scalar fluxes.

Nisbet and Chomiak propose adding a buoyancy type correction term to the scalar flux closure of the k-ε turbulence model in addition to sources in the kinetic energy and dissipation rate equations to account for additional turbulence generation and dissipation due to pressure density interactions. They then compared their model predictions with measurements in a bluff body stabilised premixed flame. Whilst they do demonstrate an improvement in the flame spreading rate over the standard k-ε model predictions, the levels of turbulence within the flame brush are still under predicted (Chomiak *et al*, 1995, Nisbet *et al*, 1994).

We have chosen here to account for the counter gradient diffusion by introducing a full second moment turbulence model. This model derives transport equations for the Reynolds stresses and fluxes, closing only the third order terms contained within these equations. A second order gradient assumption is no longer enforced so that the equations can account for anisotropy in the stress components and counter-gradient effects. A standard second moment closure model for the Reynolds stresses and scalar fluxes implemented in PHOENICS (based on Launder, 1989, Launder *et al*, 1975) has been used with additional user defined source terms to account for the influence of the variable density flow.

The general equation for the density weighted Reynolds stresses may be written as (cf. Bradley *et al*, 1994):

$$\bar{\rho}\tilde{u}_k \frac{\partial \overline{u_i'' u_j''}}{\partial x_k} = -\frac{\partial J_{ijk}}{\partial x_k} + P_{ij} + \Pi_{ij} - \left(\overline{u_i''} \frac{\partial \bar{p}}{\partial x_j} + \overline{u_j''} \frac{\partial \bar{p}}{\partial x_i} \right) - \frac{2}{3} \delta_{ij} \bar{\rho} \varepsilon \qquad (2\text{-}66)$$

where J_{ijk} is the turbulent diffusive flux, $\overline{\rho u_i'' u_j'' u_k''}$. Within PHOENICS this term is modelled in a similar fashion to the gradient approaches used for the second moment closure of the k-ε turbulence model as:

$$\frac{\partial J_{ijk}}{\partial x_k} = -\frac{\partial}{\partial x_k}\left(C_s \bar{\rho}\frac{k}{\varepsilon}\widetilde{u_i''u_l''}\frac{\partial \widetilde{u_i''u_j''}}{\partial x_l}\right) \qquad (2\text{-}67)$$

where C_s is a model constant which is usually given the value 0.22. P_{ij} is the gradient generation term:

$$P_{ij} = -\bar{\rho}\left(\widetilde{u_k''u_i''}\frac{\partial \tilde{u}_j}{\partial x_k} + \widetilde{u_k''u_j''}\frac{\partial \tilde{u}_i}{\partial x_k}\right) \qquad (2\text{-}68)$$

and Π_{ij} is the pressure-strain correlation:

$$\Pi_{ij} = \overline{\rho'\left(\frac{\partial u_i''}{\partial x_j} + \frac{\partial u_j''}{\partial x_i}\right)} \qquad (2\text{-}69)$$

This term is modelled in PHOENICS in the form recommended by Launder *et al* (1975) and in its Favre averaged form this is:

$$\Pi_{ij} = -C_1\bar{\rho}\frac{\varepsilon}{k}\left(\widetilde{u_i''u_j''} - \frac{2}{3}\delta_{ij}k\right) - C_2\left(P_{ij} - \frac{1}{3}\delta_{ij}P_{kk}\right) \qquad (2\text{-}70)$$

where the constants C_1 and C_2 take the values 1.8 and 0.6 respectively.

The fourth term on the right-hand side of the Reynolds stress transport Equation (2-66) represents the effects of the interaction between the mean pressure gradient and density inhomogeneities (Bray *et al*, 1981). The Reynolds averaged Favre fluctuation of the velocity $\overline{u''}$ is modelled on the basis of infinitely fast chemistry according to Bray and Moss (1977), such that for a homogeneous equivalence ratio:

$$\overline{u''} = \frac{\tau\rho u''c''}{\rho_r} \qquad (2\text{-}71)$$

where τ is the heat release parameter defined earlier (Equation (2-36)) and the subscript "r" implies unburnt conditions.

The general form of the density weighted equation for the scalar flux of the reaction progress variable may be written similarly (cf. Bradley *et al*, 1994):

$$\bar{\rho}\tilde{u}_k \frac{\partial \widetilde{u_i''c''}}{\partial x_k} = -\frac{\partial J_{ik}}{\partial x_k} + P_{ic} + \Pi_{ic} - \overline{c''}\frac{\partial \bar{p}}{\partial x_i} + \overline{u_i''w} \qquad (2\text{-}72)$$

Once again the turbulent diffusive transport term J_{ik} is modelled using a gradient approximation as:

$$\frac{\partial J_{ik}}{\partial x_k} = -\frac{\partial}{\partial x_k}\left(C_{st}\bar{\rho}\frac{k}{\varepsilon}\widetilde{u_k''u_l''}\frac{\partial \widetilde{u_i''c''}}{\partial x_l}\right) \qquad (2\text{-}73)$$

where the constant C_{st} is assigned the value 0.15. The form of the gradient generation term is also similar to that in the Reynolds stress equation:

$$P_{ic} = -\bar{\rho}\left(\widetilde{u_k''c''}\frac{\partial \tilde{u}_i}{\partial x_k} + \widetilde{u_k''u_i''}\frac{\partial \tilde{c}}{\partial x_k}\right) \qquad (2\text{-}74)$$

The pressure scalar term Π_{ic} was modelled in a similar fashion to the stress equation:

$$\Pi_{ic} = \overline{p'\frac{\partial c''}{\partial x_i}} = -C_{1T}\bar{\rho}\frac{\tilde{\varepsilon}}{\tilde{k}}\widetilde{u_i''c''} + C_{2T}\bar{\rho}\widetilde{u_k''c''}\frac{\partial \tilde{u}_i}{\partial x_k} \qquad (2\text{-}75)$$

where the constants C_{1T} and C_{2T} were assigned the values 3.0 and 0.5 respectively.

As with the stress equations, the fourth term on the right side of the flux equation (Equation (2-72)) represents the effects of the interaction between the mean pressure gradient and density inhomogeneities (Bray *et al*, 1981). This term has been shown to be responsible for generating counter gradient diffusion by Libby *et al* (1981) in premixed flames with modest heat release. The Reynolds averaged Favre fluctuation of the reaction progress variable, $\overline{c''}$, is modelled as:

$$\overline{c''} = \frac{\bar{\rho}}{\rho_r}\int_0^1 (1+\tau c)(c-\tilde{c})\tilde{P}(c)dc \qquad (2\text{-}76)$$

If we assume infinitely fast chemistry, such that the pdf of the reaction progress variable simplifies to two delta functions at c=0 and c=1 and insert Equation (2-38), then this equation simplifies to:

$$\overline{c''} = \frac{\tau\tilde{c}(1-\tilde{c})}{1+\tau\tilde{c}} \qquad (2\text{-}77)$$

This is the formulation proposed by Bray and Moss (1977).

The final term on the right hand side of the flux equation (Equation (2-72)) represents the fluid flow chemistry interaction. This is difficult to close generally, requiring knowledge of the joint pdf of velocity, reaction progress variable and equivalence ratio. Jones (1979) has suggested, for a homogeneous mixture fraction, expanding w in terms of powers of c'' with truncation at second-order moments. Bradley *et al* (1994) argued that this is very uncertain and that the error introduced by using this technique is probably larger than simply neglecting the term. The BML model suggests a formulation based on the assumption of fast chemistry and a prescribed form of w in terms of the reaction progress variable (Libby, 1980):

$$w(c) = \frac{\alpha w_{max} c^n (1-c^{n-1})}{1+\tau c} \qquad (2\text{-}78)$$

where α is a constant, τ is the heat release parameter, w_{max} is the maximum value of the reaction rate, and n is an integer constant which best fits the data. For this latter constant Libby (1985) has proposed a value of 5. With data on the structure of an unstrained laminar flame (Libby *et al*, 1979), assuming a Gaussian style distribution for the pdf of velocity, which was assumed to be independent of the reaction progress variable, and a linear relationship for the mean velocity between the reactant and product states Libby (1980) arrived at the expression:

$$\overline{u_i''w} = -\overline{w}\frac{\overline{\rho u_i'' c''}}{\overline{\rho}\tilde{c}(1-\tilde{c})}(\tilde{c}-\phi_n) \qquad (2\text{-}79)$$

where ϕ_n is equal to $n/(n+1)$. Given the great difficulty in the modelling of this term the considerable simplifications that were made by Libby (1980) appear justified in order to secure a closure for this term. Although it is still unclear whether or not it is better to neglect this term entirely, given the uncertainty introduced by these assumptions, this closure has been adopted here.

One final transport equation which needs to be solved is that for the dissipation rate of the turbulence kinetic energy. The density weighted form of this equation is (cf. Bradley *et al*, 1994):

$$\bar{\rho}\tilde{u}_k \frac{\partial \varepsilon}{\partial x_k} = \frac{\partial}{\partial x_k}\left(C_\varepsilon \bar{\rho} \frac{k}{\varepsilon} \widetilde{u_k'' u_l''} \frac{\partial \varepsilon}{\partial x_l} \right) + C_{\varepsilon 1} \frac{\varepsilon}{k} \frac{1}{2} P_{ii} - C_{\varepsilon 2} \bar{\rho} \frac{\varepsilon^2}{k} + C_{\varepsilon 1} \frac{\varepsilon}{k} \frac{\overline{\rho' u_k''}}{\bar{\rho}} \frac{\partial \bar{p}}{\partial x_k} \qquad (2\text{-}80)$$

where P_{ii} is the same term as that defined for the Reynolds stress equation and the constants C_ε, $C_{\varepsilon 1}$, and $C_{\varepsilon 2}$ take the values 0.18, 1.45, and 1.90 respectively. On manipulation, we note that:

$$\frac{\overline{\rho' u_k''}}{\bar{\rho}} = -\widetilde{u''} = -\tau \bar{\rho} \frac{\widetilde{u_k'' c''}}{\rho_r} \qquad (2\text{-}81)$$

which was modelled as in the Reynolds stress equation.

2.3.6 CFD Issues

It is often difficult to separate the influence of specific physical models from the underlying numerical procedures. This is particularly true when models are implemented in a commercial code where access is constrained but the code has been widely used. It is appropriate here to review briefly the background to the adoption of PHOENICS in this study and the implications of that decision.

A solution of the averaged Navier Stokes and combustion equations requires the use of a flow solver. Given that our main objective is to investigate combustion modelling issues we elected to use an existing solver. At the outset of the study two such codes were available at Cranfield. The first was the commercial software package produced by CHAM and known as PHOENICS (Spalding, 1981). This is a general purpose software package which is reasonably flexible in that it allows for the addition of user-defined transport equations and associated source terms. The package contains a range of turbulence models including the k-ε and second moment models which are of interest here. Unfortunately, the second moment turbulence model in the version of the code available did not allow solution for body fitted grids or for blockages within the grid. The k-ε turbulence model, on the other hand, was quite flexible and could be employed with any grid type, including the body fitted grids which are important for modelling a practical combustor with a complicated shape.

The second code, SOFIE, which was briefly considered, has been developed at Cranfield by Rubini (1993). This code was relatively new and did not contain the range of turbulence models or gridding options available with PHOENICS. In particular, the k-ε turbulence model was implemented however the second moment closure was not. Although a limited number of predictions were made with SOFIE and compared with

calculations using PHOENICS, the well established shortcomings in the k-ε model favoured the implementation of the various combustion models in PHOENICS, despite the limited access to other features of the code.

The extent to which it is both feasible and necessary to evaluate basic features of a commercial CFD code is a matter for debate. Inevitably, considerable weight is given to the extensive applications of PHOENICS over the last 20 years. Some 700 references have been written regarding PHOENICS since 1981 (CHAM, 1998) and there seems little to be gained by repeating this work. Of particular interest, Janssen *et al* (1993) investigate the influence of various numerical parameters on their predictions of a sudden expansion flow using PHOENICS. They looked at the influence of grid refinement, inlet conditions, choice of wall functions, turbulence models, numerical schemes and solution techniques. Their reference case used a uniform grid of 15x35 cells together with the standard k-ε turbulence model, upwind differencing scheme and log-law wall functions. To investigate the influence of grid refinement they made additional calculations on a uniform grid of 90x214 cells. For the inlet conditions they looked at two cases: the first contained constant profiles for the turbulent kinetic energy and its dissipation rate, which was used for their reference case, and the second contained fully developed profiles of these values. They compared the log-law wall function with a Blasius-law wall function and they looked at the difference between predictions made with the k-ε turbulence model to those with a simpler single equation turbulence model, the Prandtl mixing length model. In terms of numerical options they compared upwind differencing with hybrid differencing for the convective terms and they looked at harmonic averaging for the diffusive terms. They compared the slabwise solver of PHOENICS with the whole field solver which uses the tri-diagonal matrix algorithm (TDMA) method (Thomas, 1949) and the point by point solver which uses the Gauss-Seidel method (cf. Hirsch, 1988). In general they found the best results compared to measurements from the fine grid, k-ε turbulence model, log-law wall function and the fully developed inlet boundary conditions. They found that both the slabwise and point by point solvers of PHOENICS gave identical results. They could not find a converged solution with the whole field solver. Harmonic averaging for the diffusion terms was found to give very high values for the turbulence intensity compared to the standard case. Both hybrid and upwind differencing gave nearly identical results.
Other studies have also been carried out which bear some relevance to our work. Validation has been carried out regarding the second moment turbulence model incorporated within PHOENICS. These investigations, which include studies involving swirling flows, can be found in the work of Launder and his co-workers (Malin *et al*, 1990, Launder, 1989, Launder *et al*, 1975, Launder, 1975). In general, the second moment closure model performs better than the k-ε model in strongly swirling flows

where the latter model is found to be too diffusive in the radial direction. Predictions of combusting flow with PHOENICS have been performed by Shah *et al* (1990) for spark ignition engines and by Aksit (1995) for gas turbines with non-premixed combustion. Shah *et al* (1990) compared global properties of combustion and the flow field with measurements from a research engine. They applied three combustion models. The first based on the chemical time scale part of the Eddy Dissipation model, the second was the Eddy Break-up model and the third was a flame front model greatly simplified over those presented in Section 2.3.3.3. They were able to obtain a reasonably good agreement with the experiment for a tuned Eddy Break-up model and the flame front model. Results were not as good with the chemical rate model. Aksit investigated a non-premixed test combustor using a combustion model based on pdf transport techniques and he obtained a reasonable agreement between flow field measurements and the predictions made with PHOENICS. With these studies in mind it was decided to always use the slabwise solver within PHOENICS, the log-law wall functions, and hybrid differencing without harmonic averaging for the diffusion terms.

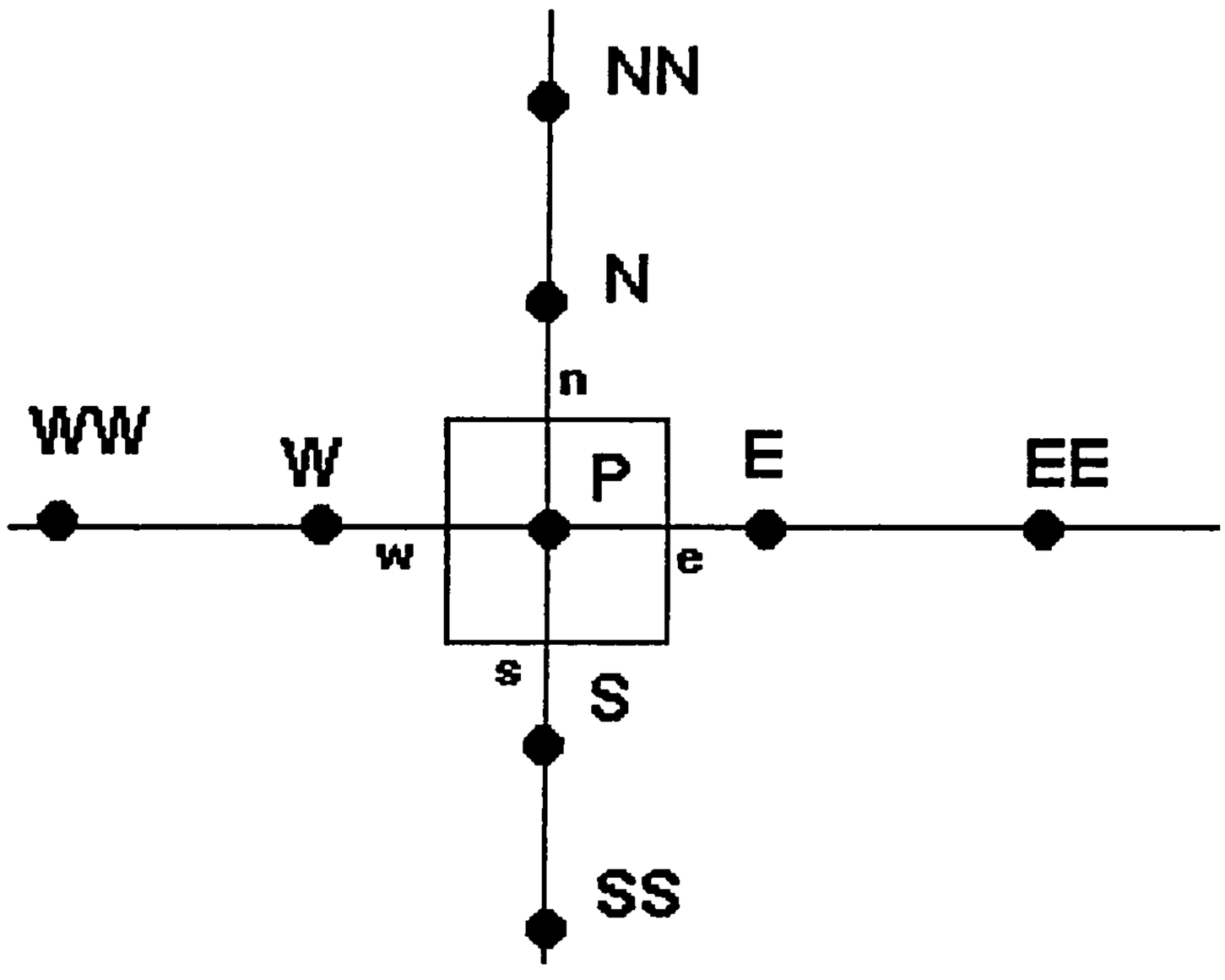

Figure 2.3.6.1 Two Dimensional Grid around the cell P

In light of recent advances in higher order differencing schemes it is worth briefly discussing the impact that these might have on the calculations. First we shall introduce some terminology by considering the general transport equation for two dimensional incompressible steady state flows (cf. Darwish, 1993):

$$\frac{\partial}{\partial x}\left(\rho u\phi - \Gamma\frac{\partial\phi}{\partial x}\right) + \frac{\partial}{\partial y}\left(\rho v\phi - \Gamma\frac{\partial\phi}{\partial y}\right) = S$$

where ϕ is any dependent variable, u and v are the x and y components of velocity respectively and ρ, Γ and S are the density, diffusivity and source terms respectively. Integrating this equation over the control volume which makes up the cell surrounding point P in Figure 2.3.6.1 and using the divergence theorem, we obtain (cf. Darwish, 1993):

$$J_e - J_w + J_n - J_s = B$$

where J_f represents the total flux of ϕ across the face f (f = e, w, n and s) and B is the volume integral of the source term S. Each of the fluxes contains a convective J^C and diffusive J^D contribution i.e.:

$$J_f = J_f^C + J_f^D$$

For a purely convective scalar flow the diffusion flux is zero while the convective flux is given by (cf. Darwish, 1993):

$$J_f^C = \left(\rho\bar{u} \bullet \bar{S}\right)_f \phi_f = C_f \phi_f$$

where S_f is the surface of cell face f, and C_f is the convective flux coefficient of cell face f. As can be seen by the above equation it is necessary to have a good estimate of the face value of ϕ in order to determine the convective flux. This value is found using some form of interpolation which is defined by the differencing technique which is being applied. The most simple approach is that of central differencing, for example (cf. Versteeg *et al*, 1995):

$$\phi_e = \frac{1}{2}\left(\phi_P + \phi_E\right)$$

This approach, which is second order accurate, works well for fine grids and for flows which are not strongly convective. It is not able to identify flow direction and gives equal weighting to the cell centre nodes on either side of it. In strongly convective flows this is not suitable as there will be a greater influence from the upwind cell (cf. Versteeg *et al*, 1995). To solve this problem upwind differencing was introduced which takes into account the flow direction:

If the velocity is from east to west $u_e = u_E$

or if it is from west to east $u_e=u_P$

Since this scheme is only first order accurate it works well with very fine grids and strongly convective flows (cf. Versteeg *et al*, 1995). A major drawback to this scheme is that it produces erroneous results when the flow is not aligned with the grid lines. It causes the distribution of transported properties to become smeared resulting in a diffusion-like appearance referred to as "false diffusion" (Versteeg *et al*, 1995). False diffusion can be minimised by using a very fine grid. To try to obtain a scheme which works well in flows with varying degrees of convection Spalding (1972) proposed the hybrid differencing scheme. This scheme uses central differencing for flows with very little convection or Peclet numbers less than two ($Pe<2$) and upwind differencing for flows which are highly convective with $Pe\geq 2$. It has the advantages of both schemes and is very stable compared to higher order schemes which will be discussed later. For this reason it is the most popular scheme in use in commercial CFD packages today. However, it suffers from only being first order accurate. To try to address this problem Patankar (1980) proposed power law differencing for one dimensional problems. In his model when the $Pe>10$ diffusion is set to zero. For $0<Pe<10$ the flux is evaluated using a polynomial expression. This scheme is more accurate than hybrid differencing for one dimensional problems. Leonard (1979) proposed the quadratic upwind differencing scheme also known as QUICK. This scheme uses three points which are upstream weighted:

if the velocity is from east to west $$\phi_e = \frac{6}{8}\phi_E + \frac{3}{8}\phi_P - \frac{1}{8}\phi_{EE}$$

or if it is from west to east $$\phi_e = \frac{6}{8}\phi_P + \frac{3}{8}\phi_E - \frac{1}{8}\phi_W$$

It is third order accurate allowing it to produce better results on coarser grids compared to the lower order differencing schemes. However, it suffers from stability problems under certain flow conditions (Versteeg *et al*, 1995). Han *et al* (1981), Pollard and Siu (1982) and Hayase *et al* (1992) have all reweighted the terms in an attempt to try to generate a more stable formulation. Hayase *et al* (1992) generalised the approach for re-arranging QUICK schemes and derived a stable and fast converging variant. Another problem which these schemes suffer from is slight overshoots and undershoots which can give rise to unbounded solutions particularly in the vicinity of steep gradients (Versteeg *et al*, 1995). Other higher order schemes have been developed, such as the third order scheme of Agarwal (1981) and the second order upwind scheme of Fromm (1968), with varying degrees of success. Many of these schemes suffer from difficulty in prescribing boundary conditions and are computationally expensive. They also suffer

from stability and boundedness problems (Syed *et al*, 1985, Turan *et al*, 1988). A class of higher order schemes have been more recently developed to overcome the boundedness problem. Basically two approaches have been adopted. The first of these follows a blending strategy, where either a limited anti-diffusive flux is added to a first order upwind scheme, to improve the resolution of steep gradients while avoiding unbounded solutions (for example the flux-corrected transport (FCT) method of Zalesak (1979)), or a smoothing diffusive flux is added to a higher order scheme to damp out oscillations (for example the filtering remedy and methodology (FRAM) scheme of Chapman (1981) and the flux blending methods of Peric (1985) and Zhu *et al* (1988)). Because of the multi-step nature of these methods they tend to be computationally very expensive and are often unable to obtain the optimum compromise between boundedness and accuracy (Darwish, 1995). The second approach to avoid the boundedness problems is based on a composite flux limiter technique. Basically the numerical flux at the cell face is limited to enforce its boundedness. The earliest schemes were based on the total variational diminishing (TVD) flux limiter scheme used for shock capturing in compressible flows. A detailed discussion of these can be found in the work of Hirsch (1990), Van Leer (1973, 1974, 1977), Borris and Brook (1973, 1976), Chakravarthey and Osher (1983), Osher (1984), Osher and Chakravarthy (1984) and Alvarez *et al* (1993). More recently new schemes (for example STOIC of Darwish (1993), SOUCOUP of Zhu and Rodi (1991), Zhu (1991), Lin and Chieng (1991), SMART of Gaskell and Lau (1988)) have been proposed based on normalised variables formulation (NVF) (Leonard, 1988, 1981). A detailed comparison of many of these composite flux limiter schemes was conducted by Darwish (1993). Three test cases were compared with steep gradients. For all three his STOIC model gave slightly better results, however all of the composite flux limiter models were shown to be a great improvement over upwind differencing. One drawback to this technique has been that it requires uniform or nearly uniform grid spacing. Darwish *et al* (1994) extended their scheme to overcome this problem successfully by introducing a new type of composite flux limiter based approach called normalised variable and space formulation (NVSF). In summary, the principal advantage of higher order schemes is the reduction of the diffusive error, which is more severe on coarse grids. This is important in real combustor geometries where complex shapes and computationally expensive combustion models usually make fine grids impractical. For schemes such as QUICK, a reduction in computational stability and the steep gradients associated with combustion, which will pose a problem for boundedness, may make this type of model impractical. Composite flux limiter schemes appear to be the most promising in terms of accuracy and boundedness however these will be computationally expensive given their relative complexity. Because of our decision to use a commercial package the opportunities to investigate such alternatives in this programme are limited but where numerical

refinements have been introduced, they are discussed in the context of particular applications.

3 Combustion Models

3.0 Introduction

In the previous chapter an overview of the various models available to close the chemical source term of the transport equation for the reaction progress variable (Equation (2-34)) were considered. Now we carry on to discuss the three specific closures considered for this study. Essentially one model from each of the three groups, of mixing based models, reduced chemistry models and detailed chemistry models was chosen.

Essentially all of the mixing based models available in the literature are variants of the original Mason and Spalding (1973) Eddy Break-up model. For this reason it was decided to concentrate on this model.

The reduced chemistry models were essentially divided up on the choice of the statistical averaging of the instantaneous chemical source term. In terms of this type of model the presumed pdf model was chosen primarily because it is the least computationally expensive of the other models.

For the detailed chemistry model, the BML Crossing Frequency model was chosen for several reasons. For one, the presumed pdf approach which was offered by some authors follows closely to the reduced chemistry presumed pdf approach in terms of concept. As we are already looking at this type of model it would be more interesting to investigate a model with a slightly different approach. As well the presumed pdf model would require the integration over the joint pdf of reaction progress variable and strain and the solution of an additional transport equation for the variance of the reaction progress variable making it very computationally expensive. Of the flame sheet models the BML Crossing Frequency model has the advantage of solving for the reaction progress variable in a similar fashion to the Presumed pdf and Eddy Break-up models. This has the advantage from a coding perspective that it makes the computation of temperature and density similar for all three of these models. It also makes it easier to compare the three models in terms of the reaction rates since they are all defined as a function of the same variable.

In addition we also consider the case where the fuel and air mixture is not completely homogeneous. The adaptations made to the three combustion models to account for this will be discussed. Finally NO_x emissions were modelled and the specifics of this model will be discussed.

Propane was assumed to be the fuel as it has similar combustion properties to kerosene (Mularz,1979). Lefebvre (1977) points out that measured values of NO_x, CO and unburnt hydrocarbon emissions from a research LPP combustor were similar for both propane and Jet A kerosene. Lean blowout limits were also found to agree closely, however propane was found to be less susceptible to autoignition than kerosene.

The flow was also assumed to be adiabatic and at a low Mach number for all of the calculations.

3.1 Eddy Break-up Model

Perhaps the simplest turbulent premixed combustion model and one of the earliest proposed is the Eddy Break-up model of Mason and Spalding (1973). This model is based on the assumption that the chemistry is infinitely fast and therefore mixing controlled such that the rate of turbulent reaction depends only on the rate of transport of chemical species and heat into the unburnt mixture. This in turn is proportional to a time scale related to the turbulence of the flow. Thus Mason and Spalding (1973) defined the mean rate of production of the reaction progress variable as:

$$\overline{w} = C\frac{\varepsilon}{k}\sqrt{\overline{Y'^2}} \qquad (3\text{-}1)$$

where C is a constant, k is the turbulence kinetic energy and ε is its dissipation rate. $\overline{Y'^2}$ is the variance of the mass fraction of the oxidant.

Given that we are interested in a closure for the reaction progress variable it is relatively simple to define such a variable in terms of the normalised mass fraction of the oxidant:

$$c = \frac{Y_r - Y}{Y_r - Y_p} \qquad (3\text{-}2)$$

where the subscripts r and p indicate the mass fraction of the oxidant in the reactant and product states respectively. And thus by inserting Equation (3-2) in Equation (3-1) and taking the density weighted form one gets:

$$\tilde{w}_c = C_c\frac{\varepsilon}{k}\sqrt{\widetilde{c''^2}} \qquad (3\text{-}3)$$

where C_c is a constant.

Mason and Spalding (1973) originally proposed solving a separate transport equation for the variance of the mass fraction of the oxidant. The transport equation for the variance of the reaction progress variable in its Favre averaged form is:

$$\frac{\partial\bar{\rho}\tilde{u}_j\widetilde{c''^2}}{\partial x_j} = \frac{\partial(-\overline{\rho u_j''c''^2})}{\partial x_j} - 2\overline{\rho u_j''c''}\frac{\partial\tilde{c}}{\partial x_j} - 2\rho\mathcal{D}\overline{\frac{\partial c''}{\partial x_j}\frac{\partial c''}{\partial x_j}} + 2\overline{\rho c''w_c} \qquad (3\text{-}4)$$

This equation requires a closure model for the last two terms on the right hand side. Mason and Spalding (1973) tackled the closure of the last term or chemical source term by simply ignoring it. They used the modelled equation for the variance of a conserved scalar offered by Launder and Spalding (1972).

Bray and Moss (1977), pointed out that, based on the assumption of infinitely fast chemistry, the probability that the reaction progress variable would take on a value between one and zero would be negligible. Thus one could assume that the probability density function or pdf of the reaction progress variable merely consisted of two delta functions one at zero and one at one. The variance can be determined from:

$$\widetilde{c''^2} = \int_0^1 (c - \tilde{c})^2 \tilde{P}(c) dc \qquad (3\text{-}5)$$

where $\tilde{P}(c)$ is the Favre pdf, and based on this two delta function form of the pdf the variance of reaction progress variable would simply be:

$$\widetilde{c''^2} = \tilde{c}(1 - \tilde{c}) \qquad (3\text{-}6)$$

As has been pointed out earlier this primarily bimodal nature to the pdf of reaction progress variable has been verified by experimental measurements in laboratory flames (Heitor *et al*, 1985, Yoshida *et al*, 1982, 1980, Moss, 1980).

Another minor distinguishing feature in the evolution of this model relates to the length scale. Mason and Spalding (1973) assumed that the rate of reaction was proportional to the rate of viscous dissipation, however Bray *et al* (1984) suggest that it should be proportional to the scalar dissipation, thereby introducing a turbulent Prandtl number. Incorporating this feature into a revised expression removes the square root over the variance:

$$\tilde{w}_c = C_{ebu} \frac{\varepsilon}{k} \tilde{c}(1 - \tilde{c}) \qquad (3\text{-}7)$$

where C_{ebu} is a constant.

This is the final form which was used for our investigation.

3.2 Presumed pdf Model

One of the main limitations of the Eddy Break-up model is that in the absence of any chemistry, it does not directly account for the effects of different fuels. To accomplish this one must also consider the direct inclusion of the chemistry in more detail.

Most practical fuels have hundreds of reactions associated with their combustion, and it is impractical to solve time averaged transport equations for each species. For our work we have chosen to simplify the chemistry down to a single step:

$$\text{fuel} + \nu \times \text{oxidiser} \Rightarrow \text{products} \qquad (3\text{-}8)$$

A simple Arrhenius expression based on experimental data can then be used to determine the rate of reaction.

Assuming that the reaction progress variable is based on the mass concentration of CO_2 and given that this is one of the products we can then readily obtain an expression for the instantaneous rate of reaction based on the reaction progress variable.

For our purposes the fuel modelled was propane and a global Arrhenius expression was adopted from the work of Westbrook and Dryer (1984).

$$\frac{\partial[C_3H_8]}{\partial t} = -8.6 \times 10^{11} \exp\left[\frac{-30000}{RT}\right][C_3H_8]^{0.1}[O_2]^{1.65} \qquad (3\text{-}9)$$

where R is the ideal gas constant in calories/(mole K), T is the temperature in K and $[C_3H_8]$ and $[O_2]$ are the molar concentration of propane and oxygen respectively.

Based on the assumption of single step chemistry, one can show that:

$$[C_3H_8] = \rho Y_{CO_2}^{c=1}\left(\frac{1}{m_T Y_{CO_2}^{c=1}} - \frac{1}{3w_{CO_2}}c\right) \qquad (3\text{-}10)$$

$$[O_2] = \rho Y_{CO_2}^{c=1}\left(\frac{5}{\phi m_T Y_{CO_2}^{c=1}} - \frac{5}{3w_{CO_2}}c\right) \qquad (3\text{-}11)$$

where c is the reaction progress variable, w_{CO_2} is the molecular mass of CO_2 in kg/mole, and $Y_{CO_2}^{c=1}$ is the mass fraction of CO_2 when the flame is fully burnt (i.e. when c=1), ρ is the density in kg/m^3, ϕ is the equivalence ratio and m_T is the total molecular mass defined as:

$$m_T = 44.01 + \frac{686.4}{\phi} \qquad (3\text{-}12)$$

Inserting Equations (3-10) and (3-11) into Equation (3-9) and making the assumption that both $Y_{CO_2}^{c=1}$ and ϕ are independent of time which is the case for a perfectly homogeneous mixture then we obtain:

$$\frac{\partial c}{\partial t} = w_c(c) = 8.6 \times 10^{11} \exp\left[\frac{-30000}{RT}\right] 3w_{CO_2} \left(Y_{CO_2}^{c=1}\rho\right)^{3/4} \left(\frac{1}{m_T Y_{CO_2}^{c=1}} - \frac{1}{3w_{CO_2}}c\right)^{0.1}$$
$$\times \left(\frac{5}{\phi m_T Y_{CO_2}^{c=1}} - \frac{5}{3w_{CO_2}}c\right)^{1.65} \qquad (3\text{-}13)$$

where $w_c(c)$ is the instantaneous rate of reaction in units of s^{-1}.

$Y_{CO_2}^{c=1}$ can be defined in two ways. One way would be to assume that when the flame is fully burnt that the chemical species have reached equilibrium. The NASA equilibrium program (Gordon and Mc Bride, 1971) could then be used to compute these correlations. This however will not necessarily lead to the reaction rate becoming zero when c=1. Another option would be to assume complete combustion, in other words to set the molar concentration of propane to zero for lean mixtures or the molar concentration to zero for oxygen for rich mixtures when c=1. This leads to the expression for $Y_{CO_2}^{c=1}$ of:

$$\phi < 1 \qquad Y_{CO_2}^{c=1} = \frac{132.03\phi}{44.03\phi + 686.4} \qquad (3\text{-}14)$$

$$\phi \geq 1 \qquad Y_{CO_2}^{c=1} = \frac{132.03}{44.03\phi + 686.4} \qquad (3\text{-}15)$$

Figure 3.2.1 illustrates a comparison of these two approaches. For lean equivalence ratios, which is what we are interested in, the proposed correlation gives almost identical results to the NASA equilibrium code. For rich mixtures however, the NASA

code predicts a lower concentration of CO_2 than does the correlation. On the lean side of the stoichiometric equivalence ratio there is more oxygen than fuel. Thus it is more likely that all of the fuel will be completely converted to CO_2. As one approaches an equivalence ratio of one the flame temperatures increases to a maximum. This will imply that the formation rate of intermediate species will be very high. Also the amount of fuel relative to the amount of oxygen is increasing and so it is more likely that there will be equilibrium concentrations of CO and possibly some unburnt hydrocarbons. On the rich side the amount of fuel relative to oxygen will increase still further making the likely hood of intermediate species even greater.

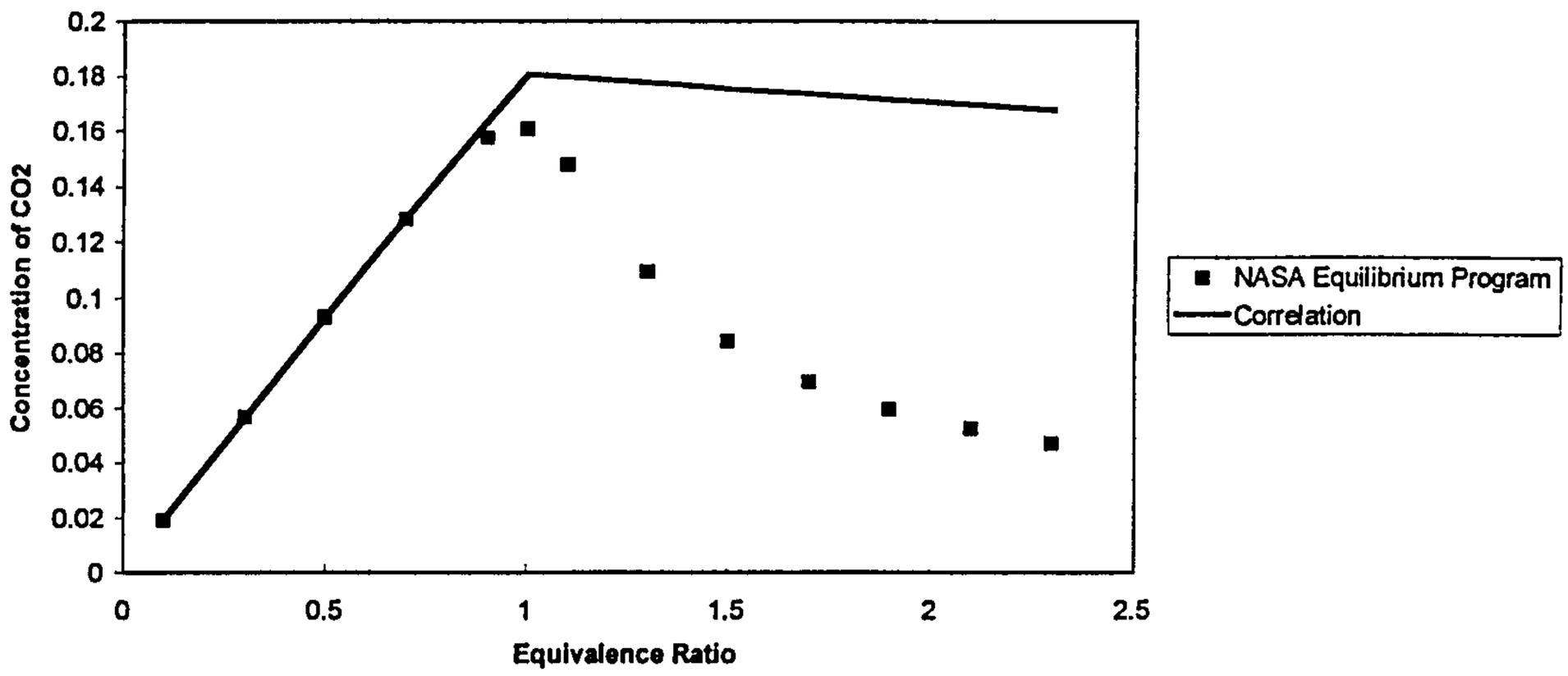

Figure 3.2.1 Fully Burnt Concentration of CO_2

To ensure that the chemical source term was zero when c=1 we chose to adopt the assumption that the chemistry was complete for $Y_{CO_2}^{c=1}$.

As was mentioned earlier, the time averaged expression needed to close the transport equation for the reaction progress variable (Equation (2-34)) can be determined by quadrature if the pdf for c is prescribed, namely:

$$\tilde{w}_c = \int_0^1 w_c(c)\tilde{P}(c)dc \qquad (3\text{-}16)$$

where $\tilde{P}(c)$ denotes the Favre probability density function (pdf).

A presumed Bray Moss style pdf was chosen because of its simplicity and for the fact that there has not been sufficient validation to verify that the more elaborate presumed pdf models such as the β-function or clipped Gaussian are any more physically representative. A comparison between the β-function and Bray Moss

style pdf's was carried out for a typical calculation. This will be discussed later in the next chapter, however the results indicate that the shapes do not differ greatly between these two. The clipped Gaussian was not tested as it has the added disadvantage that it is very computationally expensive.

In order to determine the pdf, the variance of the reaction progress variable must also be computed. To do this an additional time averaged transport equation was solved:

$$\frac{\partial \bar{\rho}\tilde{u}_j \widetilde{c''^2}}{\partial x_j} = \frac{\partial(-\overline{\rho u_j'' c''^2})}{\partial x_j} - 2\overline{\rho u_j'' c''}\frac{\partial \tilde{c}}{\partial x_j} - 2\overline{\rho \mathcal{D}\frac{\partial c''}{\partial x_j}\frac{\partial c''}{\partial x_j}} + 2\overline{\rho c'' w_c} \qquad (3\text{-}17)$$

The second last term on the right hand side of the equation, which represents the dissipation by molecular diffusion, is modelled as (Borghi, 1988):

$$2\overline{\rho \mathcal{D}\frac{\partial c''}{\partial x_j}\frac{\partial c''}{\partial x_j}} = 2\bar{\rho}\varepsilon_c = \frac{\bar{\rho}}{2}\frac{\widetilde{c''^2}}{\tau_{ex}} \qquad (3\text{-}18)$$

where ε_c is the scalar dissipation rate and τ_{ex} is the time scale representative of this rate. For τ_{ex} Borghi (1988) has recommended that the scalar dissipation rate can be related to the turbulence dissipation rate by a constant giving:

$$\frac{1}{\tau_{ex}} = 4\frac{\varepsilon}{k} \qquad (3\text{-}19)$$

More recently Mantel and Borghi (1994) have proposed, in line with Bray *et al* (1984) with regard to the Eddy Break-up model, that the ratio of this dissipation rate to that for turbulence energy is not constant. They propose that this term should be modelled with an additional transport equation. They also show that ε_c and the flame front surface area are correlated.

In the present simulations the earlier model for scalar dissipation has been adopted. Partly because the transport equation proposed by Mantel *et al* (1994) involves several additional closure assumptions which rely on an infinitely large Damköhler number (Da={turbulent mixing time}/{chemical time}) and a perfectly premixed mixture. The infinitely large Da number runs counter to the fundamental concept of the Presumed pdf model which relies on the pdf between the reaction progress variable values of 0 and 1 to be non-zero in order for there to be a chemical source

term. The second assumption, that the fuel air mixture is homogeneous, is also problematic given that we wish to be able to model a flowfield with a non-homogeneous mixture. The other reason for not using this model is that we subsequently use a full second moment closure turbulence model which is computationally intensive and additional scalar transport equations will add to this expense.

The second term on the right hand side of Equation (3-17), which represents the production by the mean gradient, was closed in a manner dependent on the flow turbulence model. For the second moment turbulence model this term was closed exactly since the scalar fluxes were computed from transport equations. For the k-ε turbulence model a gradient transport assumption was made for the scalar fluxes such that:

$$-2\overline{\rho u_j'' c''}\frac{\partial \tilde{c}}{\partial x_j} = 2\bar{\rho}\frac{\mu_t}{Sc_t}\frac{\partial \tilde{c}}{\partial x_j}\frac{\partial \tilde{c}}{\partial x_j} \qquad (3\text{-}20)$$

where μ_t and Sc_t are the turbulent viscosity and Schmidt number for c. The former was determined from:

$$\mu_t = C_\mu \bar{\rho}\frac{k^2}{\varepsilon} \qquad (3\text{-}21)$$

where the model $C\mu$ was assigned the value 0.09. The Schmidt number was assumed to be unity.

The flux of the variance, $\overline{\rho u_j'' c''^2}$, was also modelled using a gradient assumption, regardless of the turbulence model employed. This was done for the second moment turbulence model in order to both reduce computational expense and in recognition of the fact that closure terms for the transport equation of this flux do not appear to have been studied extensively.

Finally the last term on the right hand side, which represents the chemical source term, was determined from:

$$\overline{\rho c'' w_c} = \bar{\rho}\int_0^1 (c - \tilde{c}) w_c(c)\tilde{P}(c)dc \qquad (3\text{-}22)$$

3.3 Bray Moss Libby Crossing Frequency Model

The presumed pdf model for a simple scalar variable has the advantage, relative to the Eddy Break-up model, that it introduces chemistry through the assumption of a simple single-step reaction.

The BML crossing frequency model takes this one step further. It assumes that if one examines the instantaneous flame front structure then the flame will appear to be a strained laminar flamelet.

The reaction rate in such a flamelet can be evaluated using a one dimensional laminar code incorporating detailed chemistry such as those proposed by Warnatz (1983), Stahl (1988), Darabiha (1988), Rogg (1988), Kee (1988), and Dixon-Lewis (1984). Typically such codes compute the flow field of opposed jets such as that illustrated in Figure 3.3.1. Two configurations have been widely investigated in the literature.

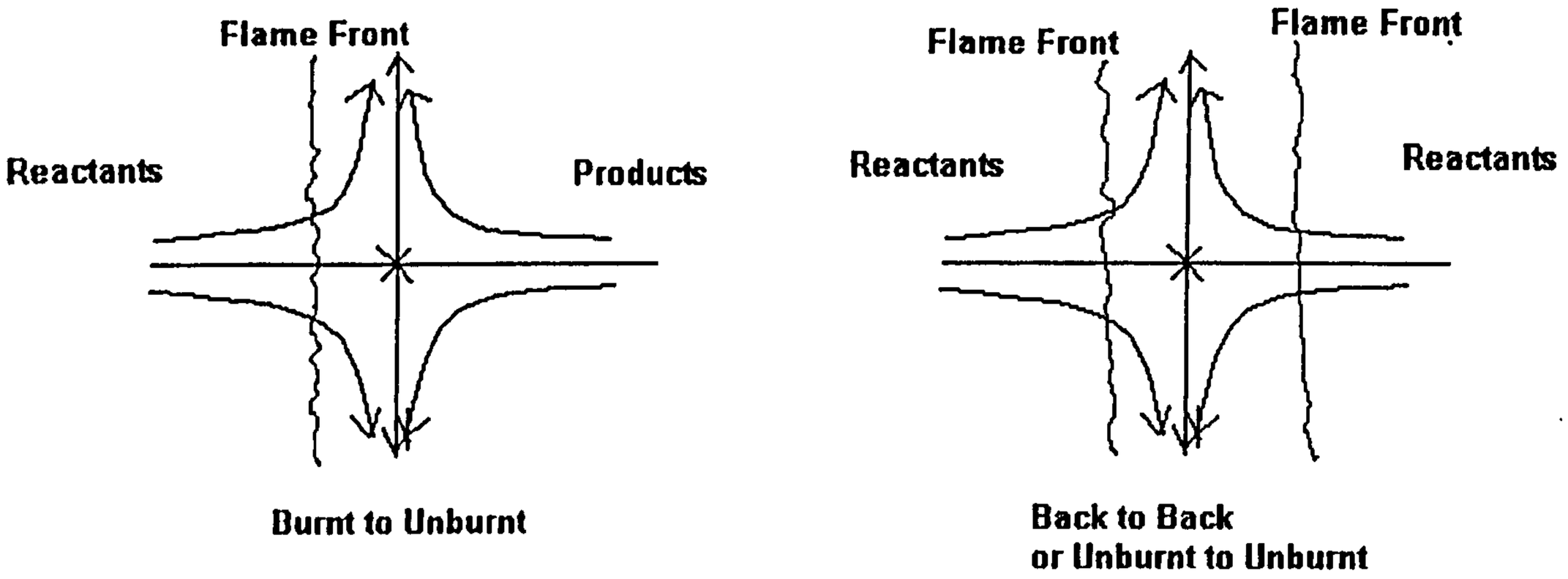

Figure 3.3.1 Counter Flowing Strained Laminar Flame Configurations

One, known as a back-to-back or unburnt-to-unburnt configuration, involves both jets having unburnt reactants. This geometry has two flame fronts either side of the stagnation point. As the velocity of the flow from either side is increased these flame fronts move towards the stagnation point. The velocity gradient parallel to the flame front increases and heat and radicals are transported away from the stagnation streamline. This can be visualised as if the flame front is being stretched. This phenomena is termed stretch or strain. Eventually if the velocities are high enough there will no longer be sufficient heat and radicals present for a given area of the flame front to sustain the flame and the flame will become quenched. The

advantage of this configuration is that there is a clear point at which the flame is quenched (Bray, 1996).

The other configuration, known as the burnt-to-unburnt configuration, has fully burnt products on one side and reactants on the other. Again as the strain rate is increased the flame front moves towards the stagnation point. However for this geometry there is not a clear point where the flame can no longer sustain itself. Heat from the jet of burnt products allows the flame to remain ignited at much higher strain rates than the back-to-back configuration (Bray, 1996). Often the existence of radicals such as OH are used to determine whether or not the flame is burning. Some in the literature argue that the advantage to this latter geometry is that it appears to simulate better the strain rate behaviour of practical turbulent flames. It is thought that in a real turbulent flame under strain rates where the flame front in a back-to-back configuration would be quenched the flame front becomes reignited by the existence of nearby pockets of fully burnt products (Bradley and Lau, 1990). With this in mind Bray *et al* (1996) have conducted an investigation into the effect of varying the enthalpy of the burnt product stream to see what effect this has on the strain rate at which flame quenching occurs. They found that above a threshold temperature of the inert stream no global extinction occurred, however below this point extinction was possible. It may equally be argued that, under conditions of very high turbulence, the flame front becomes highly contorted and even broken such that a section of the flame front may see conditions where there is very little burnt product separating it and another flame front more similar to the back-to-back configuration. Bradley and Lau (1990) point out that there is sufficient uncertainty in the statistics of the flow field to make the significance of the precise geometry of the laminar flame less important. Furthermore because of the unclear point at which flame quenching occurs, the burnt-to-unburnt geometry has remained less popular than the back-to-back configuration.

The disadvantage of computing reaction rate through a laminar one dimensional code is the amount of computational time involved. For a premixed flame with a homogeneous mixture one must compute over a range of strain rates. However for this work we are also interested in considering a non-homogeneous flame which requires also computing over a range of equivalence ratios. Djavdan *et al* (1991) suggest that the time required for such a computation is proportional to the square of the number of species. They propose using a reduced chemical scheme to speed up computations. Another option was suggested by Abu-Orf and Cant (1996), who required flamelet data for a coherent flame model (Wu and Bray, 1993). They came to the conclusion that it would be much faster to make use of existing experimental data found in the literature rather than to compute an entire flamelet library from scratch. Thus after some effort at computing a flamelet library this was the approach also adopted for this work.

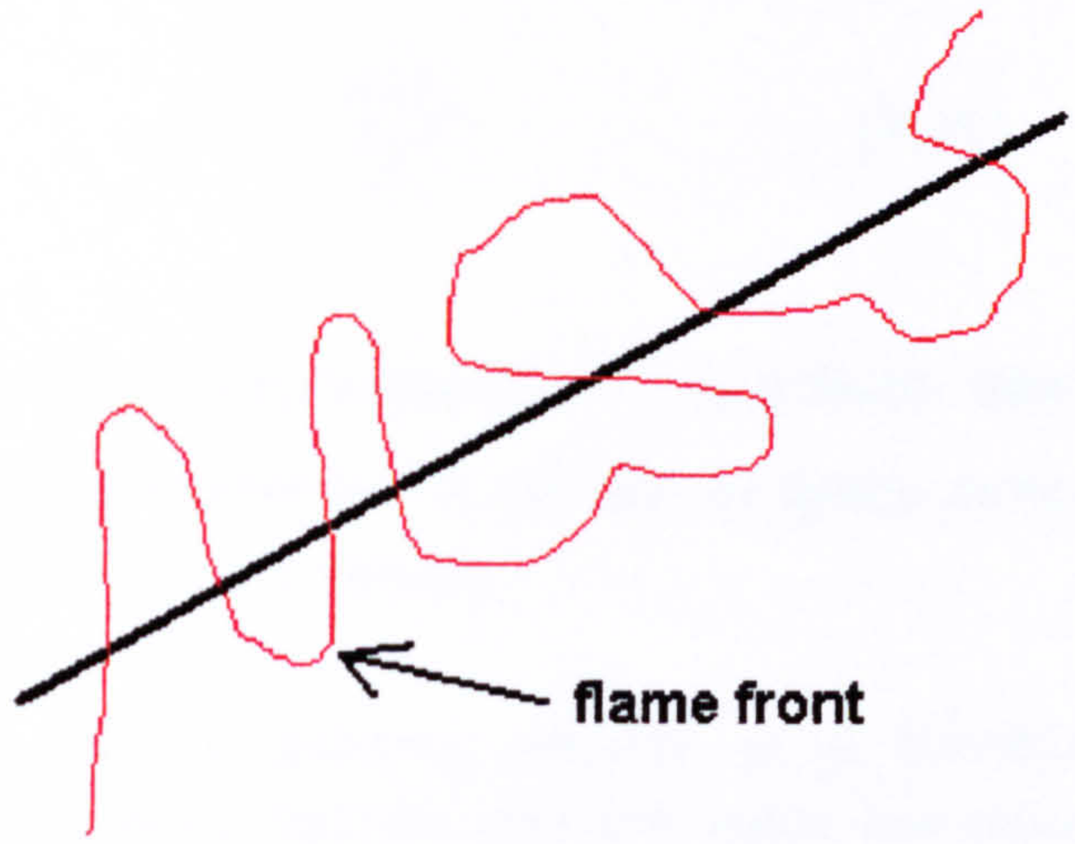

Figure 3.3.2

The BML crossing frequency model was first proposed by Bray *et al* (1984b). It is based around the idea of considering a line in space over which the flame front crosses (Figure 3.3.2). The rate of reaction is equal to the rate of reaction per crossing multiplied by the number of crossings per unit length:

$$\overline{\rho w} = \rho w_y \upsilon_y \qquad (3\text{-}23)$$

The number of crossings per unit length was proposed to be:

$$\upsilon_y = \frac{g\bar{c}(1-\bar{c})}{\hat{L}_y} \qquad (3\text{-}24)$$

where g is a constant between 1 and 2 depending on the details of the crossing frequency probability density function (Bray *et al*, 1984a,1986) (assumed to be 1.5 for our purposes), and $\hat{L}_y$ is the integral length scale of the spatial, random flamelet, crossing process. Based on experimental measurements for a Bunsen type flame Cant and Bray (1988) suggest that this value is nearly equal to the local turbulence length scale. Thus for this work $\hat{L}_y$ was assumed to be:

$$\hat{L}_y = C_\mu^{3/4} \frac{\tilde{k}^{3/2}}{\tilde{\varepsilon}} \qquad (3\text{-}25)$$

The reaction rate per crossing can be related to the rate of consumption of the reactants under a global one-step process, which in turn can be related to the burning velocity multiplied by the density of the reactants to give us:

$$\overline{\rho w_y} = \frac{\rho_R \tilde{S}_L}{\overline{|\sigma_y|}} \qquad (3\text{-}26)$$

where ρ_R is the density of the reactants, $\overline{|\sigma_y|}$ is a factor describing the mean angle of the flamelet crossing relative to the unit line in space assigned the value 0.5, and $\tilde{S}_L$ is the mean laminar burning velocity.

The instantaneous laminar burning velocity is a function of the strain rate, equivalence ratio or mixture fraction and the initial conditions of temperature and pressure. Often correlations distinguish between the function of equivalence ratio and that of the reactant temperature and pressure are offered in the form (Gülder, 1983, Metghalchi, 1980):

$$S_L^0(P, T_R, \phi) = S_{L0}^0(\phi)\left(\frac{T_R}{T_0}\right)^{\alpha}\left(\frac{P}{P_0}\right)^{\beta} \qquad (3\text{-}27)$$

where the superscript 0 implies zero strain rate, the subscript R stands for conditions for the reactants and the subscript 0 implies standard conditions of temperature and pressure (298 K and 1 atmosphere).

Abu-Orf and Cant (1996), with internal combustion engine applications in mind, used a novel equation for laminar burning velocity from Gülder (1983) which took the form:

$$S_L^0(P, T_R, \phi) = a\phi^b \exp[-c(\phi - d)^2]\left(\frac{T_R}{T_0}\right)^{\alpha}\left(\frac{P}{P_0}\right)^{\beta} \qquad (3\text{-}28)$$

where the subscript R means reactants and the subscript 0 means standard conditions of temperature and pressure (298 K and 1 atmosphere). This equation introduces difficulties at low equivalence ratios. Since the parameter b is negative the burning velocity tends to infinity. The expression is therefore unsuited to the lean mixtures of interest to this study.

Metghalchi and Keck (1980) proposed a simple polynomial relationship for propane:

$$S_L^0 = \left(38.31 + 24.84(\phi - 1) - 153(\phi - 1)^2\right)\left(\frac{T_R}{T_0}\right)^{\alpha}\left(\frac{P}{P_0}\right)^{\beta} \qquad (3\text{-}29)$$

They found that for an equivalence ratio of 0.8 that the exponents α and β were 2.27 and -0.23 respectively. Their expression works well in the range they considered from an equivalence ratio of 0.8 to 1.5. However outside of this it is not as good.

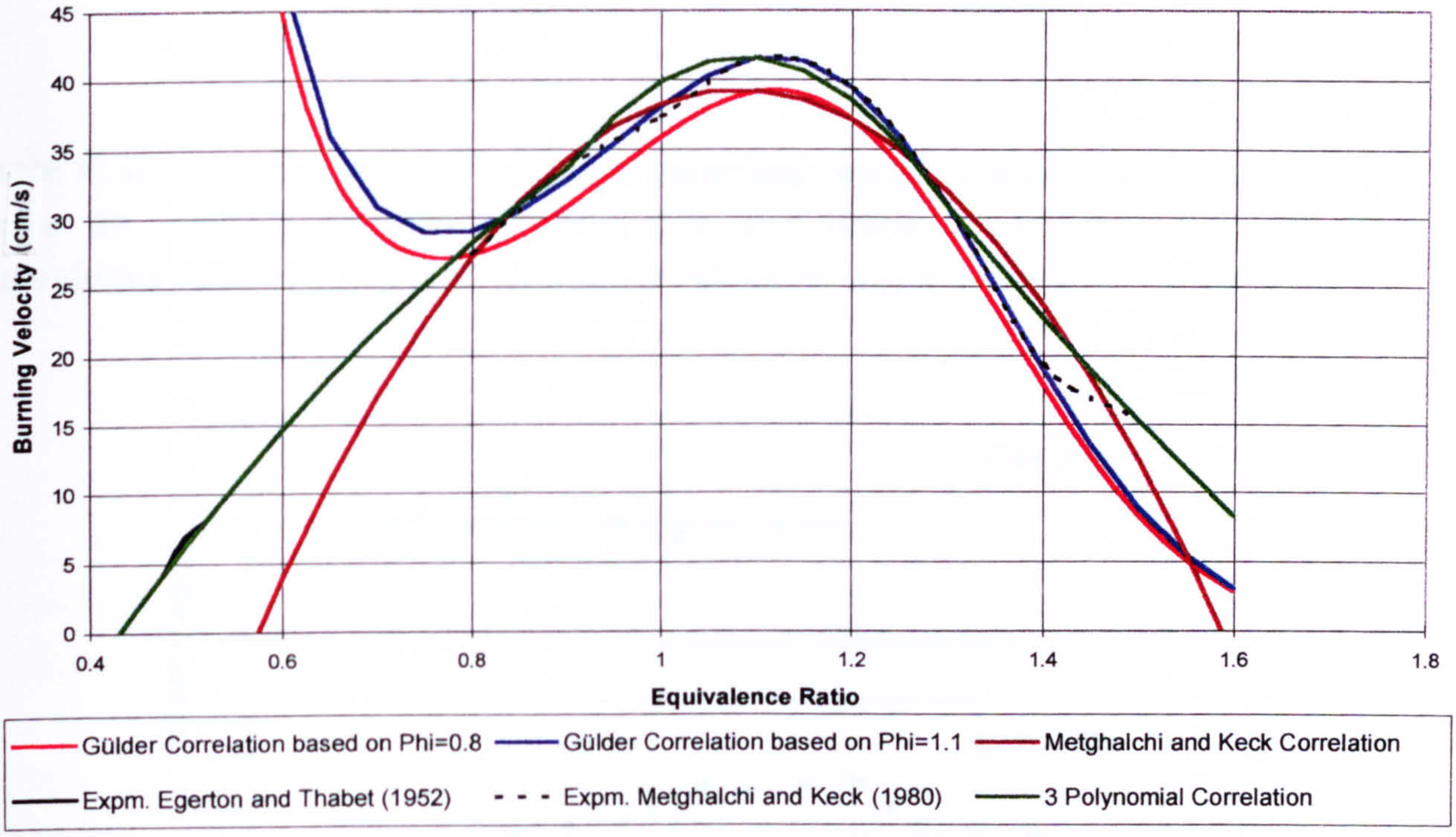

Figure 3.3.3 Burning Velocity versus Equivalence Ratio for T_0=298 K and P=1 bar

Figure 3.3.3 compares the two approaches with experimental values from Metghalchi *et al* (1980) and Egerton and Thabet (1952).

As none of the correlations worked very well over the complete range of equivalence ratios of interest to our work we have simply divided the burning velocity curve into three segments and used a polynomial curve fit for each of the three segments. This curve fit can be seen in Figure 3.3.3 and the equations are given below:

$$0.0 \le \phi \prec 0.9 \quad S_{L0}^{0} = -49.309\phi^2 + 137.071\phi - 49.824$$

$$0.9 \le \phi \prec 1.3 \quad S_{L0}^{0} = -233.75\phi^2 + 507.5\phi - 233.813$$

$$1.3 \le \phi \prec 1.5 \quad S_{L0}^{0} = 26.667\phi^2 - 152.667\phi + 184.3$$

The exponents for the reactant temperature and pressure correction were taken from Metghalchi and Keck (1980).

Thus far we have ignored the effect of strain rate on the laminar burning velocity. Law *et al* (1986) have investigated this effect in propane flames using a back-to-back counter-flowing laminar flame experiment. They proposed the relationship:

$$S_L = S_L^0\left(1+\frac{\alpha(\phi)}{\left(S_L^0\right)^2}K\right) \qquad (3\text{-}30)$$

where K is the strain rate and $\alpha(\phi)$ is a parameter which is a constant of about 0.5 above an equivalence ratio of about 0.8, and drops linearly to zero from an equivalence ratio of 0.8 to 0.5. Measured values of $\alpha(\phi)$ are shown in Figure 3.3.4.

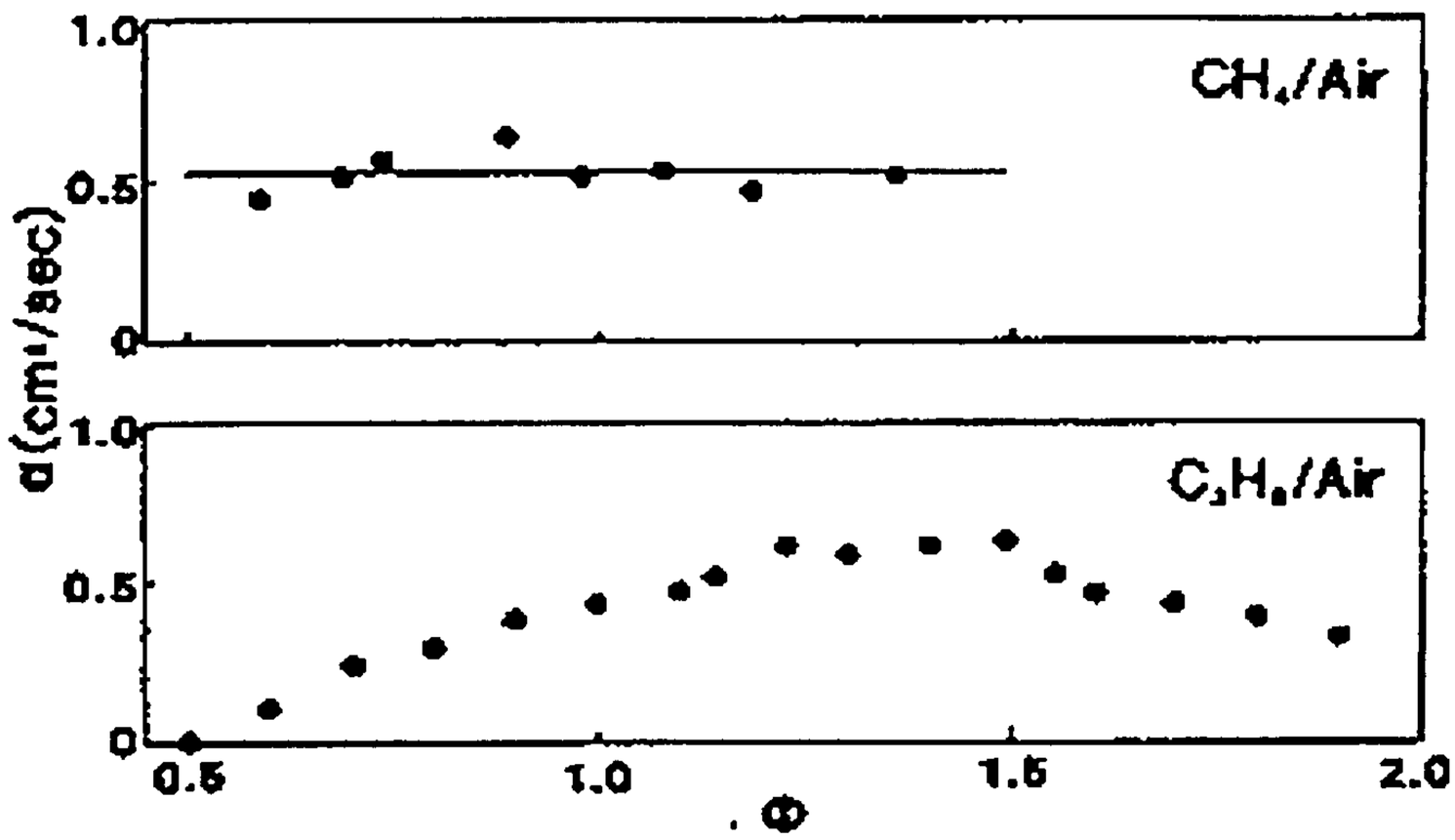

Figure 3.3.4 Measured values of $\alpha(\phi)$ form Law *et al* (1986) for Methane and Propane

To determine the mean laminar burning velocity we need to determine the joint probability density function of the strain rate and equivalence ratio (or mixture fraction). For the initial calculations the equivalence ratio was considered to be constant. However later we shall consider the equivalence ratio to be inhomogeneous. This is discussed in more detail in the next section.

In establishing a pdf of strain rate, most researchers have presumed a log-normal probability distribution for the strain rate (Abdel-Gayed *et al*, 1988, Cant *et al*, 1988, Rogg *et al*, 1986). Abdel-Gayed *et al* (1988) also proposed a quasi-Gaussian pdf and compared the predicted strain rate at which the flame would quench for both distributions with measured values for a propane-air flame in a fan-stirred reactor at several lean equivalence ratios. From these comparisons they concluded that the log-normal distribution provided slightly better agreement. Rather than compute the variance of the strain rate they propose a constant value for it, in line with most of

the literature written to date, and parameterised their pdf with only the mean of the strain rate.

Their log-normal pdf is defined as:

$$P(K) = \frac{1}{\sqrt{2\pi}\sigma K}\exp\left(-\frac{(\ln K - \mu)^2}{2\sigma^2}\right)$$

$$\sigma^2 = 0.34 \qquad (3\text{-}31)$$

$$\mu = \frac{1}{2}\left(\ln\frac{\varepsilon}{3\upsilon} - 2\sigma^2\right) - \ln 2$$

$$\overline{K} = \frac{\overline{1}}{A}\frac{\overline{dA}}{dt} = 0.422\sqrt{\frac{\varepsilon}{3\upsilon}} = 0.94\frac{u'}{\lambda}$$

where K is the strain rate, ε is the dissipation rate of the turbulence kinetic energy, ν is the kinematic viscosity, A is the flame front area, and λ is the Taylor length scale of turbulence. This definition of the strain is based around the work of Batchelor (1952) which assumes that flame front straining occurs at the Kolmogorov scales in isotropic homogeneous turbulence (Duclos *et al*, 1993). This is consistent with the original proposal for the definition of strain rate for the Crossing Frequency model (Cant *et al*, 1988). Other authors have also proposed that the rate of strain should be related to the larger time scale of the turbulence ε/k however neither of these methods have been shown to reproduce the effects of turbulence length scales and chemistry on the turbulent burning velocity (Duclos *et al*, 1993). With this in mind we have retained the original approach proposed by Cant *et al* (1988).

In order to determine the mean burning velocity we also need one more parameter, the strain rate at which the flame is quenched. We use this value as an upper limit of integration over the pdf of strain rate.

This data was taken from the measurements of the extinction strain rate of propane against equivalence ratio from Law *et al* (1986) for a back to back laminar counter-flowing propane flame experiment. This is illustrated in Figure 3.3.5. A polynomial curve fit was made of the data for use by the model.

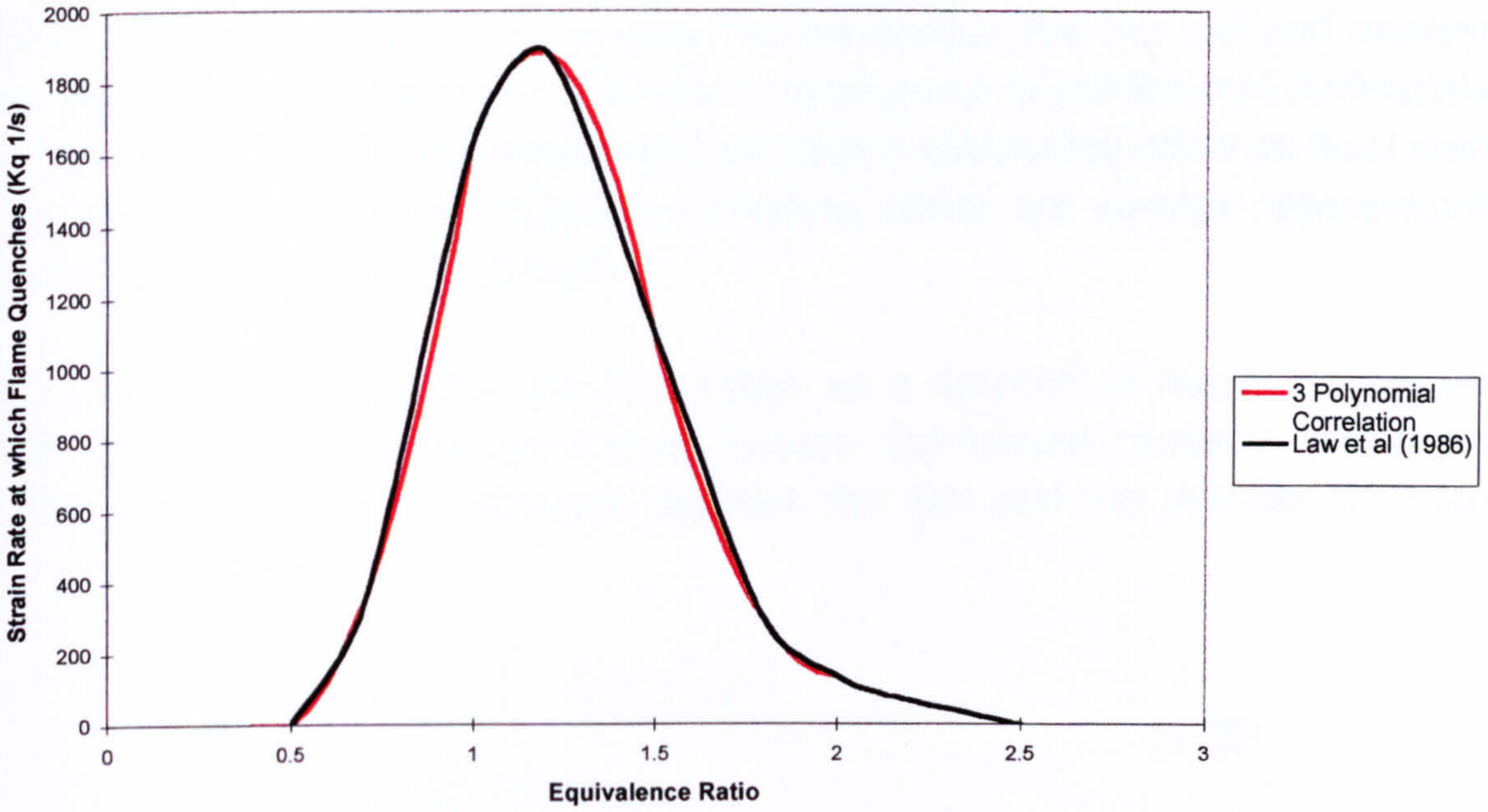

$$\phi \prec 0.5 \qquad K_q = 0.0$$

$$0.5 \leq \phi \prec 1.0 \quad K_q = 5227.667\phi^2 - 4568.7\phi + 977.433$$

$$1.0 \leq \phi \prec 1.5 \quad K_q = -7742.67\phi^2 + 18283.87\phi - 8904.8$$

$$1.5 \leq \phi \prec 2.0 \quad K_q = 3772.33\phi^2 - 15130.4\phi + 15307.8$$

Figure 3.3.5 Extinction Strain Rate of Propane from measurements by Law *et al* (1986)

3.4 Non-uniform Reactant Mixtures

All of the models discussed so far employ the assumption that the fuel and oxidiser are perfectly premixed. This is not the case in most practical combustors particularly in the gas turbine. Mixture inhomogeneity will have a substantial effect on local heat release and hence on those pollutant emissions which are strongly temperature dependent such as oxides of nitrogen.

Thus far we have treated the rate of reaction as a function of reaction progress variable alone. Now we introduce a second scalar, the mixture fraction f, such that f is a measure of the local mixedness between the fuel and the oxidiser (cf. Kuo, 1986).

$$f = \frac{\left[Y_F - (F/O)_{st} Y_O\right]_M + \left[(F/O)_{st} Y_O\right]_A}{1 + \left[(F/O)_{st} Y_O\right]_A} \qquad (3\text{-}32)$$

where Y is a mass fraction, $(F/O)_{st}$ is the stoichiometric fuel to oxidiser mass fraction, and the subscripts F, O, M and A stand for the fuel, oxidiser, mixture and air respectively. This can also be written as:

$$f = \frac{1}{1 + AFR} \qquad (3\text{-}33)$$

where AFR is the air-to-fuel mass ratio.

This scalar is conserved and bounded between [0,1], where zero denotes pure oxidiser and unity pure fuel.

The presumed pdf and crossing frequency combustion models can readily be interpreted as functions of the mixture fraction. For the presumed pdf model, the instantaneous reaction rate (Equation (3-13)) is a function of the equivalence ratio and hence the mixture fraction. The formulation of this term involves the assumption that the equivalence ratio is independent of time. For a non-homogeneous mixture this will not be the case however for small variations in the mean mixture fraction this will not be a bad assumption. In the crossing frequency model, the burning velocity can be considered to be a function of equivalence ratio or mixture fraction.

The reaction rate in the Eddy Break-up model may be considered to be a function of mixture fraction through the pre-multiplying model constant. This constant was envisaged by Mason and Spalding (1973) to be dependent on the particular flame

being considered. In their original formulation they describe the rate of reaction in terms of the mass fraction of the oxidant. If this expression is converted into a function of the mass fraction of CO_2, and normalised by the equilibrium concentration of CO_2 then a new model constant is established which is proportional to the equilibrium mass fraction of CO_2.

$$C_{EBU} = 1.2118 Y_{CO_2}^{c=1} C \qquad (3\text{-}34)$$

where C is a constant. This introduces the rather doubtful assumption that the original model constant was independent of the mixture fraction, but does introduce a dependence on mixture fraction which is reasonably close to that offered by the presumed pdf model. This latter model yields a rate expression which is proportional to the equilibrium mass fraction of CO_2 raised to the power of three quarters.

Given the instantaneous reaction rate, the mean reaction rate was then determined from:

$$\tilde{w}(c,f) = \int_0^1 \int_0^1 w(c,f)\tilde{P}(c,f)dcdf \qquad (3\text{-}35)$$

where $\tilde{P}(c,f)$ is the joint probability density function (pdf) of the reaction progress variable and the mixture fraction. Determining such a pdf is very difficult without performing a computationally intensive pdf transport calculation (Pope, 1981a,1981b,1985).

Several attempts have been made in the literature to implement presumed multi-scalar pdf's, adopting the same philosophy as the presumed pdf combustion model for a range of problems. Most have made the assumption that the pdf is uncoupled, in other words that c and f are not correlated whence:

$$\tilde{P}(c,f) = \tilde{P}(c|f)\tilde{P}(f) = \tilde{P}(c)\tilde{P}(f) \qquad (3\text{-}36)$$

Both Janicka *et al* (1978), and Correa *et al* (1992) have tackled the joint pdf of reaction progress variable and mixture fraction with an uncoupled approach. They assume a β function pdf for the pdf of the mixture fraction and a pdf consisting of three delta functions for the reaction progress variable. This latter pdf has delta functions at zero, unity and the mean of the reaction progress variable. Bradley *et al* (1990) used a similar approach but prescribe a β function pdf for the reaction progress variable as well as for the mixture fraction.

Rogg *et al* (1986) also investigated a partially premixed flame introducing a joint pdf, however they were interested in a flamelet based calculation and argue that the variables of interest were mixture fraction, scalar dissipation rate, and degree of premixedness. Again they chose a β function pdf for mixture fraction followed by a log-normal distribution for scalar dissipation and a delta function pdf for the degree of premixedness. This latter pdf has only two delta functions one at zero and the other at unity.

Girimaji (1991), on the other hand, has developed a joint β function pdf with an implied form for the variances and covariances which he claims is applicable to any number of scalars.

$$\tilde{P}(c_1, c_2, \ldots c_n) = \frac{\Gamma(\beta_1 + \beta_2 \ldots + \beta_n)}{\Gamma(\beta_1)\Gamma(\beta_2)\ldots\Gamma(\beta_n)} c_1^{\beta_1 - 1} c_2^{\beta_2 - 1} \ldots c_n^{\beta_n - 1} \delta(1 - c_1 - c_2 \ldots - c_n) \qquad (3\text{-}37)$$

where β_α is the α'th parameter of the pdf and the mean and variance of the α'th variable is respectively:

$$\tilde{c}_\alpha = \frac{\beta_\alpha}{\beta_1 + \beta_2 \ldots + \beta_n} \qquad (3\text{-}38)$$

$$\widetilde{c''^2_\alpha} = \frac{\tilde{c}_\alpha (1 - \tilde{c}_\alpha)}{\beta_1 + \beta_2 \ldots + \beta_n + 1} \qquad (3\text{-}39)$$

This representation requires the solution of transport equations for the mean of n-1 scalars plus an additional equation for a turbulent scalar energy, Q, which is defined as:

$$Q = \sum_{\alpha=1}^{n} \widetilde{c''^2_\alpha} = \frac{1 - S}{\beta_1 + \beta_2 \ldots + \beta_n + 1} \qquad (3\text{-}40)$$

where S is:

$$S = \sum_{\alpha=1}^{n} \tilde{c}_\alpha^2 \qquad (3\text{-}41)$$

Using Equations (3-38) and (3-40) then one can obtain the parameters:

$$\beta_\alpha = \tilde{c}_\alpha \left(\frac{1 - S}{Q} - 1 \right) \qquad (3\text{-}42)$$

The variance and cross-covariance are then implied by the model such that:

$$\widetilde{c''^2_\alpha} = Q\frac{\tilde{c}_\alpha(1-\tilde{c}_\alpha)}{1-S} \qquad (3\text{-}43)$$

$$\widetilde{c''_\alpha c''_\theta} = -Q\frac{\tilde{c}_\alpha \tilde{c}_\theta}{1-S} \qquad (3\text{-}44)$$

The disadvantages to this approach lie in the fact that it has not yet been experimentally validated and that the pdf of the reaction progress variable is primarily bimodal. The β function pdf does not accommodate this condition satisfactorily since it is very difficult to integrate numerically. Girimaji (1991) does however validate the β function pdf for two-scalar mixing comparing it to direct numerical simulation computations by Eswaran and Pope (1988). This comparison shows excellent results with the β function approaching a Gaussian style pdf about the mean of the mixture as the variance drops in a similar fashion to the DNS calculations. With this in mind the β function pdf is ideal for the mixture fraction.

We have adopted an uncoupled approach with a β function pdf for the mixture fraction and utilised the same averaging techniques over the reaction progress variable as implemented in the three combustion models earlier for constant mixture fraction.

Both temperature and density also need to be averaged over mixture fraction space. As reported earlier, for the constant mixture fraction case, both the temperature and density were simply related to the mean reaction progress variable.

$$\frac{\tilde{T}}{T_r} = 1+\tau\tilde{c} \qquad (3\text{-}45)$$

$$\frac{\rho}{\rho_r} = \frac{1}{1+\tau\tilde{c}} \qquad (3\text{-}46)$$

The heat release parameter τ was defined by setting the Favre mean temperature to the temperature of the fully burnt products when the Favre mean reaction progress variable was equal to unity. However the temperature of the fully burnt products, which was assumed to be the adiabatic flame temperature, is now a function of mixture fraction. Thus the heat release parameter is also a function of the mixture fraction.

Thus, for the variable mixture fraction calculations, the mean temperature was determined from the following relationship:

$$\tilde{T} = \int_0^1 \int_0^1 T(c,f)\tilde{P}(c,f)dcdf \qquad (3\text{-}47)$$

$$\tilde{T} = \int_0^1 \int_0^1 T_r(1+\tau(f)c)\tilde{P}(c,f)dcdf \qquad (3\text{-}48)$$

$$\tilde{T} = T_r \int_0^1 \int_0^1 (1+\tau(f)c)\tilde{P}(c)\tilde{P}(f)dcdf \qquad (3\text{-}49)$$

$$\frac{\tilde{T}}{T_r} = \int_0^1 (1+\tau\tilde{c})\tilde{P}(f)df \qquad (3\text{-}50)$$

and similarly for the mean density:

$$\frac{\overline{\rho}}{\rho_r} = \int_0^1 \left(\frac{1}{1+\tau\tilde{c}}\right)\tilde{P}(f)df \qquad (3\text{-}51)$$

Additionally there are terms within the second moment turbulence model which need to be modified to account for the non-uniform mixture. As with the temperature and density, models for $\overline{u''}$ and $\overline{c''}$ from Equations (2-71) and (2-76) respectively, include the heat release parameter.

Extending Equation (2-71) for flows with a variable mixture fraction one obtains:

$$\overline{u''} = \frac{\overline{\rho u'' c''}}{\rho_r} \int_0^1 \tau(f)P(f)df \qquad (3\text{-}52)$$

$$\overline{u''} = \frac{\tilde{\tau}\overline{\rho u'' c''}}{\rho_r} \qquad (3\text{-}53)$$

Similarly Equation (2-76) for the Reynolds averaged Favre fluctuation of the reaction progress variable, $\overline{c''}$, is modelled as:

$$\overline{c''} = \frac{\bar{\rho}}{\rho_r} \int_0^1 \int_0^1 (1+\tau c)(c-\tilde{c})\tilde{P}(c)\tilde{P}(f)dfdc \qquad (3\text{-}54)$$

If we assume infinitely fast chemistry, such that the pdf of the reaction progress variable simplifies to two delta functions at c=0 and c=1, then this equation simplifies to:

$$\overline{c''} = \frac{\tilde{\tau}\tilde{c}(1-\tilde{c})}{1+\tilde{\tau}\tilde{c}} \qquad (3\text{-}55)$$

This is the formulation proposed by Bray and Moss (1977) and was applied to both the Eddy Break-up model and the Crossing Frequency model. Equation (3-54) was used for the Presumed pdf model.

In order to determine the presumed pdf of mixture fraction both the mean and variance of the mixture fraction must be calculated. The mixture fraction is a conserved scalar such that the transport equations for its mean and its variance at high Reynolds number may be written:

$$\frac{\partial\left(\bar{\rho}\tilde{u}_j\tilde{f}\right)}{\partial x_j} = \frac{\partial\left(-\overline{\rho u_j'' f''}\right)}{\partial x_j} \qquad (3\text{-}56)$$

$$\frac{\partial\bar{\rho}\tilde{u}_j\widetilde{f''^2}}{\partial x_j} = \frac{\partial(-\overline{\rho u_j'' f''^2})}{\partial x_j} - 2\overline{\rho u_j'' f''}\frac{\partial\tilde{f}}{\partial x_j} - 2\rho\mathcal{D}\overline{\frac{\partial f''}{\partial x_j}\frac{\partial f''}{\partial x_j}} \qquad (3\text{-}57)$$

where all of the terms on the right hand side of these two equations may be modelled in an identical fashion to the transport equations for the mean and variance of the reaction progress variable (cf. Equations (2-34) and (3-17)).

The closure of the scalar flux term in Equations (3-56) and (3-57) was conducted in a similar fashion to those of the reaction progress variable. For the second moment turbulence model the general form of the transport equation for the scalar flux is similar to that of the reaction progress variable (Equation (2-72)) minus the chemistry source term. The only other difference in the modelling between these two equations lies in the source term for the interaction between the pressure gradient and the density inhomogeneity. In this term the Reynolds averaged Favre fluctuation of the mixture fraction is modelled as:

$$\overline{f''} = \frac{\bar{\rho}}{\rho_r} \int_0^1 \int_0^1 (1+\tau c)(f-\tilde{f})\tilde{P}(f)\tilde{P}(c)dfdc \qquad (3\text{-}58)$$

which reduces to:

$$\overline{f''} = \frac{\tilde{f''}}{1+\tilde{\tau}\tilde{c}} + \frac{1}{1+\tilde{\tau}\tilde{c}} \int_0^1 \tau(f-\tilde{f})\tilde{P}(f)df \qquad (3\text{-}59)$$

for the Eddy Break-up and Crossing Frequency models which both assume infinitely fast chemistry.

3.5 NO_x Model

As was discussed earlier oxides of nitrogen in lean premixed flames are believed to be formed by one of three main routes: the thermal NO mechanism, the prompt NO mechanism, and the nitrous oxide route. It is not known how much importance the nitrous oxide route has for lean premixed gas turbine combustors. This mechanism has also not been well investigated in terms of turbulent combustion modelling and so it will not be considered here.

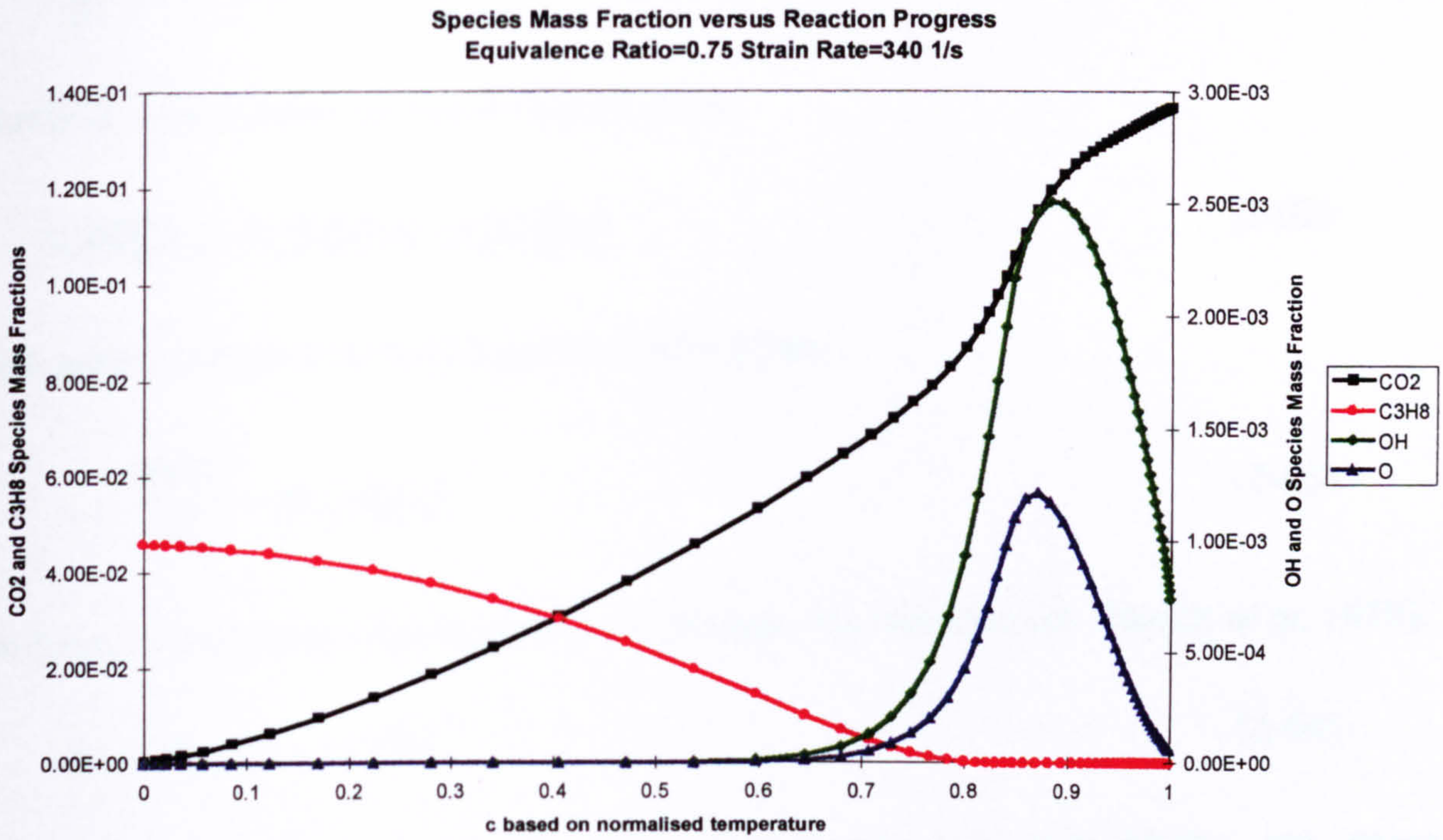

Figure 3.5.1 Species Mass Fraction versus Reaction Progress Variable

In order to solve for the formation rate of NO for Zeldovich NO_x many researchers make the assumption that the temperature and O, OH and N radical concentration may be considered to be in equilibrium. This is especially true of gas turbine conditions where the pressures and temperatures are high. This assumption however, tends to underpredict the formation rate of NO by this mechanism especially during the initial phases of NO formation when the radical concentrations are not near equilibrium. Figure 3.5.1 shows mass fractions of various species against reaction progress variable based on normalised flame temperature for a burnt-to-unburnt laminar flame calculation of a propane-air mixture. O and OH species peak before dropping to their equilibrium values. Miller (1989) points out that despite this the quantitative rates of formation during the early stages of the reaction are very low so that the net underprediction is modest when compared with the total concentration of NO formed. As combustors are deigned for lower and lower emissions this is possibly a factor which will be more important in the future.

Based on the reaction mechanism of Equations (2-1) through (2-3) and assuming that the concentration of NO is sufficiently small that the reverse reactions can be ignored (Jones and Pridden, 1978).

$$\frac{d[NO]}{dt} = k_1[O][N_2] + k_2[N][O_2] + k_3[N][OH] \qquad (3\text{-}60)$$

$$\frac{d[N]}{dt} = k_1[O][N_2] - k_2[N][O_2] - k_3[N][OH] \qquad (3\text{-}61)$$

assuming steady state for the N radical gives:

$$k_2[N][O_2] + k_3[N][OH] = k_1[O][N_2] \qquad (3\text{-}62)$$

which when substituted into Equation (3-60) gives:

$$\therefore \quad \frac{d[NO]}{dt} = 2k_1[O][N_2] \qquad (3\text{-}63)$$

The oxygen radical can be related to O_2 through the reaction (cf. Baulch *et al*, 1976):

$$O_2 + M \Leftrightarrow O + O + M \qquad (3\text{-}64)$$

where the forward and reverse rate coefficients, assuming $M=O_2$, are given respectively by (Baulch *et al*, 1976):

$$k_f = 9.8 \times 10^{18} T^{-2.5} \exp\left(\frac{-59380}{T}\right) \quad \frac{m^3}{mole\ s} \qquad (3\text{-}65)$$

$$k_r = 4.7 \times 10^{11} T^{-2.5} \quad \frac{m^6}{mole^2\ s} \qquad (3\text{-}66)$$

where T is temperature in K.

The rate of formation of the O radical is then:

$$\frac{d[O]}{dt} = k_f[O_2][M] - k_r[O]^2[M] \qquad (3\text{-}67)$$

Assuming equilibrium then:

$$\frac{d[O]}{dt} = 0 \tag{3-68}$$

thus:

$$[O] = \sqrt{\frac{k_f}{k_r}}[O_2]^{1/2} = K_c[O_2]^{1/2} \tag{3-69}$$

where K_c is the equilibrium constant:

$$\frac{d[NO]}{dt} = 2k_1K_c[O_2]^{1/2}[N_2] \tag{3-70}$$

The molar concentration of oxygen can be related to the reaction progress variable through a modified version of Equation (3-11) to account for the existence of NO:

$$[O_2] = \rho Y_{CO_2}^{c=1} Y_{NO}^{c=1}\left(\frac{5}{\phi m_T Y_{CO_2}^{c=1} Y_{NO}^{c=1}} - \frac{5}{3w_{CO_2} Y_{NO}^{c=1}}c - \frac{1}{2w_{NO} Y_{CO_2}^{c=1}}c_{NO}\right) \tag{3-71}$$

where $Y_{NO}^{c=1}$ is the equilibrium concentration of NO which was determined from the NASA equilibrium code (Gordon and Mc Bride, 1971), m_T is defined by Equation (3-12), w_{NO} is the molecular mass of NO and c_{NO} is the progress variable of the reactions for the formation of NO. Similarly:

$$[N_2] = \rho Y_{NO}^{c=1}\left(\frac{18.8}{\phi m_T Y_{NO}^{c=1}} - \frac{1}{w_{NO}}c_{NO}\right) \tag{3-72}$$

Inserting Equations (3-71) and (3-72) into the right hand side of Equation (3-70), normalising the molar concentration of NO on the left side to put it in terms of the progress variable c_{NO} and making the assumption that $Y_{NO}^{c=1}$ is independent of time one obtains the reaction rate $w_{c_{NO}}$ for Equation (2-59):

$$w_{C_{NO}} = \frac{dc_{NO}}{dt} = 6.94 \times 10^{11} \exp\left(\frac{-68140}{T}\right) w_{NO} \sqrt{\rho Y_{CO_2}^{c=1} Y_{NO}^{c=1}}$$

$$\times \left(\frac{5}{\phi m_T Y_{CO_2}^{c=1} Y_{NO}^{c=1}} - \frac{5}{3 w_{CO_2} Y_{NO}^{c=1}} c - \frac{1}{2 w_{NO} Y_{CO_2}^{c=1}} c_{NO}\right)^{1/2} \left(\frac{18.8}{\phi m_T Y_{NO}^{c=1}} - \frac{1}{w_{NO}} c_{NO}\right) \tag{3-73}$$

Prompt NO unlike thermal NO forms quickly in the flame front. Thus a fast chemistry model is required to predict its formation rate. There are two potential ways to do this. One is to compute the full NO chemistry within the laminar flamelet calculations. The mean source term for the formation rate of NO could then be closed with a presumed pdf approach. Since we decided against computing laminar flamelets for our detailed chemistry model, this was not an option. Dupont *et al* (1993a, 1993b) have proposed an alternate approach which involves making several assumptions on the main reaction mechanism (Equations (2-7) through (2-10)). They have considered the first reaction (Equation (2-7)) to be the rate limiting step. Assuming OH and O are in partial equilibrium and proposing a mechanism for the formation of CH they obtain an expression for the rate of formation of NO by this mechanism for methane fuel. Dupont *et al* (1993a, 1993b) raise several questions concerning the validity of their assumptions not the least the validity of assuming equilibrium for the O and OH radicals near the flame front. This will be much more important for prompt NO because most of the reaction takes place within the flame front. Thus for this reason we decided to consider only the thermal NO mechanism.

For calculations made with a non-uniform reactant mixture the mean chemical source for NO production, $\tilde{w}_{C_{NO}}$, was determined in a similar fashion to the chemical source term for the main heat release. The joint pdf of c, c_{NO}, and f $\tilde{P}(c, c_{NO}, f)$ which replaces $\tilde{P}(c, c_{NO})$ in Equation (2-59) was determined from the assumption the f was uncoupled from the other two:

$$\tilde{P}(c, c_{NO}, f) = \tilde{P}(c, c_{NO})\tilde{P}(f) = \tilde{P}(c_{NO} | c = 1)\tilde{P}(f) \tag{3-74}$$

where $\tilde{P}(f)$ is the same as that used for the combustion models.

4 Model Evaluation on Simple Geometries

4.0 Introduction

In order to systematically evaluate the combustion models comparisons have been made in the framework of a simple geometry. A large number of primarily two dimensional ducted turbulent premixed combustion experiments have been performed over the last three decades. Most have focused on bluff-body or sudden expansion stabilised flames. Some examples of these were conducted by Howe *et al* (1963), Stull *et al* (1974), Ganji *et al* (1980), Pitz *et al* (1981, 1983), Proctor II *et al* (1987b) and Sjunnesson *et al* (1991a, 1991b). Others have examined swirl stabilised flames, for example Hillemanns *et al* (1988) and Philipp *et al* (1992), however less measurement data are available in the literature from these configurations. A few experiments have also been conducted in flows with pilot stabilised flames (Moreau, 1974, 1977, Moreau *et al*, 1976, 1980).

From the standpoint of Reynolds averaged CFD prediction, an underlying difficulty with bluff-body or sudden expansion stabilised flames is that the general flow field is often characterised by large coherent eddies. These eddies can be clearly seen in the Schlieren photographs (Figure 4.0.1) from the Pitz and Daily (1981) backward facing step experiment. They have also been noted to be present in high Reynolds number cold flows across backward facing steps (Lasher *et al*, 1992, Eaton *et al*, 1981). Steady state calculations of such phenomena tend to underpredict the degree of mixing within the shear layer and hence, in mixing limited combustion, the rate of reaction. Hsiao *et al* (1984) attempted to predict the backward facing step stabilised flame experiment of Ganji *et al* (1980) using a rather elaborate random vortex method in place of a standard turbulence closure which allowed them to solve the Navier Stokes equations without averaging. They solved for combustion by assuming that the flame front could be discritised into small line segments each of which were thinner than the smallest grid cell. The orientation of the flame front was then determined based on the value of the reaction progress variable within each cell and its surrounding neighbours. The flame front is then displaced according to turbulence and volumetric expansion. Hsiao *et al* (1984) concluded that the flowfield was dominated by large scale eddies which assisted the flame front to spread across the duct. Other researchers (Olovsson, 1992, Lindstedt and Vaos, 1995, Fureby *et al*, 1995) using somewhat simpler steady state models reported an inability to capture the flame front spreading for similar flows. Despite this largely unfavourable background, the configuration and the understanding of the flowfield derived from so

many experiments make it a useful test problem for evaluating alternative combustion model implementations. We have therefore also attempted to compute the backward facing step experiment of Pitz and Daily (1981, 1983) and bluff body experiment of Howe and Shipman (1963) using the models described in Chapter 3. One can see from Figures 4.0.2 and 4.0.3 that the turbulence intensity is substantially underpredicted in both the cold and combusting calculations of the backward facing step. From Figure 4.0.4 we observe that the experimental velocity profile recovers much faster than the predictions due to the greater degree of mixing caused by the large eddies. Figure 4.1.2.9 illustrates the underprediction of the flame front spreading by the experiment in the wake of a bluff body.

In reviewing these calculations, ducted flows also provide two additional features which have been found to strongly influence the flame front spreading rate. The first is acoustic interaction which can play a significant role even for small flame holders (Lewis and Moss, 1979). The second is a strong induced axial pressure gradient which may give rise to enhanced counter-gradient transport. This latter feature was noted in a backward facing step experiment by Shepherd *et al* (1982) which did not appear to contain coherent eddy structures and yet produced a high rate of flame spreading across the duct from a small step height.

The existence of large coherent structures in most of these experiments has tended to direct the modelling effort of such flows towards transient calculations. Recently, Olovsson (1992), Lindstedt and Vaos (1995) and Fureby *et al* (1995) have employed either transient Reynolds stress model calculations or large eddy simulation to capture the large coherent structures and improve their predictions of the effective reaction rate in bluff-body stabilised flames.

Earlier researchers, for example Mason and Spalding (1973), circumvented the shedding problem by starting their calculation downstream of the flame holder and prescribing the inlet levels of turbulence.

Since the primary objective of this thesis is to investigate the application of steady state models to a practical lean prevaporised premixed combustor, no attempt has been made to reproduce the transient behaviour of these two dimensional geometries. Rather they will be used as a convenient framework to compare the various models being investigated.

With this in mind, the Pitz and Daily (1981, 1983) experiment was chosen as the basis for a comparison of the combustion models because of the large amount of experimental data associated with it. The experiment of Moreau *et al* (Moreau, 1974, 1977, Moreau *et al*, 1976, 1980) was selected as a test of the NOx model since it contains measurements of NOx concentrations.

a) $Re_H = 1.5 \times 10^4$, $\tau_{exp} = 74\mu s$

Figure 4.0.1 Schlieren Photographs from the Pitz and Daily (1981) Experiment

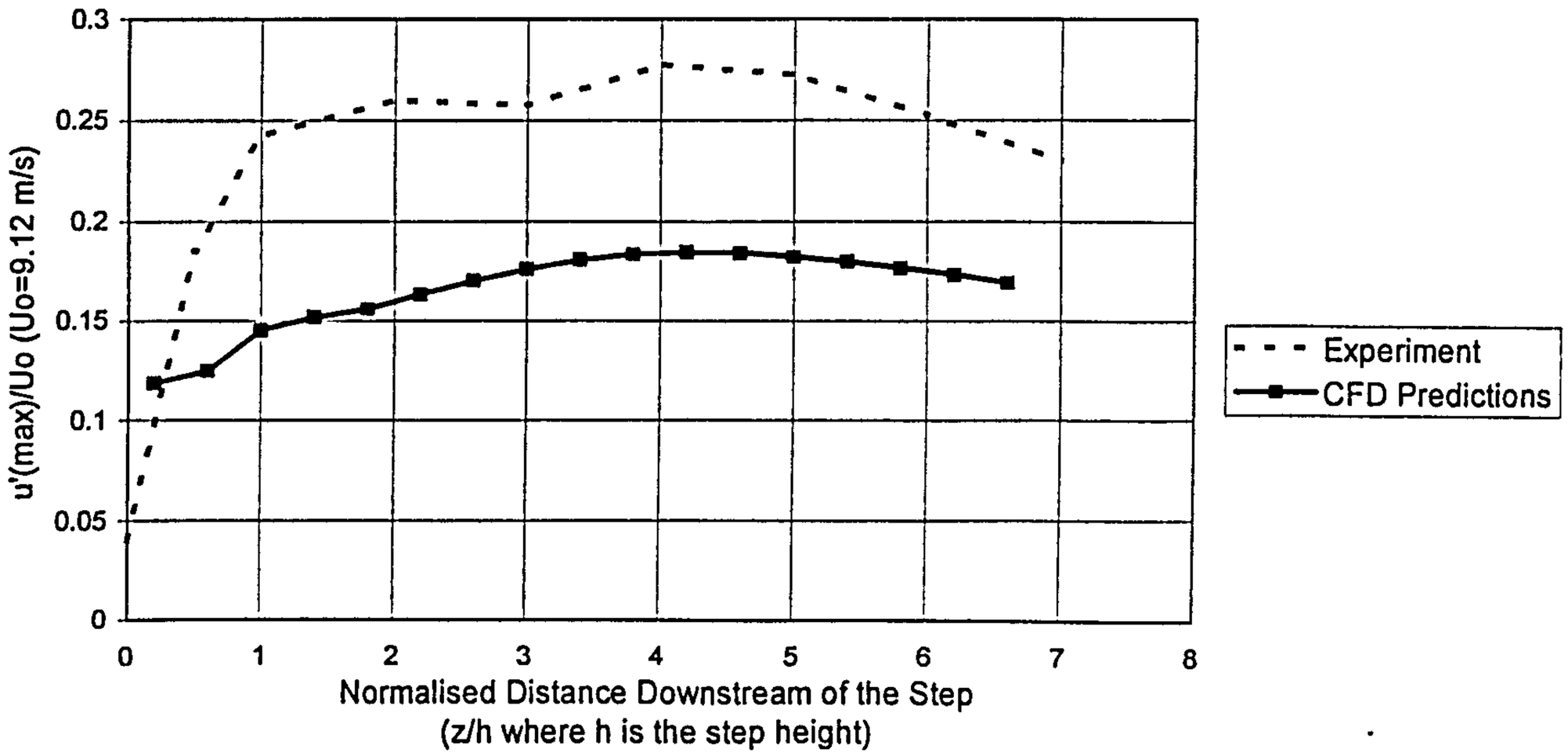

Figure 4.0.2 Axial Variation of Local Peak Turbulence Intensity (Cold Flow)

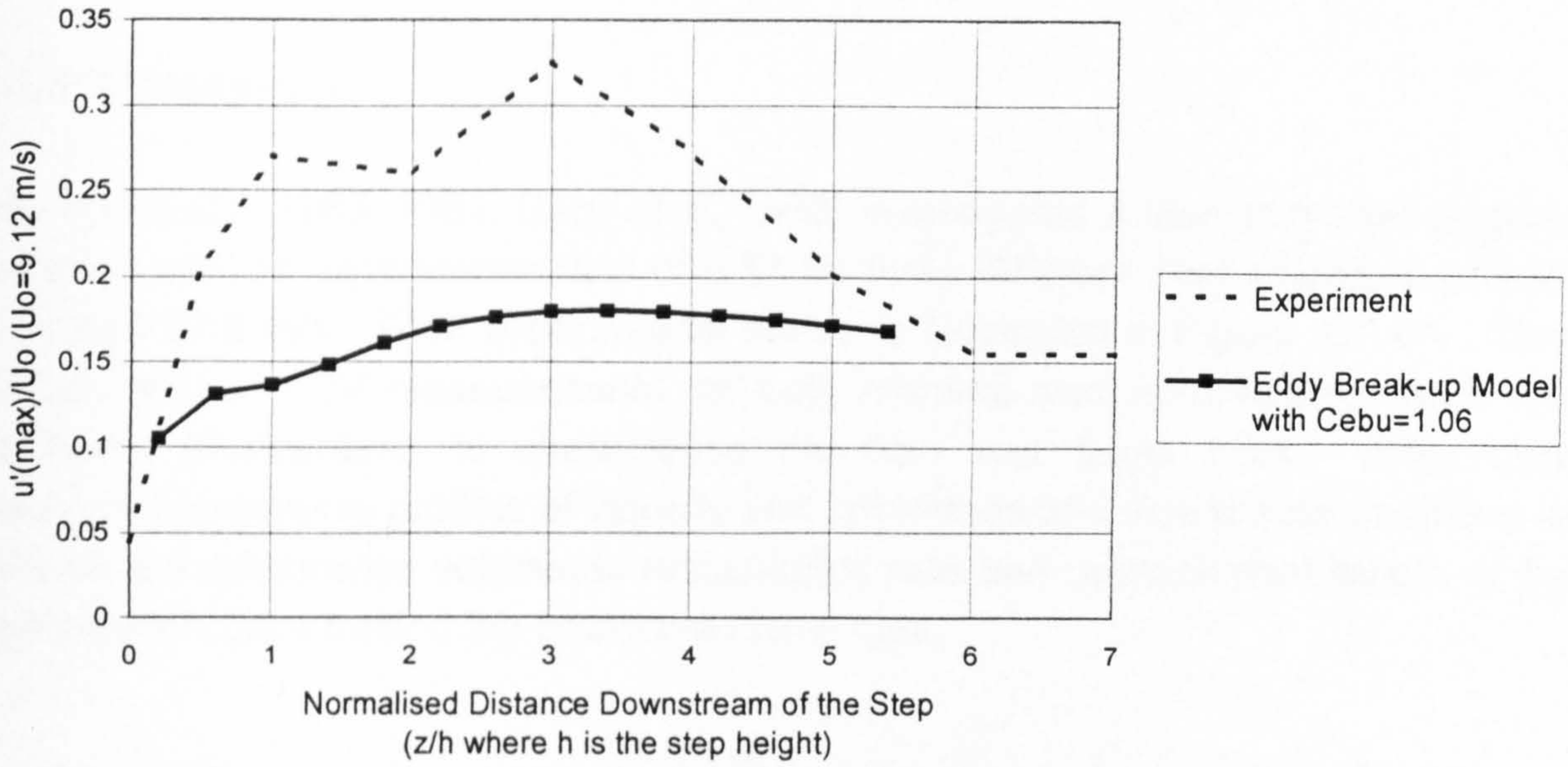

Figure 4.0.3 Axial Variation of Local Peak Turbulence Intensity (Combusting Flow)

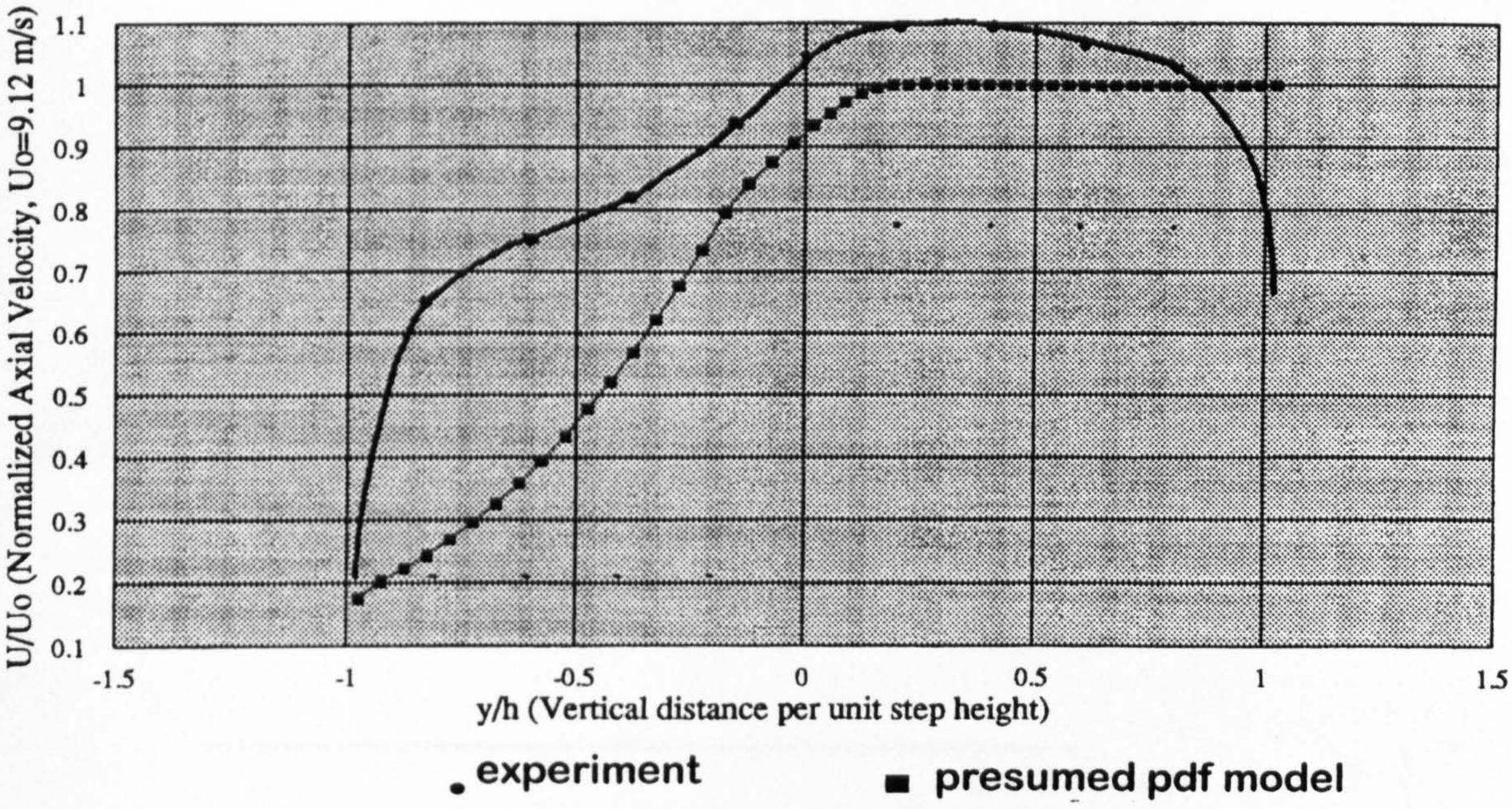

Figure 4.0.4 Transverse Distribution of Axial Velocity
6 Step Heights Downstream of the Sudden Expansion

4.1 Comparison of the Combustion Models

4.1.1 Introduction

Pitz and Daily (1983, 1981, Ganji *et al*, 1980) investigated a lean premixed propane air flame with an equivalence ratio of 0.57 for three different inlet velocities of 9.12, 13.3 and 22.2 m/s. Their experimental set-up is illustrated in Figure 4.1.1.1. They report detailed LDV measurements on both reacting and non-reacting flows and Schlieren photographs to characterise the flow and flame front. They have measured transverse profiles of velocity and turbulence at discrete axial positions as well as the streamwise volumetric recirculation rate and reattachment length of the recirculation zone behind the backward facing step.

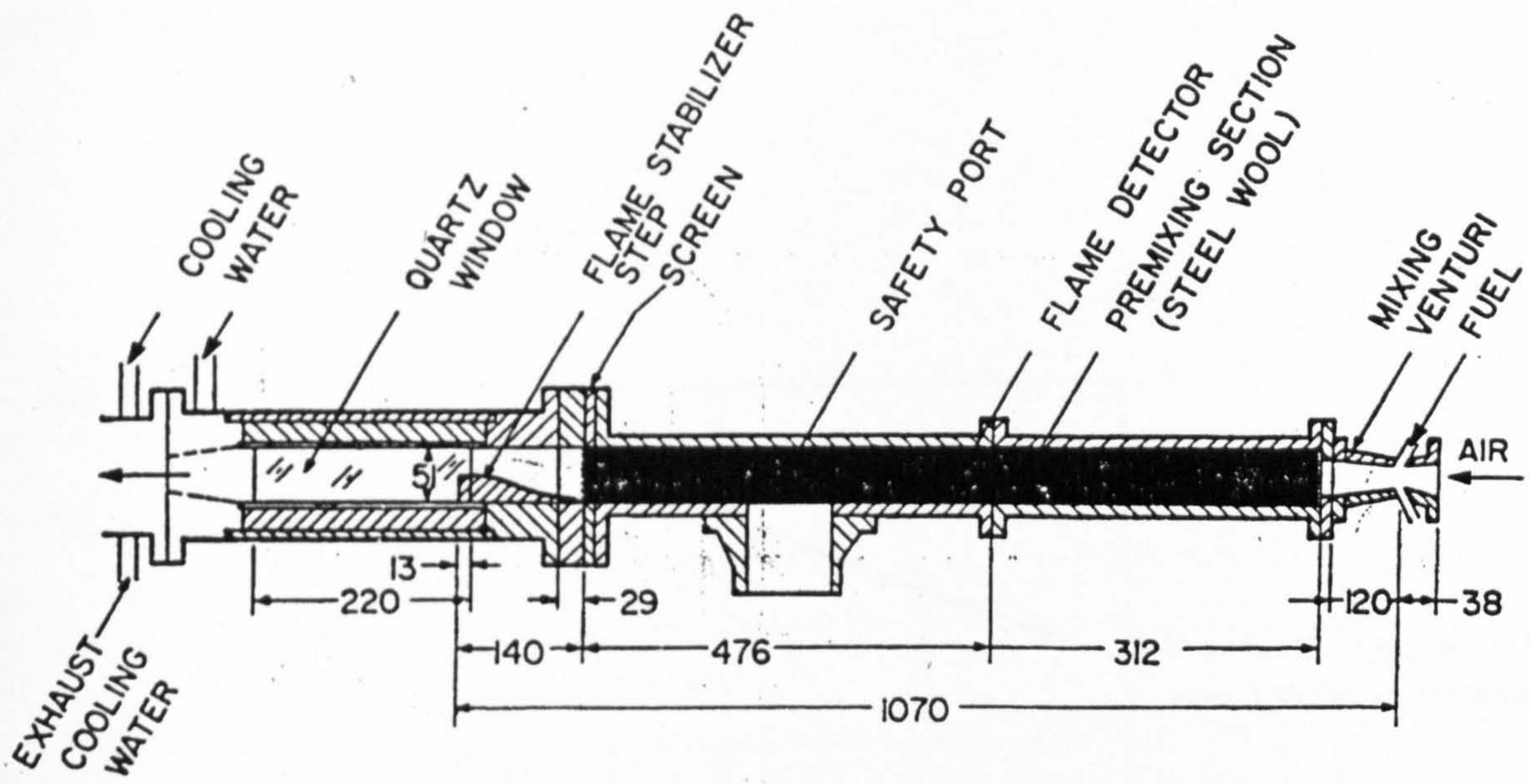

Figure 4.1.1.1a Pitz and Daily Experimental Set-up
(all dimensions in mm)

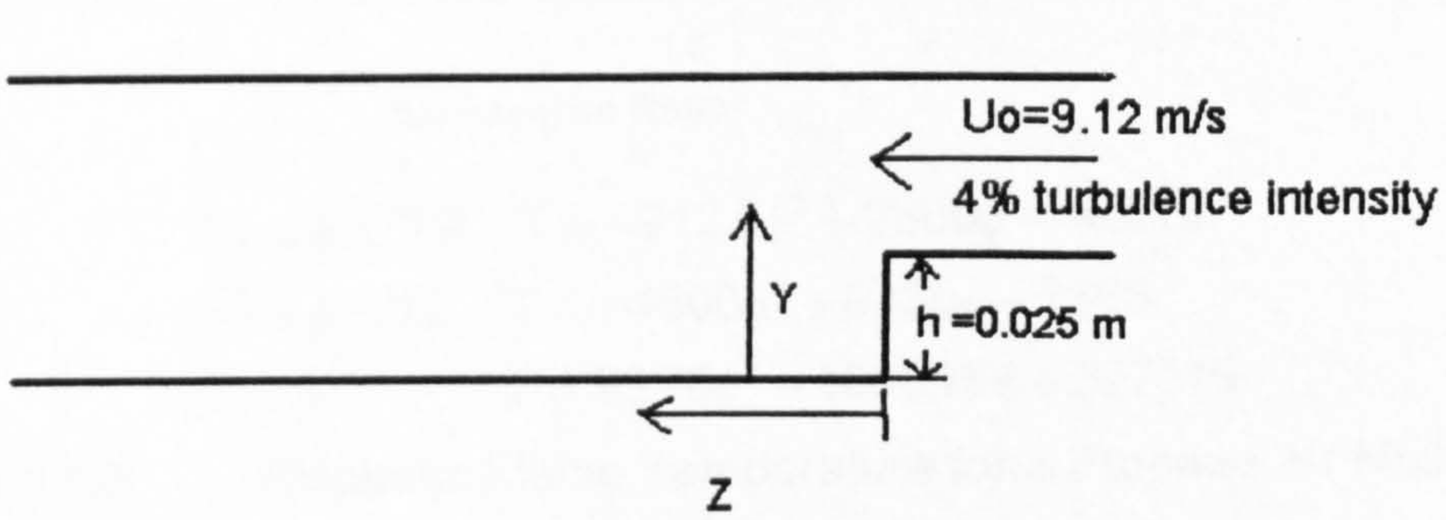

Figure 4.1.1.1b Pitz and Daily Experiment Calculation Domain

The specific condition investigated here is that of the inlet velocity (Uo) of 9.12 m/s since this appeared to exhibit the most uniform profile of inlet turbulence intensity ($u'/Uo = 0.04$).

All the calculations on this geometry were performed with the k-ε turbulence model. Hybrid differencing was employed and no sensitivity analysis to the differencing scheme was carried out.

Cold calculations were first conducted to establish a suitable grid. These were followed by combusting calculations with both the Eddy Break-up and Presumed pdf combustion models. Combustion was assumed to be adiabatic in all cases and the relationship between adiabatic flame temperature and mixture strength was computed using the NASA equilibrium program (Gordon and Mc Bride, 1971) (cf. Figure 4.1.1.2).

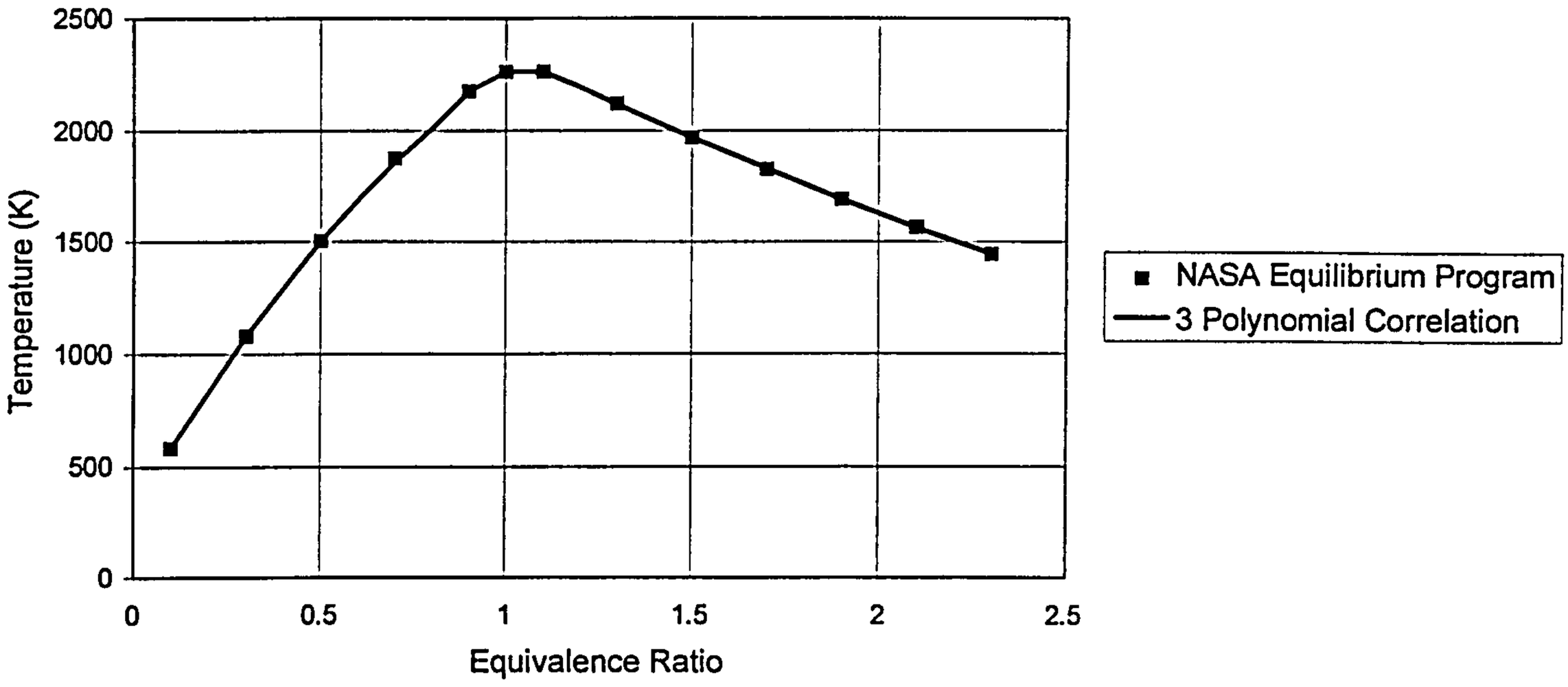

$0.0 \leq \phi \prec 0.9 \quad T = -912.5\phi^2 + 2860\phi + 302.13$

$0.9 \leq \phi \prec 1.2 \quad T = -4500\phi^2 + 9430\phi - 2666$

$1.2 \leq \phi \quad T = 93.75\phi^2 - 1008.75\phi + 3271.19$

Figure 4.1.1.2 Adiabatic Flame Temperature for a Propane Air Mixture with To=298 K Po=1 atm

4.1.2.1 Cold Flow Predictions

In order to gain some insight into the sensitivity of this flowfield to mesh density, two dimensional cold flow predictions were conducted using the three grids illustrated in Figures 4.1.2.1 to 4.1.2.3. The first two of these grids simply introduce a variation in the density of cells present. The third grid further modified the higher density grid by making additional refinement on top of the step and a reduction in the grid density near the exit of the domain. For all cases standard wall functions were applied to all surfaces and the inlet velocity and root mean square turbulence intensity were assumed to be uniform across the duct at values of 9.12 m/s and 4% respectively. The inlet conditions were set at 3.8 inlet duct widths upstream of the sudden expansion. A fixed static pressure was assumed at the exit which was set at 11.8 duct widths downstream of the sudden expansion.

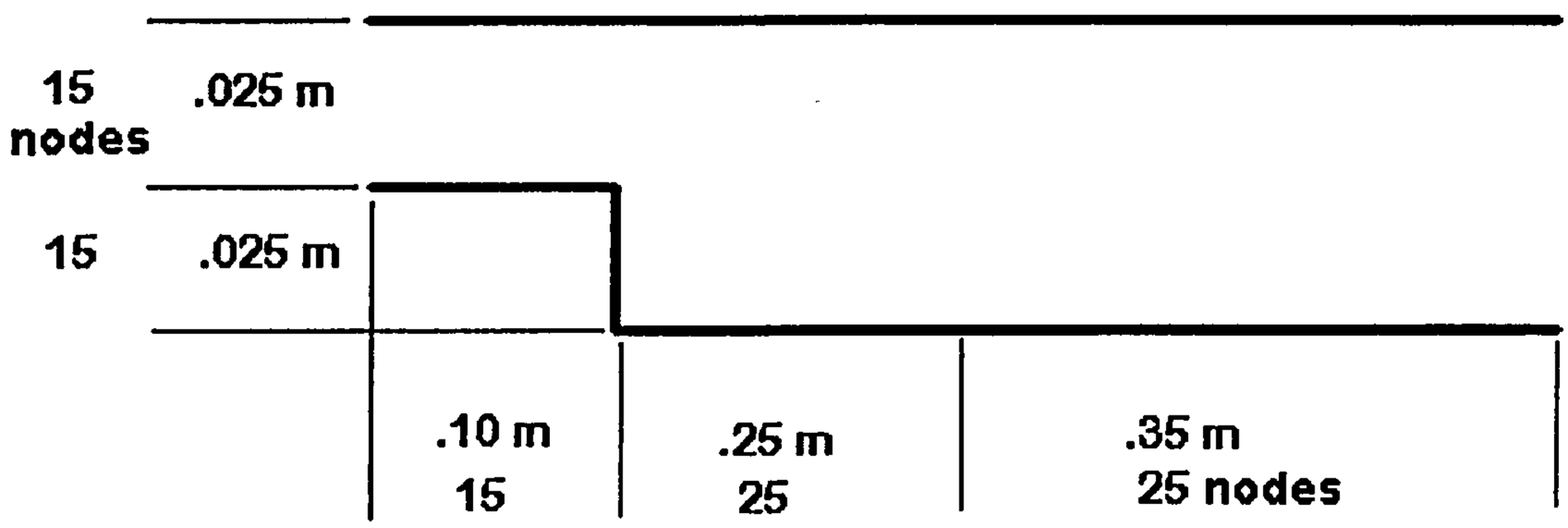

Figure 4.1.2.1 Low Density Grid (30×65)

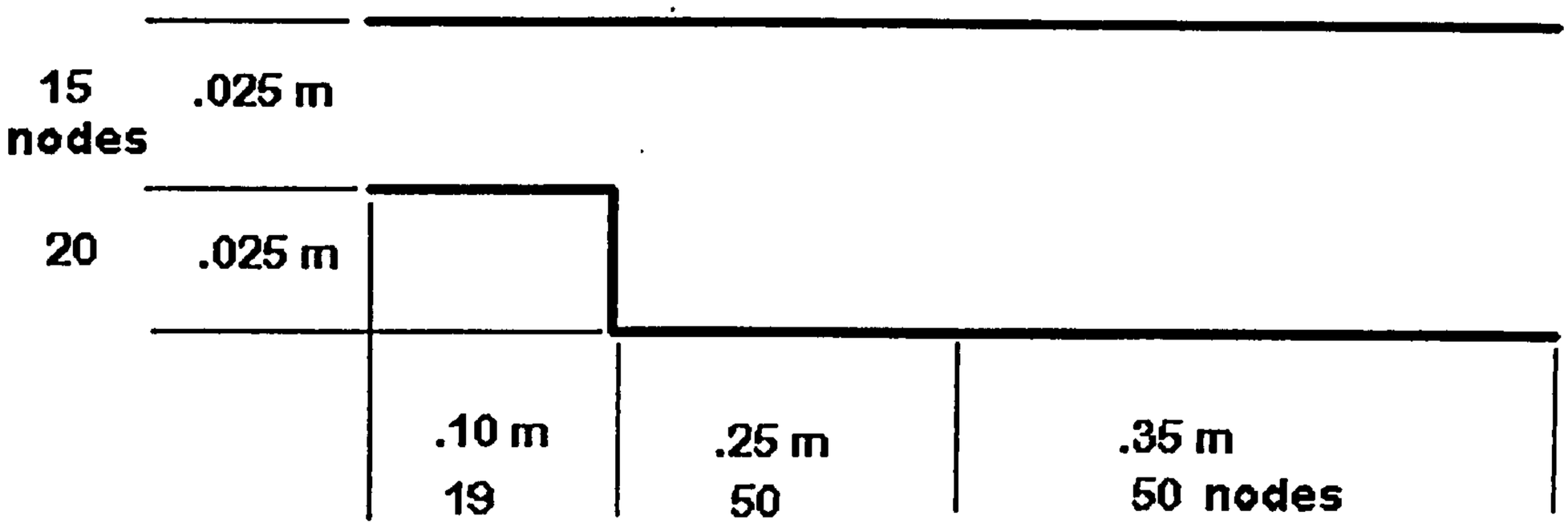

Figure 4.1.2.2 High Density Grid (35×119)

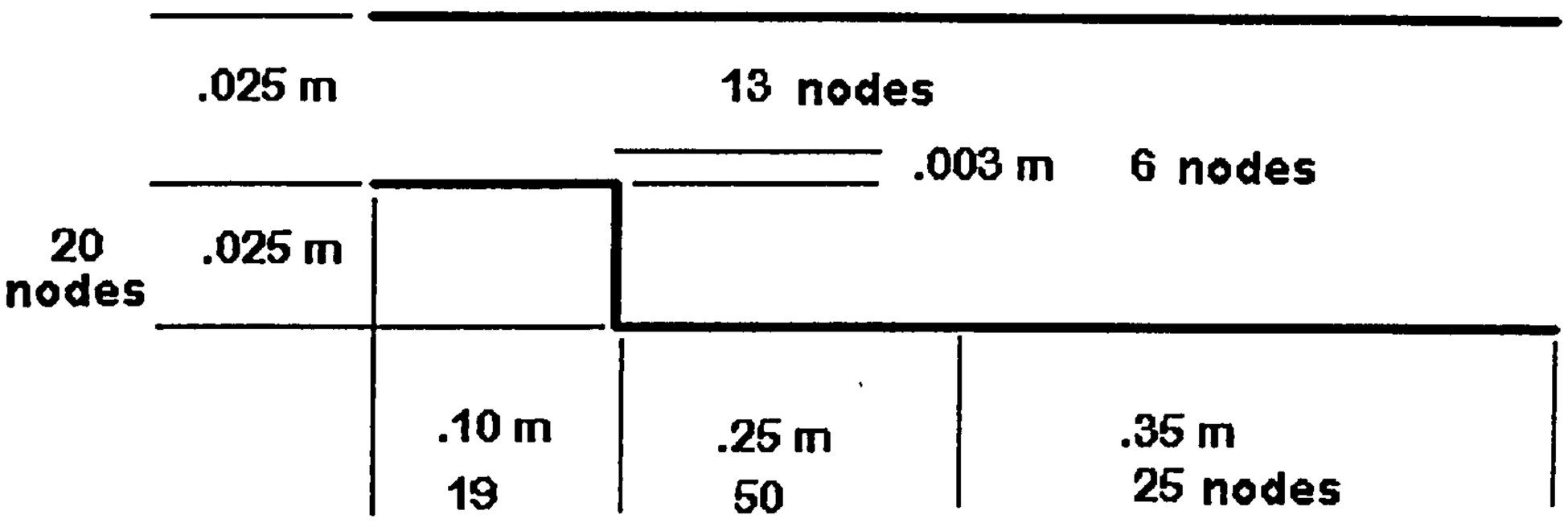

Figure 4.1.2.3 Refined Boundary Layer Grid (39×94)

Generally speaking, the global features of the flow field were captured by all of the predictions. A plot of the velocity vectors along with the measured velocities can be seen in Figure 4.1.2.4. The boundary layer next to the lower wall, downstream from the step, appears to be under predicted by the calculations.

More critically, Table 4.1.2.1 lists the predicted and measured values of the reattachment length. Both the high density grid and the refined boundary layer grid over predict the reattachment length. In fact, the greater the refinement, the greater the over prediction. The low density grid, which will be more numerically diffusive, under predicted the recirculation length slightly. Although the trend that the reattachment length should increase with increasing grid refinement is not unexpected the overprediction of this relative to the experimental measurements with the k-ε turbulence model is unusual. Typically predictions made with the k-ε turbulence model tend to underpredict the recirculation length by up to 30% (Chieng *et al*, 1980, Autret *et al*, 1988). This underprediction gets worse as the ratio of the step height to channel width becomes smaller because the pressure drop is smaller and the correct prediction of the turbulence becomes more important (Lasher *et al*, 1992). The fact that the recirculation length is overpredicted in our calculations indicates that there is a process occurring within the experiment which is enhancing

the mixing above that predicted. This is likely due to vortex shedding and large coherent structures within the flow.

Comparisons were also made with the measured maximum negative velocity within the recirculation zone and the peak velocity fluctuations. Both of these values can be seen normalised by the mean inlet velocity in Figures 4.1.2.5 and 4.1.2.6. The strength of the recirculation is under predicted for all of the cases, but the axial location of the peak appears to best predicted by the grid with the refined boundary layer. The coarser grid appears to increase slightly the magnitude of the maximum reverse flow velocity and to displace the peak closer to the step. The maximum turbulence intensity is over predicted next to the step but seriously under predicted further downstream. The grid refinement does not have a significant impact on this parameter away from the step. However in the near vicinity of the step the refined boundary layer grid tends to agree slightly better with the experiment.

In general, the underprediction of the peak velocity fluctuation once again gives evidence that coherent structures exist within the flow. Figure 4.0.1 shows two Schlieren photographs taken from the experiment of this case. One can make out clearly large vortex structures in the wake of the step which will be responsible for the measured increase in the turbulence intensity. As was discussed earlier these features are not predicted by the steady state k-ε turbulence model.

Recirculation Length per unit Step

		Length (/h)	% error
Cold	Experiment	6.50	
	High Density Grid	6.59	1.32%
	Refined Boundary Layer	7.04	8.36%
	Low Density Grid	6.47	0.49%
Hot	Experiment	4.55	
	C_{EBU}=1.06	5.17	13.55%
	C_{EBU}=2.12	3.73	17.98%
	C_{EBU}=2.12b	3.83	15.72%
	C_{EBU}=3.18	2.63	42.16%
	Pres. PDF Bray-Moss 5*WWE84	3.66	19.57%

Note: b - case without wall function on upper wall

Table 4.1.2.1 Normalised Reattachment Length
(h is the step height)

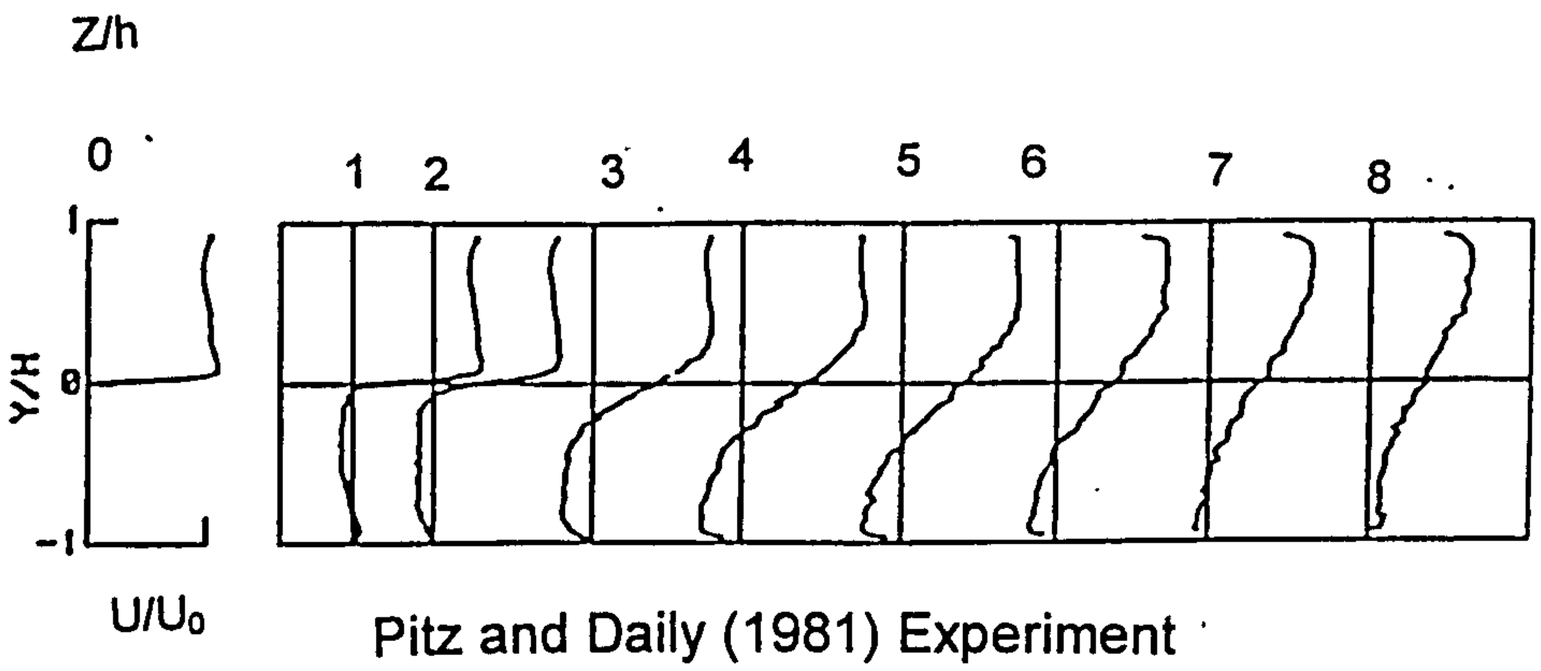

Pitz and Daily (1981) Experiment

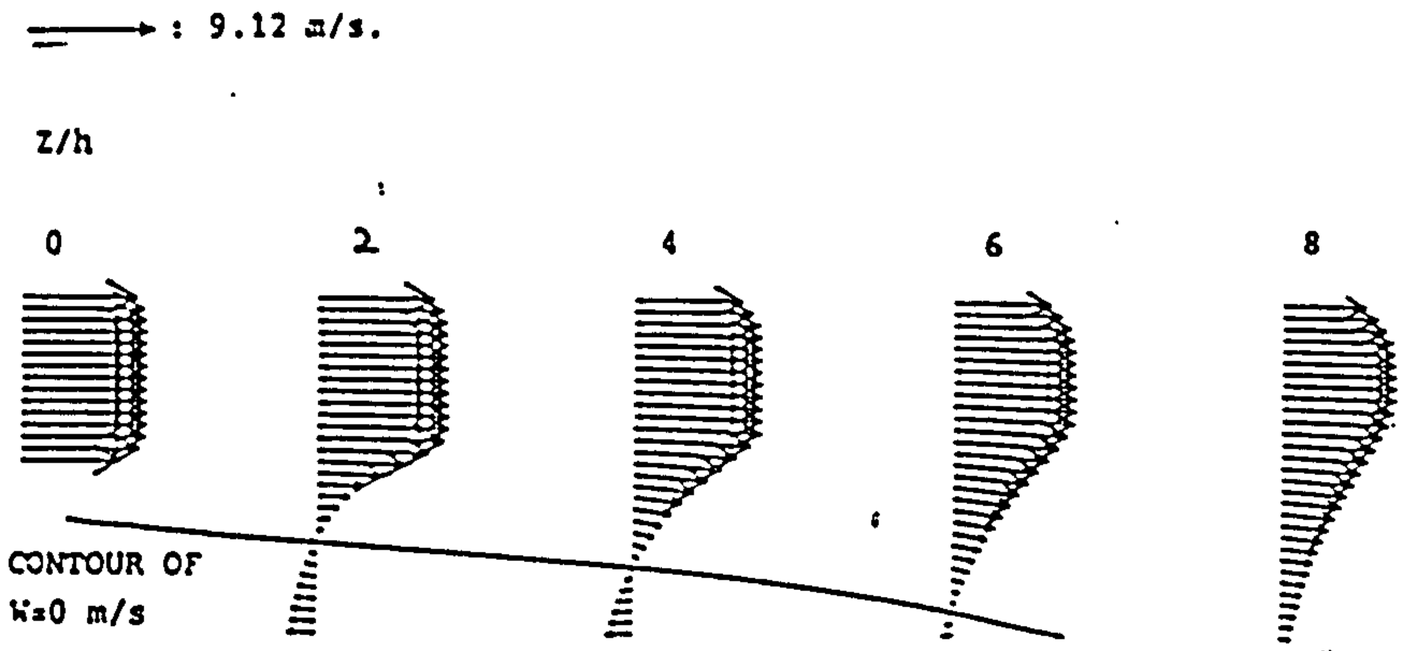

Low Density Gird

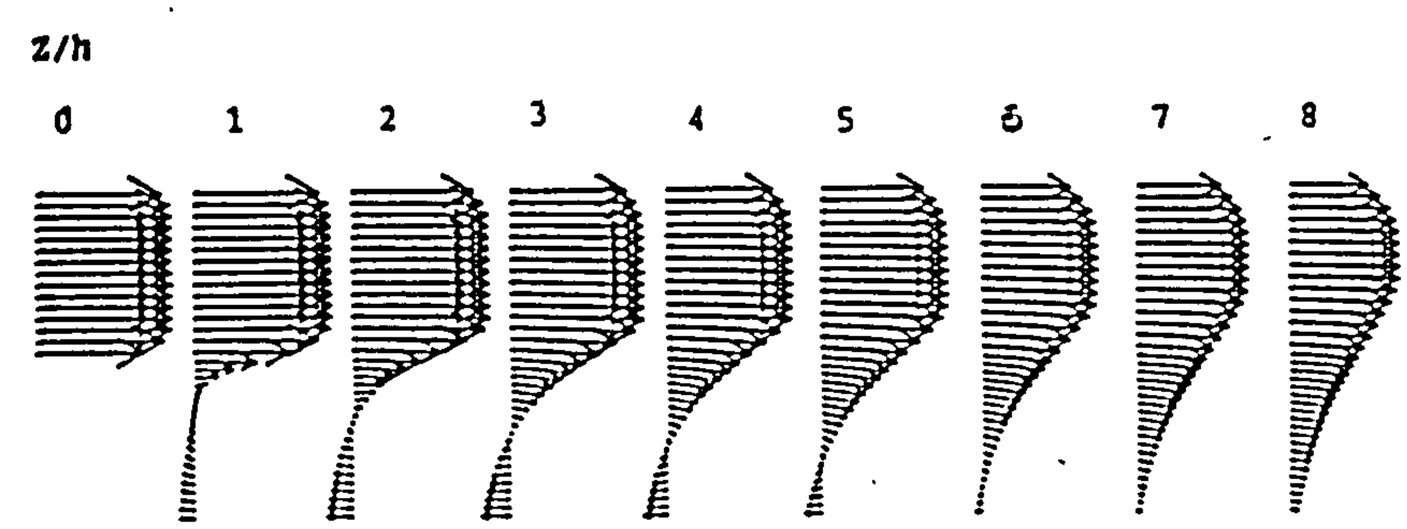

High Density Grid

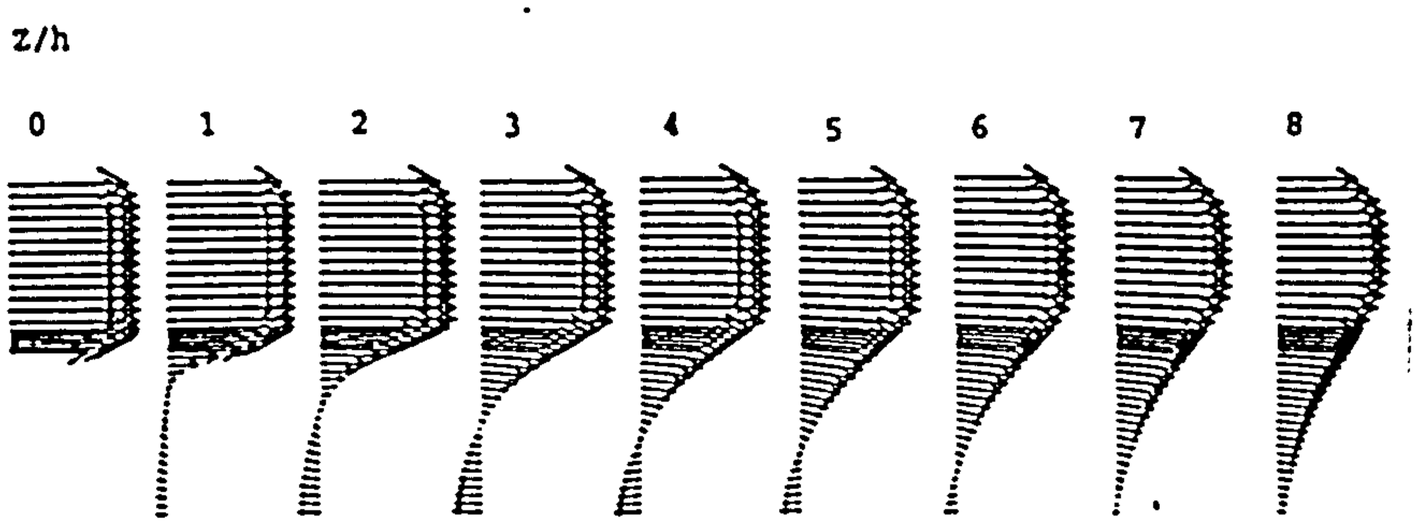

Refined Boundary Layer Grid

Figure 4.1.2.4 Comparison of Velocity Vectors for Cold Flow

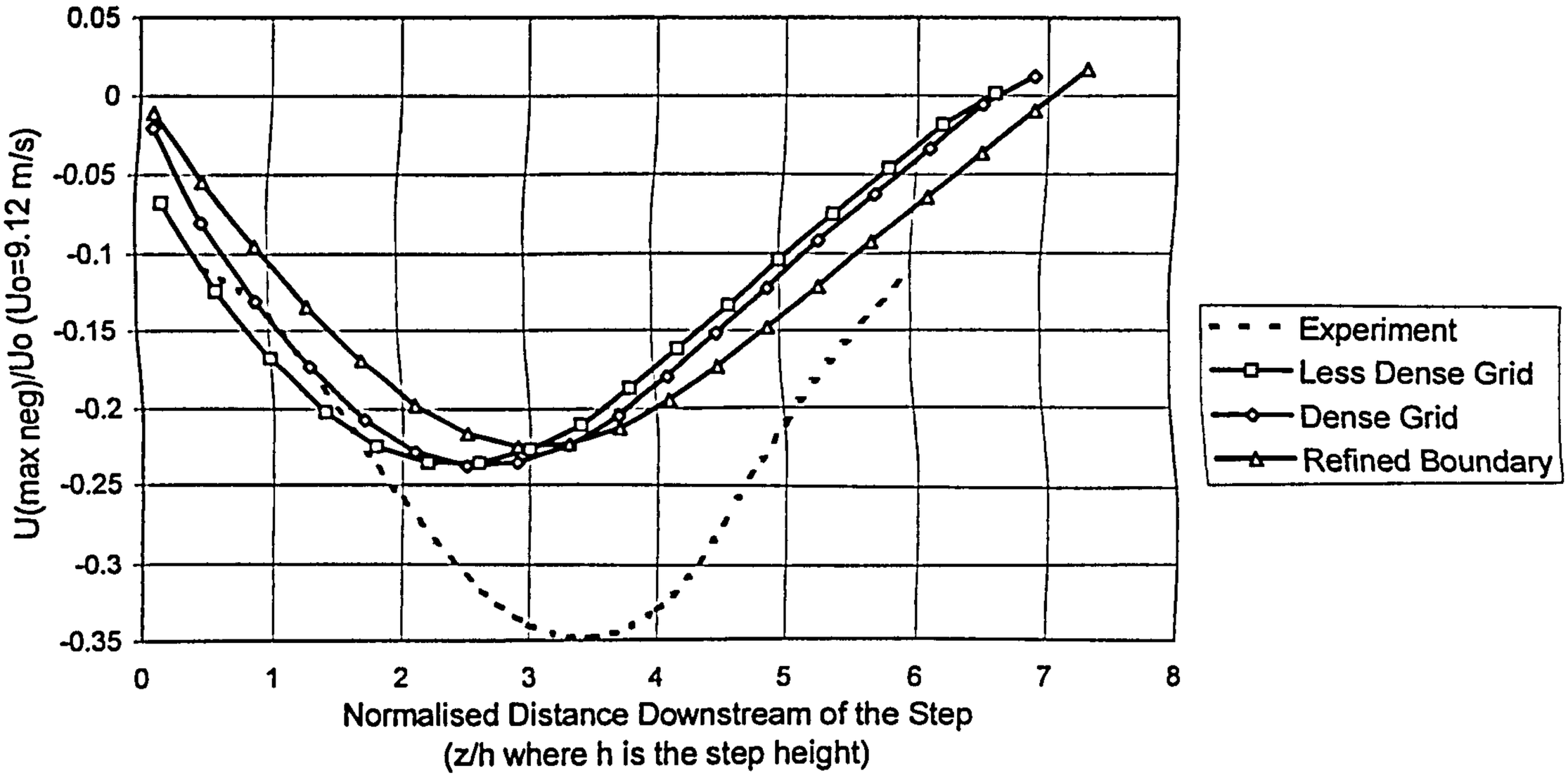

Figure 4.1.2.5 Axial Variation of Peak Negative Velocity in the Recirculation Zone

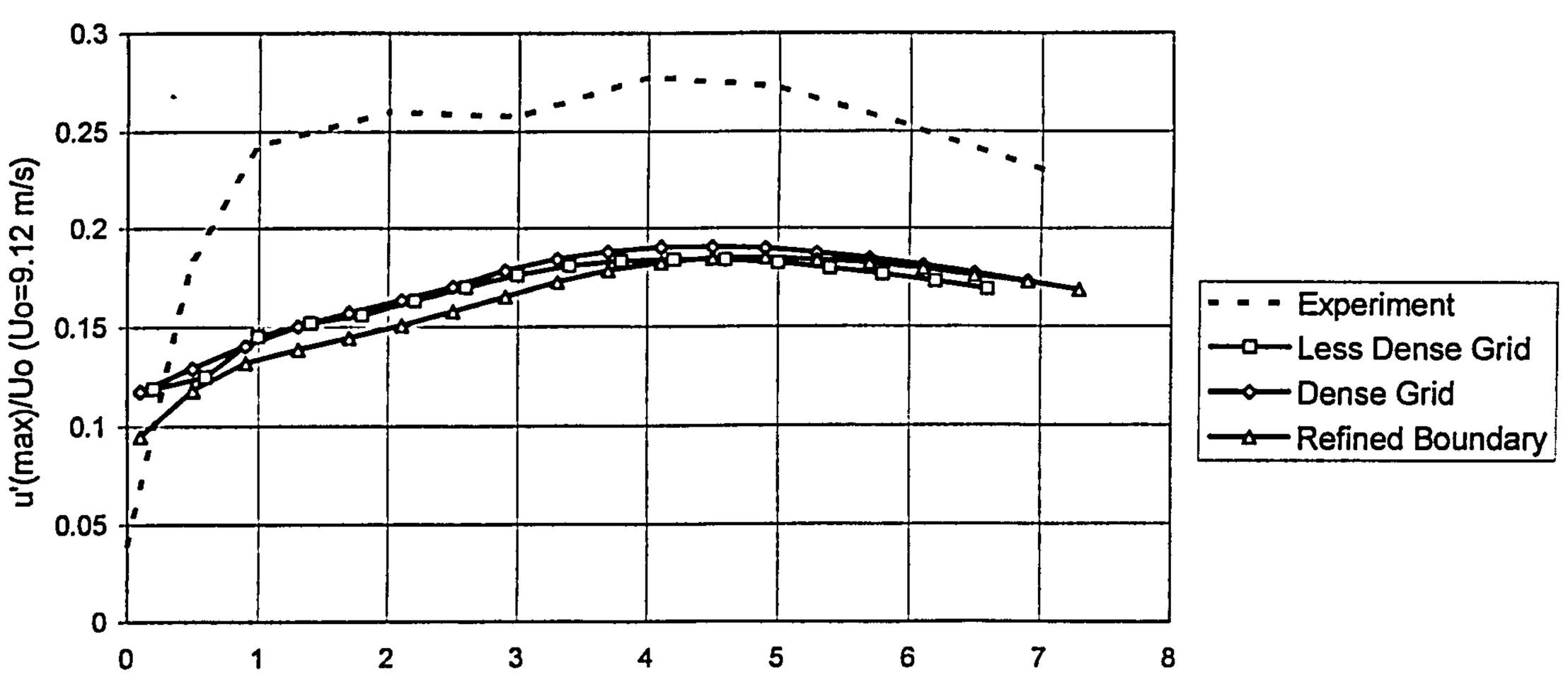

Figure 4.1.2.6 Axial Variation of Local Peak Turbulence Intensity

In summary, all three grids captured the principle time-averaged features of the flow field to a greater or lesser degree, but the influence of large scale transient features were not represented. The coarse grid was therefore chosen for the implementation of the combustion models in order to permit a reasonably quick solution of the combusting cases.

4.1.2.2 Combusting Flow Predictions

The Eddy Break-up model was first investigated with three values of the Eddy Break-up model constant (C_{EBU}), 1.06, 2.12, and 3.18. The first of these was based on the original value proposed by Mason and Spalding (1973) and the other two are twice and three times this value respectively. For the lowest value of C_{EBU}, wall functions were applied on all of the walls. For values of 2.12 and greater, the turbulence time scale is such that the flame stabilises in the boundary layer of the upper wall. This is evidently not physical. The flow is here assumed adiabatic whilst in practise any flame which tried to stabilise next to the wall would lose heat and radicals to the wall by diffusion and most probably would be extinguished. Thus for the calculations with C_{EBU}=2.12 (2.12b in Table 4.1.2.1) and 3.18 the wall function was turned off for the upper wall. The Presumed pdf calculations were also performed without the wall function on this upper wall.

Velocity vectors from the three Eddy Break-up model computations and measured contours of velocity are represented in Figure 4.1.2.8. Similar global features of the flow are predicted by each case. The flame front is assumed to be the contour of the mean reaction progress variable $\tilde{c} = 0.5$. Both the spreading rate of the flame front into the unburnt mixture and the recovery of the velocity near the lower wall are under predicted. Increasing the value of the combustion model constant improves both of these features. Colour contours of the reaction progress variable for these four cases are reported in Figure 4.1.2.9. As expected, increasing the model constant, and hence the turbulent reaction rate, also reduces the thickness of the flame brush.

Plots of the maximum recirculating velocity and maximum velocity fluctuations normalised by the inlet velocity can be found in Figures 4.1.2.10a and 4.1.2.10b. As in the cold flow predictions, the maximum negative velocity in the recirculation zone is under predicted by all of the calculations. Increasing the Eddy Break-up model constant shifts the peak of this value closer to the step as well as to a higher magnitude. In contrast the lowest value of the model constant shows the best agreement with the axial location of this peak. The turbulence intensity is also again seriously under predicted. Increasing the model constant appears to damp the turbulence such that this under prediction gets worse. The experiment indicates that close to the step the turbulence is enhanced, however further downstream it is damped over the cold flow predictions. The enhancement is probably caused by the same vortex shedding which was found in the cold flow and which is not captured by these predictions. However the turbulence damping is consistent with the predictions. The reattachment length shown in Table 4.1.2.1 is over predicted for the lowest value of the Eddy Break-up model constant and under predicted for all

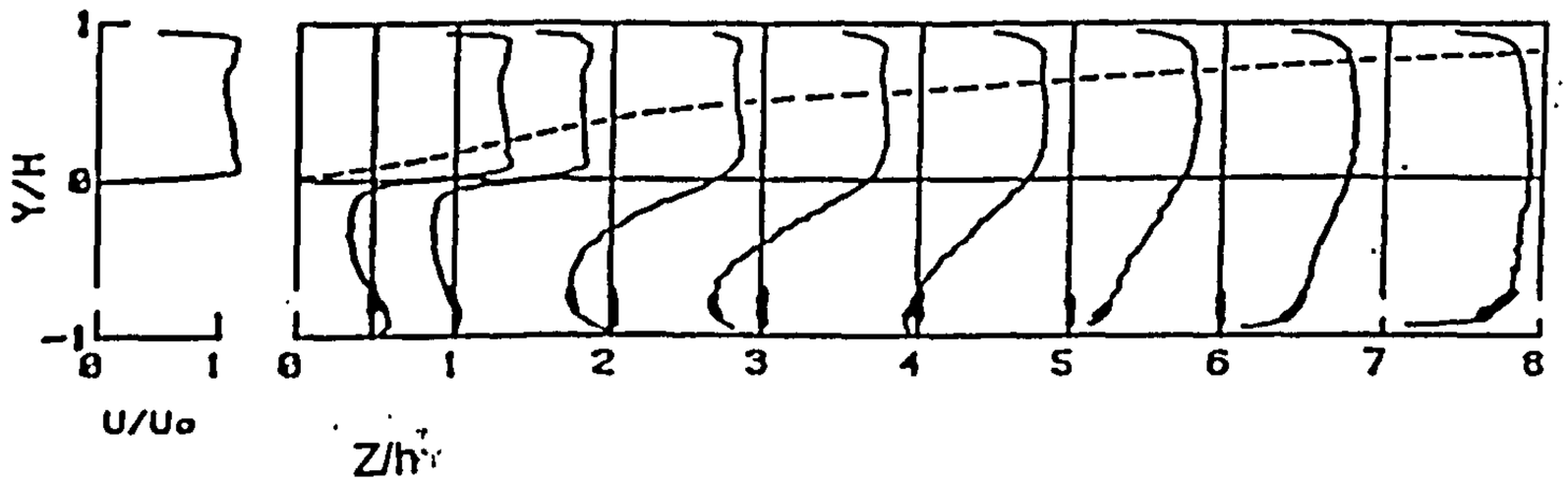

Pitz and Daily (1981) Experiment

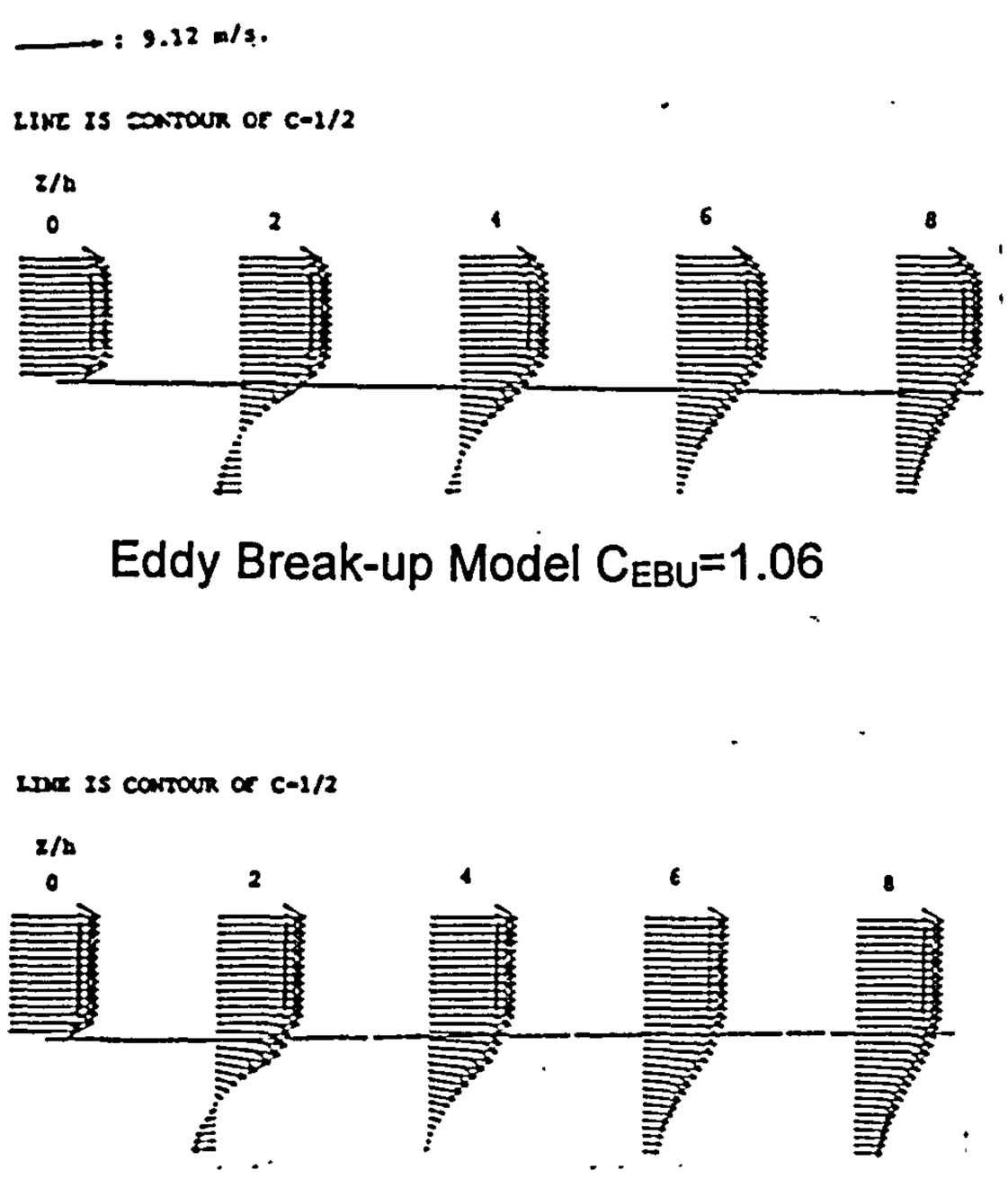

Figure 4.1.2.8 Comparison of the Velocity Vectors for Combusting Flow

Eddy Break-up Model C_{EBU}=1.06

Eddy Break-up Model C_{EBU}=2.12

Eddy Break-up Model C_{EBU}=3.18

Figure 4.1.2.9 Comparison of the Mean Reaction Progress Variable

other cases. This under prediction becomes worse as the model constant is increased. The main point which can be drawn from all of this is that although increasing the combustion model constant can increase the spreading rate of the flame front (and eventually produce a realistic looking flame front compared to the experiment) it has a deleterious effect on the flowfield predictions.

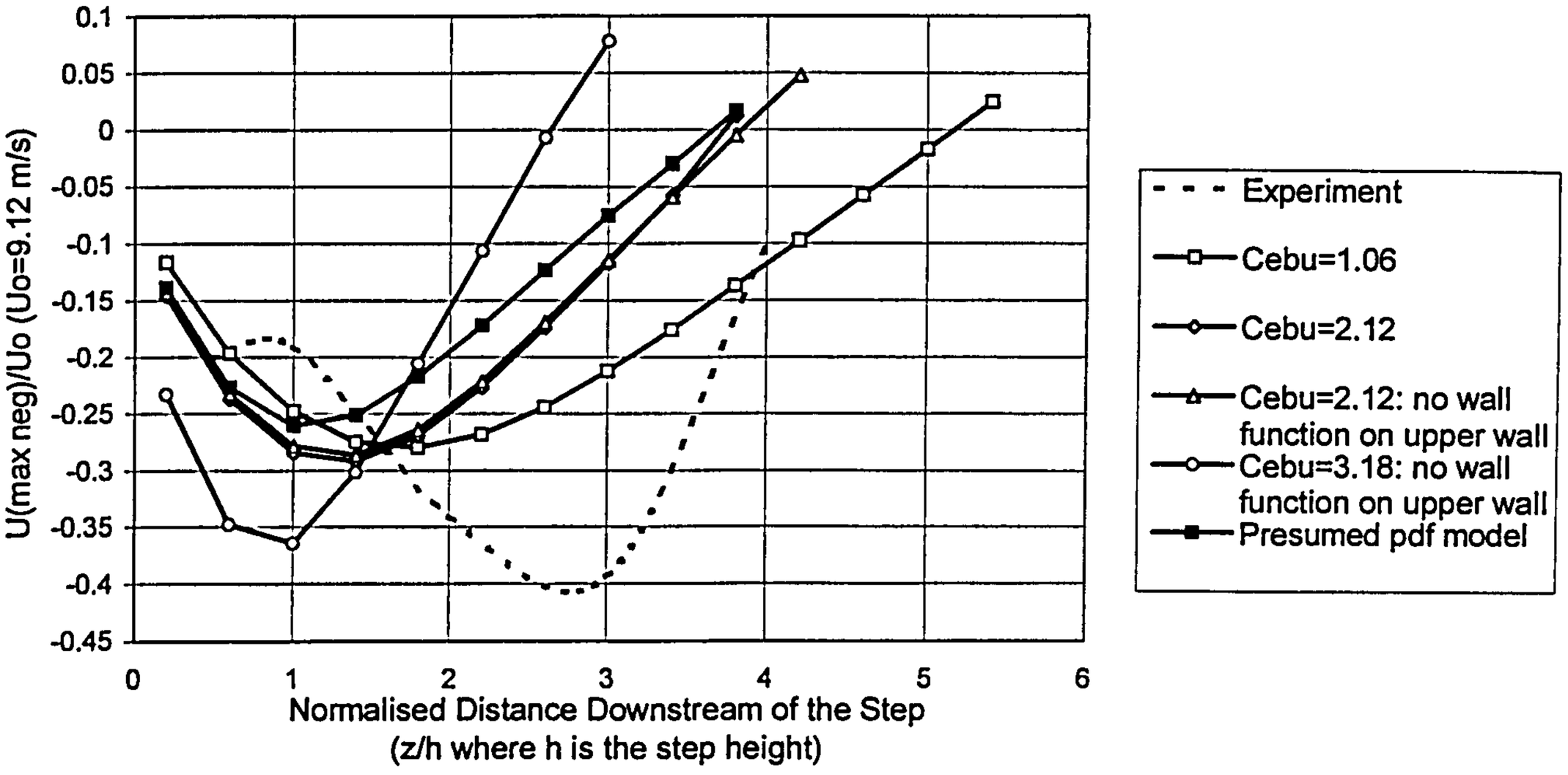

Figure 4.1.2.10a Axial Variation of Peak Negative Velocity in the Recirculation Zone

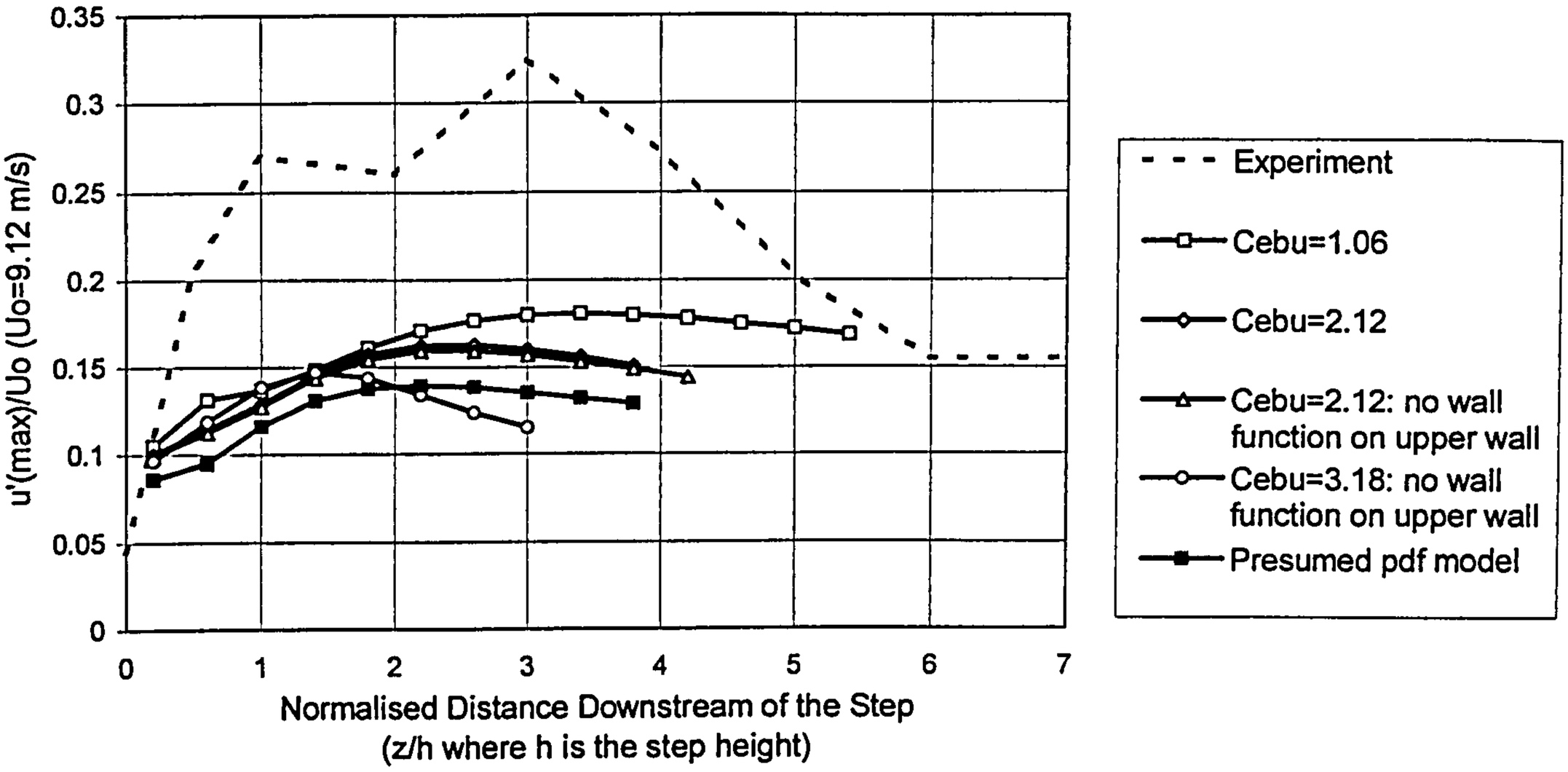

Figure 4.1.2.10b Axial Variation of Local Peak Turbulence Intensity

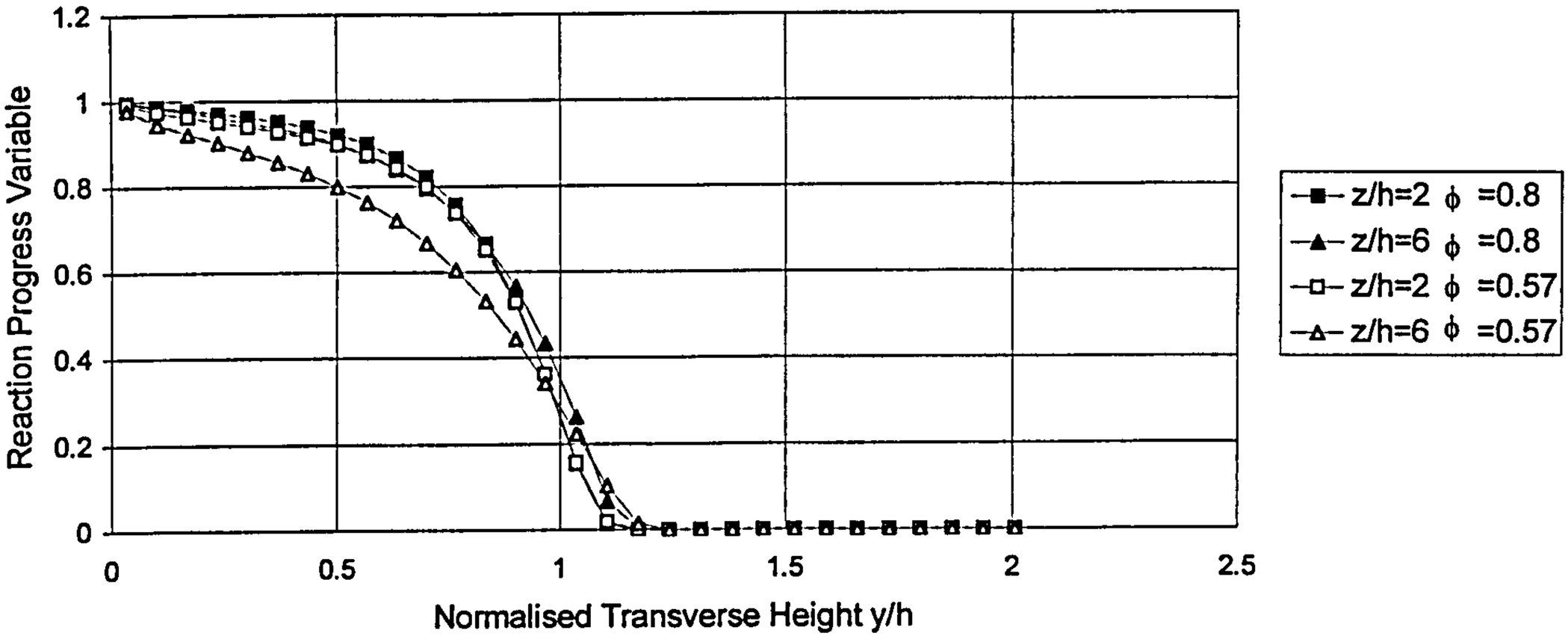

Figure 4.1.2.11 Reaction Progress Variable at Discrete Axial Positions (ϕ=0.8 and 0.57)

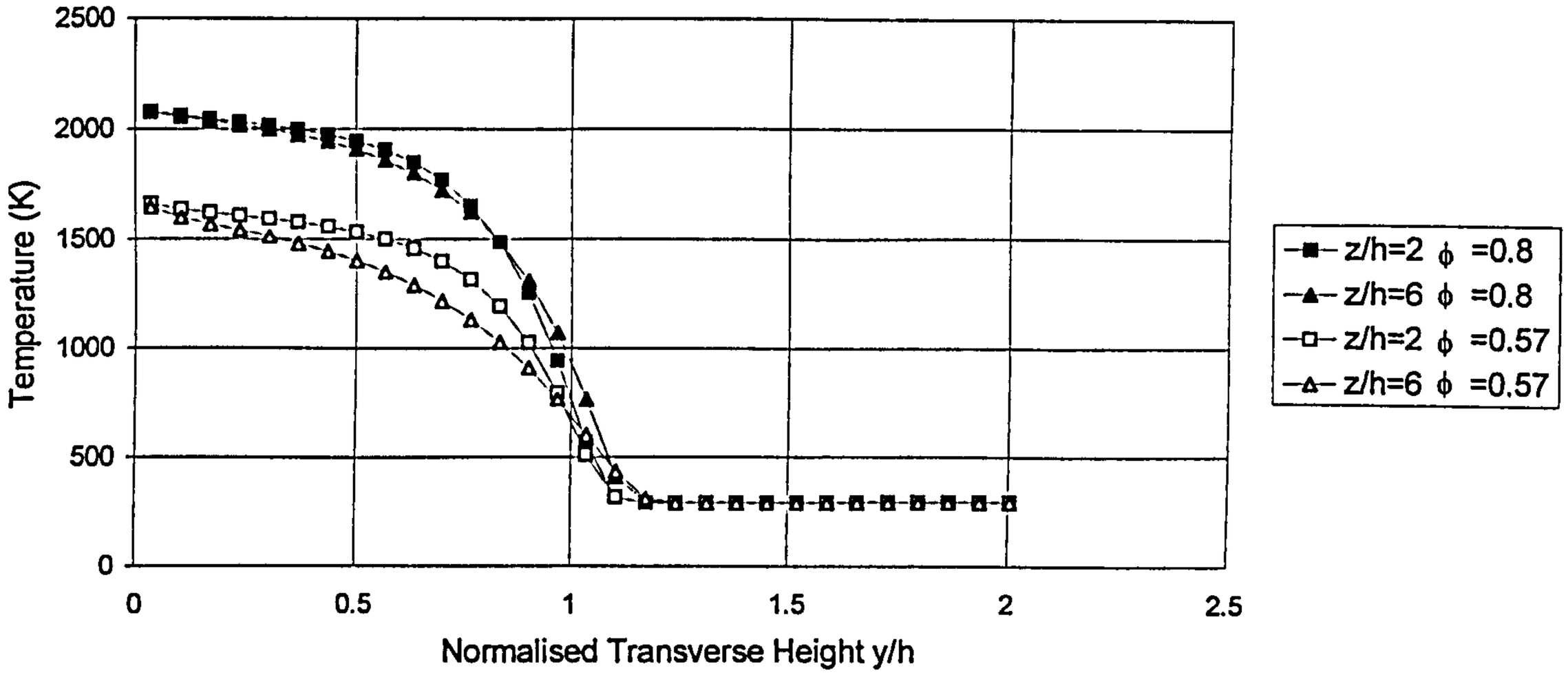

Figure 4.1.2.12 Mean Temperature at Discrete Axial Positions (ϕ=0.8 and 0.57)

A comparison of the predictions made with the Eddy Break-up combustion model for equivalence ratios of 0.57 (C_{EBU}=2.12) and 0.8 (C_{EBU}=2.94 -based on the assumptions introduced in Section 3.4) can be seen in Figures 4.1.2.11 and 4.1.2.12. The closer the equivalence ratio is to one the stronger the chemical source term. This appears to generate more of the reaction progress variable in the recirculation zone and causes the flow to sustain this further downstream of the recirculation zone. However the rate of spread of the flame front as defined by lower values of the reaction progress variable is not significantly different from that of the lower equivalence ratio case. The influence of the difference in adiabatic flame temperature which will affect the density appears to manifest itself primarily in an acceleration of the flow rather than in an expansion of the flow. The latter of these cases would have resulted in a greater spreading of the flame front.

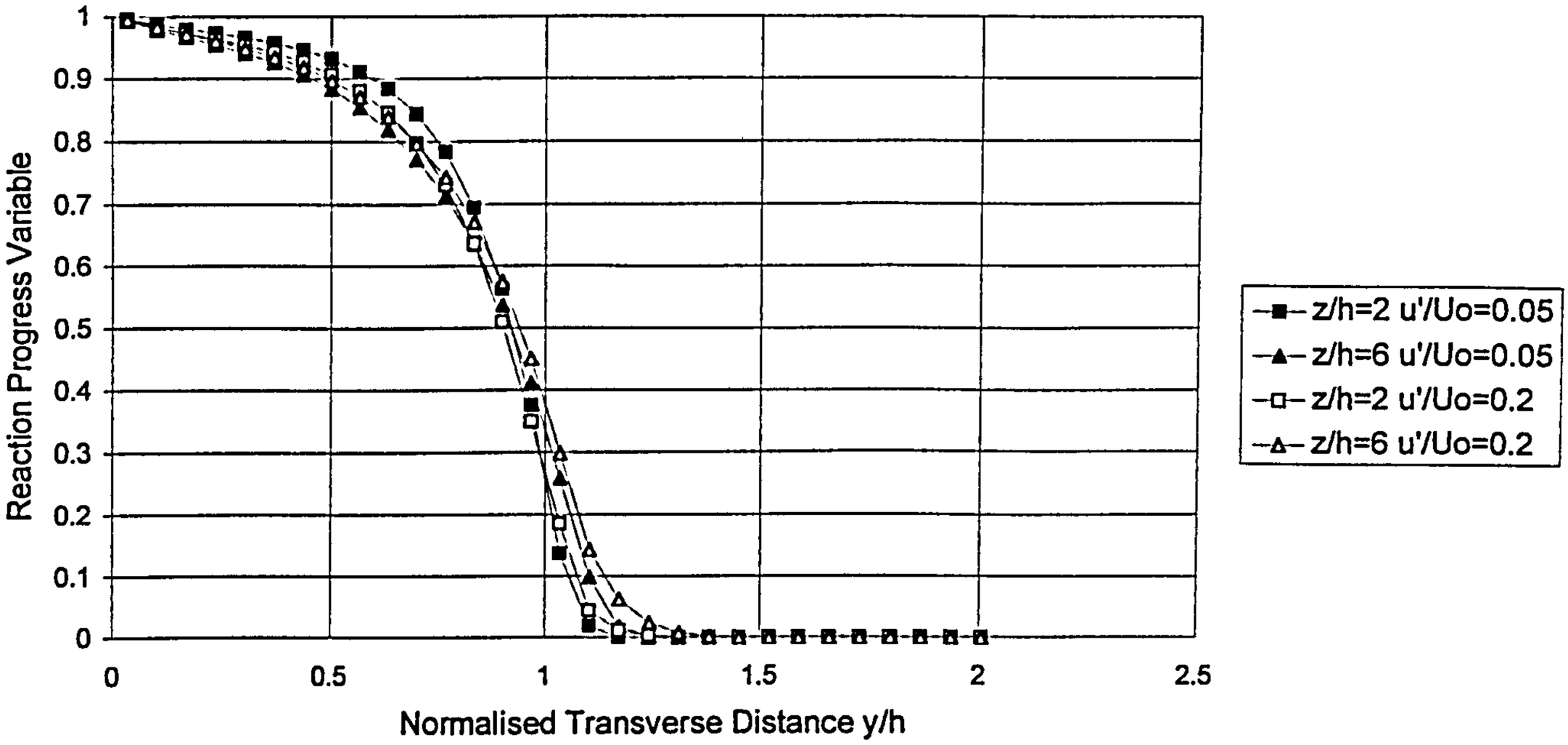

Figure 4.1.2.13 Reaction Progress Variable at Discrete Axial Positions (ϕ=0.8 C_{EBU}=2.94)

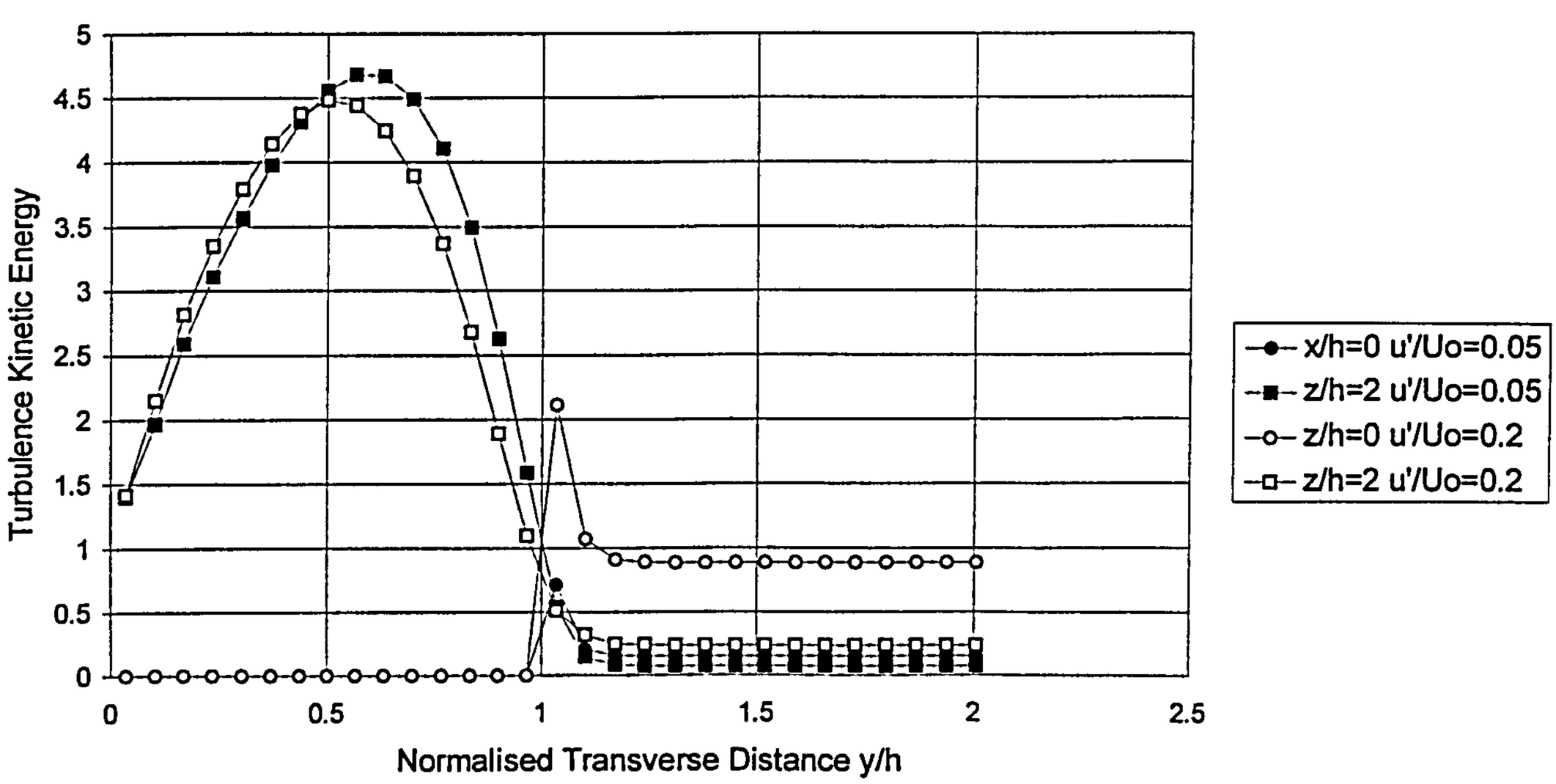

Figure 4.1.2.14 Turbulence Kinetic Energy at Discrete Axial Positions (ϕ=0.8 C_{EBU}=2.94)

A measure of the sensitivity of the Eddy Break-up predictions to the level of turbulence intensity is illustrated in Figure 4.1.2.13. The higher inlet turbulence intensity (20%) has the effect of enhancing the spreading rate for the lower values of the reaction progress variable, however this improvement is only slight considering the large increase in inlet

intensity. This suggests that the inlet turbulence is dissipated rapidly before the step, which is proven in Figure 4.1.2.14. With this in mind investigations were also carried out with a reduced inlet length, however similar results were found. Thus the flowfield of the backward facing step is dominated by the turbulence generated by the shear layer at the top of the step, and is relatively independent of the inlet turbulence intensity.

The effect of the inlet turbulence frequency (ε_0/k_0) on the Eddy Break-up model was also investigated. Figures 4.1.2.15 through 4.1.2.16 show the reaction progress variable and turbulence frequency profiles for inlet values of 4922 1/s (based on a turbulence length scale of 0.03% of the duct width) and 3375 1/s (based on a turbulence length scale of 0.05% of the duct width). More extreme values, coming from an earlier comparison of Mason and Spalding's (1973) calculations of Howe and Shipman's (1963) experiment, of 6469 1/s and 0.5 1/s were also investigated but showed similar trends in terms of the downstream values of the turbulence frequency. In general, the flame front is not affected by the inlet value of turbulence frequency. The effects are only felt in the inlet stream. The values of frequency predicted in the recirculation zone were found to be nearly identical in all cases regardless of the value in the free stream.

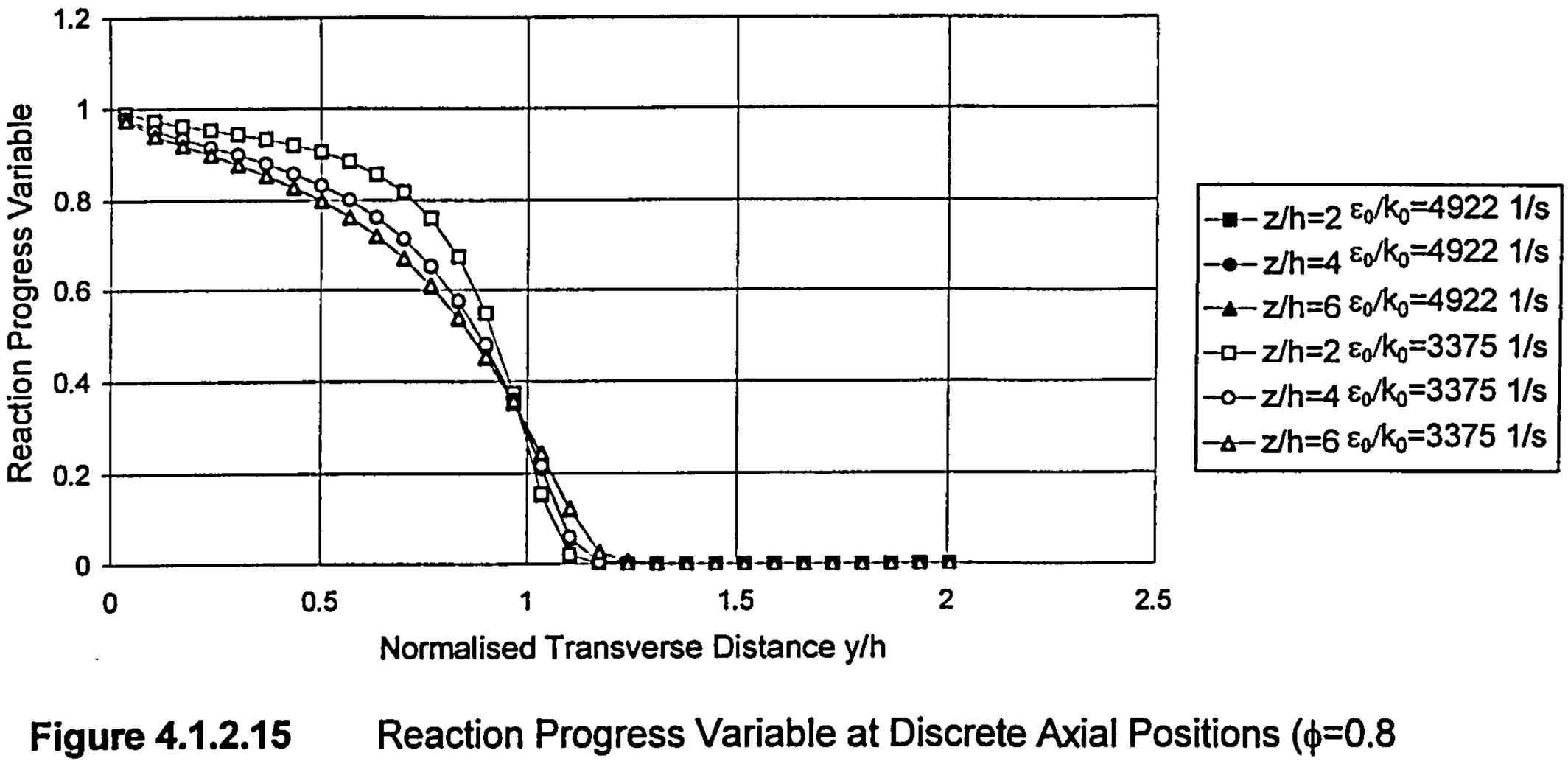

Figure 4.1.2.15 Reaction Progress Variable at Discrete Axial Positions (ϕ=0.8 C_{EBU}=2.94)

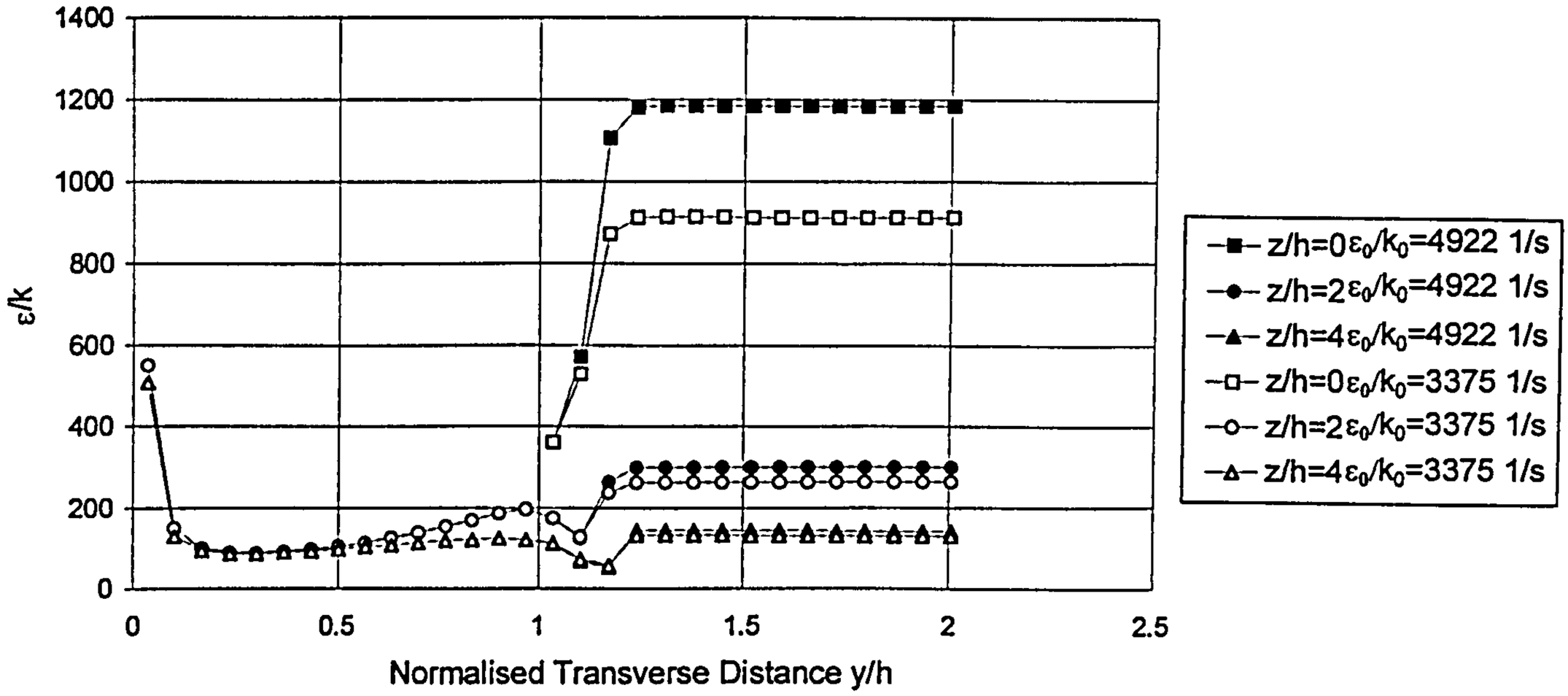

Figure 4.1.2.16 Turbulence Frequency at Discrete Axial Positions (ϕ=0.8 C_{EBU}=2.94)

The grid used for the Presumed pdf computations was the same in the streamwise direction as that for the Eddy Break-up model. However computations with this grid and the Presumed pdf model were found to have convergence problems which were related to the degree of coarseness in the cross stream direction. A grid with 20 cells covering the step and 30 cells covering the inlet duct was found to give reasonably stable convergence properties.

Figures 4.1.2.19 and 4.1.2.20 illustrate contours of the mean reaction progress variable of the Presumed pdf model described in Section 3.2 with its source term scaled arbitrarily by a factor of 5 and the Eddy Break-up (with C_{EBU}=2.12) model respectively. The scaled Presumed pdf case produces a similar flame front spreading to the Eddy Break-up model with C_{EBU}=2.12, and it is these computations which will be described in subsequent sections.

Figures 4.1.2.21 and 4.1.2.22, which compare the axial velocity measured with that predicted by this model at 2 step heights and 6 step heights downstream of the sudden expansion, indicate that this model both underpredicts the strength of the recirculation behind the step and the acceleration of the flow downstream of it. Both are indicating that not as much material is being consumed and hence accelerated, due to the reduction in density across the flame front, as is occurring in the experiment. Hence they both indicate that the reaction rate is not strong enough.

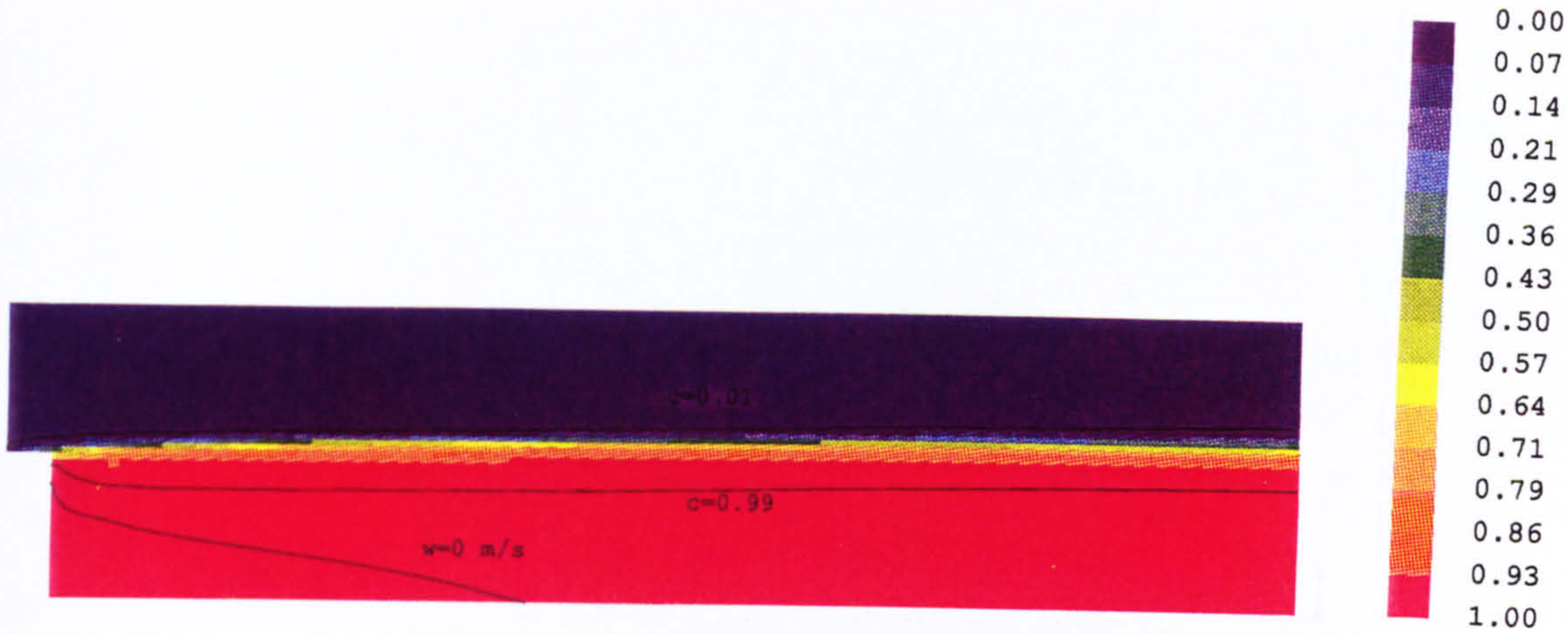

Figure 4.1.2.19 Mean Reaction Progress Variable for the Presumed pdf Model with 5 times the original chemical source term

Figure 4.1.2.20 Mean Reaction Progress Variable for the Eddy Break-up Model with C_{EBU}=2.12

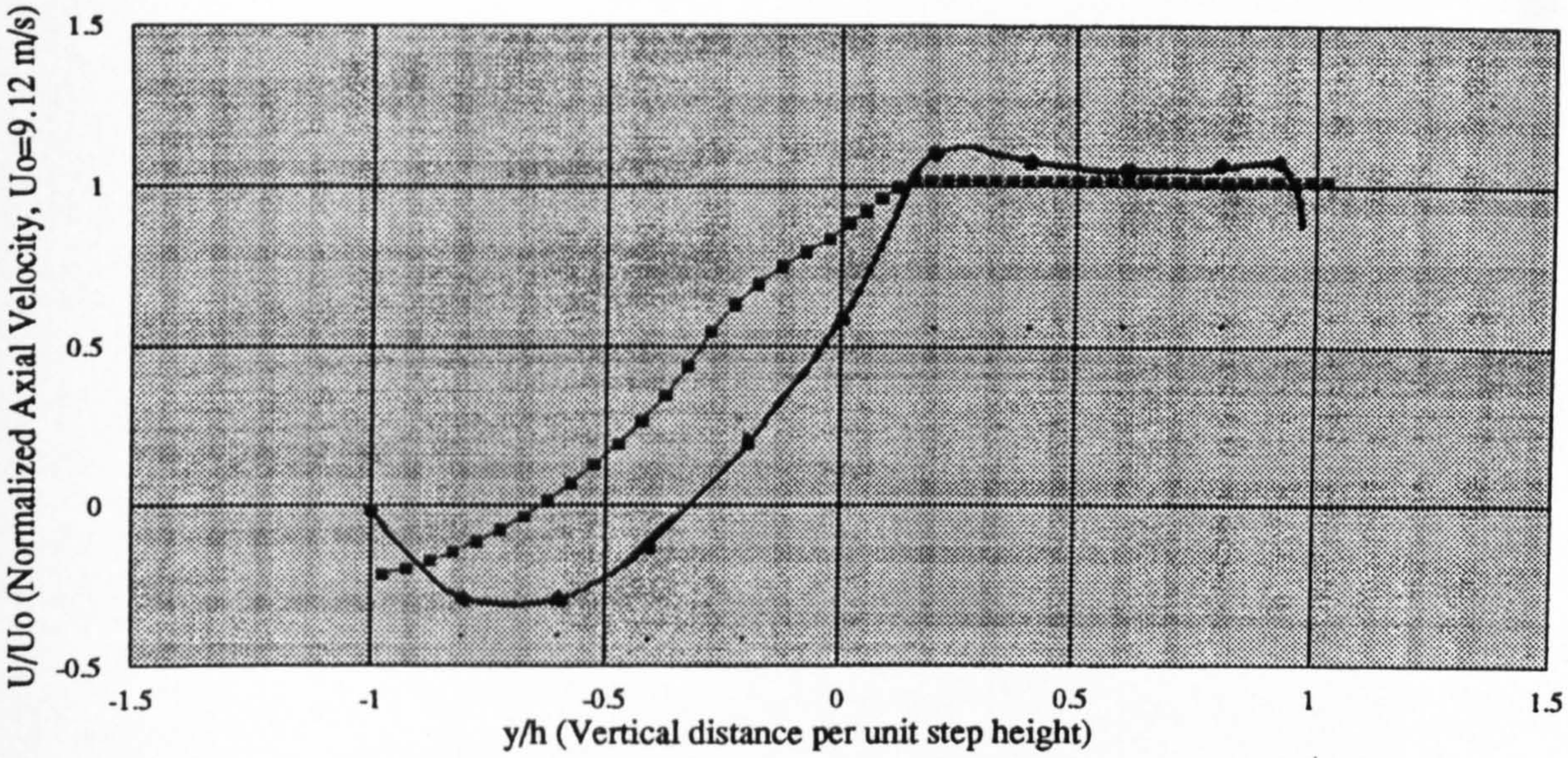

Figure 4.1.2.21 Transverse Profile of Axial Velocity 2 Step Heights Downstream of the Sudden Expansion

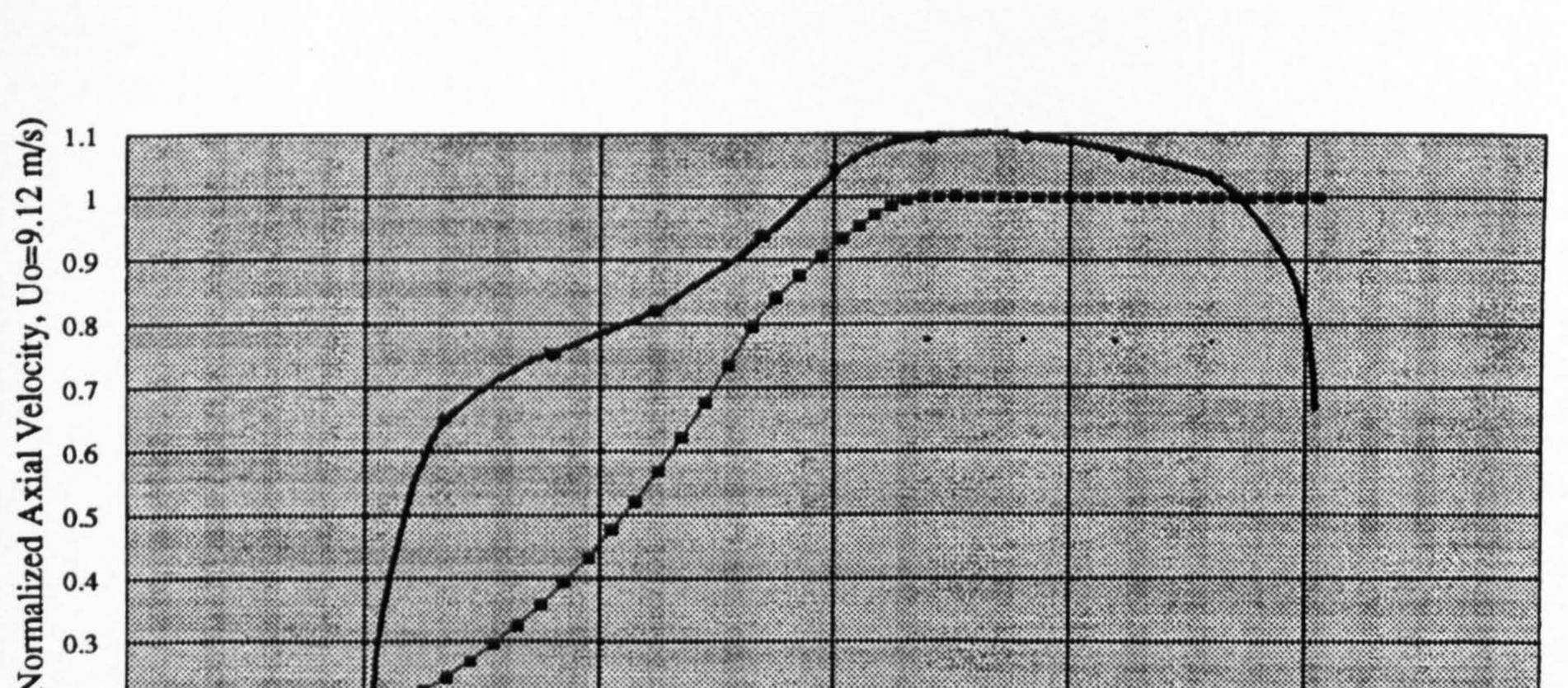

Figure 4.1.2.22 Transverse Profile of Axial Velocity 6 Step Heights Downstream of the Sudden Expansion

Figure 4.1.2.23 Mean Chemical Source Term (1/s) for the Presumed pdf Model with 5 times the original chemical source term

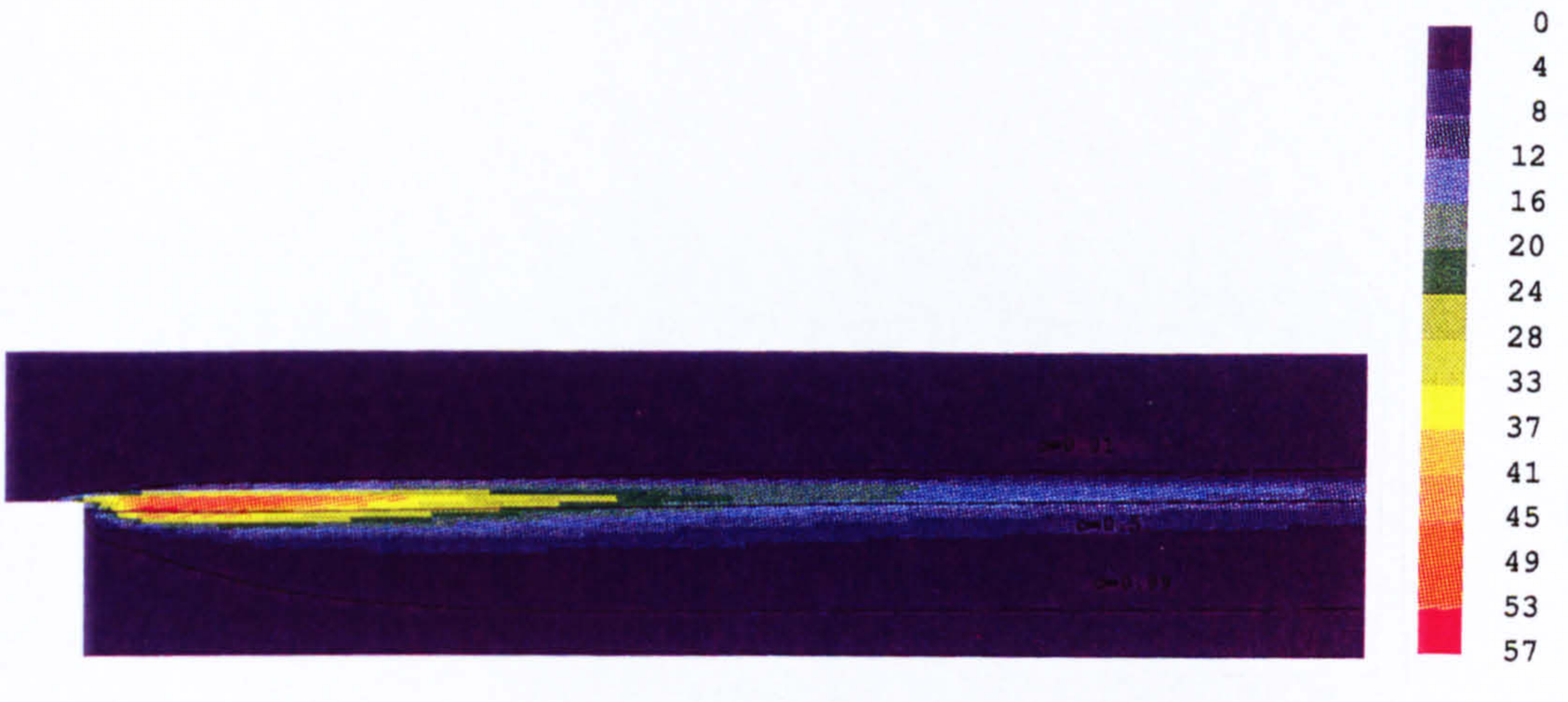

Figure 4.1.2.24 Mean Chemical Source Term (1/s) for the Eddy Break-up Model with C_{EBU}=2.12

Figure 4.1.2.25 Presumed pdf parameter α for Simple Block pdf of Figure 2.3.3.2.1

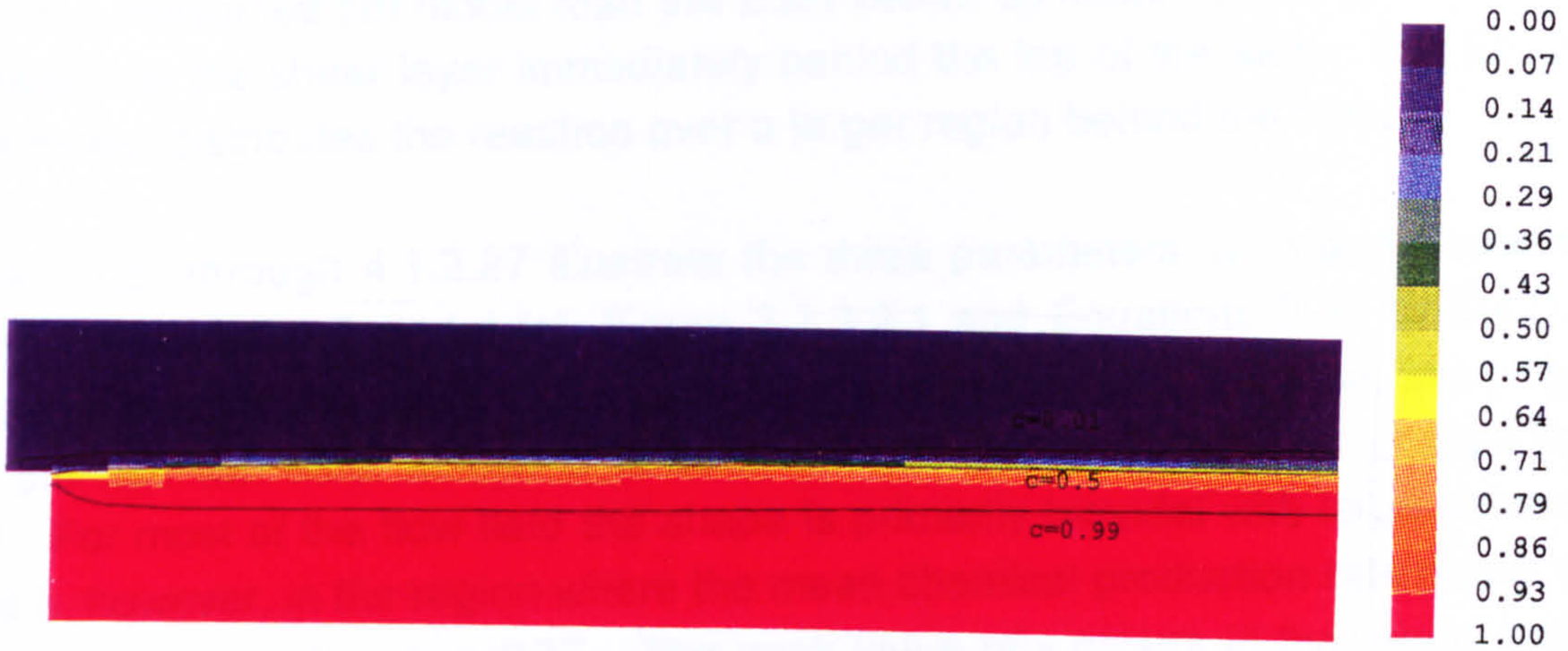

Figure 4.1.2.26 Presumed pdf parameter β for Simple Block pdf of Figure 2.3.3.2.1

Figure 4.1.2.27 Presumed pdf parameter γ for Simple Block pdf of Figure 2.3.3.2.1

Figures 4.1.2.23 and 4.1.2.24 show contours of the chemical source term for both the Presumed pdf and Eddy Break-up models. The peak chemical source term is higher for the Presumed pdf model than the Eddy Break-up model, but is confined to a small region in the shear layer immediately behind the top of the step. The Eddy Break-up model distributes the reaction over a larger region behind the step.

Figures 4.1.2.25 through 4.1.2.27 illustrate the three parameters, α, β and γ which define the Presumed pdf model (cf. Figure 2.3.3.2.1 and Equations 2-40 to 2-42). The shape of the pdf was always of type δ=1 for this particular calculation, implying that the pdf had two delta functions at zero and one and a rectangular section in between. For most of the flow field the shape is primarily bimodel with large values for α and β, however, in the region where the mean chemical production rate peaks γ also reaches a high value $\gamma \leq 0.37$. The peak value of γ occurs in the region just downstream of the sudden expansion where the variance of the reaction progress variable is still relatively small. A plot of α, β and γ across the flame front at a plane 8 step heights downstream of the sudden expansion is presented in Figure 4.1.2.28. Figure 4.1.2.29 illustrates the accompanying mean and variance of the reaction progress variable. The peak in γ occurs roughly where the mean reaction progress variable takes on the value 0.5 and the variance is also a maximum. We might expect that the higher the variance the smaller would be γ. As discussed earlier, the maximum variance for the reaction progress variable would be $\tilde{c}(1-\tilde{c})$,

corresponding to γ=0. This gives a value of 0.25 for a mean reaction progress variable of 0.5 which is close to the maximum value obtained, and although γ is a maximum here it also has a very small magnitude compared to α and β.

A budget for the source terms of the transport equation for the variance of the reaction progress variable (Equation (3-17)) and the diffusion term in the transport equation of the mean reaction progress variable (Equation (2-34)) is illustrated in Figures 4.1.2.30 and 4.1.2.31 for the plane 2 step heights downstream of the expansion. The dominant source terms in the variance equation are the dissipation by molecular diffusion (or scalar dissipation) term and the chemical production term. The first acts primarily as a sink and peaks close to $\tilde{c} = 0.5$ where the variance of the reaction progress variable peaks. The chemical source term at the leading edge of the flame brush acts as a source increasing the variance. Near the rear of the flame brush it flips sign to become a sink. The mean gradient term, which contains the scalar flux of the reaction progress variable, is modelled using a gradient approximation as is usual for the k-ε turbulence model. As has been pointed out counter gradient diffusion has been found to be significant in ducted flames (Shepherd *et al,* 1982). If this is present it will make this term a sink rather than a source which will help to reduce the variance. As was just pointed out the lower the variance the larger γ is in the pdf and thus the larger the chemical source term for the reaction progress variable. This will improve the flame spreading however given that the magnitude of this term is not high compared to the other two this may not be that significant for this particular flow field. Thus it is not expected that the additional modelling of counter gradient diffusion will significantly affect the prediction of the flame front.

Additionally, for the Presumed pdf model a comparison was made between the pdf shapes formed by a β-function pdf and the simple block style pdf of Figure 2.3.3.2.1. Figure 4.1.2.32 illustrates the ratio of the two pdfs at various distances across the plane of the duct at 8 step heights downstream of the sudden expansion. Despite a large difference in the mean values of the reaction progress variable, the ratio of the two pdf types is very similar for all three points. The difference between the two is the highest for values of reaction progress variable near zero and unity. This reflects the fact that the β-function pdf tends to infinity at these bounds, but is accounted for by delta functions in the Bray Moss pdf. Between these values, their ratio is of order unity and there is little difference between the different forms of the pdf.

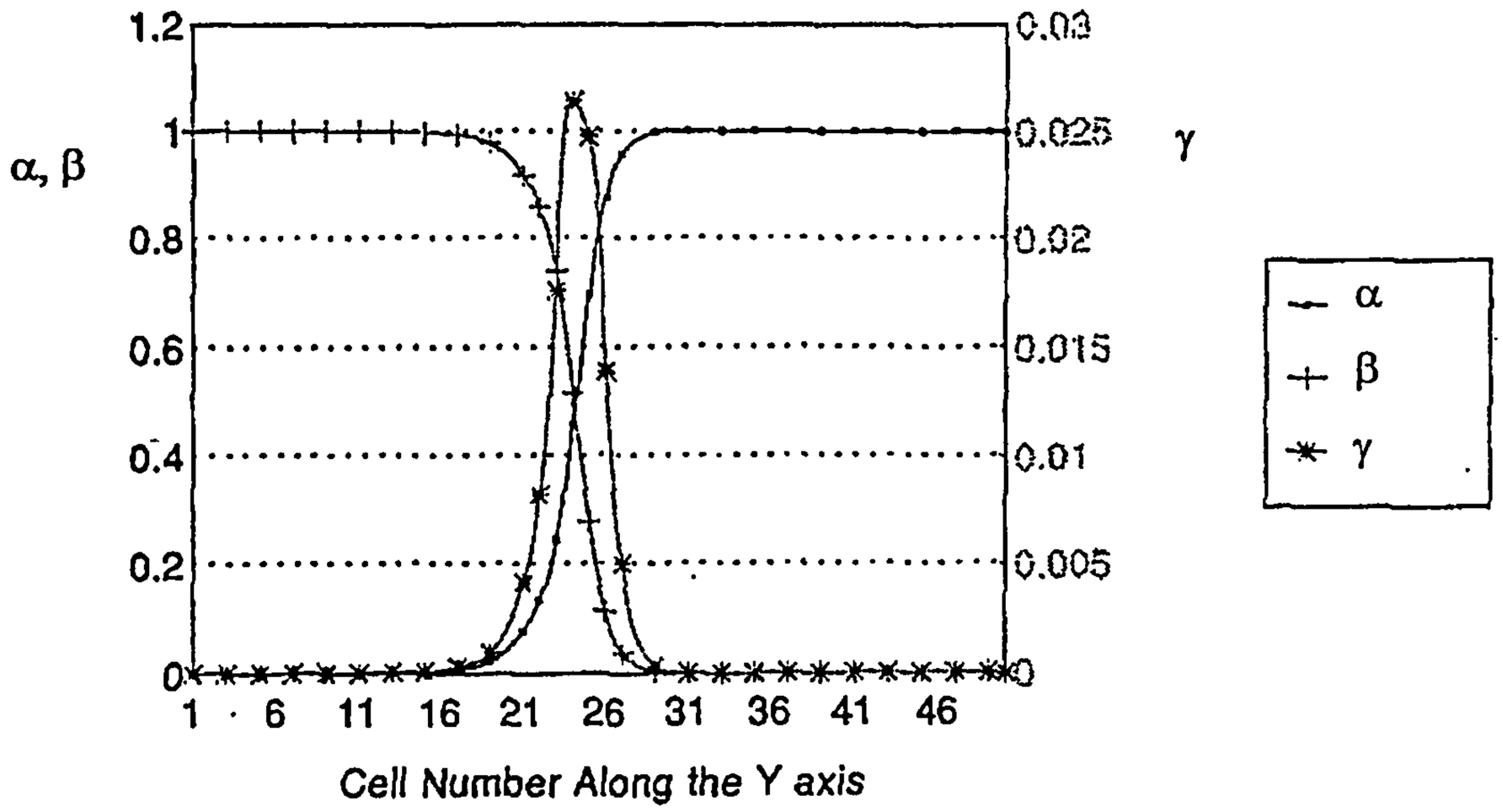

Figure 4.1.2.28 Profiles of the Presumed pdf Parameters at Z/h=8

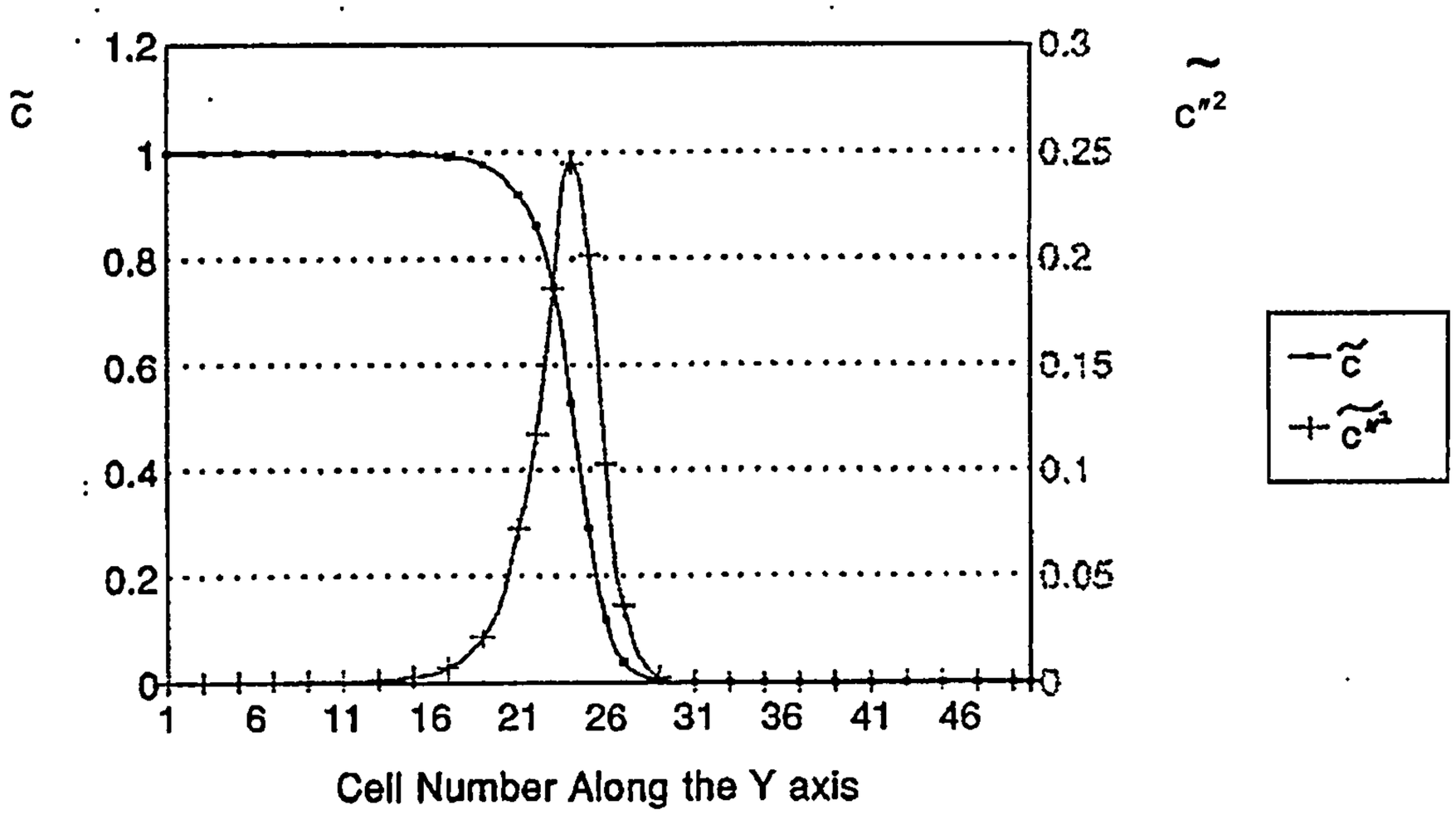

Figure 4.1.2.29 Mean and Variance of the Reaction Progress Variable at Z/h=8 for the Presumed pdf Model

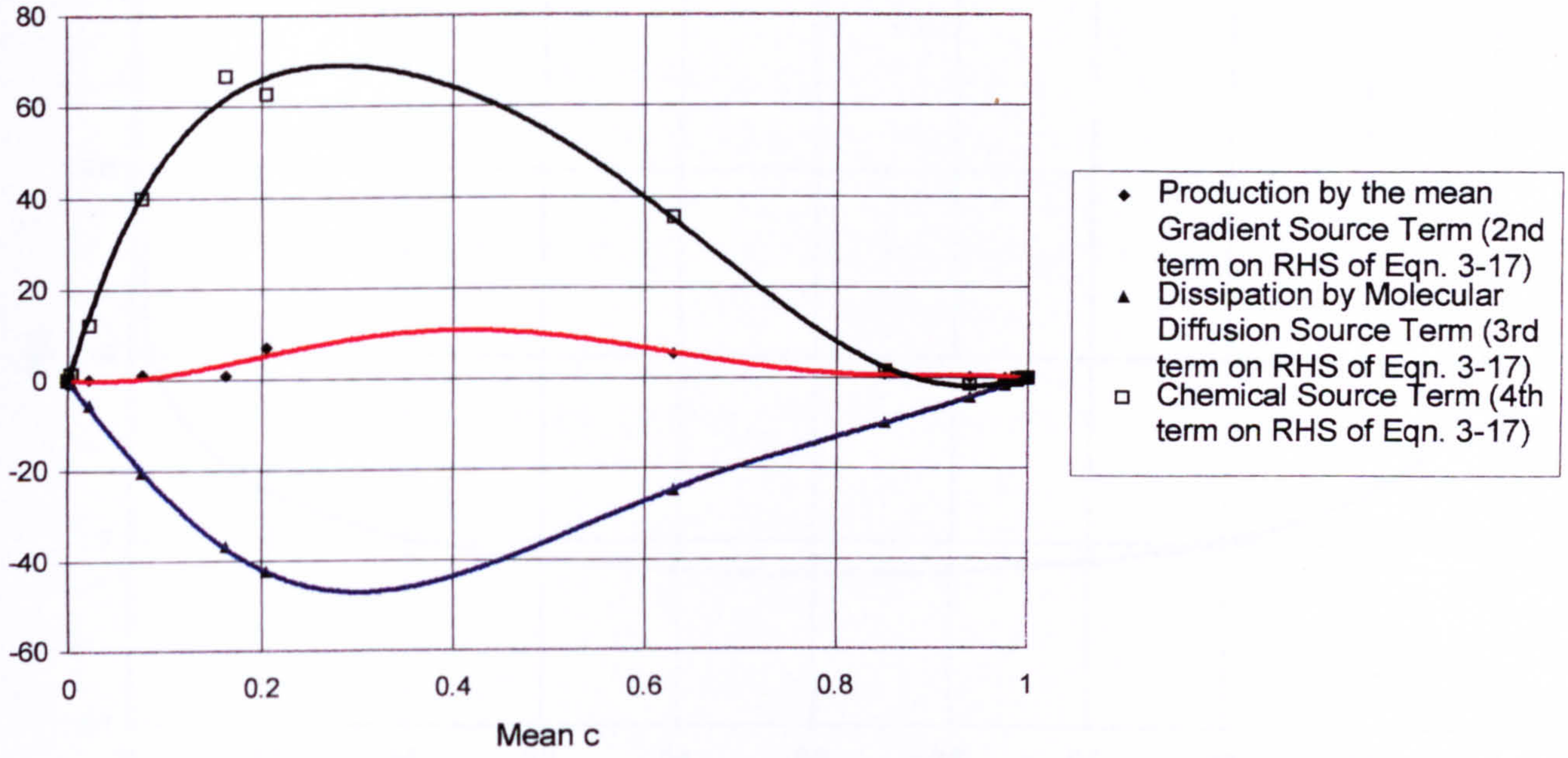

Figure 4.1.2.30 Budget for the Source Terms of the Variance of the Reaction Progress Variable at Z/h=2

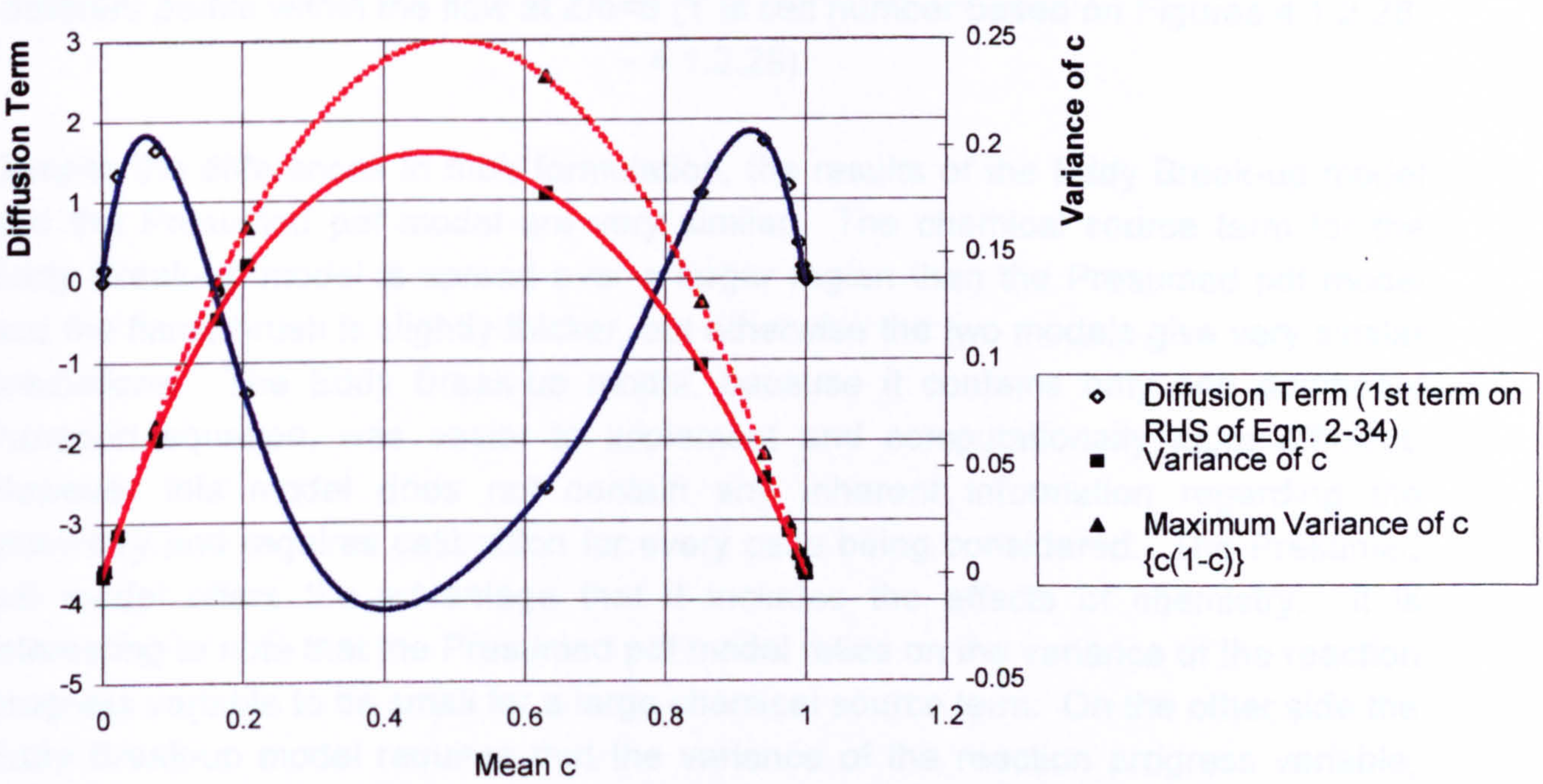

Figure 4.1.2.31 Variance of the Reaction Progress Variable and the Diffusion term for the Mean Reaction Progress Variable at Z/h=2

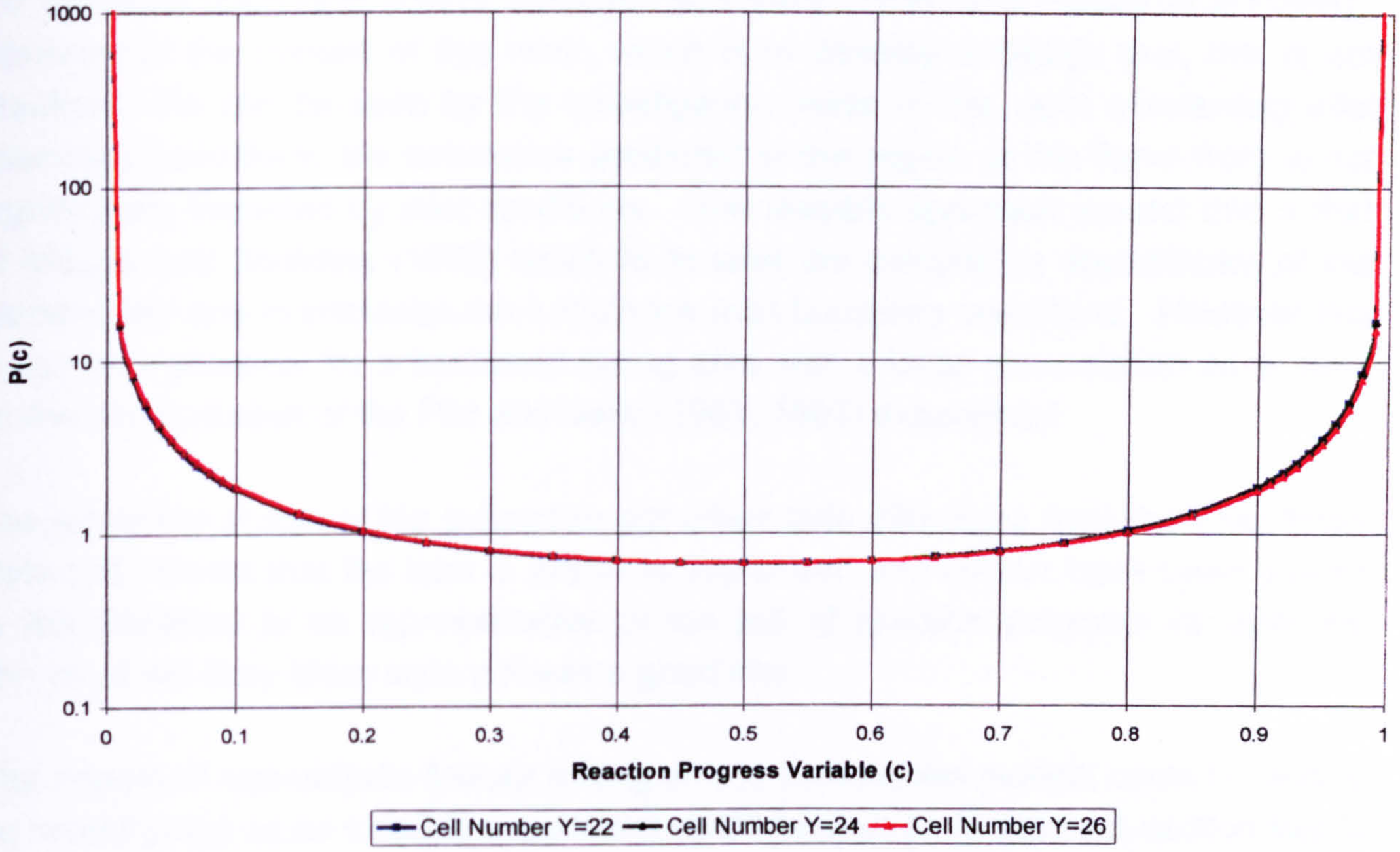

Figure 4.1.2.32 Ratio of the β function pdf to the Simple Block style pdf at different points within the flow at Z/h=8 (Y is cell number based on Figures 4.1.2.28 – 4.1.2.29)

Despite the differences in their formulation, the results of the Eddy Break-up model and the Presumed pdf model are very similar. The chemical source term for the Eddy Break-up model is spread over a larger region than the Presumed pdf model and the flame brush is slightly thicker, but otherwise the two models give very similar predictions. The Eddy Break-up model, because it contains only one additional transport equation, was easier to implement and computationally more efficient. However this model does not contain any inherent information regarding the chemistry and requires calibration for every case being considered. The Presumed pdf model offers the advantage that it includes the effects of chemistry. It is interesting to note that the Presumed pdf model relies on the variance of the reaction progress variable to be small for a large chemical source term. On the other side the Eddy Break-up model requires that the variance of the reaction progress variable, which it assumes is always a maximum, be large for a large chemical source term. Despite this fundamental difference between the models, it is interesting that both give very similar results.

In the context of the backward facing step it is clear that the flame front position and strength is strongly dependent on the turbulent shear layer. A correct prediction of this would require transient calculations, such as those investigated more recently in

the literature (Olovsson (1992), Lindstedt and Vaos (1995) and Fureby *et al* (1995)). However in the context of this work, which is to develop a design tool, this is not practical. As can be seen by the investigation made in this work concerning inlet boundary conditions, the turbulence predicted in the region of the flame front is not significantly impacted by inlet conditions. One feasible approach around this is that of Mason and Spalding (1973) which is to start the calculation downstream of the flameholder and to prescribe the turbulence inlet boundary conditions. However this is not very practical for a backward facing step with a large recirculation zone such as the configuration of the Pitz and Daily (1981, 1983) experiment.

The smoother shape of the β-function pdf offers little difference from the Bray Moss style pdf. Given that the later is easier to implement and neither have been proven in the literature to be representative of the pdf of reaction progress variable the choice of the Bray Moss style pdf was a good one.

The impact of non-uniform fuel air mixing on the combustion models could not easily be investigated as no suitable experiment could be found. In the next section this is explored in the context of NOx predictions where it is felt that this will have the greatest impact. Additionally the relative influence of counter gradient diffusion on the models is fully investigated in the next chapter in the context of the experimental LPP combustor.

4.2 Assessment of the NO_x Model

Assessment of the NO_x model and its implementation was undertaken by making a comparison with measured concentrations of NO_x from the experiment by Moreau *et al* (1980). This experiment was based on a rig which was comprehensively investigated during the late 1970's both experimentally (Moreau *et al*, 1980, Moreau, 1977, Moreau *et al*, 1976, Moreau, 1974) and theoretically (Moreau *et al*, 1980, Borghi *et al*, 1977b).

In this ducted experiment a lean premixed methane-air mixture, was stabilised by a parallel hot stream of fully burnt product at 2000 K. The rig is illustrated in Figure 4.2.1. The duct was 100 mm wide of which the product stream was 20 mm and the reactant stream was 80 mm. The reactant stream had a mean velocity of 55 m/s, temperature of 600 K and an equivalence ratio of 0.8, and the fully burnt product stream had velocity of 110 m/s and an equivalence ratio of unity. Since we have developed our models for adiabatic flow, we assumed that the equivalence ratio of the fully burnt stream was 0.67, which has an adiabatic flame temperature of roughly 2000 K. We also assumed that the equivalence ratio was uniform across both inlet streams. The variance of the mixture fraction across the fully burnt stream was assumed to be zero. Across the reactant stream four values of the variance of the mixture fraction were set such that the root mean square of the fluctuation of the equivalence ratio normalised by the mean equivalence ratio was 1%, 20%, 40% and 442%. 1% was chosen to simulate a nearly perfectly homogeneous mixture and 442% to simulate a completely unmixed mixture. 20% was investigated as this corresponded to a representative value measured within the experimental test burner (Chapter 5) and 40% was chosen to see the effect of doubling this value. One additional case was investigated where the variance was set to 1% and the burnt stream was given the equivalence ratio of 1.0 and subsequent adiabatic flame temperature of about 2370 K. This latter case was conducted to see the sensitivity of the temperature of the fully burnt inlet stream on the NOx produced.

Given that the combustion heat release model was not being tested here, the Eddy Break-up model was used with a model constant selected to give good agreement between the predicted and the measured flow velocities. A value of C_{EBU}=2.12 was found to give good results as can be seen in the comparison of the measured and predicted velocity profiles of Figures 4.2.2 and 4.2.3. All but the case with the highest inlet variance for the mixture fraction gave good agreement in terms of the acceleration of the flow as one moved downstream. This case had the highest possible variance which implied that the reactants were initially completely unmixed. Thus the flame front was delayed slightly as the reactants had to mix before they were able to burn.

Inlet conditions for the velocity were assumed to be a plug flow based on the previous CFD calculations of Borghi *et al* (1977b) for this experiment. The inlet conditions of turbulence kinetic energy and its dissipation rate in the k-ε turbulence model were also taken from the work of Borghi *et al* (1977b) who obtained good agreement for the heat release rate for identical conditions to those measured in Moreau *et al* (1980).

Moreau *et al* (1980) also made predictions using two models based on the Zeldovich mechanism. The first model accounted for the superequilibrium of O atoms however ignored turbulent fluctuations. The second model assumed equilibrium for the O atoms as we have done and accounted for turbulent fluctuations with a presumed pdf approach in terms of the mass fraction of the fuel. They found that the super equilibrium based model agreed within 30% of the measured values while the other model underpredicted the production rate of NOx by a factor of between 10 and 100. Moreau *et al* (1980) assumed that the product stream contained 50 ppm of NOx based on measurements 22 mm downstream of the start of the combustor. However looking at these measurements they have a peak value of closer to 80 ppm near the wall and fall off gradually to zero about 30 mm from the wall. To be consistent with Moreau *et al* (1980) we have also assumed a uniform inlet NOx concentration of 50 ppm.

Since the fuel was methane and all of the correlations had been previously set up for propane these needed adjusting. The flame temperature and the equilibrium concentration of NO was computed by the NASA equilibrium code (Gordon and Mc Bride, 1971). Figures 4.2.4 and 4.2.5 illustrate the computed values with the correlation used to fit this data.

Equation (3-12) for the total molecular mass, m_T, for methane becomes:

$$m_T = 16.01 + \frac{274.56}{\phi}$$

and the fully burnt mass fraction of CO_2, $Y_{CO_2}^{c=1}$, becomes:

$$\phi \prec 1 \qquad Y_{CO_2}^{c=1} = \frac{44.01\phi}{16.01\phi + 274.56}$$

$$\phi \geq 1 \qquad Y_{CO_2}^{c=1} = \frac{44.01}{16.01\phi + 274.56}$$

Figure 4.2.6 compares these last two equations with the predictions of the NASA equilibrium code. Once again a similar trend is noted as with propane where the fully burnt equation for $Y_{CO}^{c=1}$ compares well with the equilibrium values for lean equivalence ratios, which are of interest to us, and poorly for rich ones.

Results from these calculations for the mean concentration of NO formed can be seen in Figures 4.2.7 and 4.2.8. Given that we are not predicting the oxidation of NO to form NO_2 it is better to compare our predictions with the concentrations of NO_x measured by the experiment. For the case with the smallest variance in the mixture fraction the agreement is quite good in the region downstream of the reactant inlet, which stretches across the upper 80 mm of the duct. Production rates here appear to be slightly under predicted which can be accounted for by the fact that we assumed equilibrium for oxygen and ignored other non-Zeldowich mechanisms of NOx formation. Downstream of the fully burnt product stream the NO_x levels are seriously under predicted. This is most probably due to NO_x which was produced by this stream before entering the measurement section which was not properly accounted for. Increasing the variance of the mixture fraction increases the rate of formation of the NO_x as has been mentioned earlier. This trend is well predicted apart from the case with the highest possible variance. This case has a reduced rate of reaction for the main heat release as the fuel and oxidiser are initially unmixed and must mix before they can burn. Thus the level of NO_x produced further away from the burnt product stream is underpredicted because the flame spreading rate is reduced. However closer to the burnt product stream where the flame front is located the rate of NO_x production is much higher than for the other cases. The final case, which was run with a equivalence ratio of unity for the fully burnt stream, grossly over predicted the quantity of NO_x downstream of this section of the duct due to the very high flame temperature. However it had a negligible affect on the NO_x concentrations predicted downstream of the reactant inlet. An error in the measured inlet temperature of the fully burnt stream may also be a cause in the difference between the predicted and measured concentration of NO_x downstream of it. The results of this latter computation though indicate that this does not affect the validity of the comparison made of the NO_x produced downstream of the reactant inlet stream.

Generally speaking these predictions indicate that the NO_x model is doing a good job at predicting the levels of NO_x produced. The variance of the mixture fraction in the experiment was not measured, however given the long premixing section it is likely to be very low. Increasing the variance of the mixture fraction gives the expected increase in the level of NO_x produced as was discussed in Section 2.1.1. This can also be seen in Figure 4.2.9 which illustrates the affect of the mean and the variance of the equivalence ratio on the mean production rate of NO. Clearly it would be

instructive to evaluate this model against an experiment in which the variance of the mixture fraction is well defined, however such an experiment does not appear to have been reported in the literature.

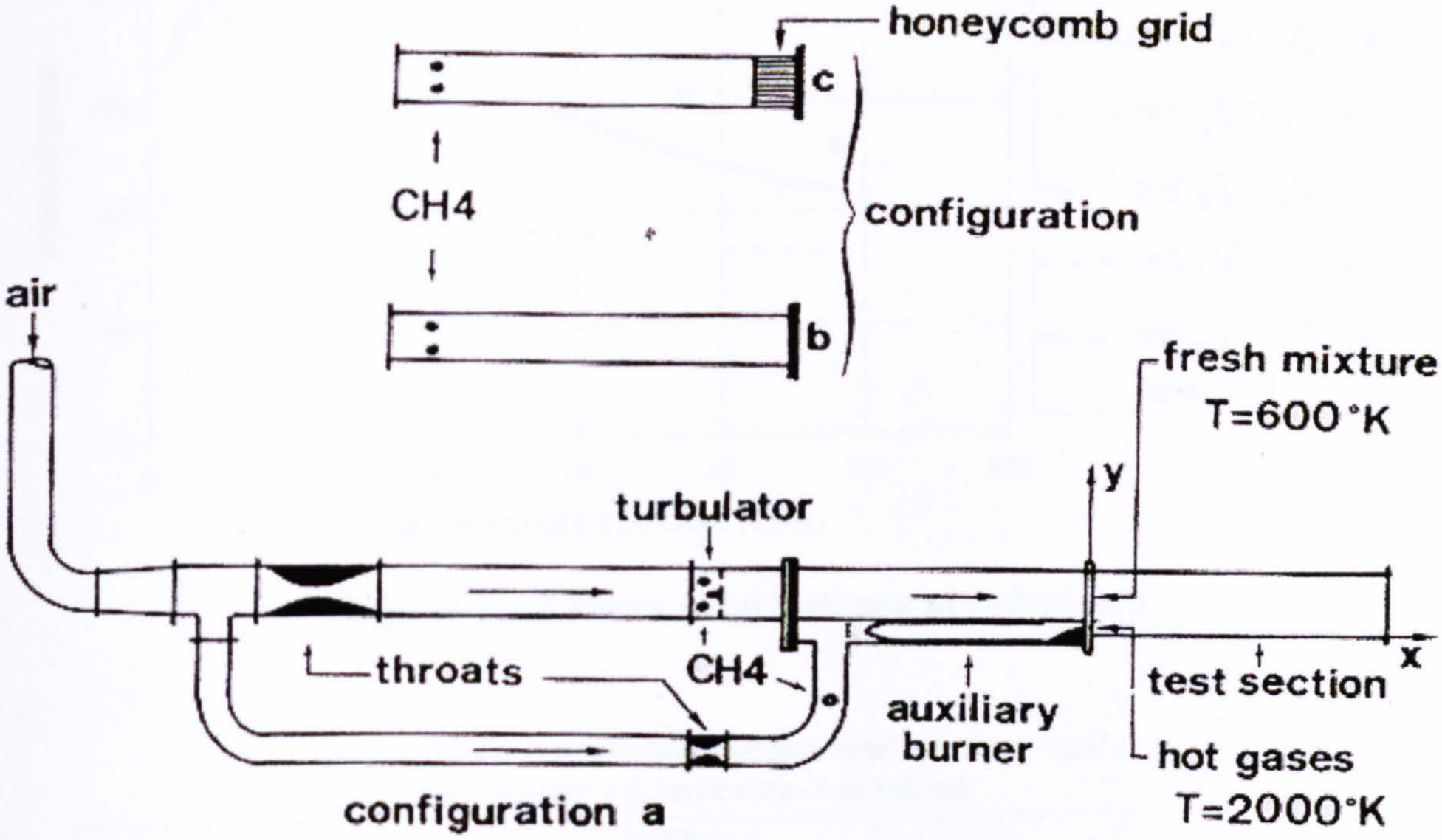

Figure 4.2.1 Experimental Configuration

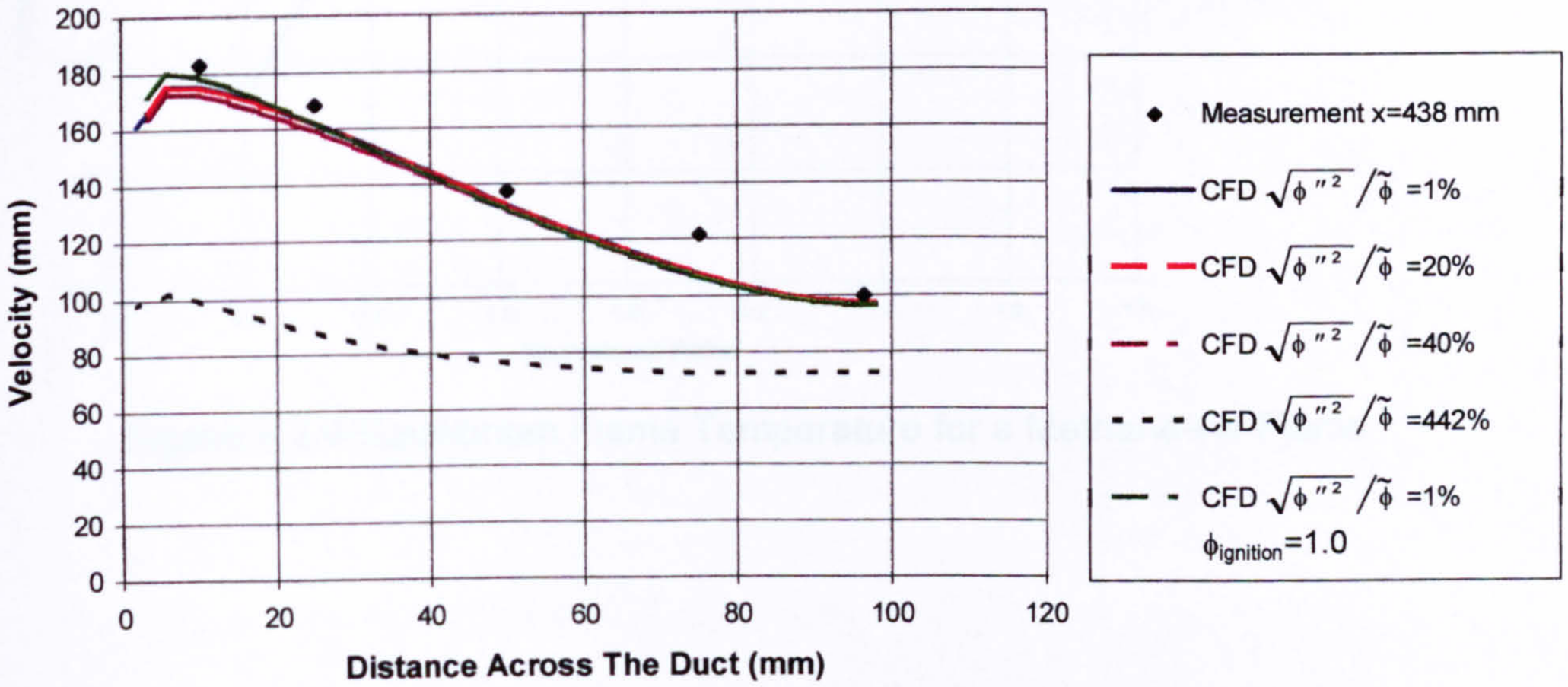

Figure 4.2.2 Mean Axial Velocity at x=438 mm

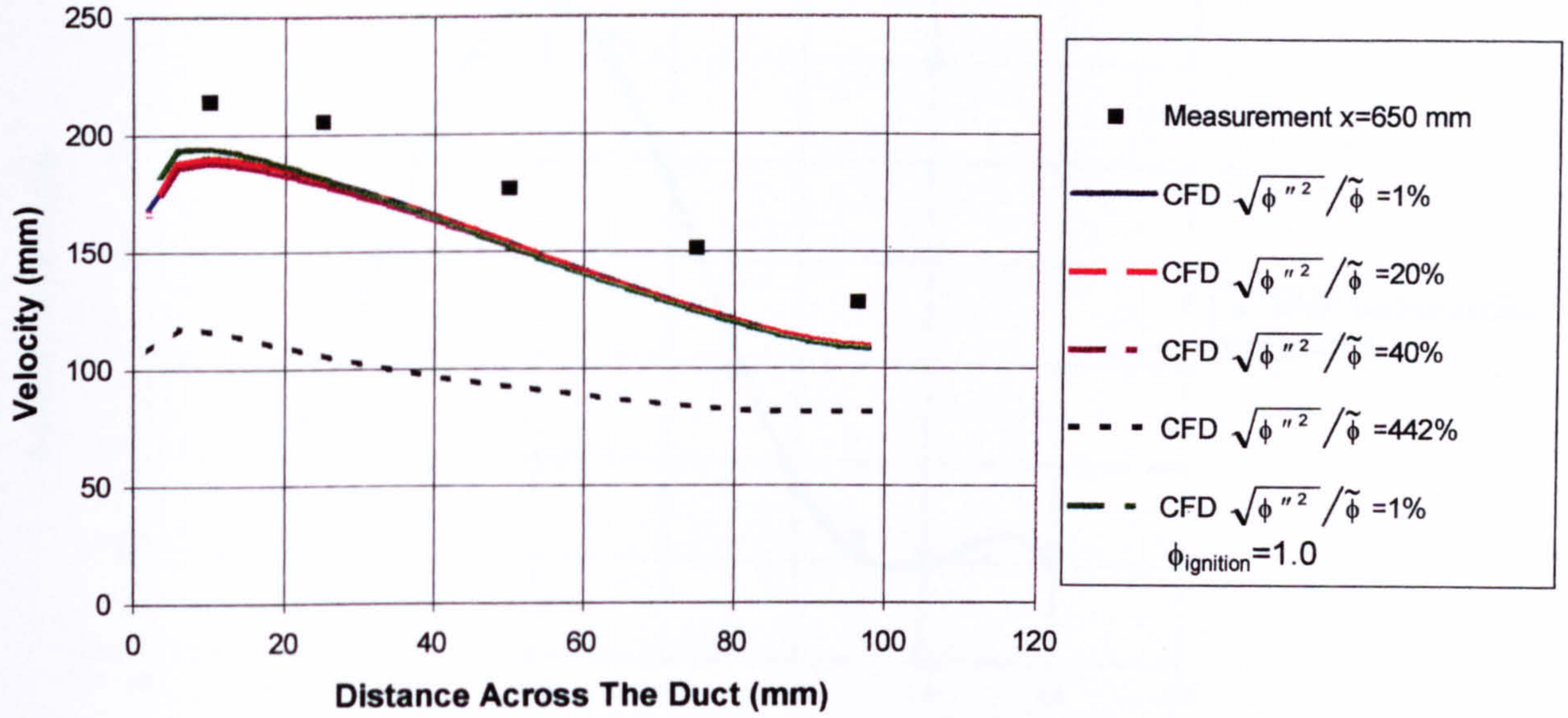

Figure 4.2.3 Mean Axial Velocity at x=650 mm

$$y = -6.0393E+03x^6 + 3.6437E+04x^5 - 8.6294E+04x^4 + 1.0180E+05x^3 - 6.4135E+04x^2 + 2.2443E+04x - 1.8444E+03$$

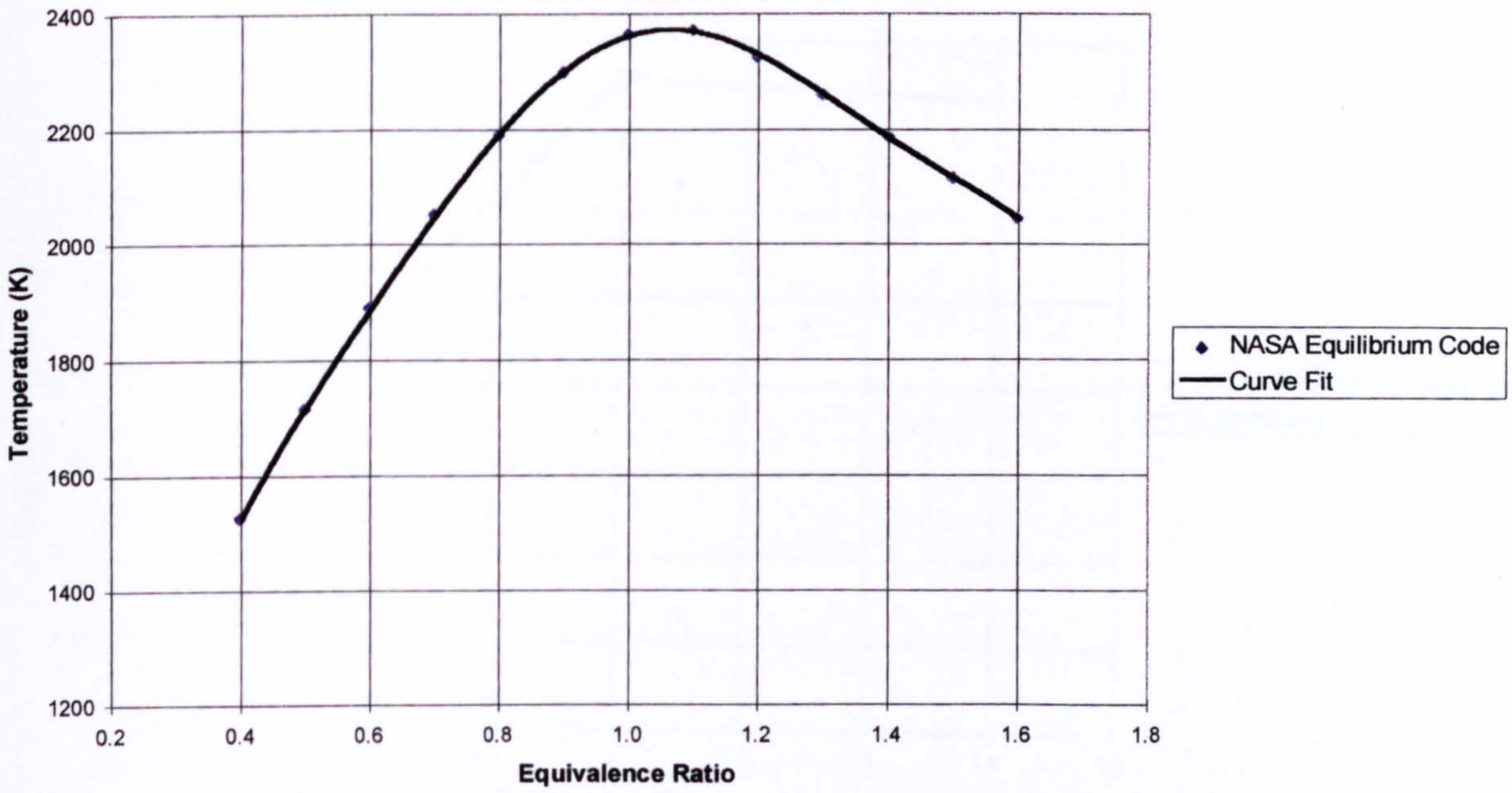

Figure 4.2.4 Equilibrium Flame Temperature for a Methane-Air Flame

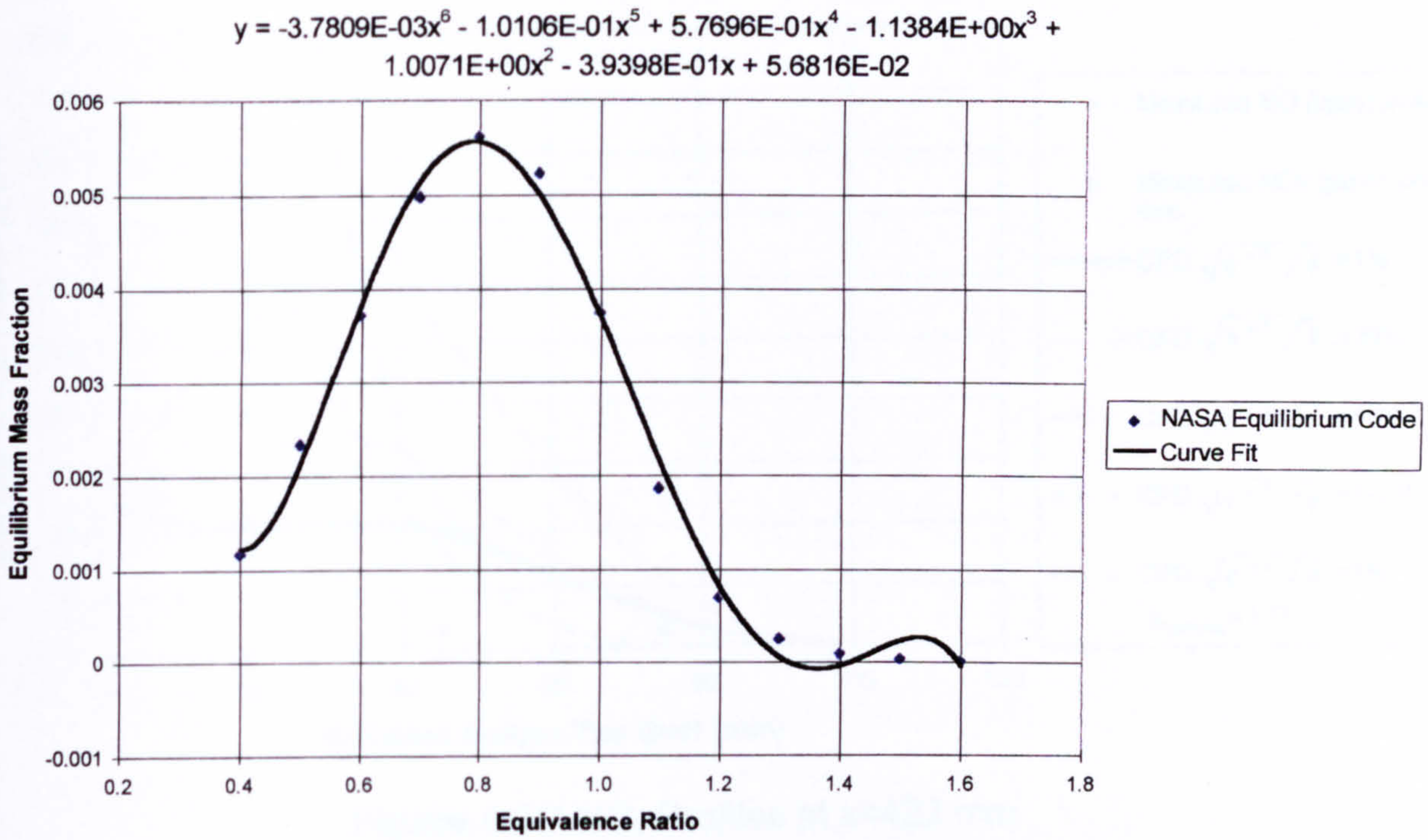

Figure 4.2.5 Equilibrium Mass Fraction of NO for a Methane-Air Flame

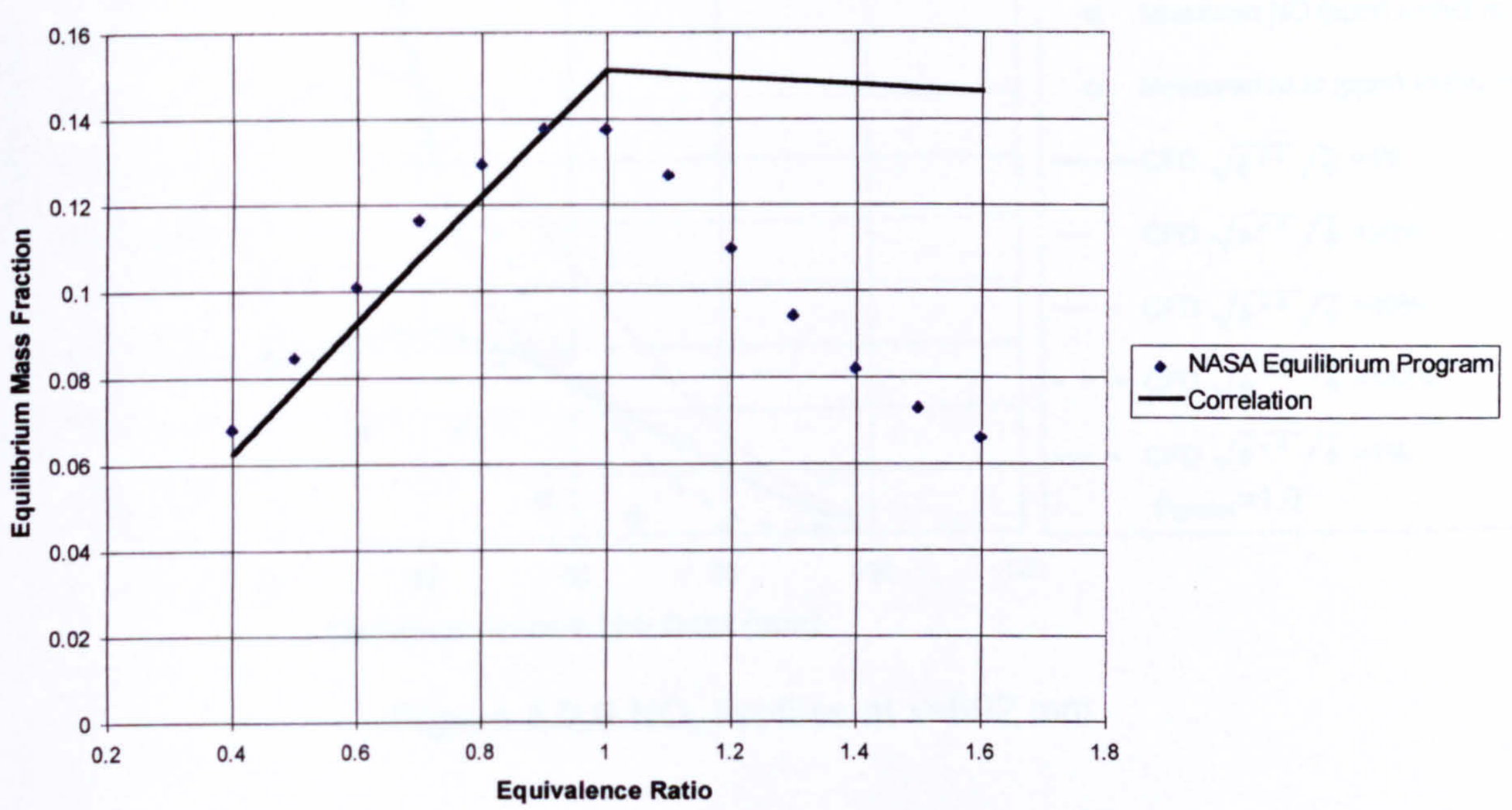

Figure 4.2.6 Equilibrium Mass Fraction of CO_2 for a Methane-Air Flame

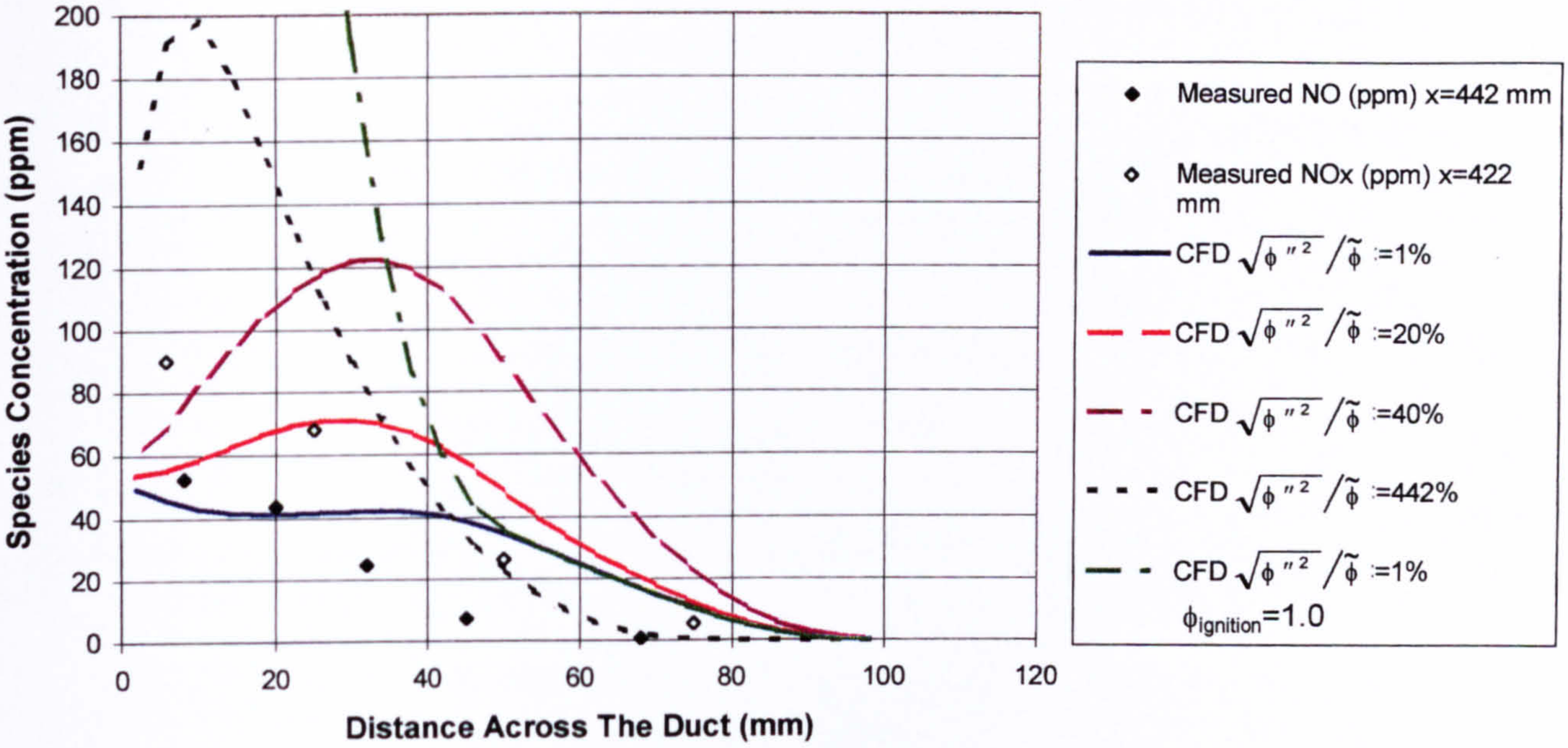

Figure 4.2.7 NO_x Profiles at x=422 mm

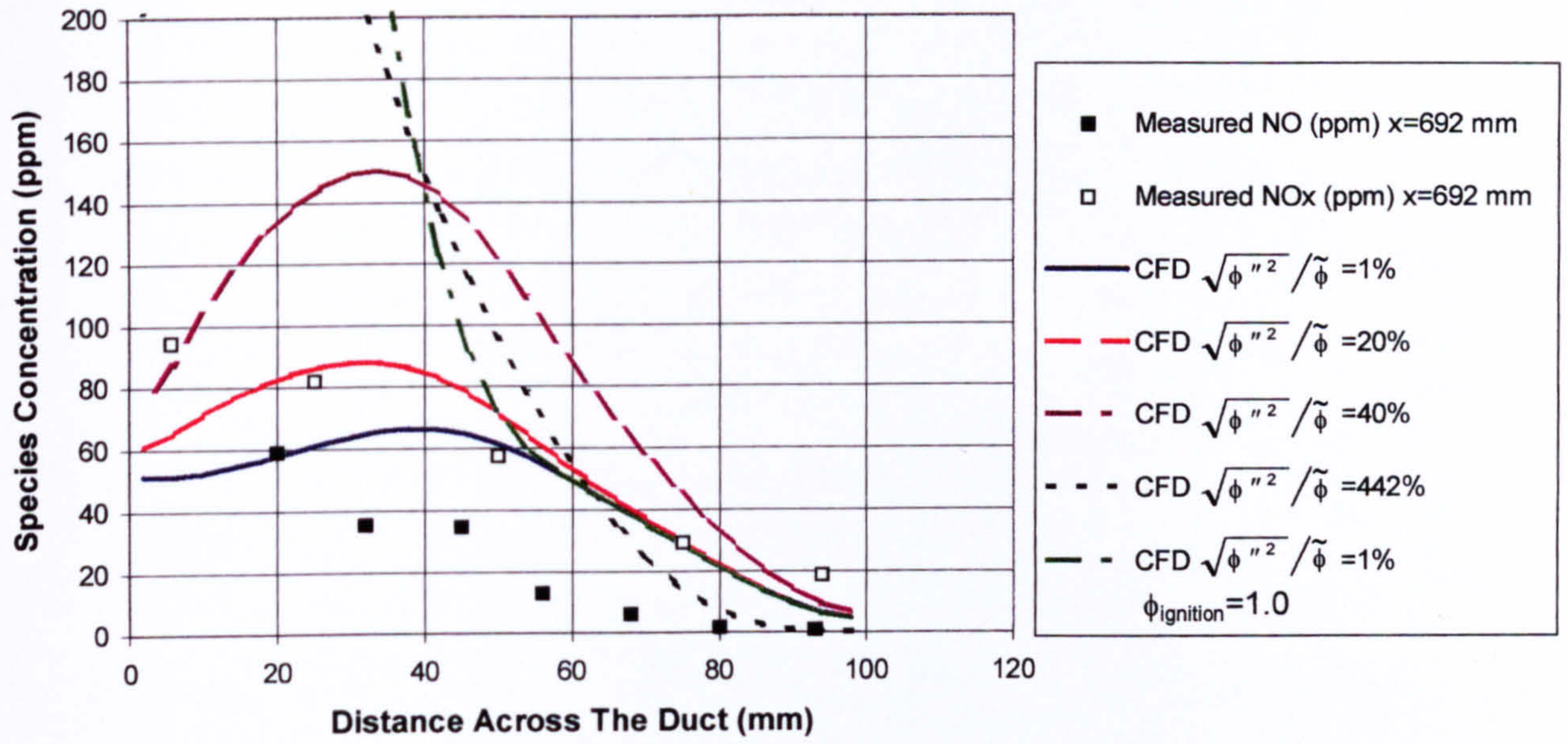

Figure 4.2.8 NO_x Profiles at x=692 mm

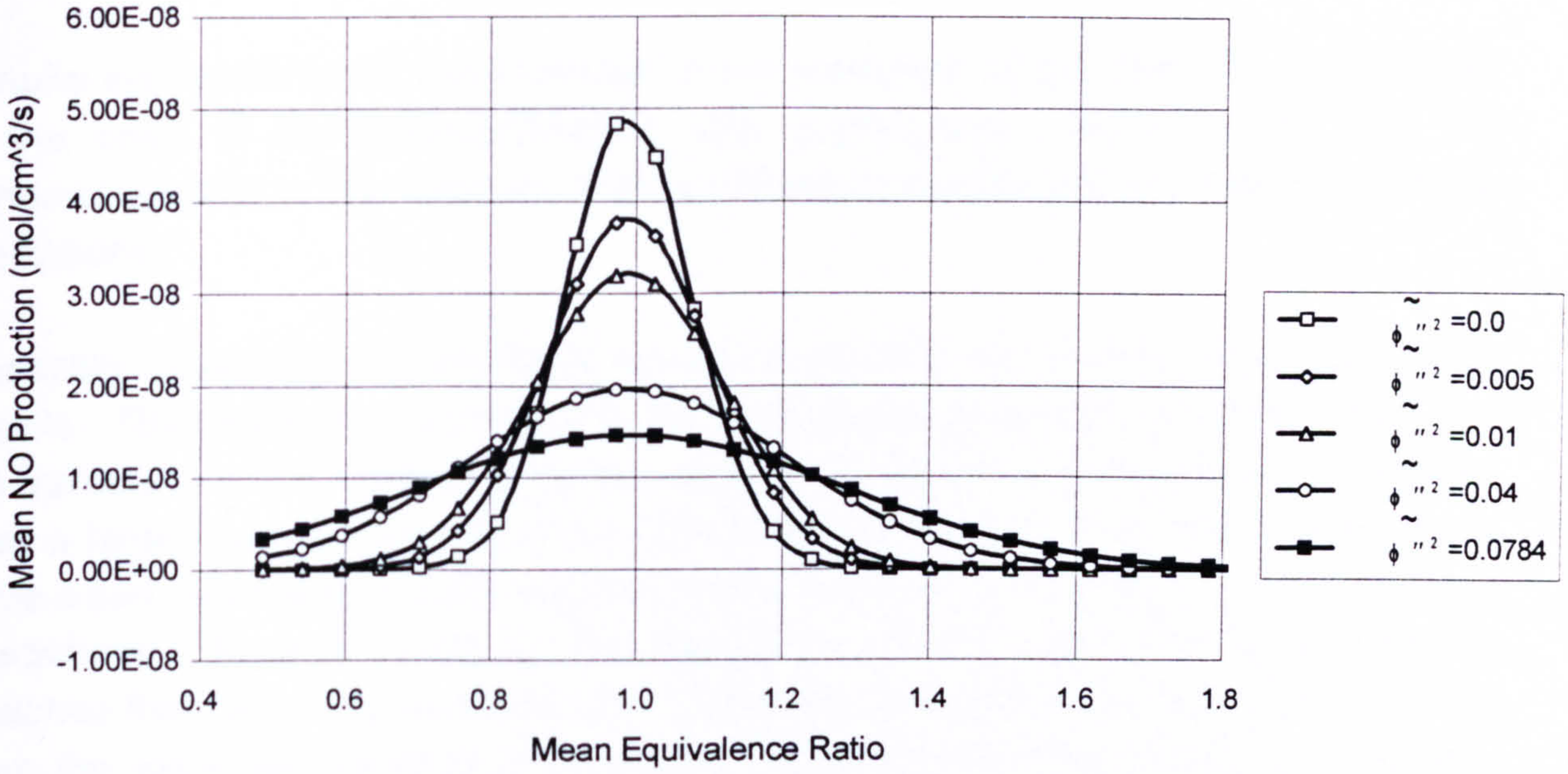

Figure 4.2.9 Influence of the Mean and Variance of the Equivalence Ratio on the Mean Rate of Production of NO for a Propane-Air Flame at Atmospheric Conditions

4.3 Conclusions

Despite well established shortcomings in the prediction of the flame front spreading in the case of the backward-facing step experiments, useful insight into the performance and implementation of the combustion models can be drawn from these predictions.

Generally speaking the Eddy Break-up and Presumed pdf models generated similar results. The chemical source term in the Eddy Break-up model, which assumes that the variance of the reaction progress variable is always a maximum, is distributed over a larger region than that of the Presumed pdf model. This latter model would have a zero source term if the variance was a maximum and relies primarily, in these predictions (Figure 4.1.2.30), on the dissipation by molecular diffusion to keep the variance from obtaining its maximum. This works to achieve the maximum deviation from the maximum variance at a reaction progress variable near 0.5. This also coincides with the maximum value of the maximum possible variance which is where the Eddy Break-up model which is proportional to this value would also have its peak chemical source term. Thus for this geometry both combustion models have their peak chemical source term at the same value of reaction progress variable. Given that the variance of the reaction progress variable predicted by the Presumed pdf model approaches the maximum variance as one approaches either zero or one (Figure 4.1.2.31) then one can see that the chemical source term will have a sharper peak at its maximum than the Eddy Break-up model.

Expanding on the inherent differences between the two models, the Eddy Break-up model assumes that only products and reactants exist and that the creation of products from reactants is instantaneous. The mean rate of reaction depends on the concentration of both these species. If there are only products present then the temperature is sufficient for combustion but there aren't any reactants to react. And vice versa if there are only reactants then there is material to react but not sufficient temperature for it to occur. Thus the maximum mean rate of reaction will occur when there is an even mixture of the two. The presumed pdf model does not assume that the conversion from reactants to products is instantaneous. However, in a similar fashion to the Eddy Break-up model the instantaneous rate of reaction (Equation (3-13)) requires the existence of product or at least a high inlet temperature and reactants for it to be non-zero. If the variance of the reaction progress variable was at its maximum then at any instant in time only product or reactants would exist and there would not be a mixture of the two. Thus, provided the inlet temperature was not sufficiently high to self ignite the mixture, the mean source term of the presumed pdf model would be zero. In the case of the Eddy Break-up model such a mixture would never exist since as soon as it did it would instantly react to form product. However in the case of the presumed pdf model there is a finite time scale

associated with the rate of reaction and so such mixtures are possible and in fact are required for reaction to occur. As the rate of reaction is increased the chemical source term in the variance equation (Equation (3-17)) will increase. This is the dominant positive source term for the variance (Figure 4.1.2.30) and will cause the variance to move closer to its maximum. At the same time the reduction in the mean reaction rate due to the increased variance will be compensated for by the increased instantaneous reaction rate. Therefore it is expected that in the limit as the chemical reaction rate approaches infinity the presumed pdf model will reduce to a model similar to the Eddy Break-up model.

A number of distinct features emerge from the solutions. The flame front strength in this flow field appears to be dominated by the formation of the shear layer at the step. Turbulence frequency (ε/k) within the recirculation appears to be substantially independent of the inlet conditions of turbulence, upstream of the step. It is not possible to influence the flame front spreading by modifying the inlet boundary conditions and thus in order to obtain a reasonable prediction of the flame front spreading with steady state models it would be necessary to initiate the calculation downstream of the formation of the shear layer as was done by Mason and Spalding (1973). Additionally, comparisons of the shapes of both Bray-Moss style and β function pdf's indicate that the largest difference between the two for this flow field lie near zero and one. However generally speaking, these two pdf's are very similar and, given that there are no specific physical arguments for the β function pdf and it is more complicated to integrate when the variance is large, the Bray-Moss style pdf is the best choice.

The NOx computations indicated that the model, as described in Section 3.5, gives satisfactory predictions of the growth of NOx concentrations as the flame front expands. Initial values of NOx were not reported in the experiment and pilot stream levels are lower than those in the experiment, however the levels in the reactant stream behind the flame front follow closely to those measured in the experiment. The parametric analysis of inlet fuel air mixture inhomogeneity indicate that this is a very important factor in increasing NOx formation rates.

5 Experimental LPP Combustor

5.0 Introduction

The main objective of this study was to evaluate a range of combustion models on a practical combustor geometry. To accomplish this, predictions were made of an experimental lean prevaporised premixed (LPP) combustor which was tested at Cranfield under atmospheric conditions by Harding (1996). Unfortunately the data available from this experiment are somewhat limited and can only provide a qualitative basis for comparison of the various combustion models.

The configuration which is illustrated in Figure 5.1 is similar to most LPP combustors which are either commercially available or currently being researched. It incorporates a premixing duct which is fed air through radial in-flow swirlers. Fuel is injected radially outward, with a tangential component of velocity in the same direction as the swirlers, from a central lance which also admits non-swirling air through its centre. The air fuel mixture then passes through a converging and then diverging section of duct, before it enters the combustion chamber via a sudden expansion. The combination of swirl and the sudden expansion induce a reverse flow zone along the central axis of the duct near the end of the premixing section which acts to stabilise the flame. Detailed dimensions of the experimental rig can be found in Harding's thesis (Harding, 1996).

This numerical investigation involved two phases. The first assessed the cold flow predictions by comparison with the experimental measurements made within the premixing duct. This phase included a comparison of simulations employing a variety of grids and turbulence models. The second phase involved a comparison of the three combustion models, two turbulence models and NO_x model.

5.0.1 Modelling Issues

PHOENICS was used for the flowfield computation and all three user-defined combustion models were investigated with both the k-ε and second moment turbulence models. The PHOENICS implementation of the second moment closure was severely limited in that applications are restricted to cartesian or cylindrical grids without any internal blockages. For the k-ε turbulence model such restrictions do not apply. Thus three grids were created. One detailed grid describing the complete combustor was created starting with a plenum chamber upstream of the premixing duct. This grid is illustrated in Figure 5.2. It was used for cold flow calculations to establish boundary conditions for the other two grids, which were cylindrical and

permitted the implementation of all the combustion models in conjunction with the k-ε and second moment turbulence models. The radial inflow swirlers in the detailed grid were modelled using source terms in the momentum equations to ensure that the correct radial velocity was imparted to the flow. The pressure drop across the swirlers due to losses was not accounted for in the absence of experimental pressure measurements. The fuel injector which consisted of individual holes distributed around the circumference of the lance, could not be resolved and was simulated as a single slot. This permitted a quasi-2 dimensional treatment of the geometry. The grid was generated as a two dimensional axisymmetric grid but the calculation included all three orthogonal velocity components (axial, radial, and tangential). The pre-processor of FLUENT was used to generate the body fitted grid. The two cylindrical grids are illustrated in Figures 5.3 and 5.4. The first begins at the inlet of the convergent divergent duct with the wall created using blocked cells. The second grid started at the exit of this duct and was used for the second moment calculations.

Inlet boundary conditions for the first of these grids came from the cold calculations of the body-fitted grid and inlet conditions for the final grid came from the k-ε calculations of the second grid. The reason for re-computing the k-ε cases on the second grid was to ensure that both the second moment and k-ε cases had a similar grid layout. The addition of the premixing duct section for the k-ε calculations allowed for the inclusion of any combustion that might occur within this duct and its impact on the velocity field.

A fixed static pressure boundary was applied to the outlet conditions and standard wall functions were applied to all walls. Hybrid differencing was used for all calculations.

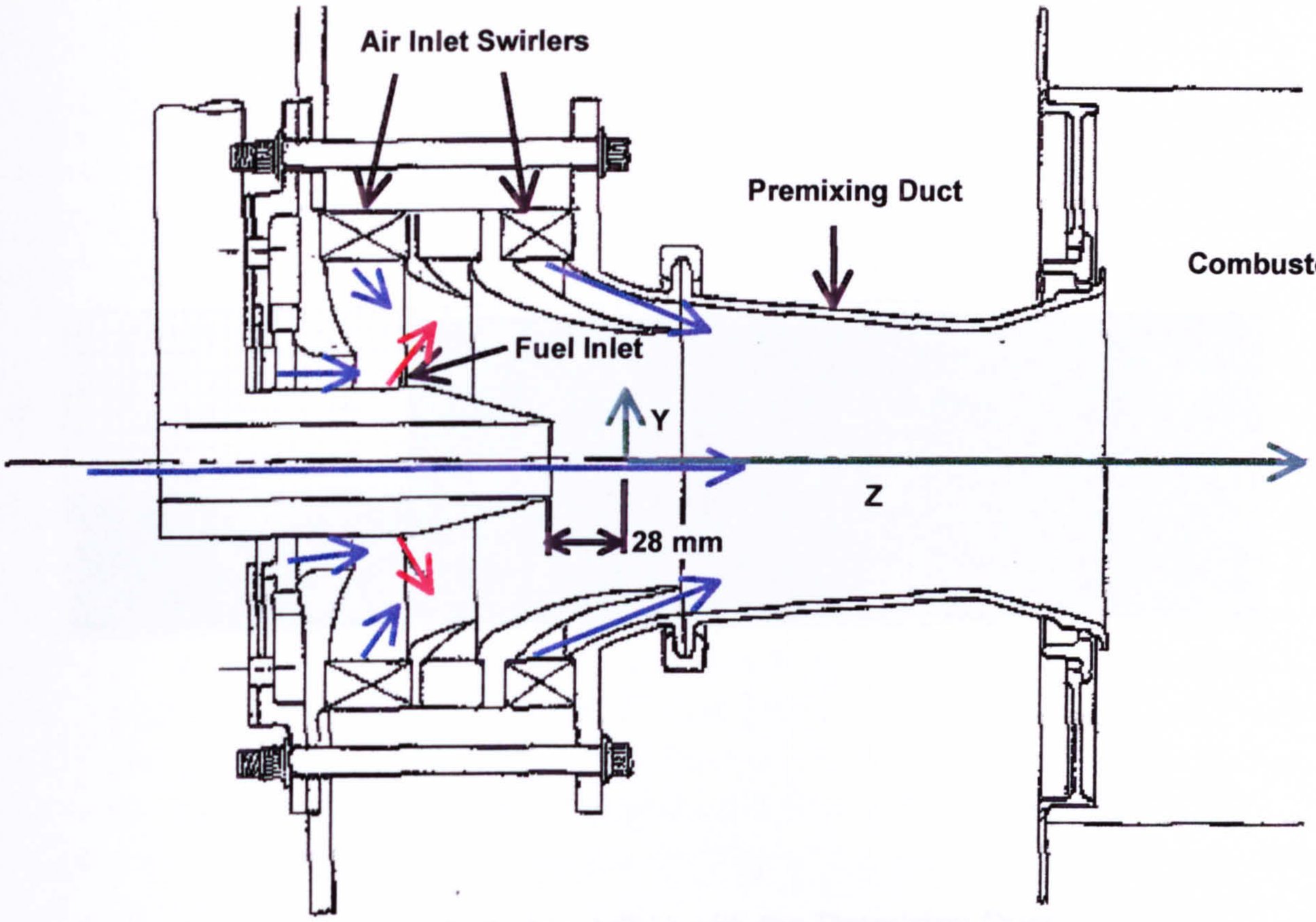

Figure 5.1 Generic LPP Test Combustor

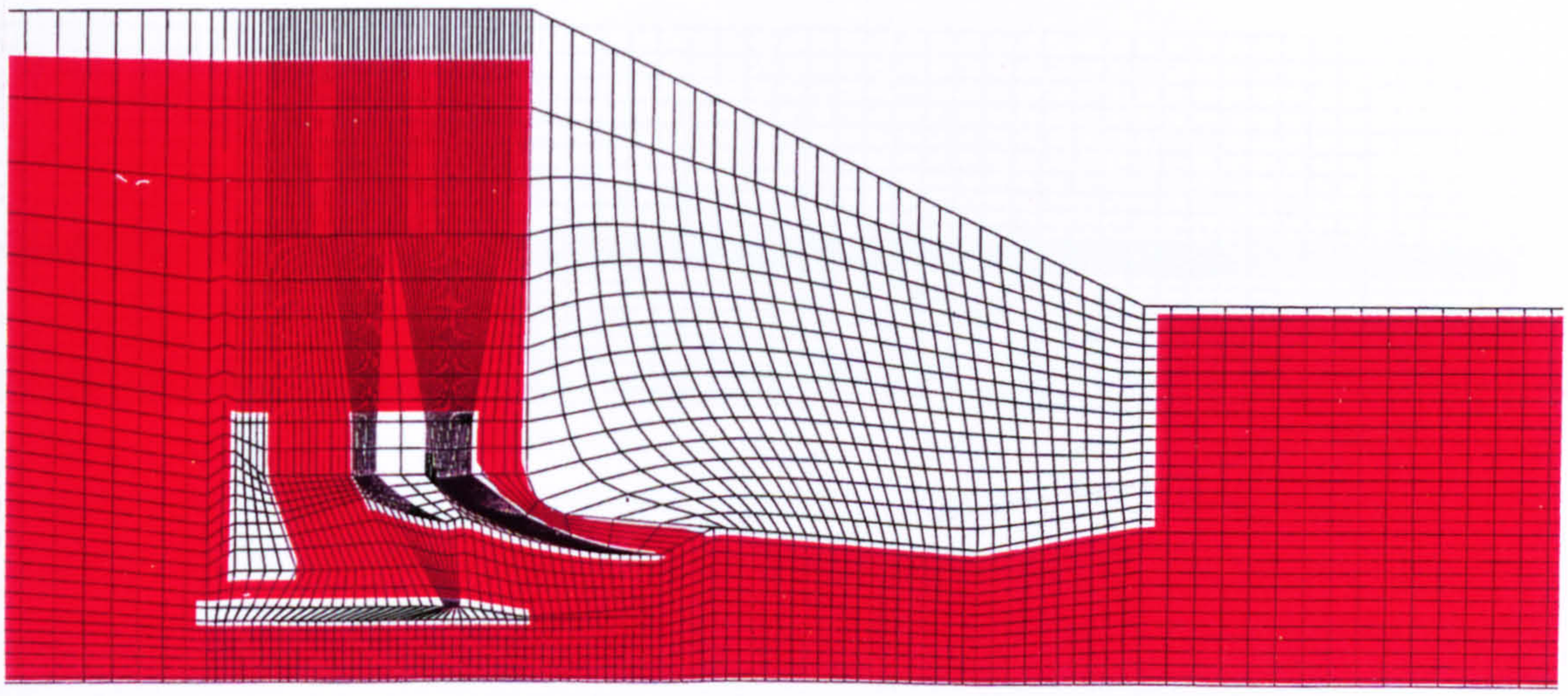

Figure 5.2 Body Fitted Combustor Grid in region of Premixing Duct
(Red colour denotes cells which are active)

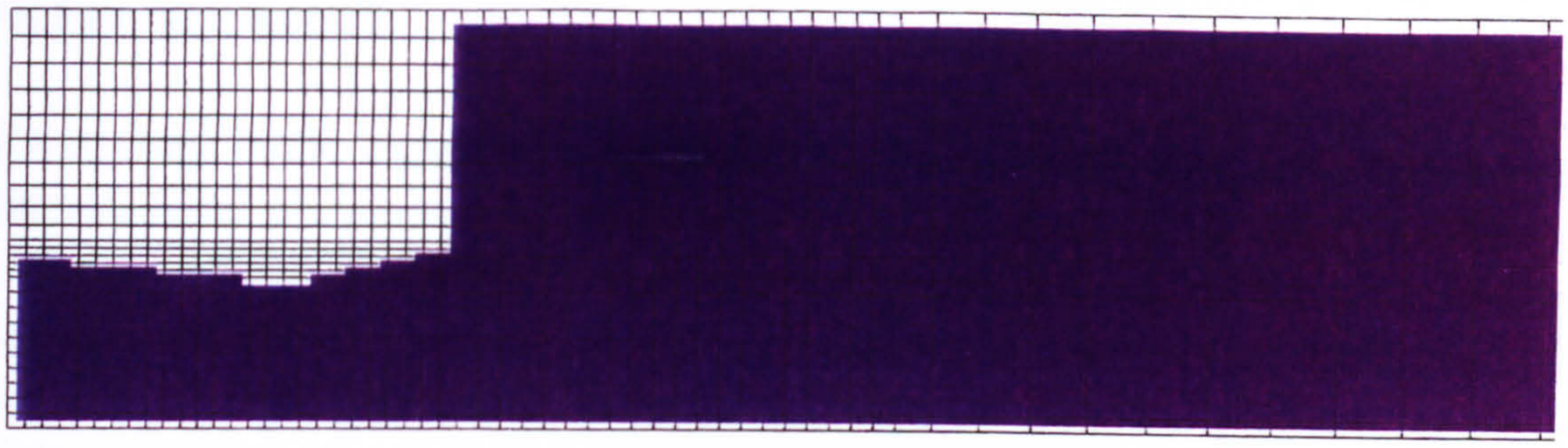

Figure 5.3 Cylindrical Grid with the Premixing Duct
(Blue indicates cells which are active)

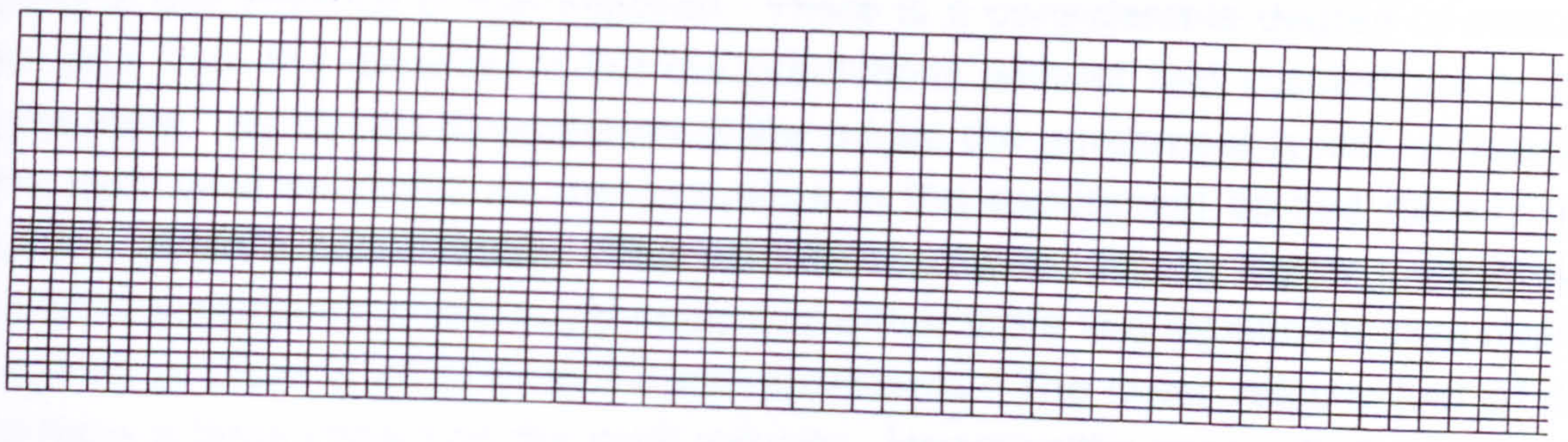

Figure 5.4 Cylindrical Grid starting downstream of the Premixing Duct

5.1 Isothermal Predictions

Isothermal predictions were made using all three grids and both k-ε and second moment turbulence models. Inlet conditions for the calculation, made with the body fitted grid, were taken from the experiment (Harding, 1996b). The air mass flow was 0.107 kg/s with a temperature of 1000 K and pressure around one atmosphere. The air to fuel ratio was 22.

The fuel used in the experiment was liquid kerosene. The two-phase flow brings an additional level of complexity, which was not considered to be within the scope of this study. Many researchers have chosen gaseous propane as a substitute for kerosene because of some similarity in combustion characteristics (Lefebvre, 1977). However, the boundary condition at the fuel injector posed a problem for gaseous injection. In order to predict the same distribution of the fuel within the channel the fuel penetration should be the same for the gaseous fuel as for the liquid. We decided to investigate two velocities for the fuel jet, one with a Mach number just under the speed of sound with a value of Mach 0.8 or 507.10 m/s and the other with a velocity of 225.36 m/s or 8 times the velocity of the fuel given the experimental geometry.

5.1.1 Mixing Duct Predictions: Body Fitted Grid

Figures 5.1.1 through 5.1.4 illustrate radial profiles of the mean axial velocity within the premixing duct. The axial position z is based on the co-ordinate system illustrated in Figure 5.1 and starts 28 mm downstream of the exit from the central fuel lance. The air velocity measurements were made by laser doppler anemometry (LDA) in the absence of fuel injection. There is a considerable degree of scatter in the data from the experiment but the predictions without fuel injected are in good agreement. By 25 mm downstream of the origin, the agreement is less satisfactory. The high axial velocities on the centreline in the experiment spread radially more rapidly, giving a flatter profile. The velocities on average are higher than those of the CFD predictions which would imply that either there is a significant asymmetry in the flow, or there is an error in the measurements. The lower velocity fuel jet does not have a large impact on the axial velocity. However the case with the higher fuel jet velocity tends to produce a region of lower velocities immediately downstream of its injection point which is compensated at a larger radius as the air is displaced. In practice the fuel is injected through distinct holes around the circumference of the lance and the air will be able to penetrate between the fuel jets. In the predictions, the annular fuel sheet presents a more impenetrable barrier.

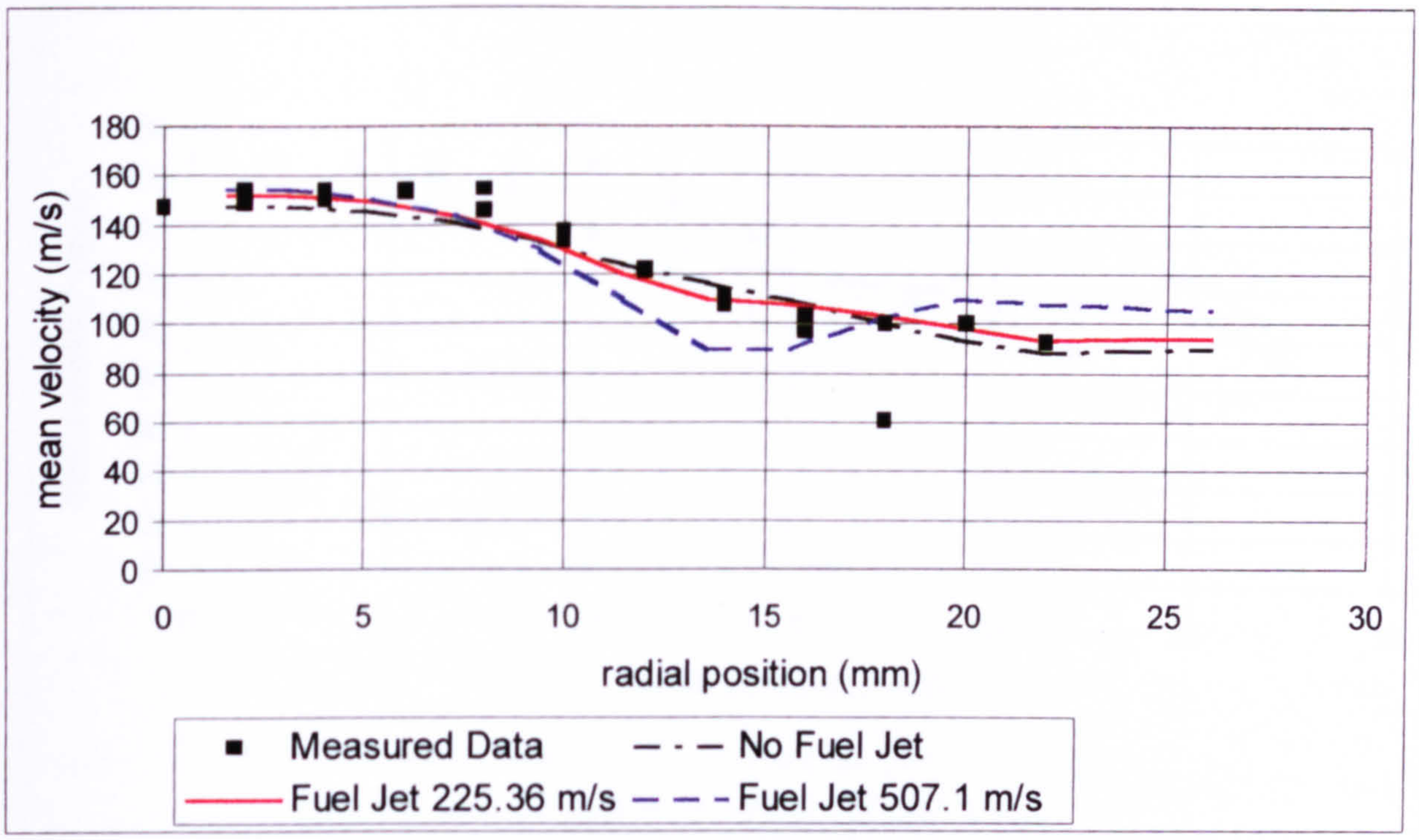

Figure 5.1.1 Mean Axial Velocity at z=0 mm

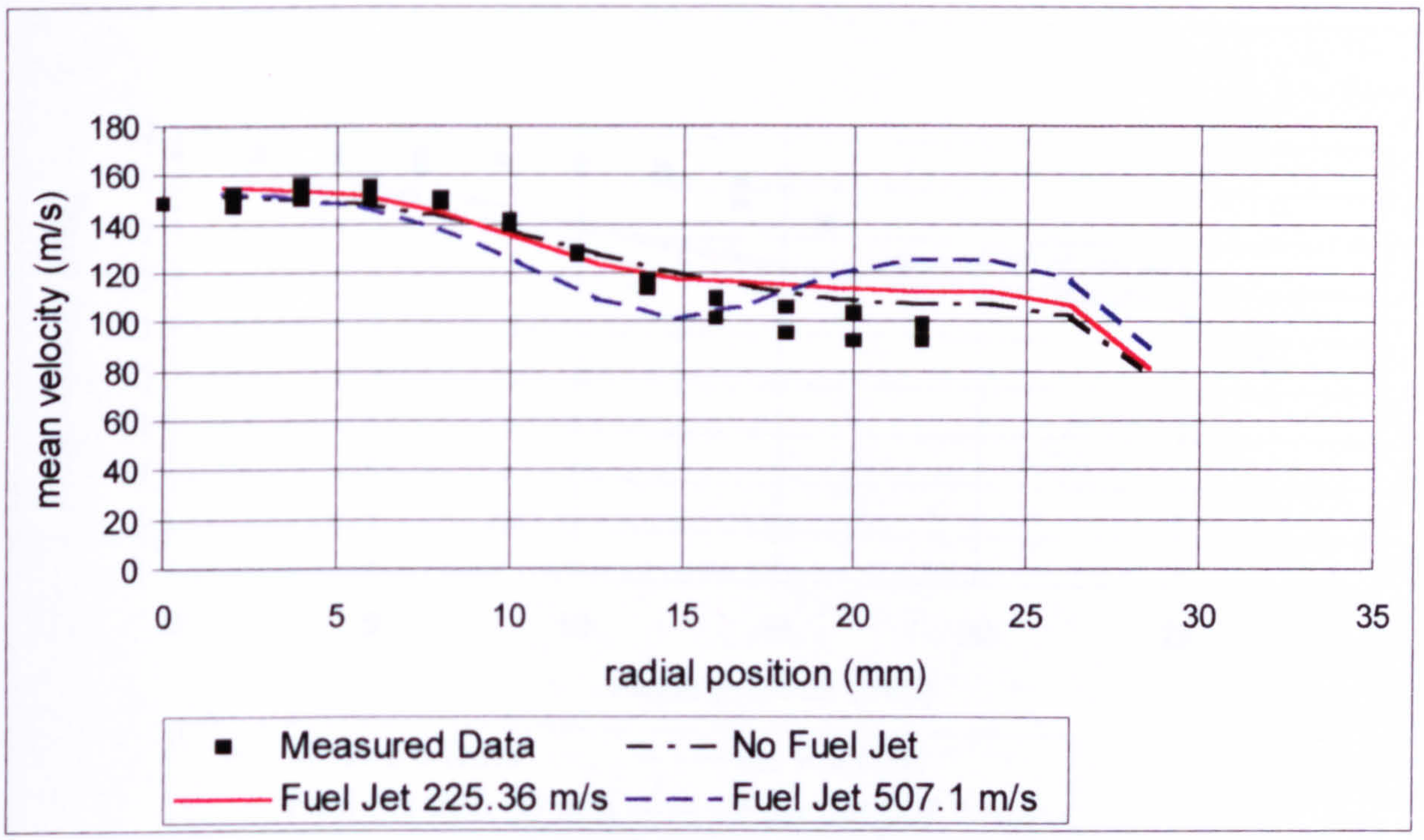

Figure 5.1.2 Mean Axial Velocity at z=10 mm

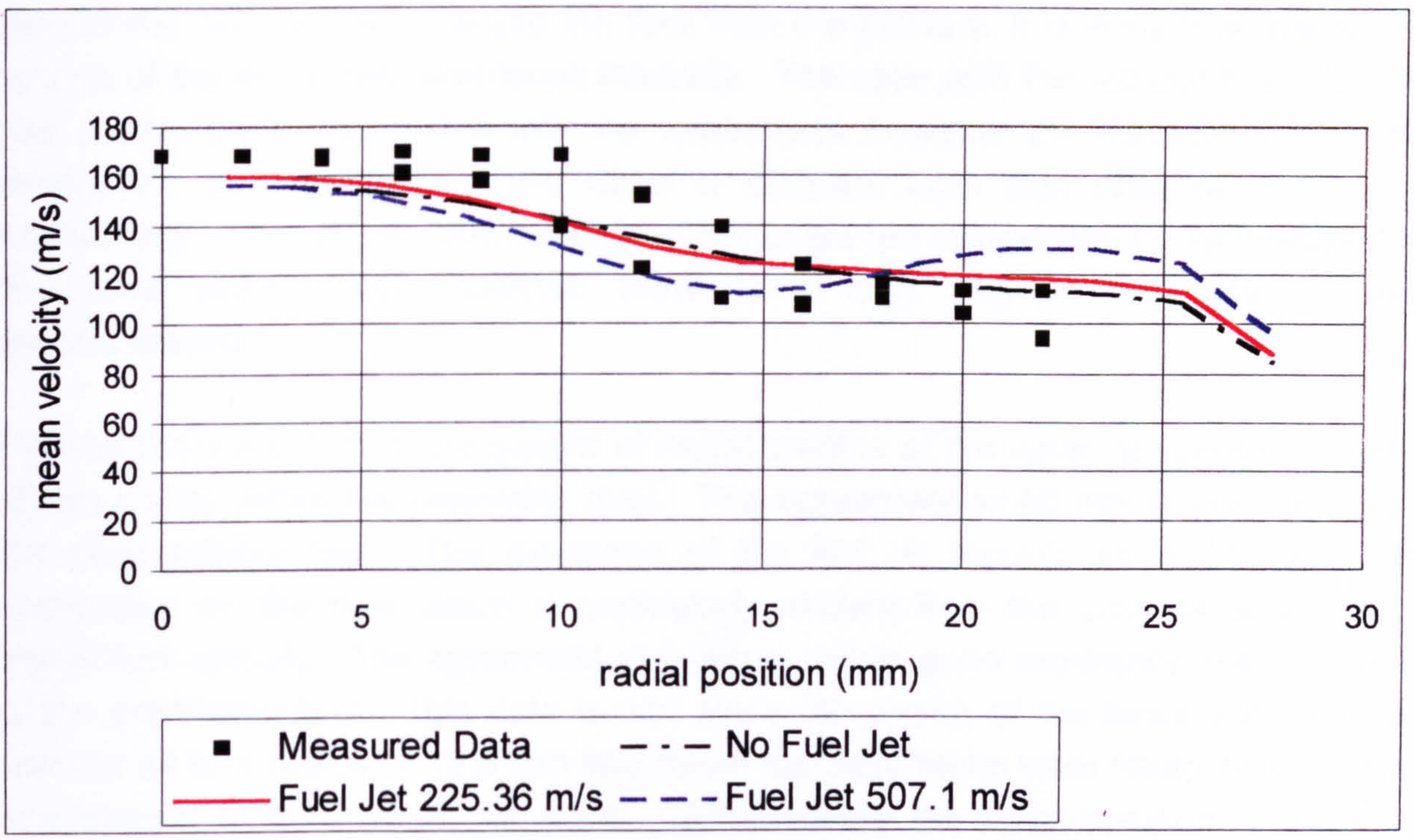

Figure 5.1.3 Mean Axial Velocity at z=20 mm

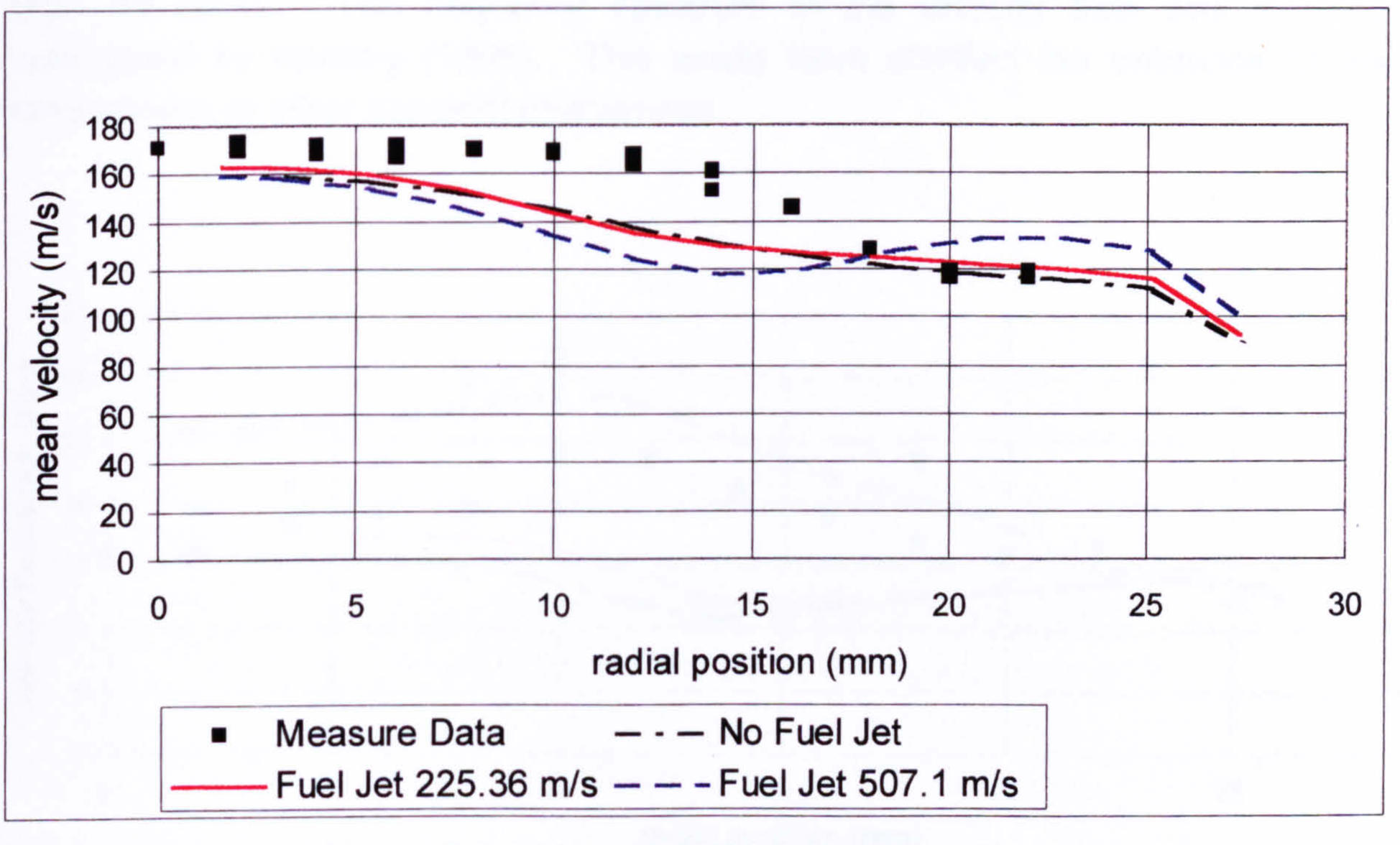

Figure 5.1.4 Mean Axial Velocity at z=25 mm

Figures 5.1.5 through 5.1.8 present radial profiles of the root mean square of the axial velocity at the same axial positions as the plots of mean axial velocity. The agreement for these predictions is not quite as good for the case without fuel flow. The turbulence intensities are generally underpredicted. Given that the peak in turbulence intensity for the case at 0 mm is in the region of the shear layer between

the central non-swirling flow and the flow from the swirlers, it is likely that this is the source of the enhanced turbulence intensity. The case with the highest fuel velocity has a very good agreement with the experiment however the mechanism for the production of turbulence in this case is different from that observed from the experiment. After 20 mm downstream of the origin the agreement is much better for the case without fuel, however there is a high degree of scatter in the measurements.

Figures 5.1.9 and 5.1.10 are graphs of radial profiles of the mean tangential velocity at two points within the premixing duct. The agreement at 40 mm is very good for the case without fuel. The existence of the fuel jet imparts an additional swirl component on the flow, which is particularly evident from the predictions with the higher fuel velocity. The agreement at 0 mm is not as good especially near the axis of the premixing duct. This data is odd since the centre of the lance admits non-swirling air to a radius of 12.5 mm and these measurements were taken only 28 mm downstream of the end of the lance. Unfortunately the measurements were only made from one side of the duct and it is not possible to verify that this large swirl velocity was on the centreline of the burner and not that the measurements were taken off centre. The frequency spectrum of the velocity data was also not investigated by Harding (1996). This would have clarified the existence of any unsteadiness or other transient phenomena.

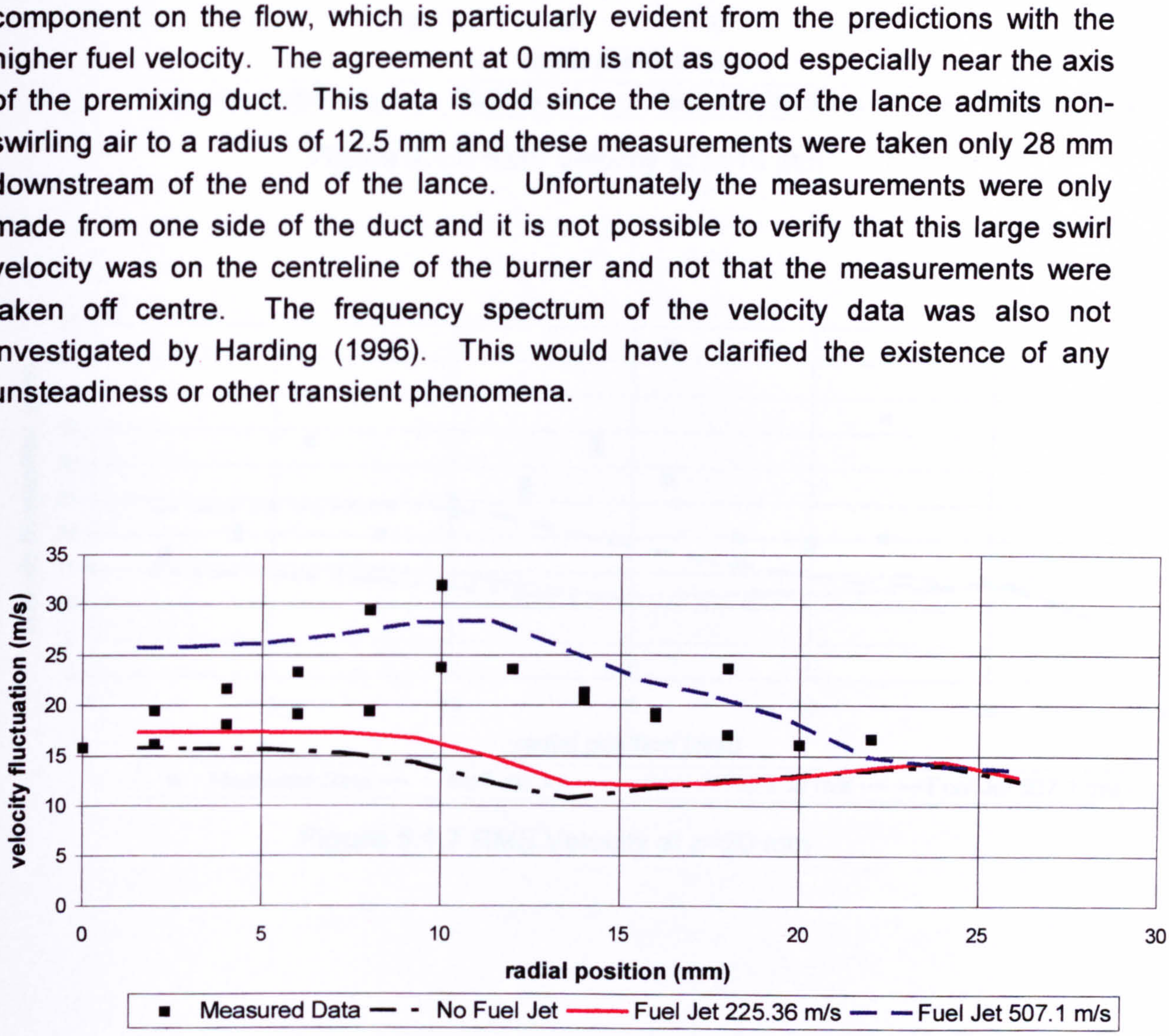

Figure 5.1.5 RMS Velocity at z=0 mm

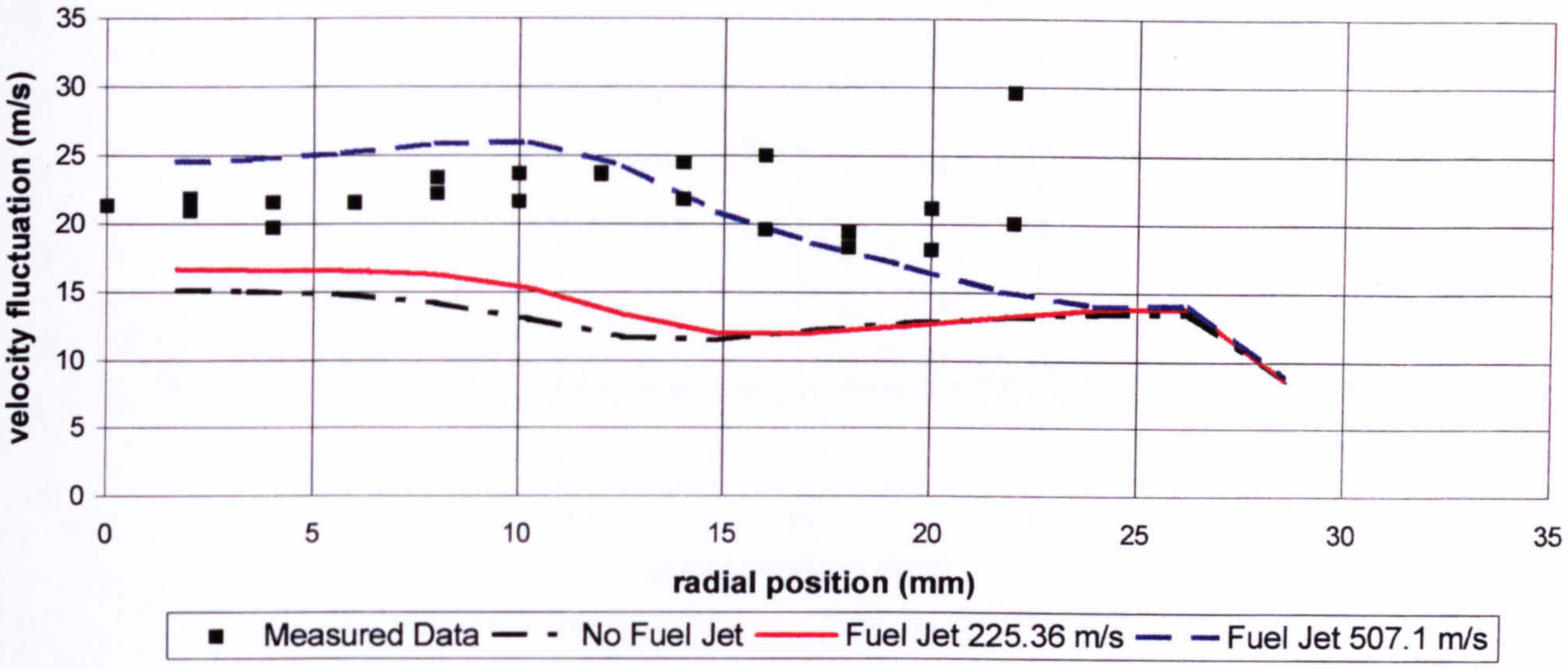

Figure 5.1.6 RMS Velocity at z=10 mm

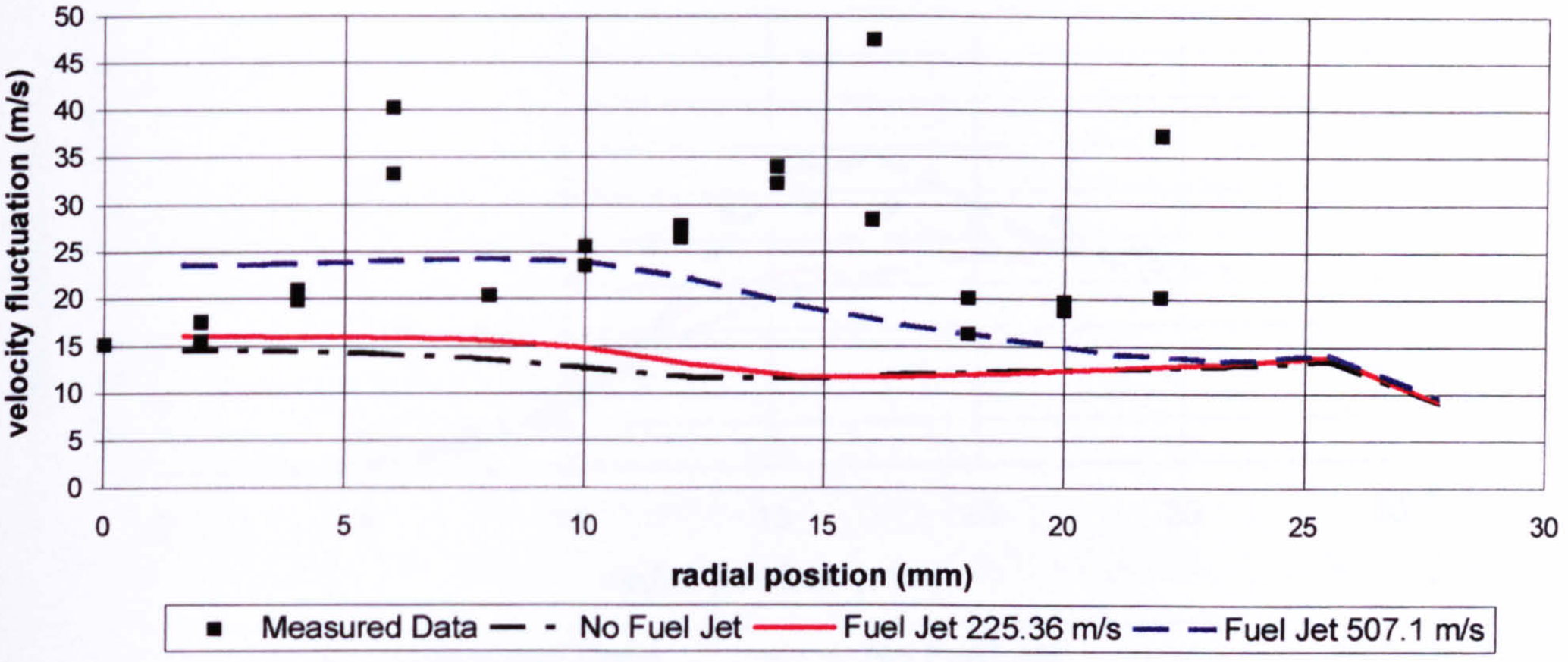

Figure 5.1.7 RMS Velocity at z=20 mm

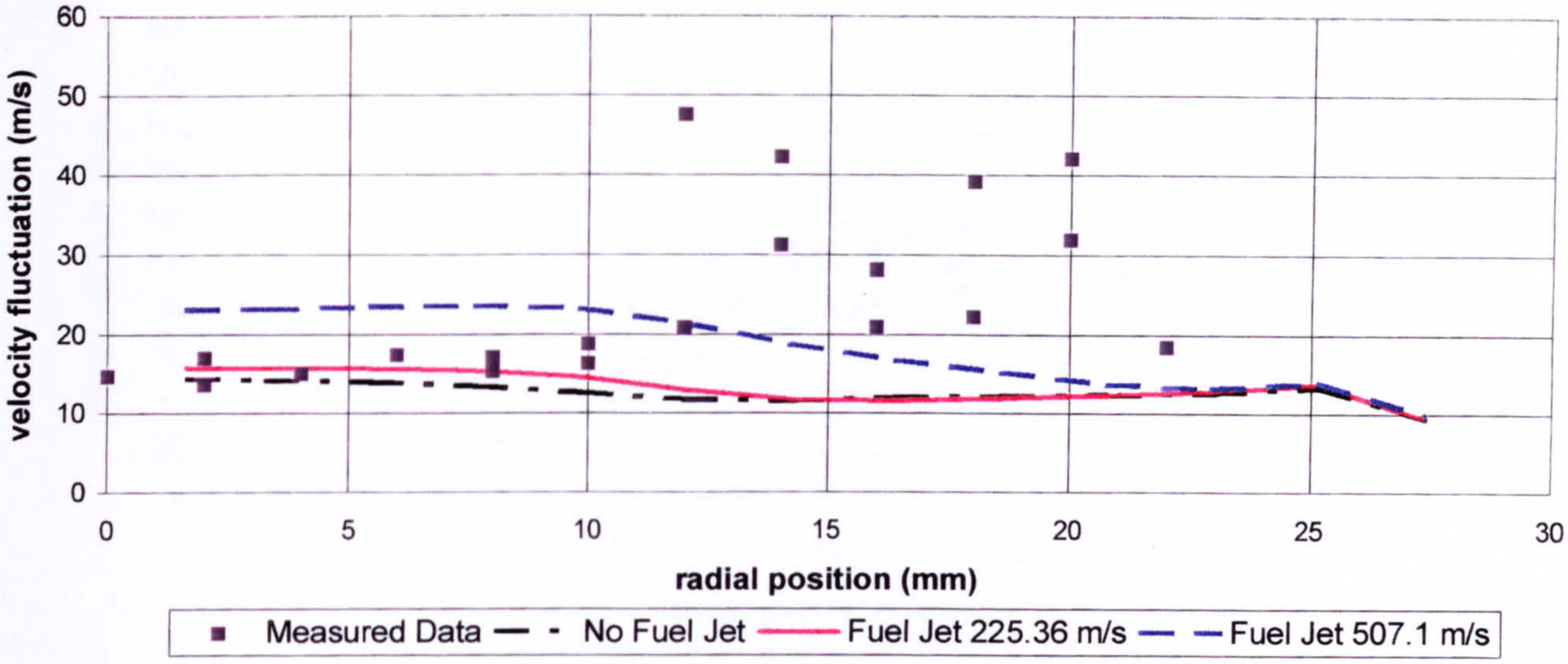

Figure 5.1.8 RMS Velocity at z=25 mm

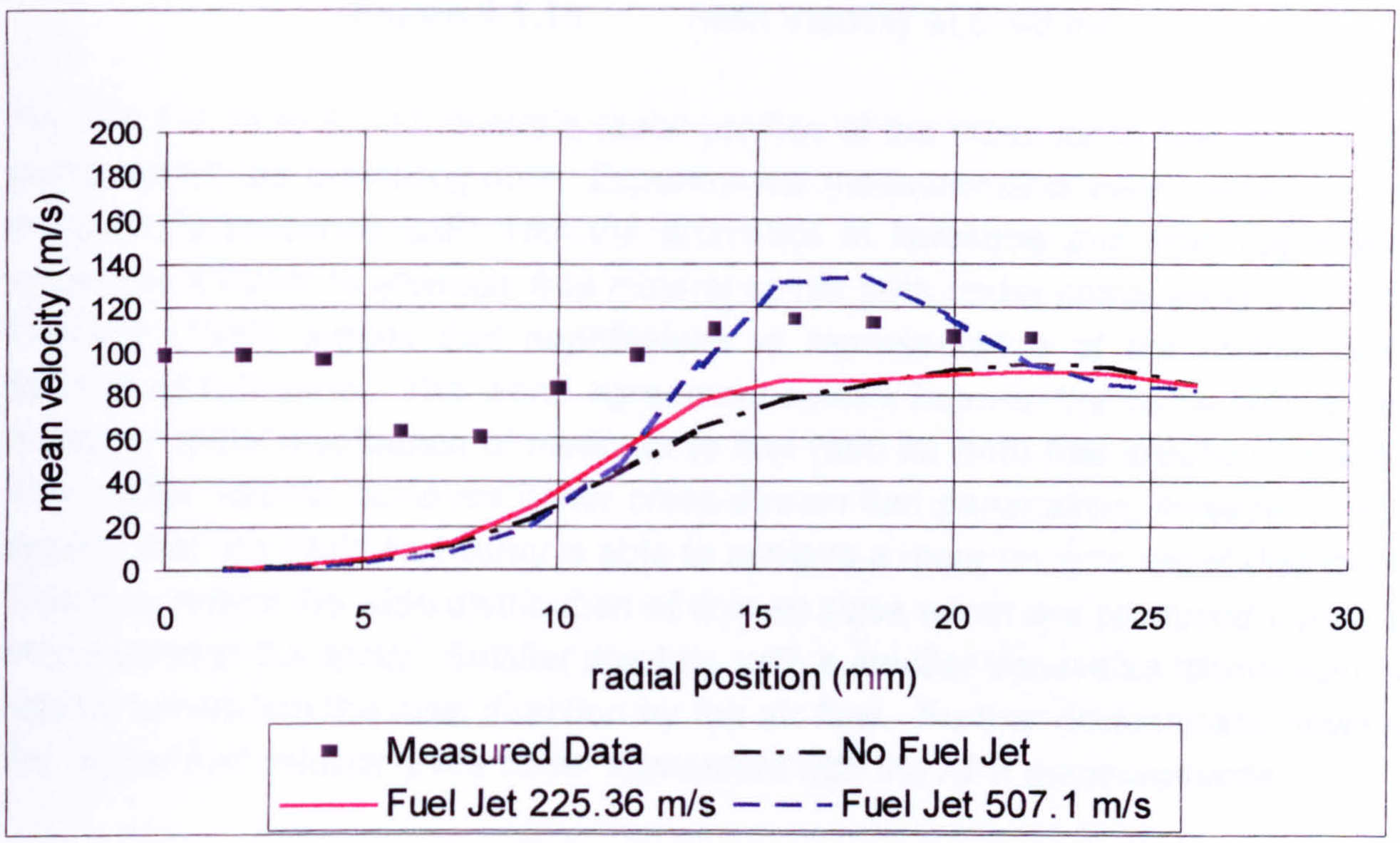

Figure 5.1.9 Swirl Velocity at z=0 mm

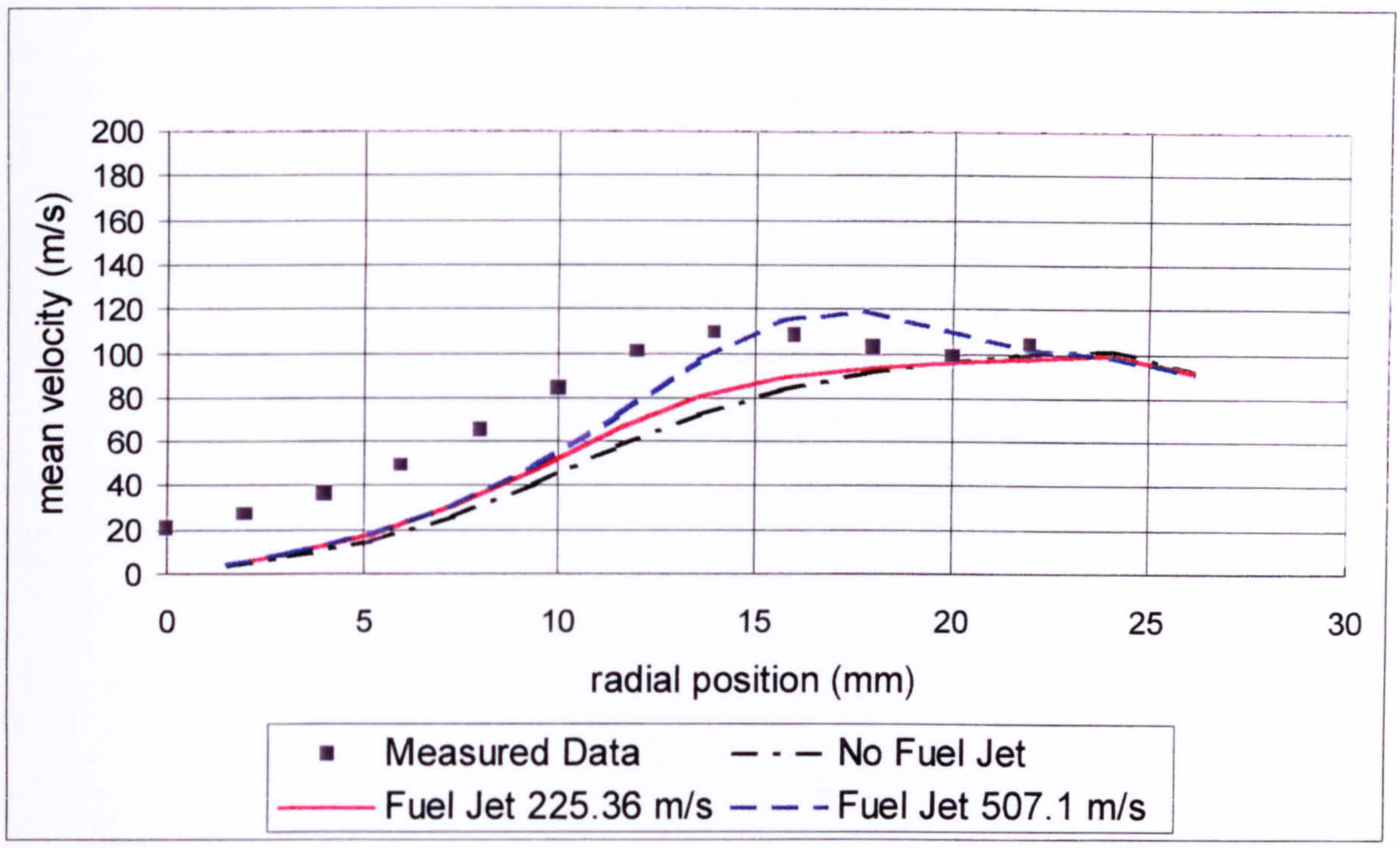

Figure 5.1.10 Swirl Velocity at z=40 mm

Figures 5.1.11 to 5.1.13 illustrate radial profiles of the mean air to fuel ratio at three points within the premixing duct. Experimental measurements were made with laser induced fluorescence (LIF) from the aromatics in kerosene and from naphthalene added as a tracer to aromatic free mineral spirits both under combusting conditions. Harding (1996) argues that naphthalene is representative of the middle boiling fraction of kerosene. The worst agreement occurs nearest the lance with a much narrower radial distribution of mean air to fuel ratio for both fuel injection velocities. The higher velocity achieves better cross-stream fuel penetration, however it would appear that the liquid fuel spray is able to achieve a more uniform radial distribution. This may reflect the wide distribution of droplet sizes which are produced during the atomisation of the spray. Smaller droplets, with a smaller transverse momentum, are rapidly turned into the axial direction by the air flow. Further downstream, however, the higher fuel velocity gives better agreement with the AFR measurements.

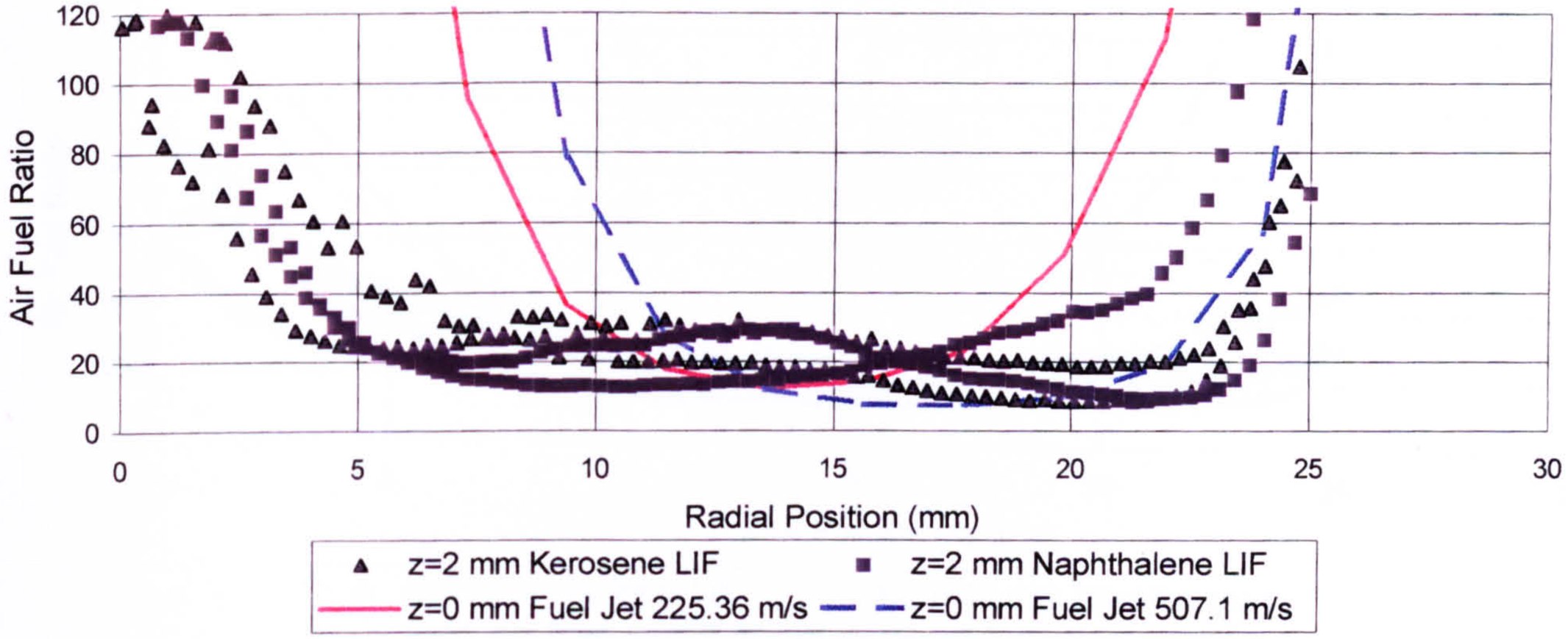

Figure 5.1.11 Air to Fuel Ratio at z=0 mm

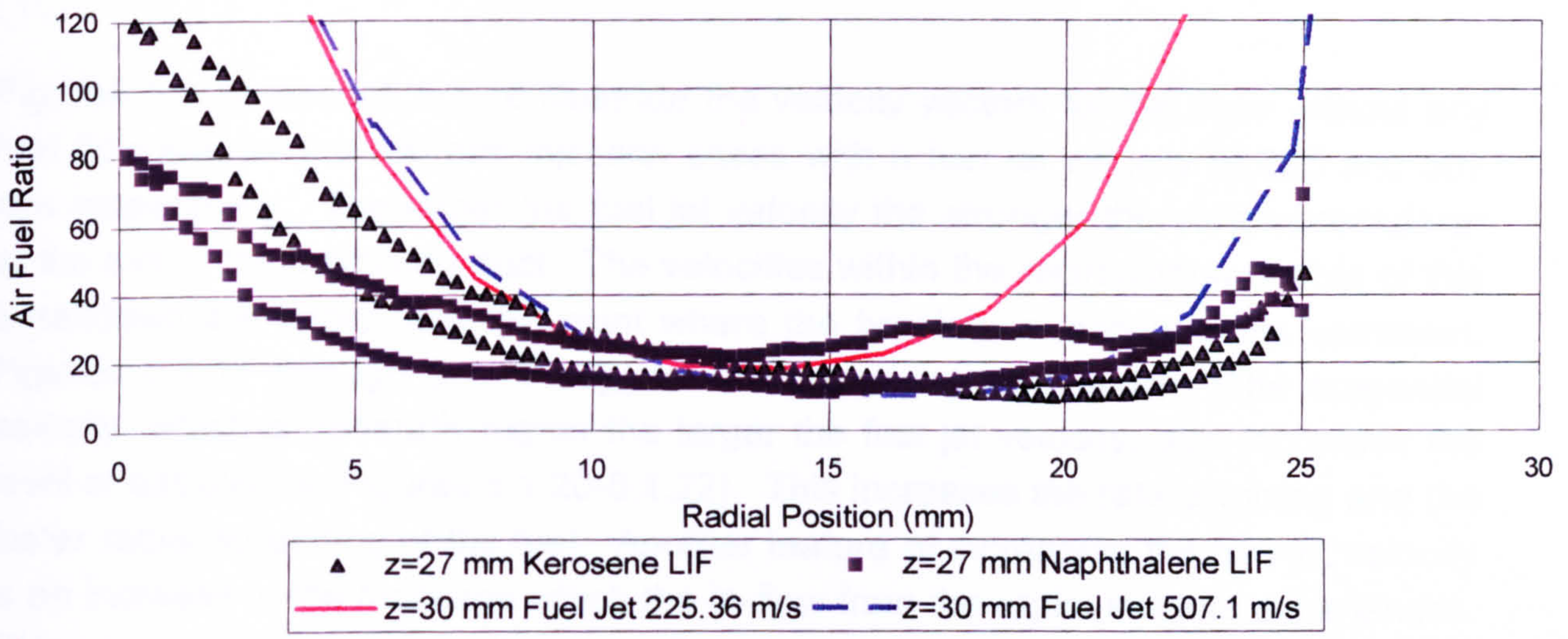

Figure 5.1.12 Air to Fuel Ratio at z=30 mm

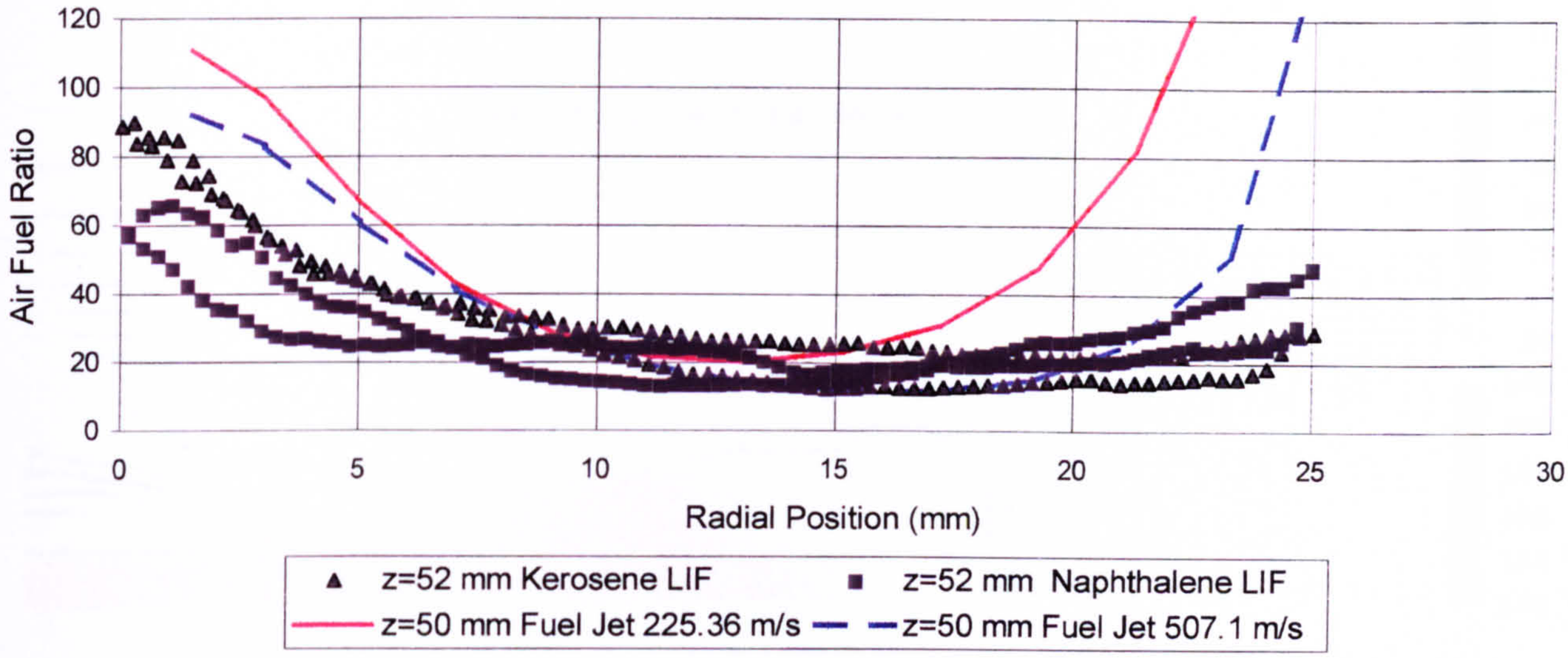

Figure 5.1.13 Air to Fuel Ratio at z=50 mm

Unfortunately this is all of the quantitative mixing data available from the isothermal experiment.

Figures 5.1.14 through 5.1.16 illustrate the velocity vectors for the case without any fuel flow and for the two gas injection cases with a fuel jet velocity of 225 and 507 m/s respectively. The larger the fuel jet velocity the stronger the vortex breakdown at the exit of the premixing duct. The velocities within the recirculation bubble of this breakdown are larger, and the point where the breakdown occurs shifts upstream. Figures 5.1.17 through 5.1.19 suggest the underlying mechanism. The tangential velocity, which is generally higher the larger the fuel jet velocity, also increases the level of turbulence (Figures 5.1.20-5.1.22). This increases the rate of mixing and the faster radial spreading of the fuel. Another feature of increasing the fuel jet velocity is an increase in the blockage which the in-flow from the radial swirlers experiences. This causes an increase in the mass flow through the centre of the lance which is non-swirling and opposes the upstream movement of the vortex breakdown point. The flow through the swirlers will also be forced radially outwards and will have an increase in their tangential velocity to preserve angular momentum. The net effect is to increase the swirl number of the flow causing the vortex breakdown point shift upstream.

Based on these comparisons it was decided to adopt the case with the higher fuel jet velocity in subsequent computations with combustion.

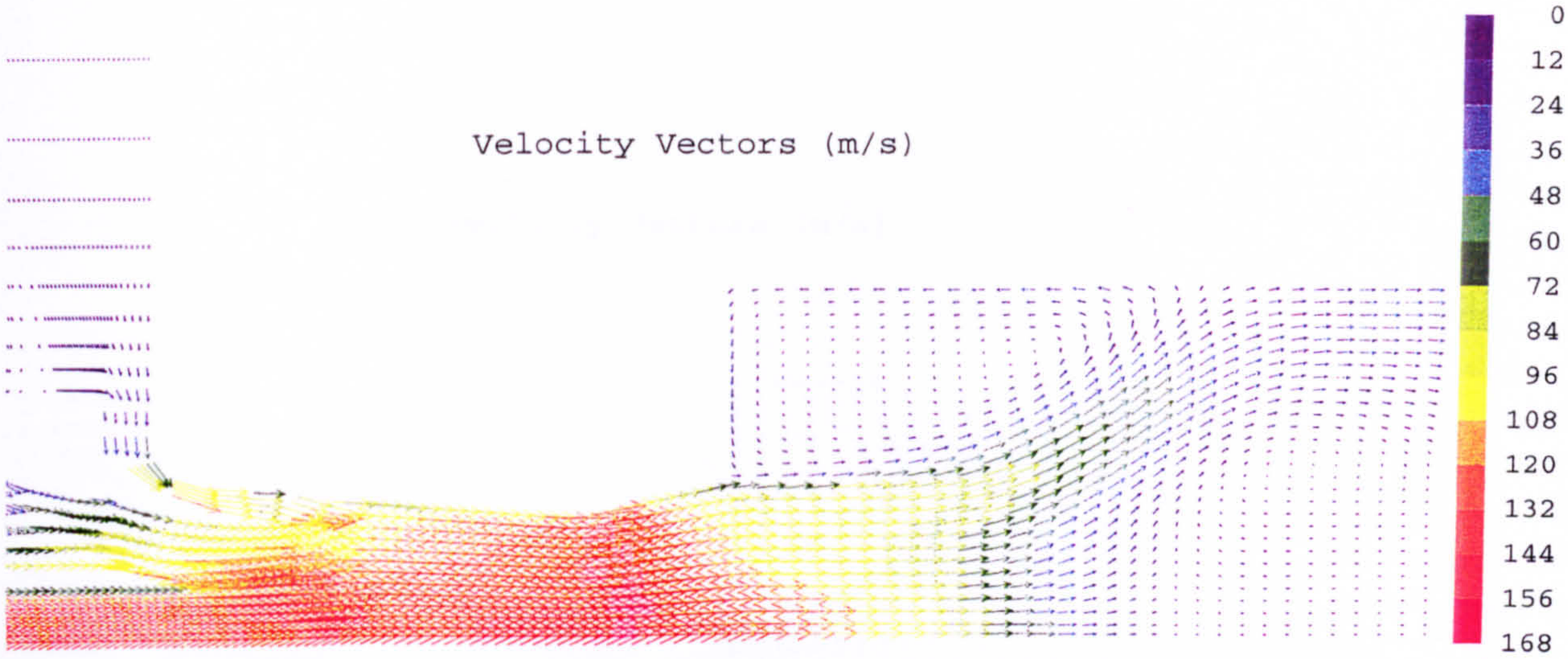

Figure 5.1.14 Velocity Vectors without Fuel

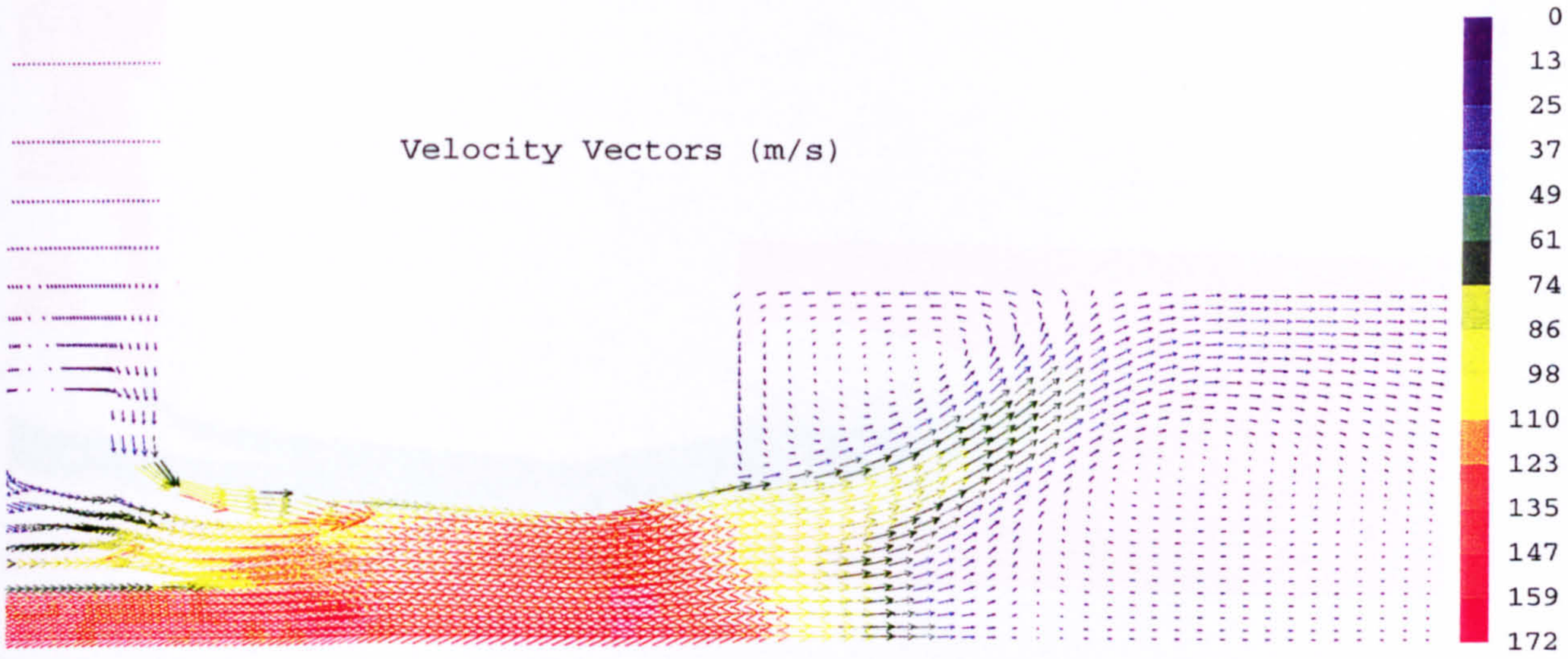

Figure 5.1.15 Velocity Vectors with a Fuel Jet Velocity of 225 m/s

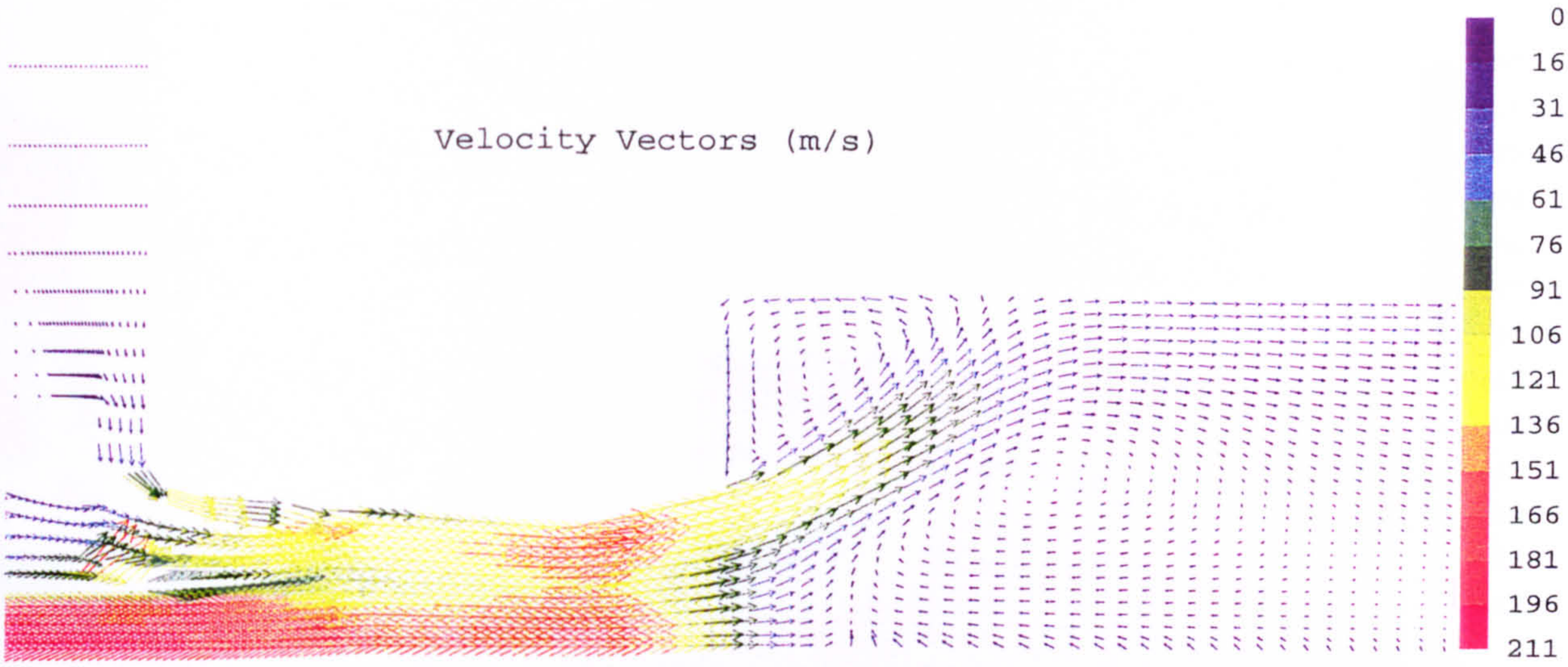

Figure 5.1.16 Velocity Vectors with a Fuel Jet Velocity of 507 m/s

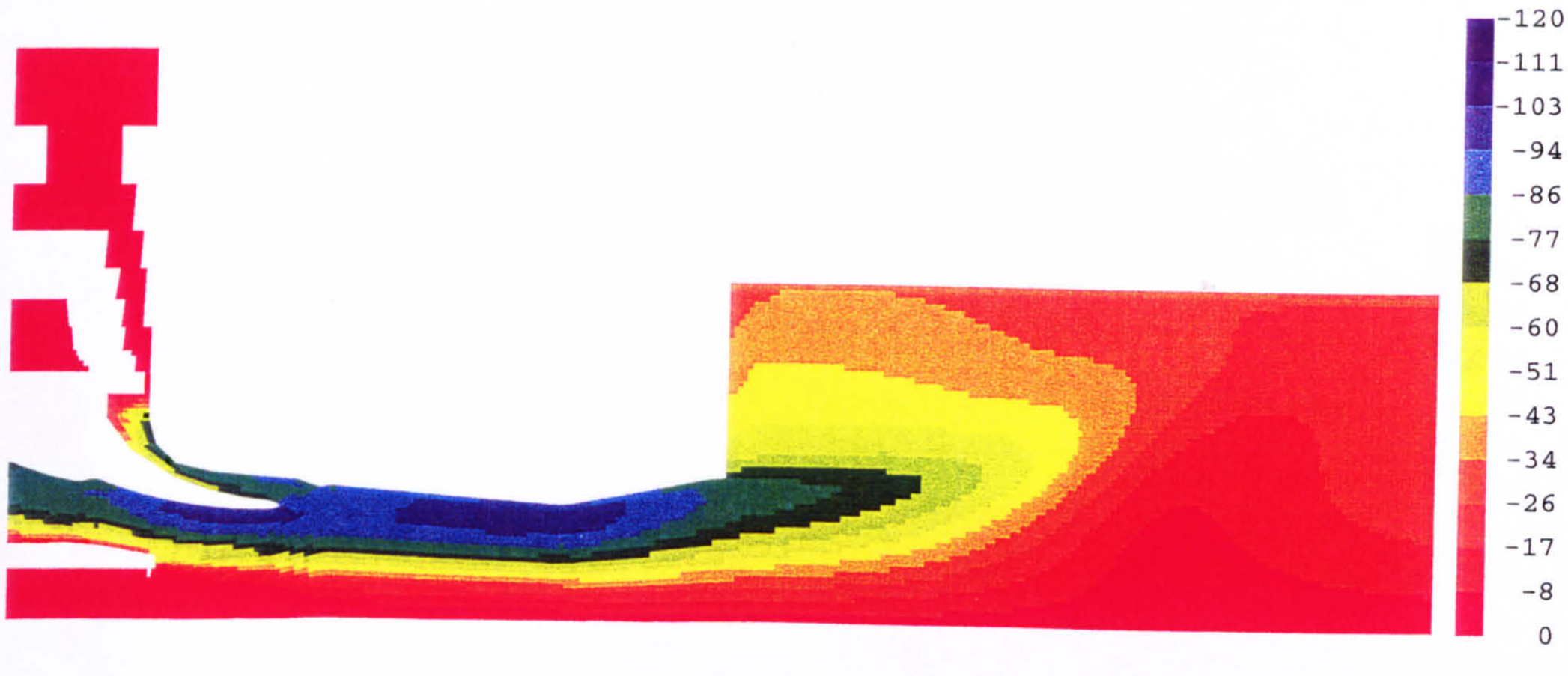

Figure 5.1.17 Tangential Velocity (m/s) with no Fuel

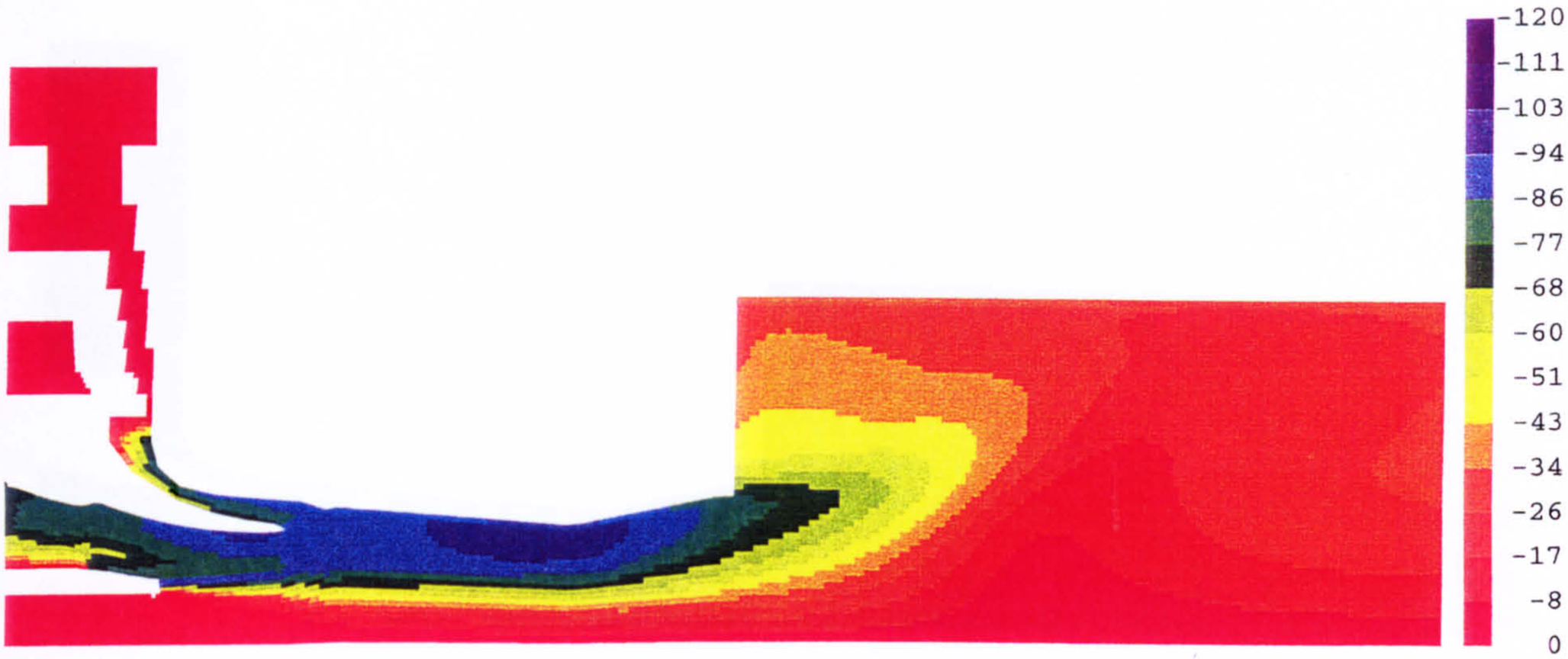

Figure 5.1.18 Tangential Velocity (m/s) with a Fuel Jet Velocity of 225 m/s

Figure 5.1.19 Tangential Velocity (m/s) with a Fuel Jet Velocity of 507 m/s

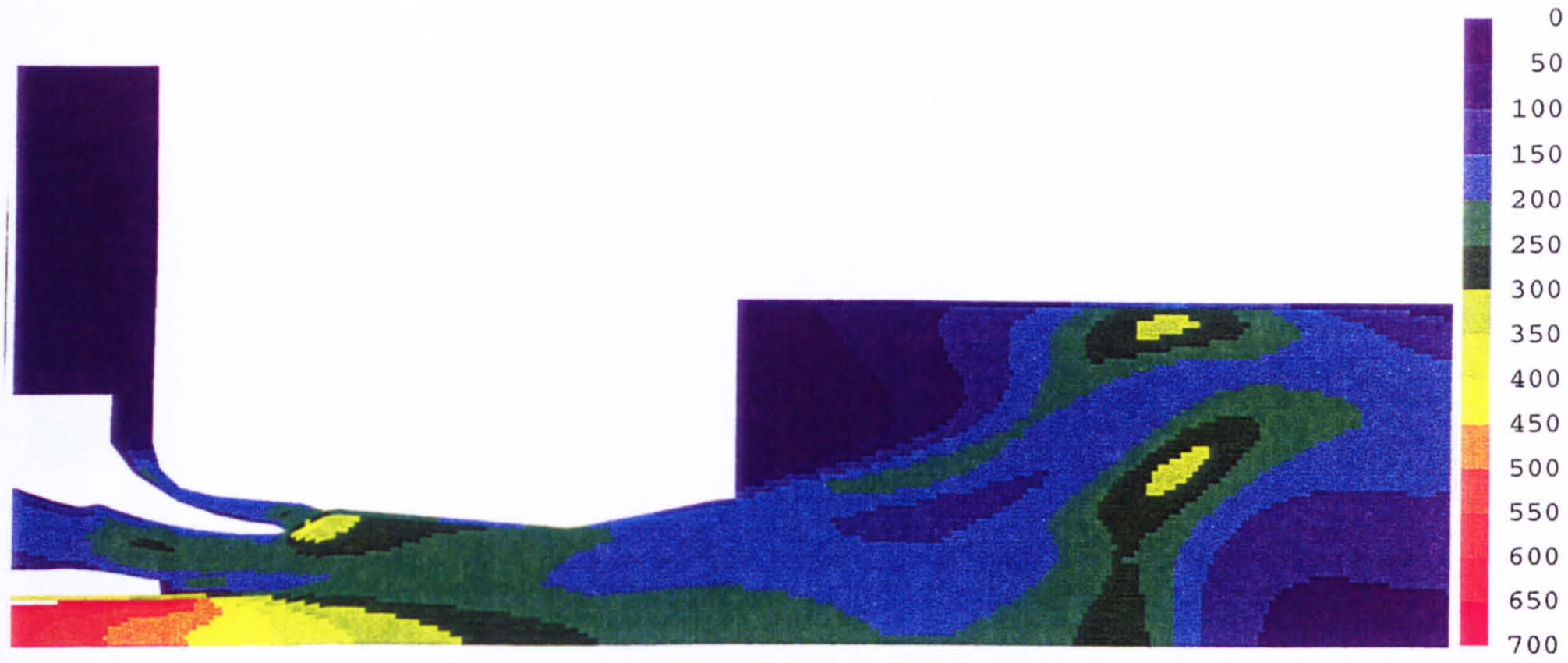

Figure 5.1.20 Turbulence Kinetic Energy $(m/s)^2$ with no Fuel

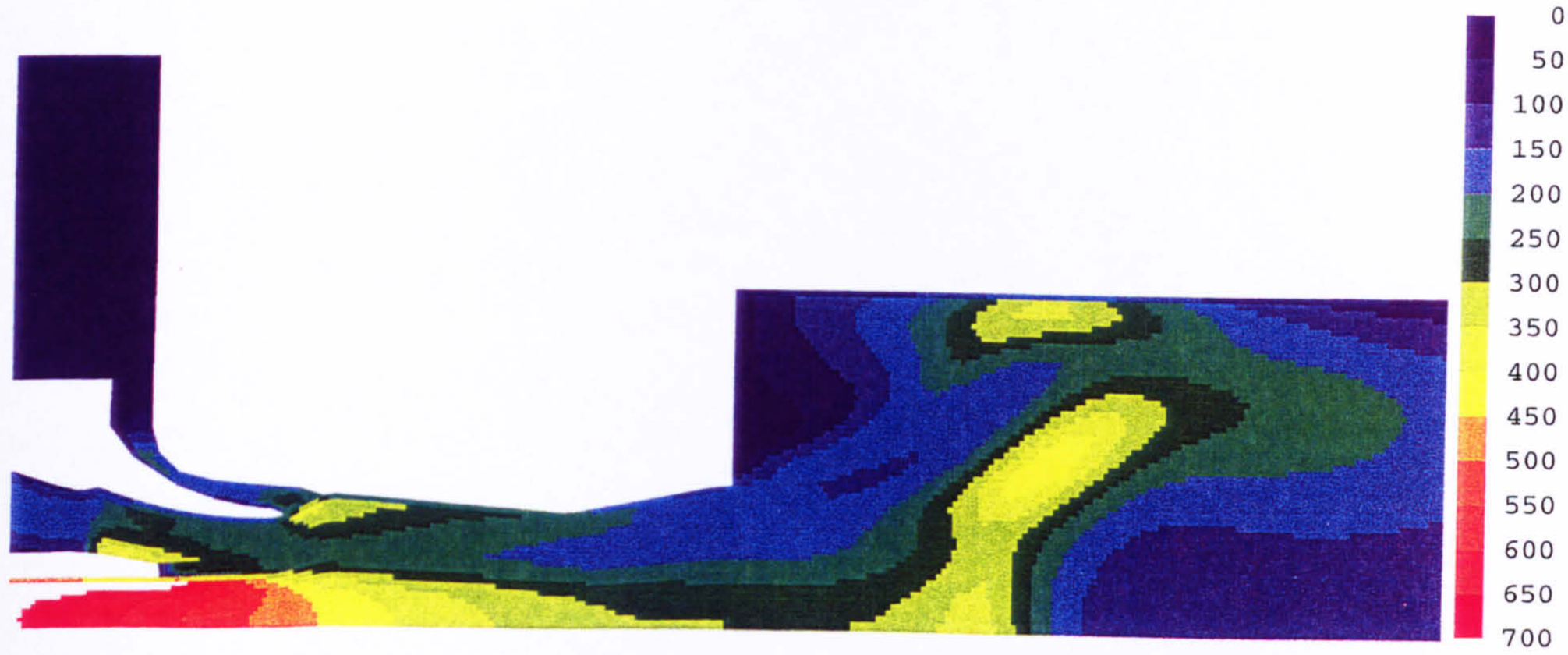

Figure 5.1.21 Turbulence Kinetic Energy $(m/s)^2$ with a Fuel Jet Velocity of 225 m/s

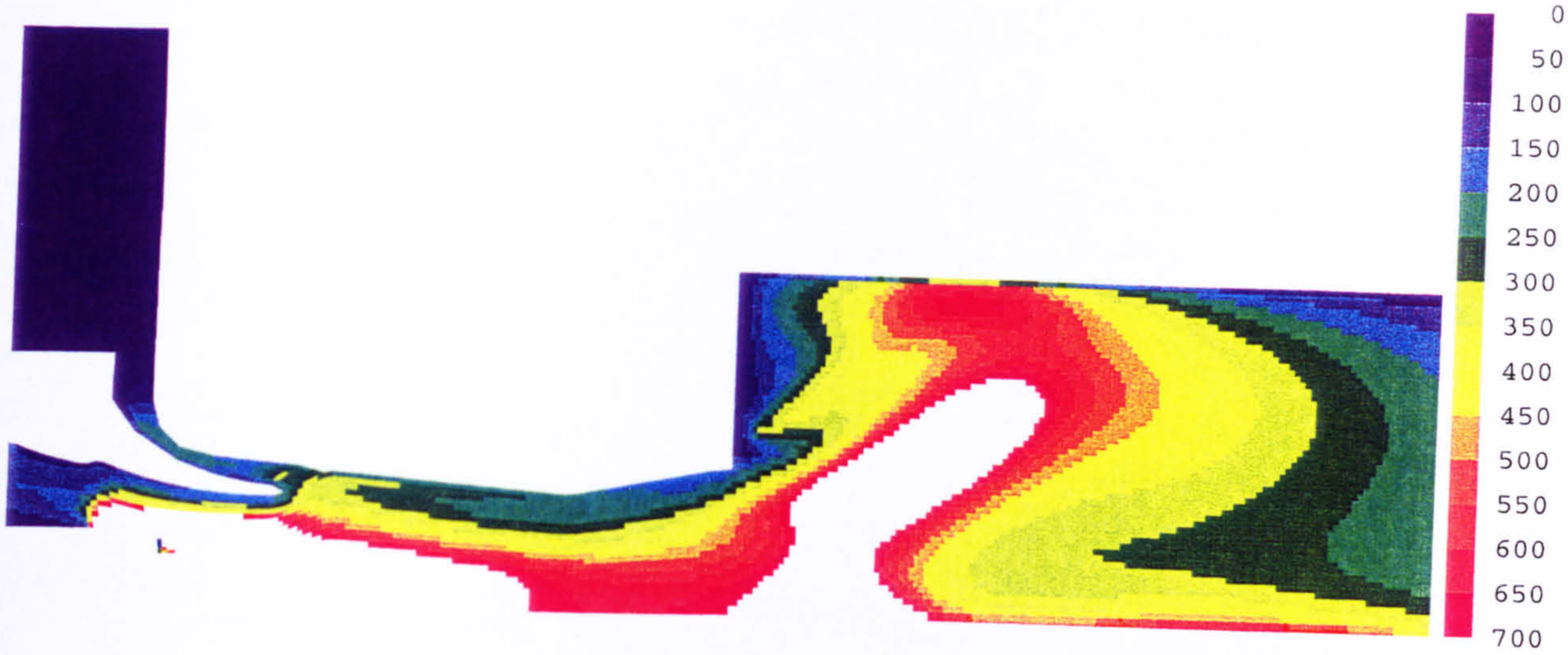

Figure 5.1.22 Turbulence Kinetic Energy $(m/s)^2$ with a Jet Velocity of 507 m/s

5.1.2 Mixing Duct Predictions: Cylindrical Grid

In order to explore alternative models for turbulence and combustion, calculations were performed on the cylindrical grid with the premixing duct. Figure 5.1.23 and 5.1.24 compare the predicted distributions of mean mixture fraction for the complete body-fitted and cylindrical grids. The two cases exhibit a very similar distribution. The full grid suggests that the flow mixes slightly faster than that with the cylindrical grid, especially after the exit of the premixing duct. This may in part reflect the fact that the latter grid is slightly finer and so there will be less artificial diffusion in this region. However the differences are not large and demonstrate that there is a sufficient degree of grid independence to encourage the further comparison of combustion models. Similar comparisons can be made for the velocity field. Figure 5.1.25 shows a plot of the velocity vectors for the cylindrical grid. Comparing with Figure 5.1.16 one can see that the results are almost identical except in the region next to the outer wall of the premixing duct where the irregular edges of the cylindrical grid (cf. Figure 5.3) disturb the flow locally. Figure 5.1.26 shows contours of the tangential velocity which are also very similar to those for the body fitted grid (Figure 5.1.19). Around the point of the vortex breakdown the full grid calculations show an increase in the magnitude of the tangential velocity near the axis which is not predicted by the cylindrical grid case. It is however recovered by the second moment turbulence model as shown in Figure 5.1.29. This may be simply software related and explained by the fact that both the second moment turbulence model and the quasi two dimensional body fitted grid required the use of a new co-located solver in PHOENICS, which solves the velocities along with all the other variables at the cell centres. The cylindrical grid with the k-ε turbulence model used the standard staggered solver in PHOENICS where the velocities were calculated at the cell faces and the remaining variables at the cell centres. Figure 5.1.27 illustrates contours of the turbulent kinetic energy which, when compared to Figure 5.1.22, indicates that the castellated outer wall of the premixing duct also generates additional turbulence. This explains the greater level of turbulence in the shear layer between the flow leaving the premixing duct and the recirculating flow in the upper corner behind the expansion step. The turbulence generated by the vortex breakdown is also slightly larger for the cylindrical grid. Generally speaking, however the flow field calculations are very similar despite some substantial differences in the detail of the mesh geometries.

Inlet conditions for the investigation of the second moment turbulence model on the second cylindrical grid (Figure 5.4) were taken from the cylindrical k-ε model grid at the outlet plane of the premixing duct. A plot of the velocity vectors for this case can be seen in Figure 5.1.28. The point of the vortex breakdown remains unchanged relative to the k-ε turbulence model, however given its close proximity to the exit of

the premixing duct this may be largely influenced by the inlet conditions, which were prescribed from the calculations made with the k-ε model. The breakdown bubble for this case is much longer than with the k-ε model and the flow pattern within the bubble is very different. Rather than a single recirculation there are two. One near the axis of the combustor which is in the opposite direction to that generated by the predictions with the k-ε model. The second is further away from the axis and stretches much further downstream. Figure 5.1.29 shows contours of the tangential velocity. As mentioned earlier, this case shows an increase in the magnitude of the tangential velocity near the axis starting around the point of the vortex breakdown. The radial profile of the tangential velocity also tends to exhibit free vortex behaviour with the absolute peak in velocity about a quarter of the radius from the centre of the combustor. The k-ε model calculations on the other hand tend to suggest a solid body rotation with the peak tangential velocity at the outer wall of the combustor (Figure 5.1.26). The turbulence kinetic energy is also around half that of the k-ε model calculations in the vortex breakdown region and even less in the shear layer behind the expansion step. This can be seen in Figure 5.1.30.

The main conclusion from these cold flow simulations is that the three grids give broadly similar results. Some questions arise over the patching together of flow fields in particular, how much influence the inlet boundary condition and its proximity to the vortex breakdown exerts on the second moment closure grid. In the absence of a complete second moment closure which is applicable to a curvilinear body-fitted geometry, this uncertainty remains unresolved. The choice of an exaggerated inlet fuel velocity of 507 m/s produced good agreement with the experimental measurements within the premixing duct. Additionally, the penetration of the fuel jet was found to have a strong influence on the swirl strength and hence position of the vortex breakdown bubble. Harding (1996) felt that the existence of the combustion alone somehow was responsible for this shift in the position of the vortex breakdown. However he did not make any non-combusting measurements with fuel. This adds an extra element to explain why the vortex breakdown appears to be closer to the exit of the premixing duct under combusting circumstances.

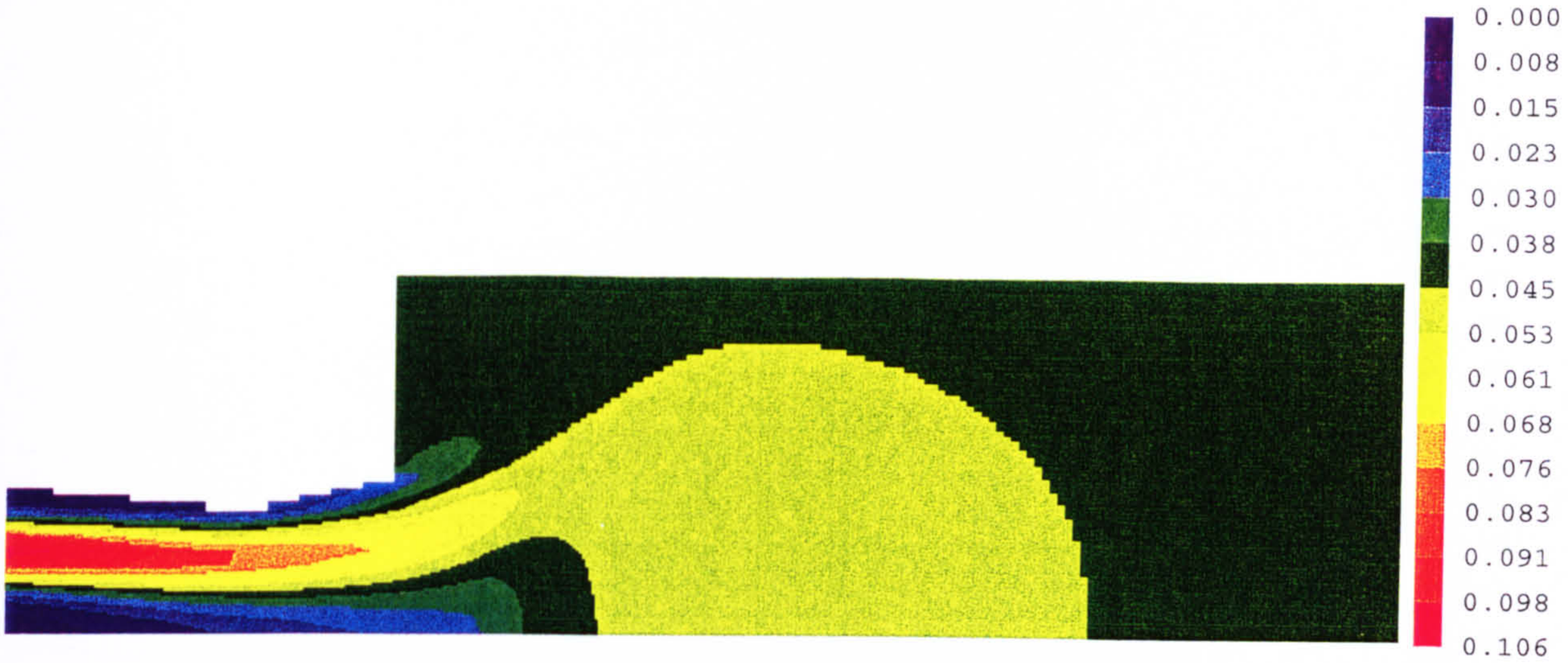

Figure 5.1.23 Mean Mixture Fraction with a Fuel Jet Velocity of 507 m/s on the Cylindrical Grid

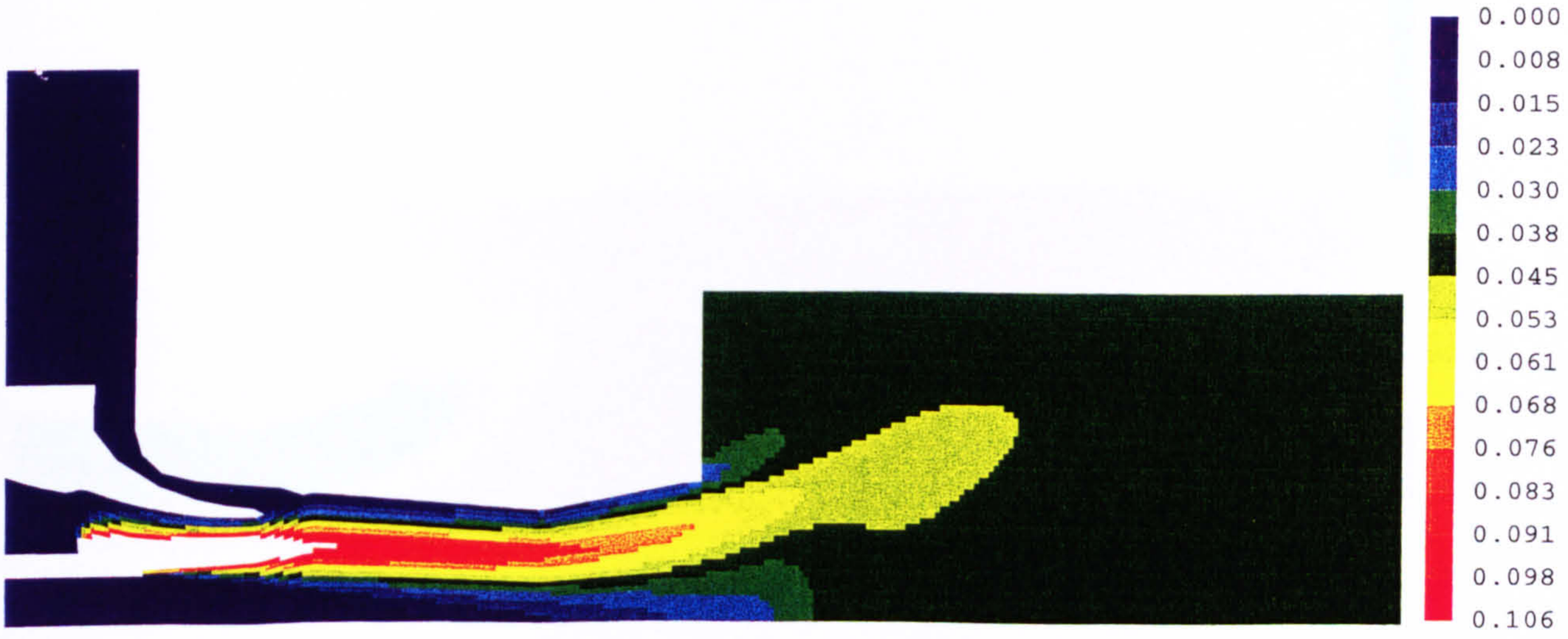

Figure 5.1.24 Mean Mixture Fraction with a Fuel Jet Velocity of 507 m/s on the Body Fitted Grid

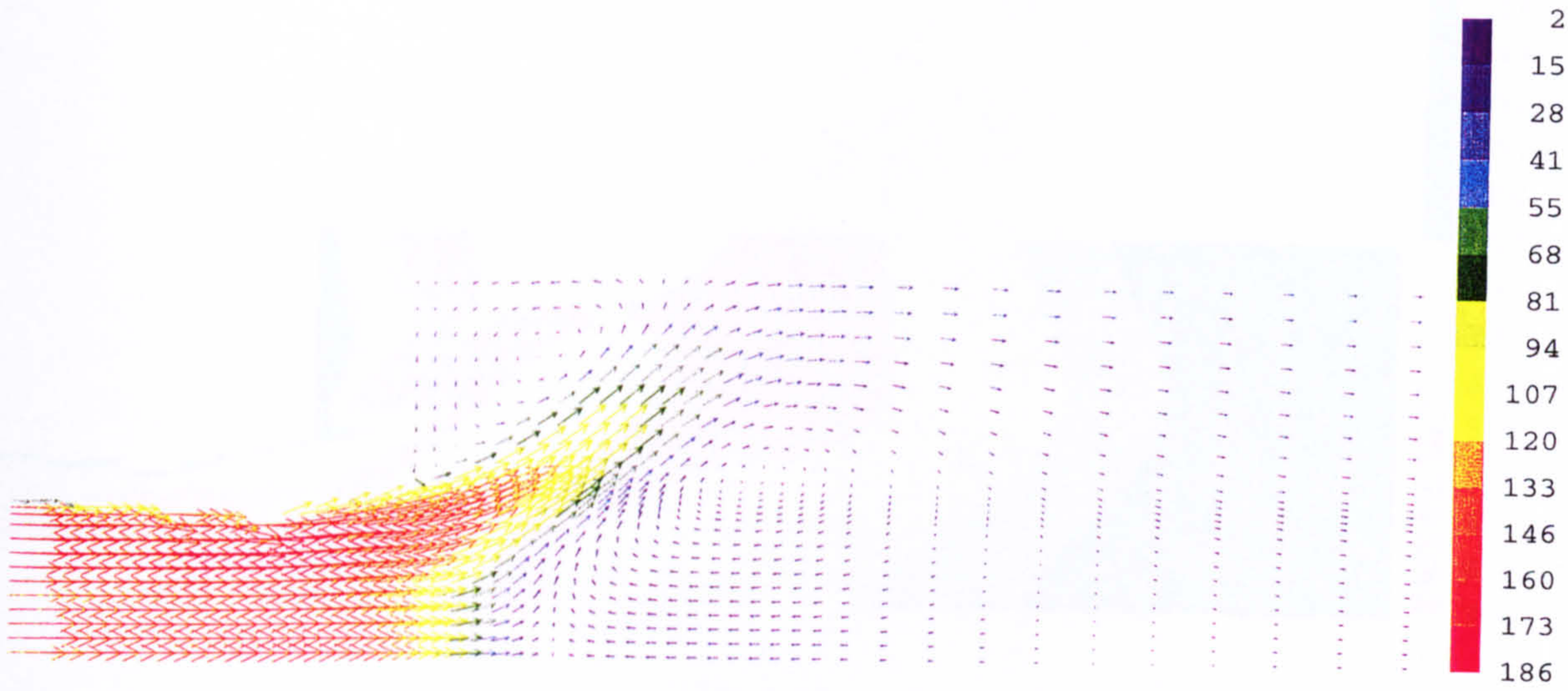

Figure 5.1.25 Velocity Vectors (m/s) from the k-ε Turbulence Model Cylindrical Grid

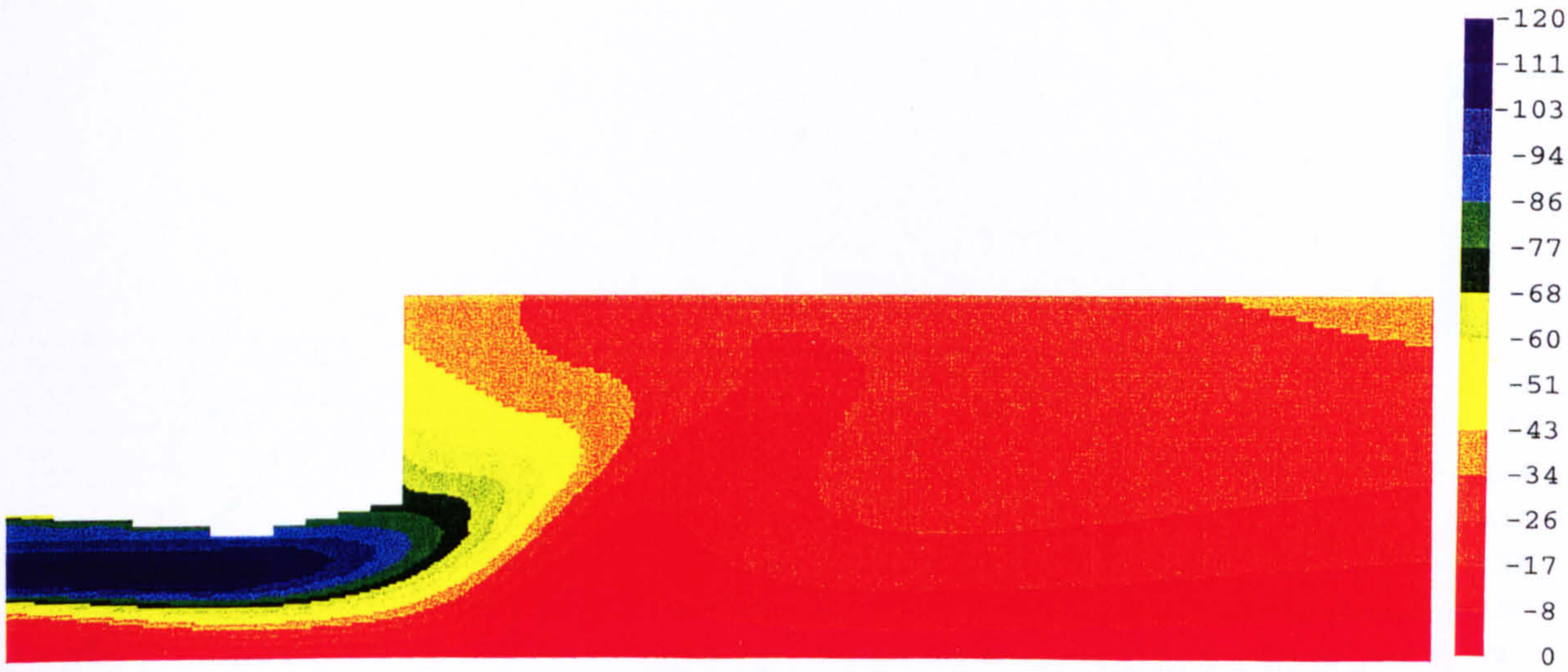

Figure 5.1.26 Tangential Velocity (m/s) from the k-ε Turbulence Model Cylindrical Grid

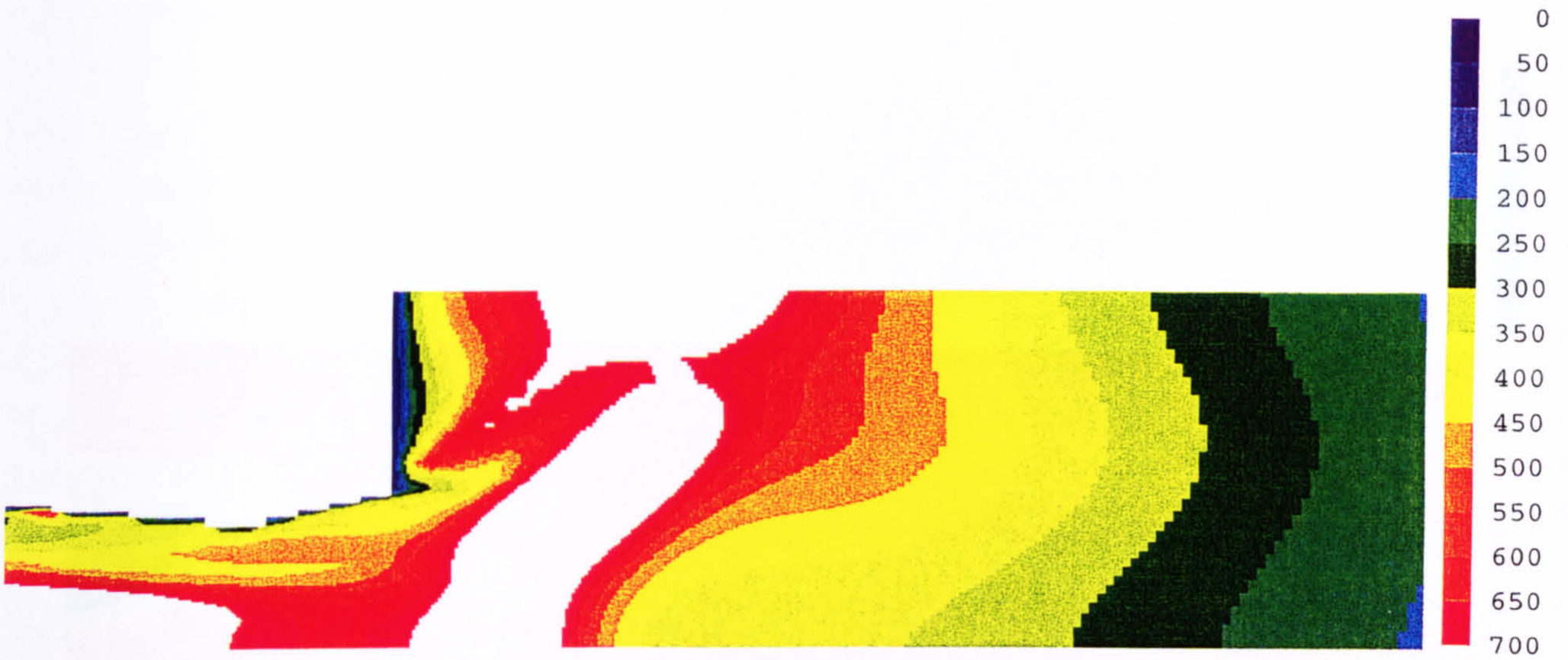

Figure 5.1.27 Turbulence Kinetic Energy $(m/s)^2$ from the k-ε Turbulence Model Cylindrical Grid

Figure 5.1.28 Velocity Vectors (m/s) from the Second Moment Turbulence Model Cylindrical Grid

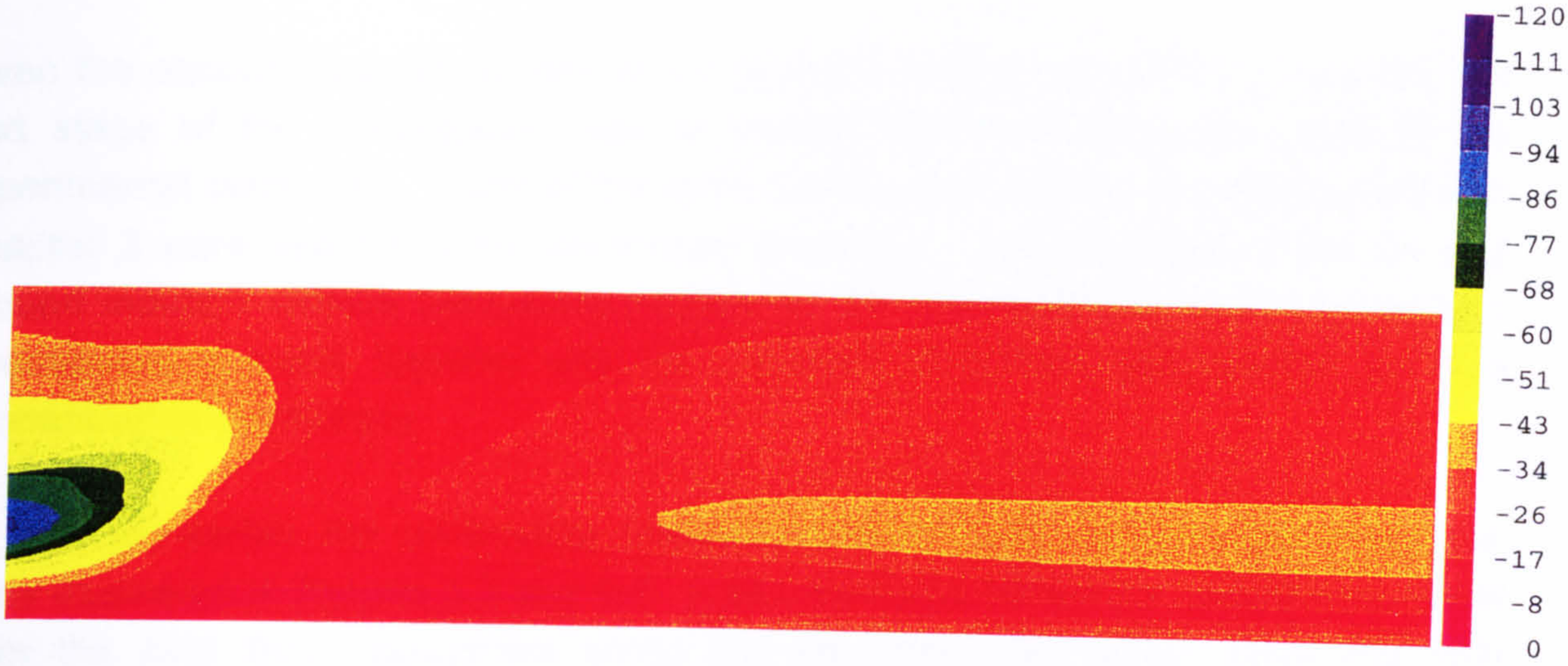

Figure 5.1.29 Tangential Velocity (m/s) from the Second Moment Turbulence Model Cylindrical Grid

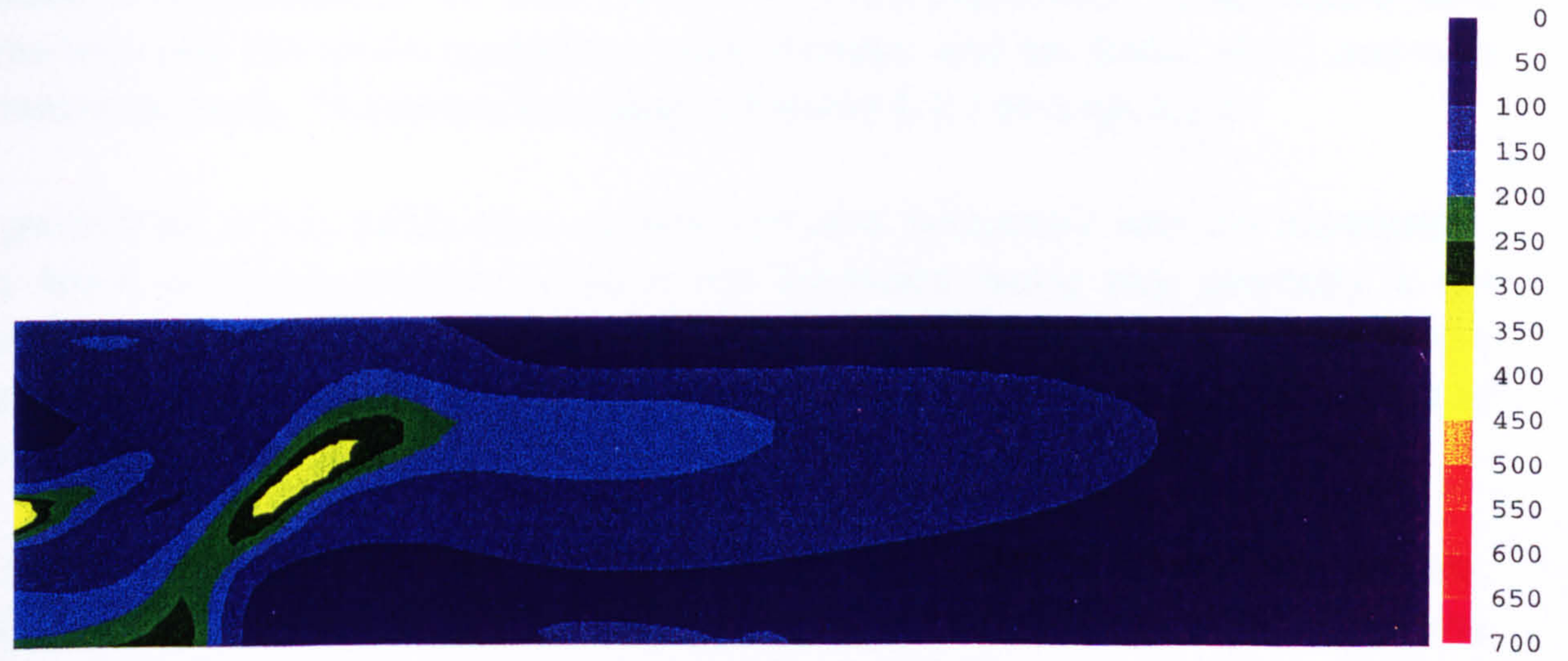

Figure 5.1.30 Turbulence Kinetic Energy $(m/s)^2$ from the Second Moment Turbulence Model Cylindrical Grid

5.2 Combusting Flow Predictions

5.2.0 Introduction and Modelling Issues

Given the encouraging simulations of the isothermal flow with differing meshes, the next stage of the investigation was to predict the combusting flow field of the experimental combustor. Each of the three combustion models discussed earlier in Chapter 3 were applied to the combustor geometry. The influence of the k-ε and second moment closure turbulence models on the flow field and scalar fluxes was investigated in detail, together with the influence of mixture homogeneity on NOx concentration predictions.

As reported earlier, the combusting calculations were made using the two cylindrical grids illustrated in Figures 5.3 and 5.4. Inlet conditions for the k-ε calculations came from the cold flow calculations using the full body-fitted grid. Thus the inlet conditions for the fuel and air are the same as those for the isothermal ones. The calculations made with the second moment turbulence model used combustor inlet conditions derived from the combusting k-ε calculations at the exit of the premixing duct.

The earlier 2-dimensional calculations, which were used to initially investigate the combustion models, had fuel and air inlet temperatures of 298 K. This meant that the correlations for flame temperature, and the equilibrium concentration of NO needed to be updated for the new conditions of this experiment. Calculations were performed with the NASA equilibrium code (Gordon and Mc Bride, 1971) and new correlations made. These are illustrated in Figures 5.2.1 through 5.2.2.

In general all of the combustion models compare favourably with the experiment. The flame spreading problem noted in the backward facing step geometry is not apparent in the predictions of this flow field. This is most probably due to the absence of large transient features in the flow which so influenced the flow field of the backward facing step.

To establish which combustion regime the flame in the LPP test combustor fell into, predicted properties of the flame and flow field for the calibrated BML Crossing Frequency model were plotted on a Borghi diagram similar to that of Figure 2.3.1.4. Figure 5.2.3 indicates that all of the points fall into the distributed reaction zone. In this zone the chemical time is still significantly shorter than the mixing time scale however high levels of turbulence in the flow will cause local extinctions. Thus it is important to consider flame front straining.

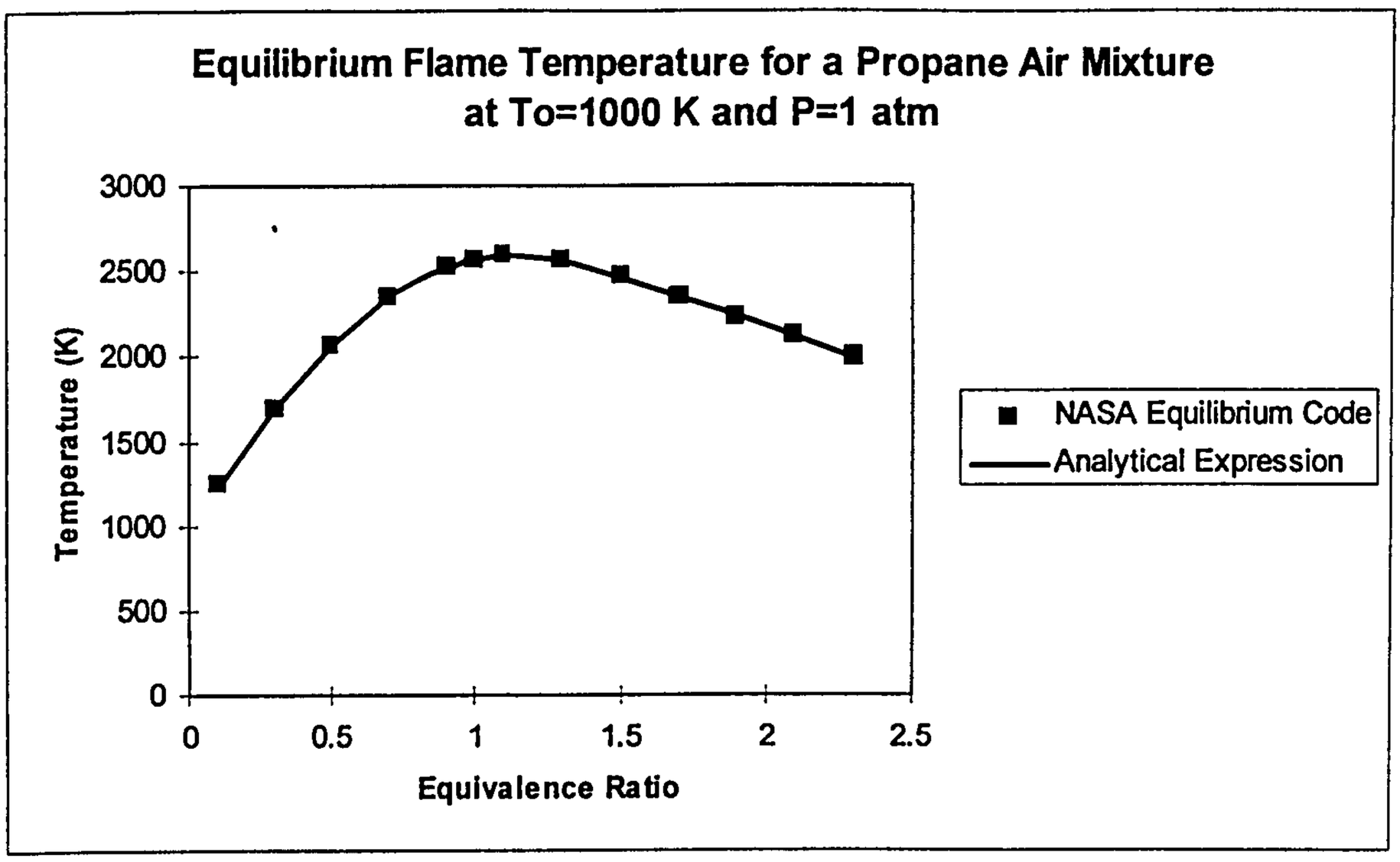

$0 \leq \phi \leq 0.7 \qquad T = 1125\phi^2 + 2785\phi + 958.75$

$0.7 < \phi \leq 1.3 \qquad T = 1200\phi^2 + 2746.667\phi + 1022.333$

$1.3 < \phi \qquad T = 90.625\phi^2 - 245.625\phi + 3037.469$

Figure 5.2.1 Polynomial Curve Fit of Equilibrium Flame Temperature for Propane-Air Mixtures

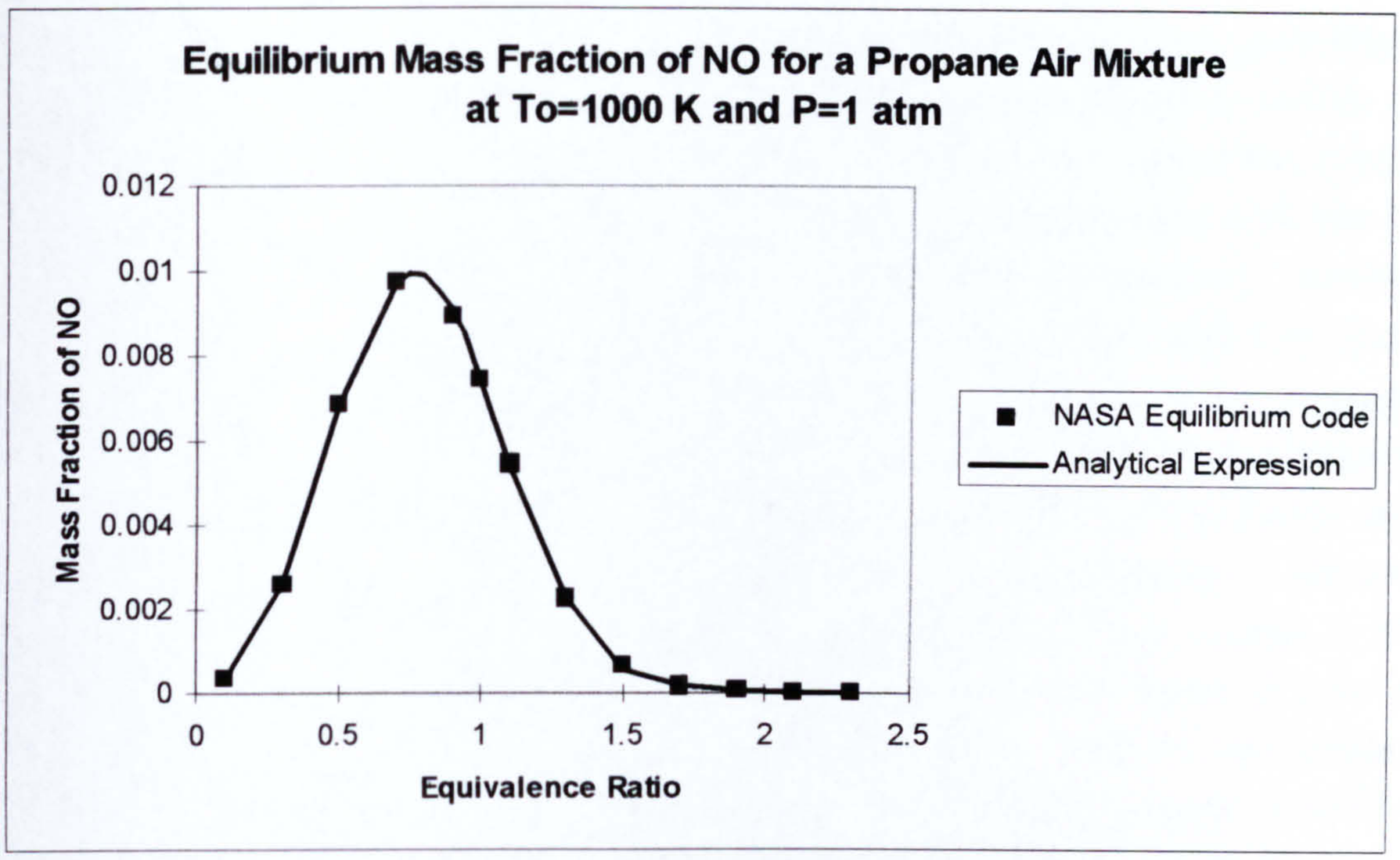

$$0 \le \phi \le 0.5 \qquad Y_{NO}^{c=1} = 0.02484\phi^2 + 0.00142\phi - 0.000088$$

$$0.5 < \phi \le 1.1 \qquad Y_{NO}^{c=1} = 0.04471\phi^2 + 0.06827\phi - 0.01612$$

$$1.1 < \phi \le 1.7 \qquad Y_{NO}^{c=1} = 0.01697\phi^2 - 0.05618\phi + 0.04664$$

$$1.7 < \phi \qquad Y_{NO}^{c=1} = 0.001349\phi^2 - 0.00552\phi + 0.005653$$

Figure 5.2.2 Polynomial Curve Fit of Equilibrium Mass Fraction of NO

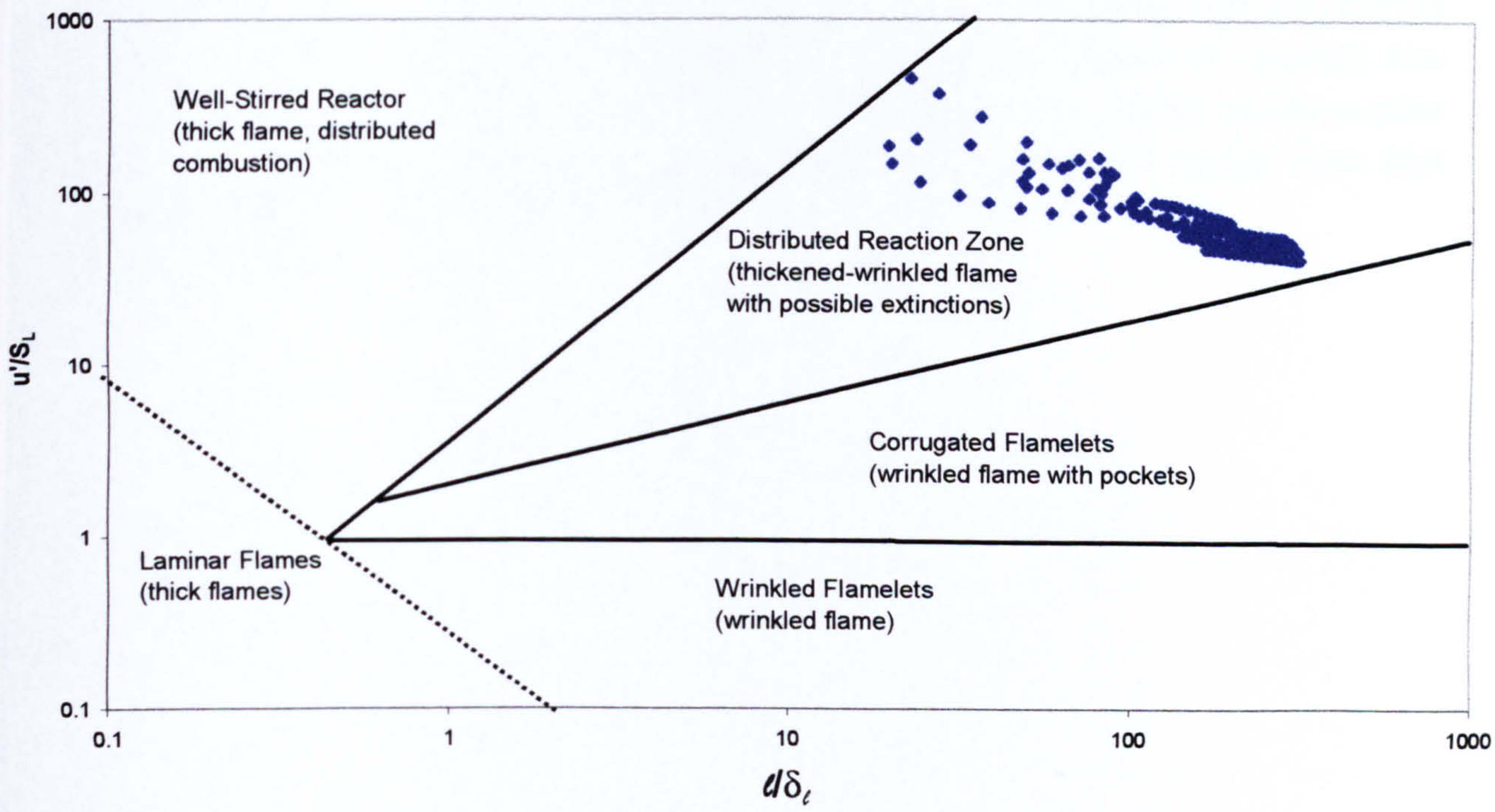

Figure 5.2.3 Borghi Diagram with Calibrated BML Crossing Frequency Model Predictions within the Combustion Chamber

One feature of note from the combusting computations was the prediction of the mean temperature. Harding (1996) made measurements along a radius near the exit of the premixing duct within the combustor. He does not report the precise axial location of these measurements however they agree qualitatively with the contours of mean temperature predicted by all three of the combustion models. His measurements and predictions using the Eddy Break-up model, with both the k-ε and second moment turbulence models, can be found in Figures 5.2.4 through 5.2.6. Harding (1996) notes that the peak temperature is well below the adiabatic flame temperature. This he attributes to the cooling air, which is introduced along the outer wall of the combustor in the experiment with a temperature of about 300 K, effectively quenching the flame. Convective and radiative heat losses to the outer wall may be another explanation for this. However a similar trend is also found in the predictions which do not include the cooling air. Mixture inhomogeneity is predicted such that the region next to the outer wall contains a mean mixture fraction which is lower than the mean of the overall flow. This is illustrated by the k-ε predictions with the Eddy Break-up combustion model in Figure 5.2.7. The second moment turbulence model predictions reproduce better the relatively flat trend in the peak temperature observed by Harding. This relates to the observation that the chemical source term is higher for this turbulence model as will be discussed later. Importantly for the NO_x calculations, we note as well that the temperatures predicted are significantly higher than those measured. This may be partly explained by the introduction of the cooling air which would lower the mean mixture fraction even further. It might be possible that the cooling air is also quenching the flame as is suggested by Harding (1996) through an enhancement of the mixing rate and hence local flame front strain rates however there is insufficient evidence to quantify this effect. Additionally the inlet conditions for the calculations are based on the earlier reported temperature of 1000 K (Harding, 1996b) which is 100 K higher than that later reported by Harding (1996).

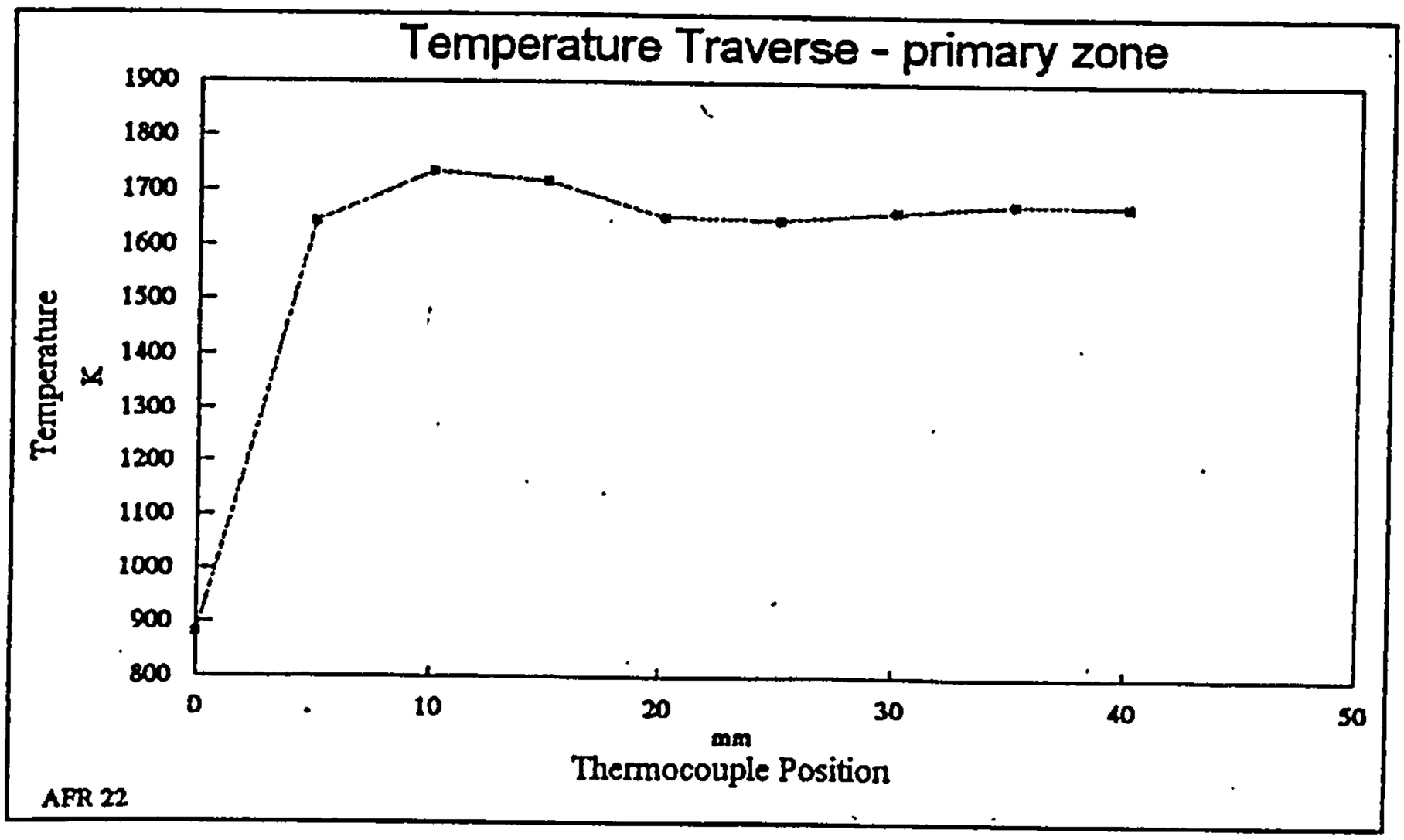

Figure 5.2.4a Temperature Measurements (Harding, 1996)
(thermocouple position denotes radial distance)

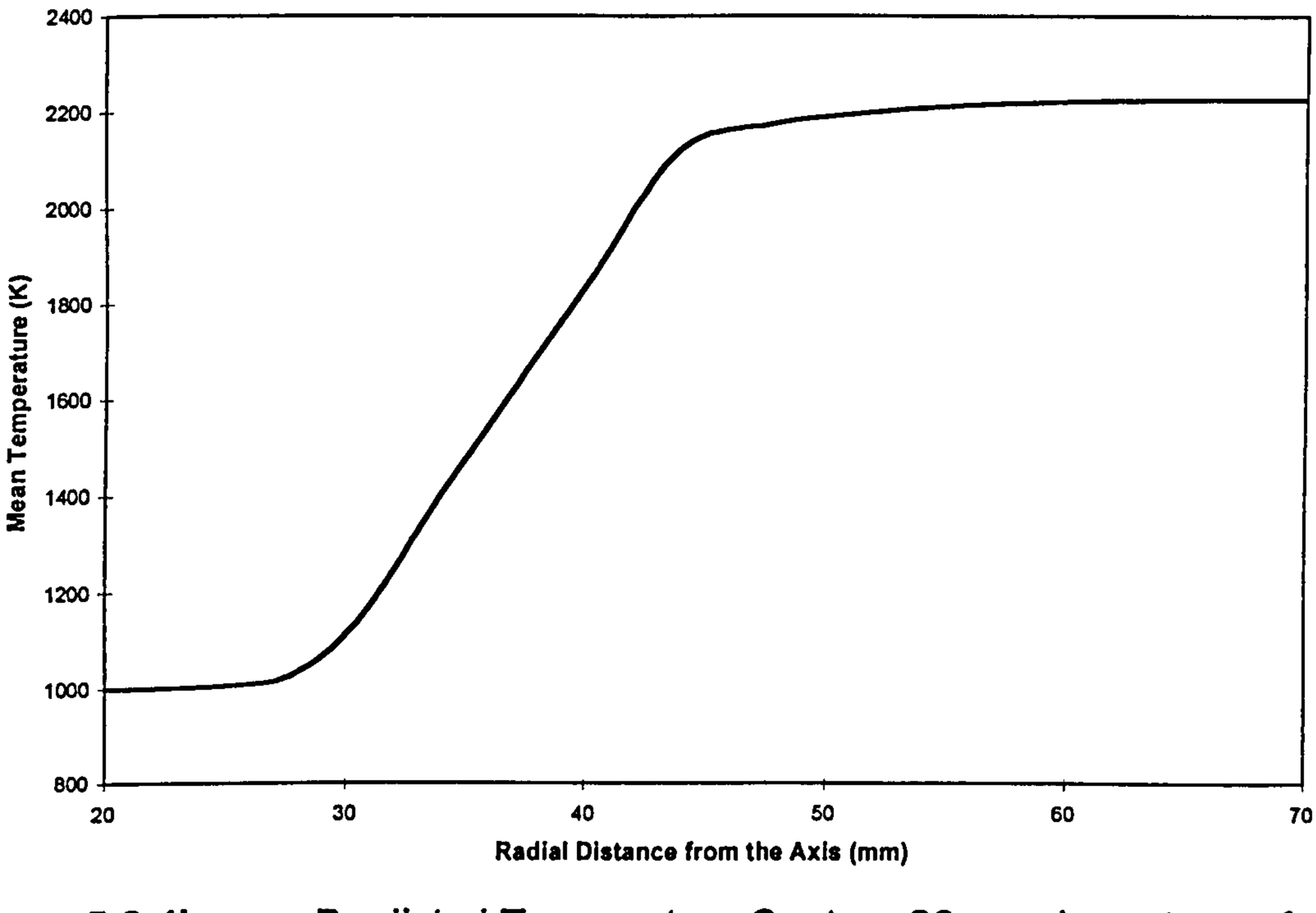

Figure 5.2.4b Predicted Temperature Contour 20 mm downstream from the exit of the Premixing Duct for the Eddy Break-up and Second Moment Closure Models

Apart from this radial measurement of temperature, Harding (1996) conducted some LIF measurements of the aromatic content within the kerosene fuel within the combustor at the exit of the premixing duct. With these measurements he defined a reaction progress variable based on the concentration of the unburnt fuel. A sample

of mean and instantaneous contours of the reaction progress variable based on LIF images can be seen in Figures 5.2.8 and 5.2.9 respectively.

Figure 5.2.5 Mean Temperature (K) Contour for the Eddy Break-up and k-ε Models

Figure 5.2.6 Mean Temperature (K) Contour for the Eddy Break-up and Second Moment Models

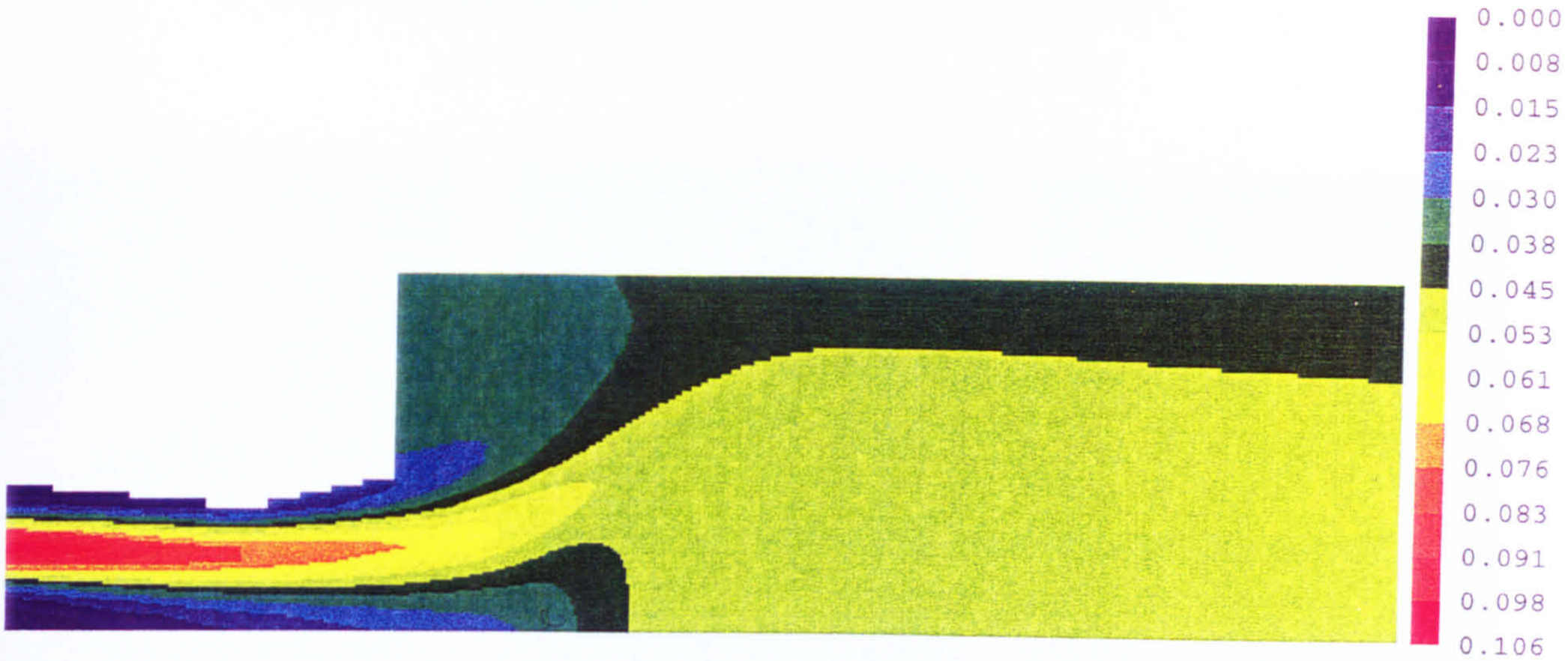

Figure 5.2.7 Mean Mixture Fraction Contour for the Eddy Break-up and k-ε Models

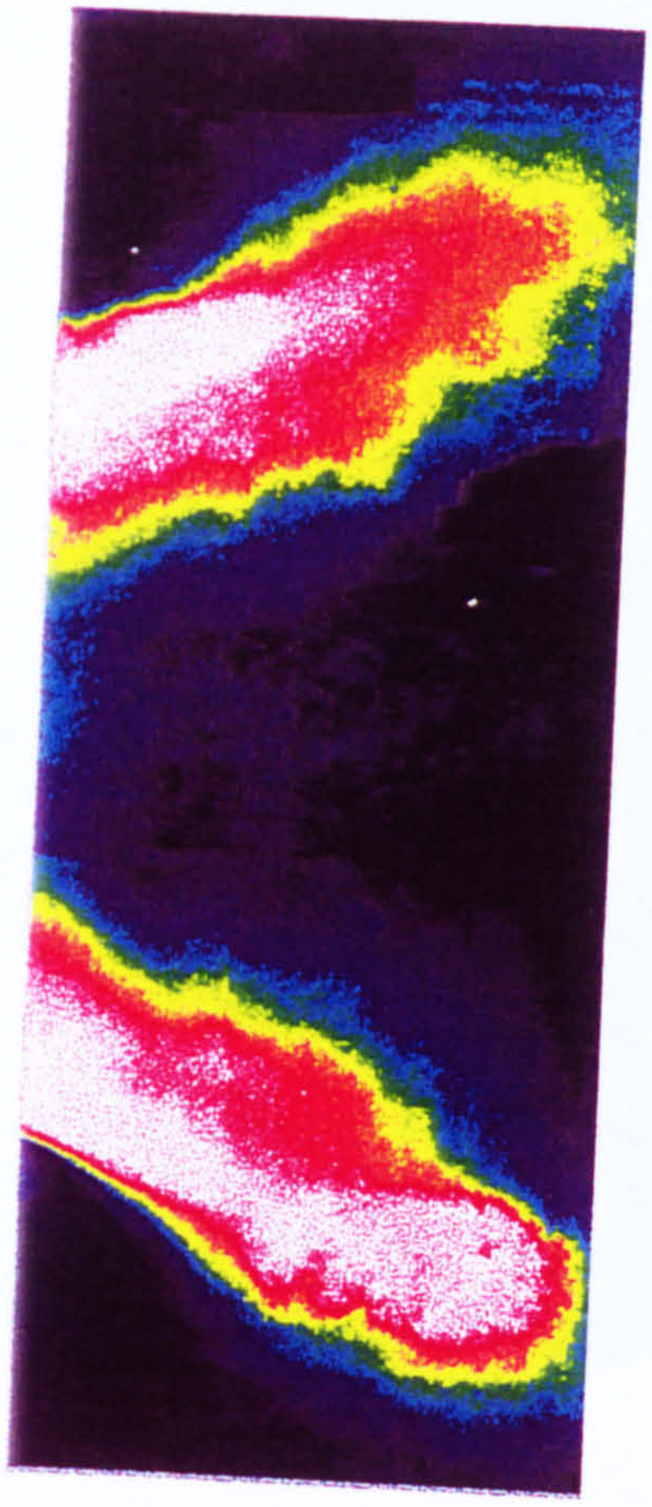

Figure 5.2.8 Mean LIF Image of the Fuel (Harding, 1996)

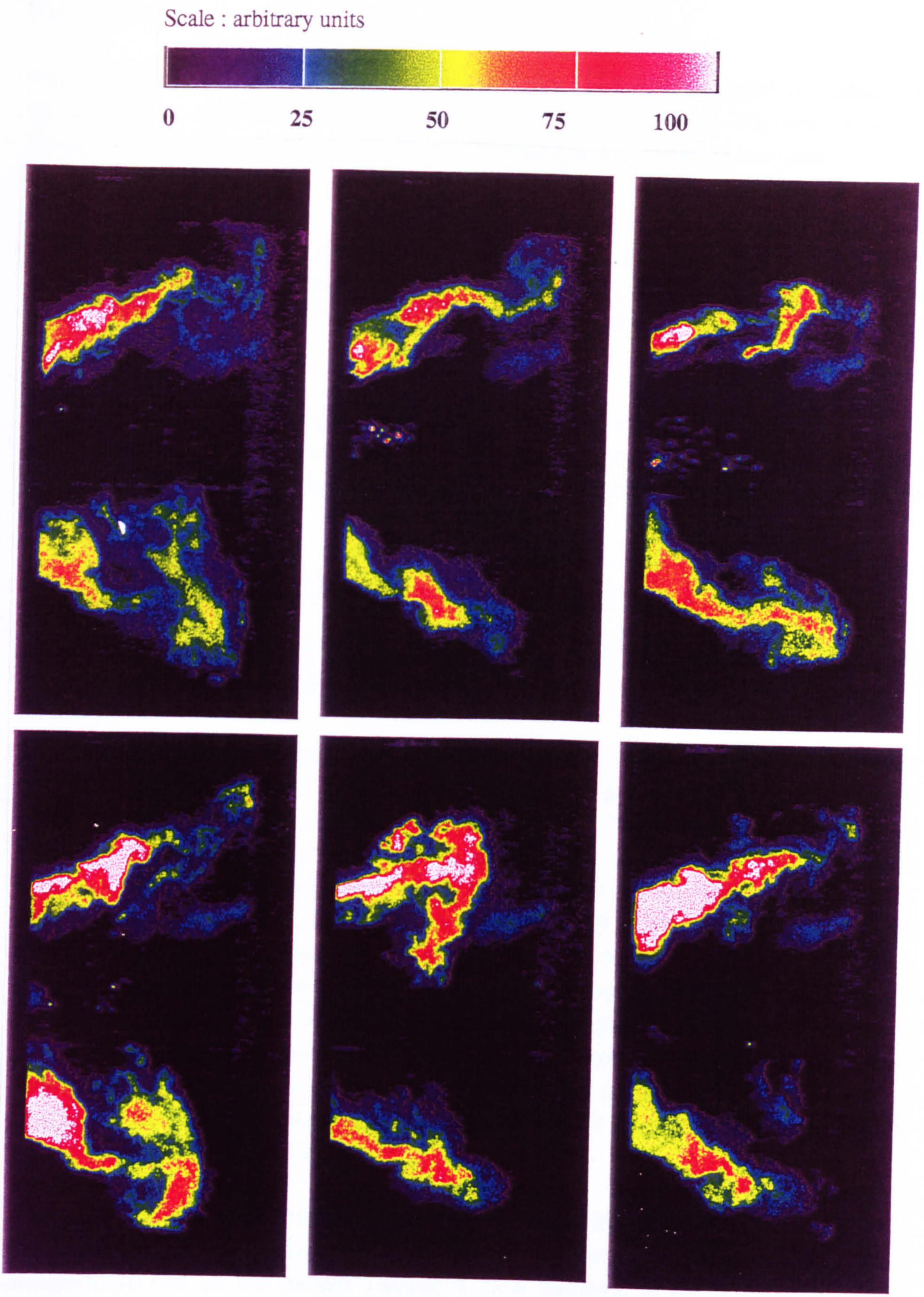

Figure 5.2.9 Instantaneous LIF Images of the Fuel (Harding, 1996)

5.2.1 Eddy Break-up Model

For the Eddy Break-up model the model constant, C_{EBU}, was assigned the value 2.43 for the mean equivalence ratio of 0.712, based on Equation (3-34), and C_{EBU}=2.12 for an equivalence ratio of 0.57, based on the earlier two dimensional work.

Figures 5.2.1.1 through 5.2.1.4 illustrate plots of the velocity vectors, contours of tangential velocity, mean reaction progress variable, and variance in the mixture fraction for predictions made with the k-ε turbulence model. The mean mixture fraction and mean flame temperature are illustrated in the Figures 5.2.7 and 5.2.5 respectively.

Generally speaking the results of these predictions compared qualitatively with the experimental measurements which were available, as was discussed in the previous section. A discussion of how these results compared with the other models will be presented later.

5.2.2 Presumed PDF Model

Figures 5.2.2.1 through 5.2.2.6 illustrate distributions of the same properties with the k-ε turbulence and Presumed pdf models.

The Presumed pdf model produced qualitatively similar results to the Eddy Break-up model. The chemical source term was slightly stronger and, in fact, predicted a small degree of reaction within the premixing duct. The initial temperature of the mixture is high enough for the Arrhenius reaction rate expression of Equation (3-9) to give a non-zero rate when c=0. Given that the spontaneous ignition temperature for propane in air at atmospheric pressure is about 766 K (cf. Glassman, 1987) and the inlet temperature of this experiment is around 1000 K then the model reflects a feature of the full chemistry that is entirely missing from the Eddy Break-up model. Part of the reason for this over prediction of the chemical source term is related to the factor of 5 which was introduced during the backward facing step investigations. There, this factor was needed to give a reasonable prediction of the flame front position relative to the Eddy Break-up model. However for this combustor geometry this factor is evidently too large.

The existence of a small amount of heat release within the premixing duct also had a large impact on the variance of the mixture fraction. The effect of the small temperature rise on the density caused a local damping of the turbulence kinetic energy. This in turn caused an increase in the molecular diffusion sink term in Equation (3-57) reducing the variance of the mixture fraction.

The results with the second moment closure model will be discussed later.

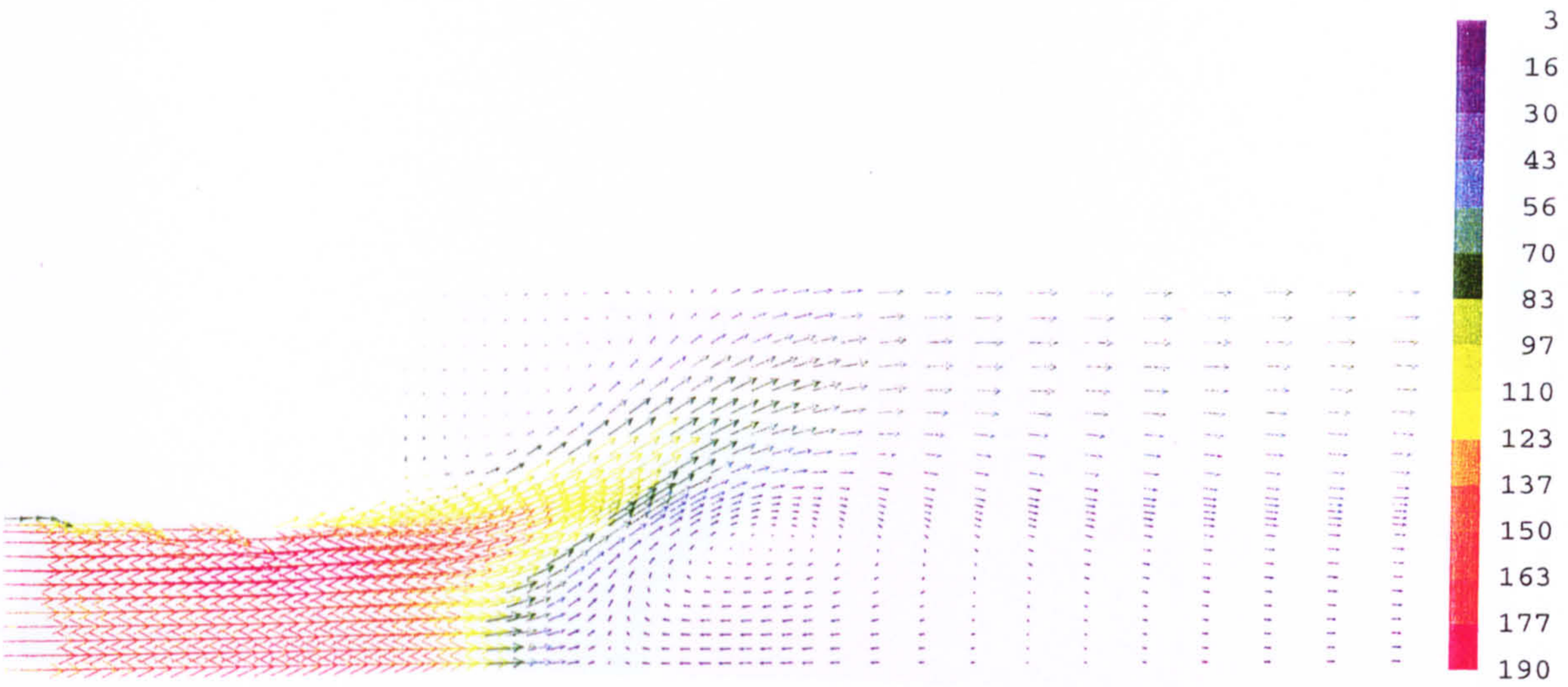

Figure 5.2.1.1 Velocity Vectors (m/s) for the Eddy Break-up and k-ε Models

Figure 5.2.1.2 Tangential Velocity (m/s) for the Eddy Break-up and k-ε Models

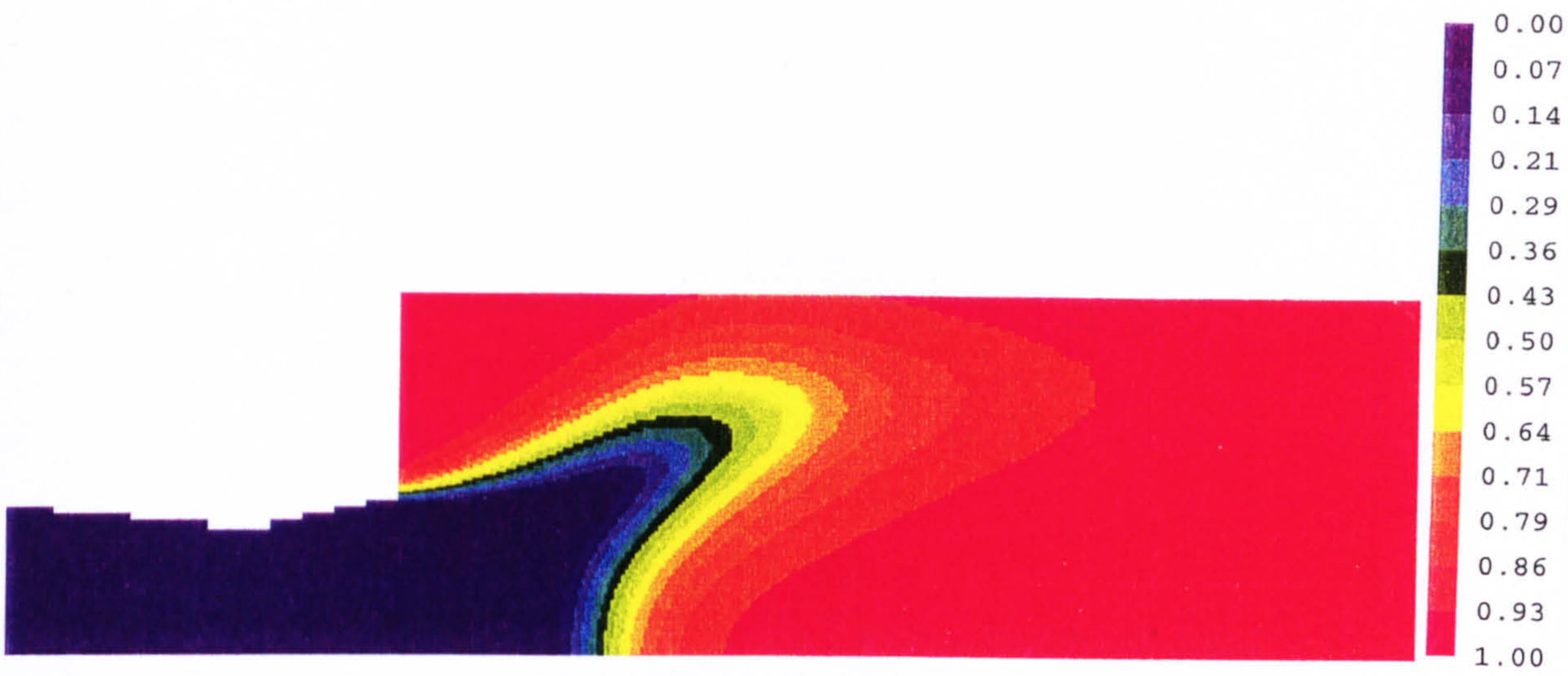

Figure 5.2.1.3 Mean Reaction Progress Variable for the Eddy Break-up and k-ε Models

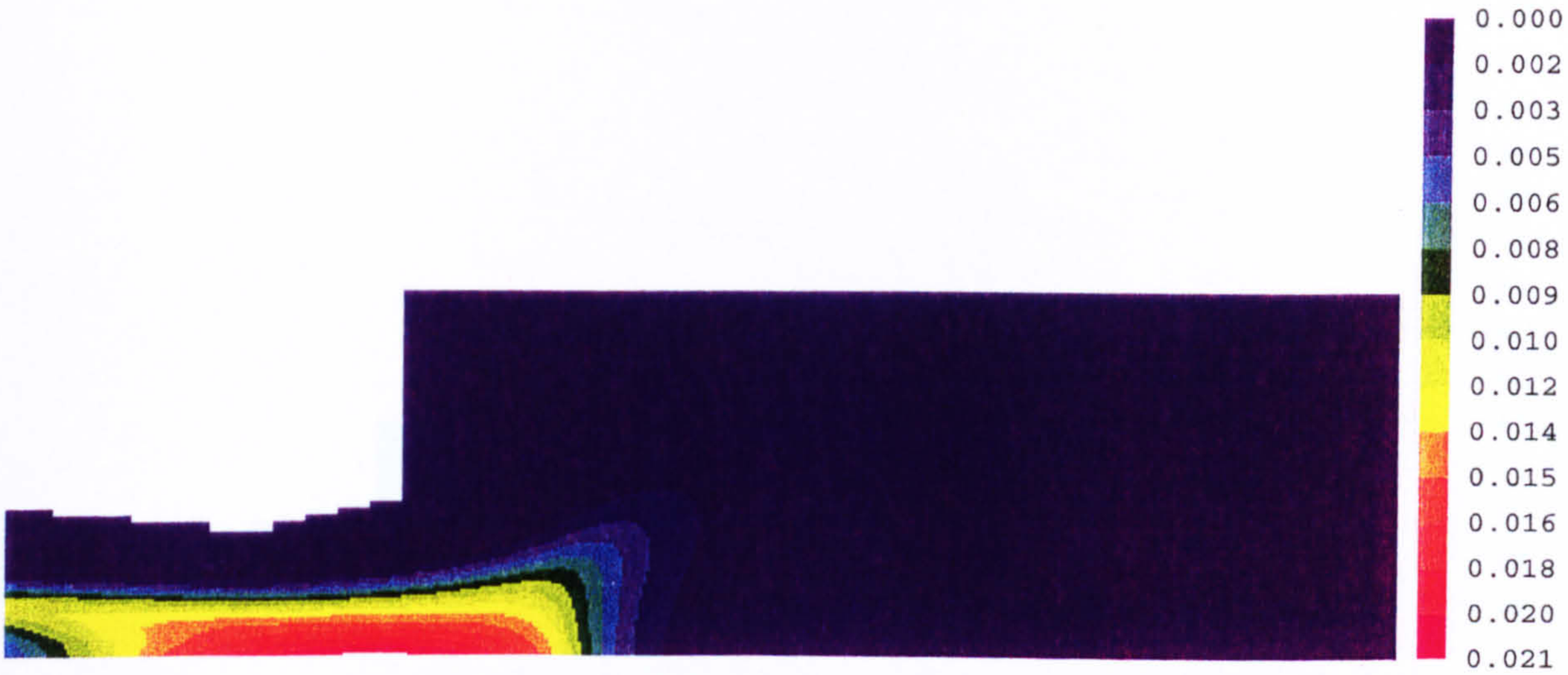

Figure 5.2.1.4 Variance of the Mixture Fraction for the Eddy Break-up and k-ε Models

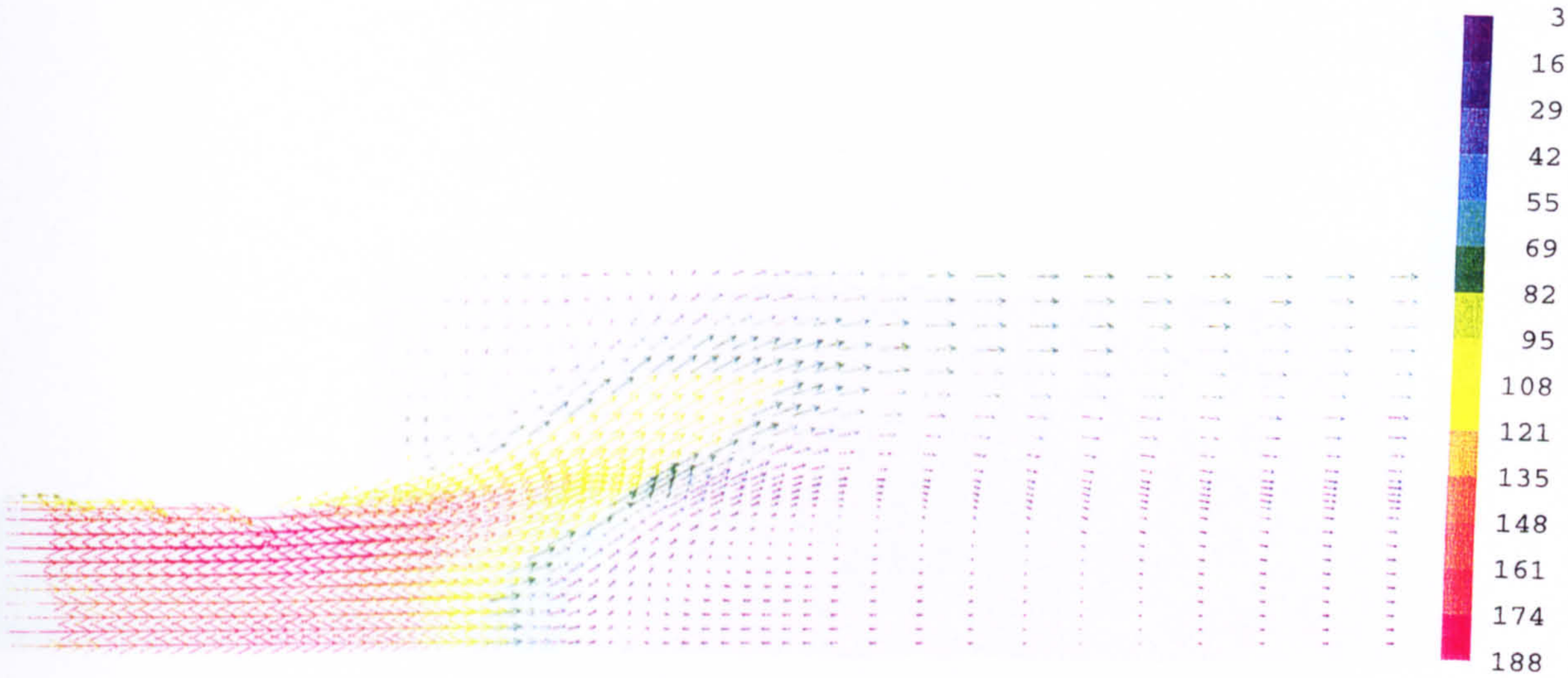

Figure 5.2.2.1 Velocity Vectors (m/s) for the Presumed pdf and k-ε Models

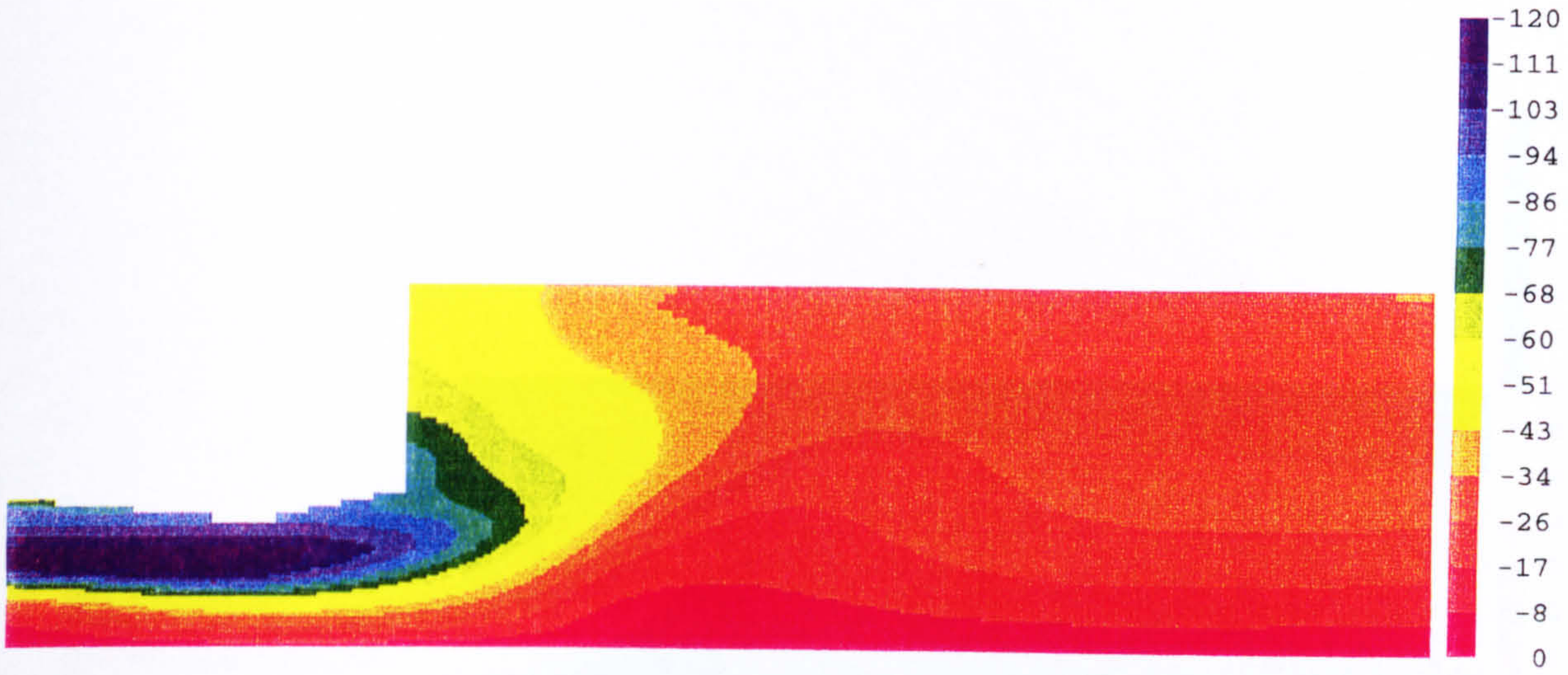

Figure 5.2.2.2 Tangential Velocity (m/s) for the Presumed pdf and k-ε Models

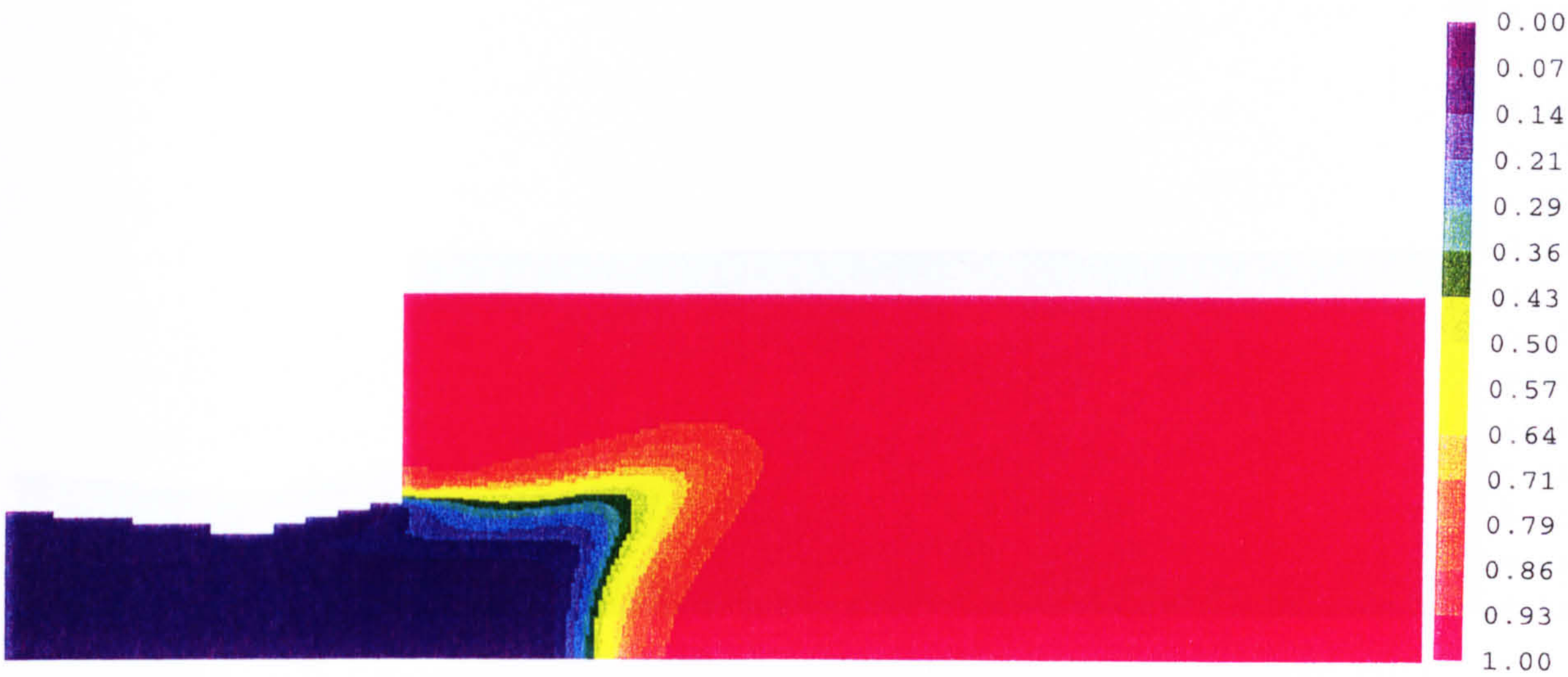

Figure 5.2.2.3 Mean Reaction Progress Variable for the Presumed pdf and k-ε Models

Figure 5.2.2.4 Mean Mixture Fraction for the Presumed pdf and k-ε Models

Figure 5.2.2.5 Variance of the Mixture Fraction for the Presumed pdf and k-ε Models

Figure 5.2.2.6 Mean Temperature (K) for the Presumed pdf and k-ε Models

5.2.3 Bray Moss Libby Crossing Frequency Model

Figures 5.2.3.1 through 5.2.3.6 illustrate plots of the velocity vectors, contours of tangential velocity, mean reaction progress variable, mean mixture fraction, variance in the mixture fraction and mean flame temperature for predictions made with the k-ε turbulence and BML Crossing Frequency models.

The BML Crossing Frequency model again presents qualitatively similar results to the Eddy Break-up model. More like the Eddy Break-up model than the Presumed pdf model, combustion does not occur until the unburnt reactants come into contact with burnt products at the edge of one of the two recirculation zones. Adopting the model constants suggested in the literature (Cant *et al*, 1988), this model appears to substantially underpredict the mean reaction rate. Combustion is not completed within the combustor (cf. Figures 5.2.3.3, 5.2.3.6). In order to enhance this, the value of $\overline{|\sigma_y|}$, the mean direction cosine of the flamelet crossing relative to the unit line in space, was modified. The original constant, 0.5, was based on the assumption that the mean crossing angle was 60° from the suggestion of Cant *et al* (1988). If this angle is 84° then $\overline{|\sigma_y|}$ becomes 0.1. This value gives a much better agreement with the Eddy Break-up model as can be seen by Figures 5.2.3.7 through 5.2.3.12. These figures illustrate distributions of the velocity vectors, contours of tangential velocity, mean reaction progress variable, mean mixture fraction, variance in the mixture fraction and mean flame temperature for the new constant. It seems plausible that $\overline{|\sigma_y|}$ be combustor geometry dependent and coupled with the degree of turbulence around the flame front. The greater the intensity of the turbulence, the more contorted the flame front and hence the steeper the mean angle between the flame front and a unit line in space.

Another factor in the underprediction of the heat release rate by the original calculations lies in the high levels of strain rate present in the flow field. This will be discussed in more detail later, however, its effect is to leave a large fraction of the flame front quenched as seen in Figure 5.2.3.13. Increasing the peak quenching strain rate from 1850 1/s, which is representative of the unburnt-to-unburnt laminar flame geometry on which we based our model, to a level of 5000 1/s, which is more representative of an unburnt-to-burnt laminar flame geometry, causes a large reduction in the fraction of the flame front which is quenched. For the second moment closure, 60 mm downstream of the exit of the premixing duct, the minimum percentage of the flame front which is quenched falls from about 98% down to 75%.

We may compare the absolute levels of the mean strain rate predicted from the Kolmogorov length scale, which was adopted for the predictions described by

Equation (3-31), with that based on the eddy dissipation rate ε/k. Radial profiles of these two rates at various distances downstream of the exit of the premixing duct are plotted in Figure 5.2.3.14. The two cases are qualitatively similar, however, the strain rate based on the eddy dissipation is an order of magnitude smaller than that based on the Kolmogorov length scale. This will clearly have an important effect given that the mean strain rate for the latter case is well above the maximum quenching strain rate. This will also contribute to the underpredicted rate of reaction of the calculations made with $\left|\overline{\sigma_y}\right|$=0.5. The strain rate based on the eddy dissipation rate near the premixing duct exit was also smaller on the axis, relative to its peak value, than the Kolmogorov length scale based strain rate. Additionally, it reduced in magnitude faster, relative to its peak near the premixing duct exit, as one moved downstream. Based on this, a stronger reaction rate would be predicted with the strain rate defined by the eddy dissipation rate.

The calculations made with the second moment closure model will be discussed next.

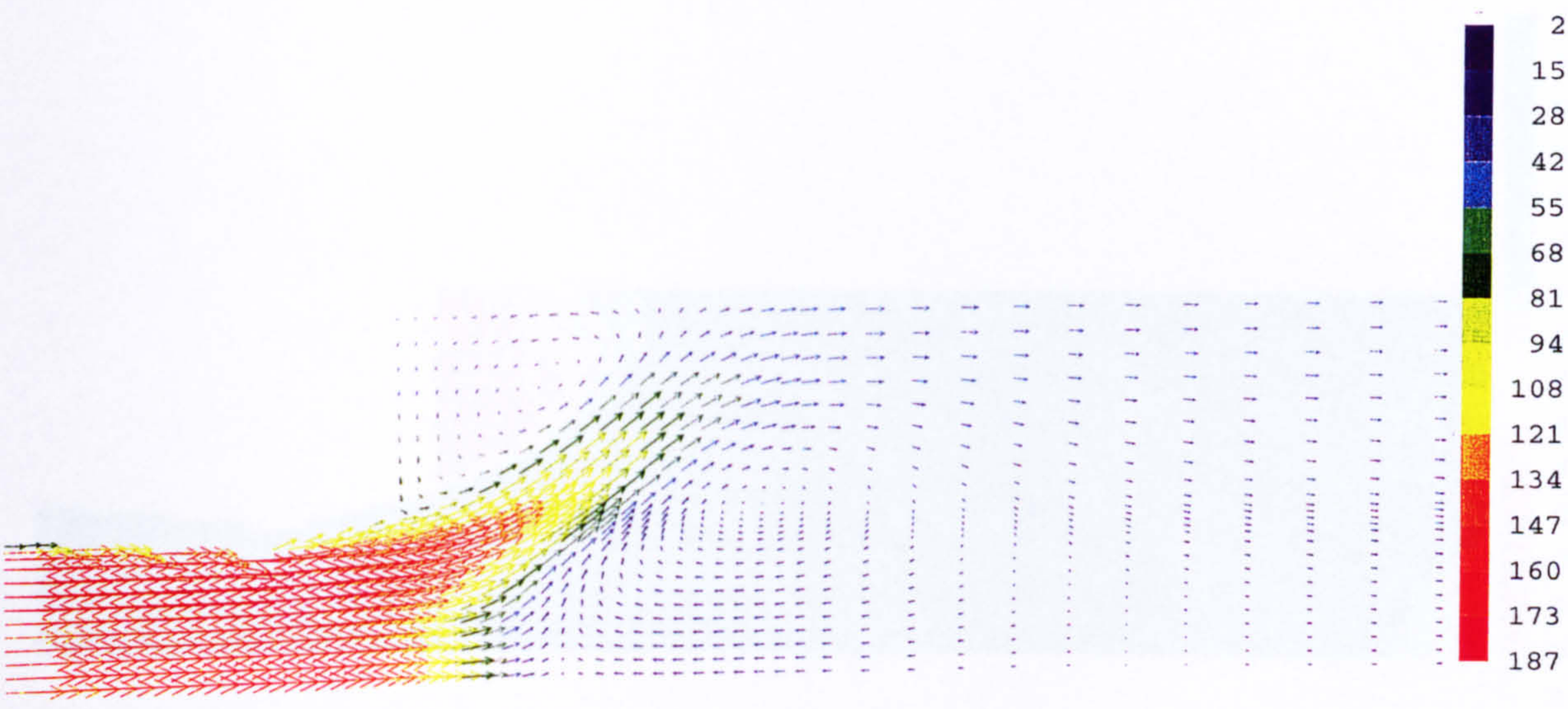

Figure 5.2.3.1 Velocity Vectors (m/s) for the original BML Crossing Frequency and k-ε Models

Figure 5.2.3.2 Tangential Velocity (m/s) for the original BML Crossing Frequency and k-ε Models

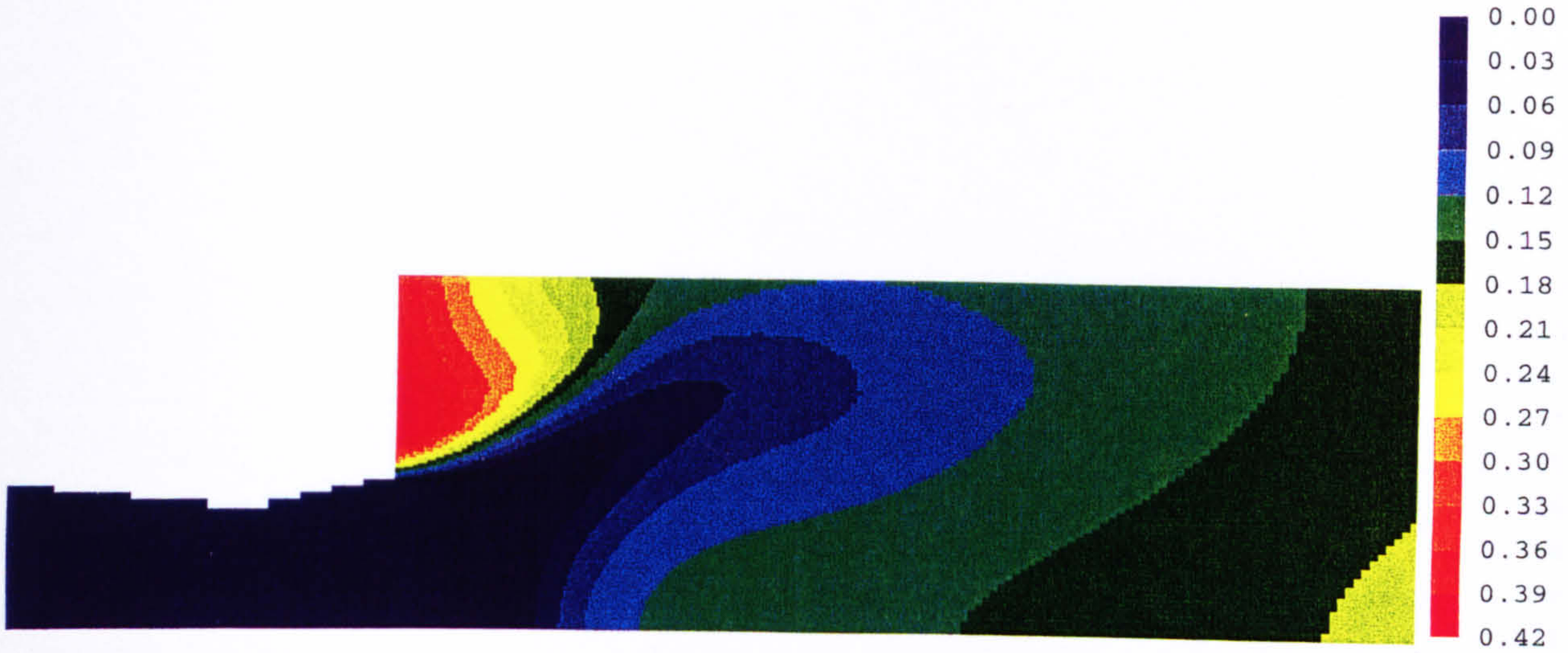

Figure 5.2.3.3 Mean Reaction Progress Variable for the original BML Crossing Frequency and k-ε Models

Figure 5.2.3.4 Mean Mixture Fraction for the original BML Crossing Frequency and k-ε Models

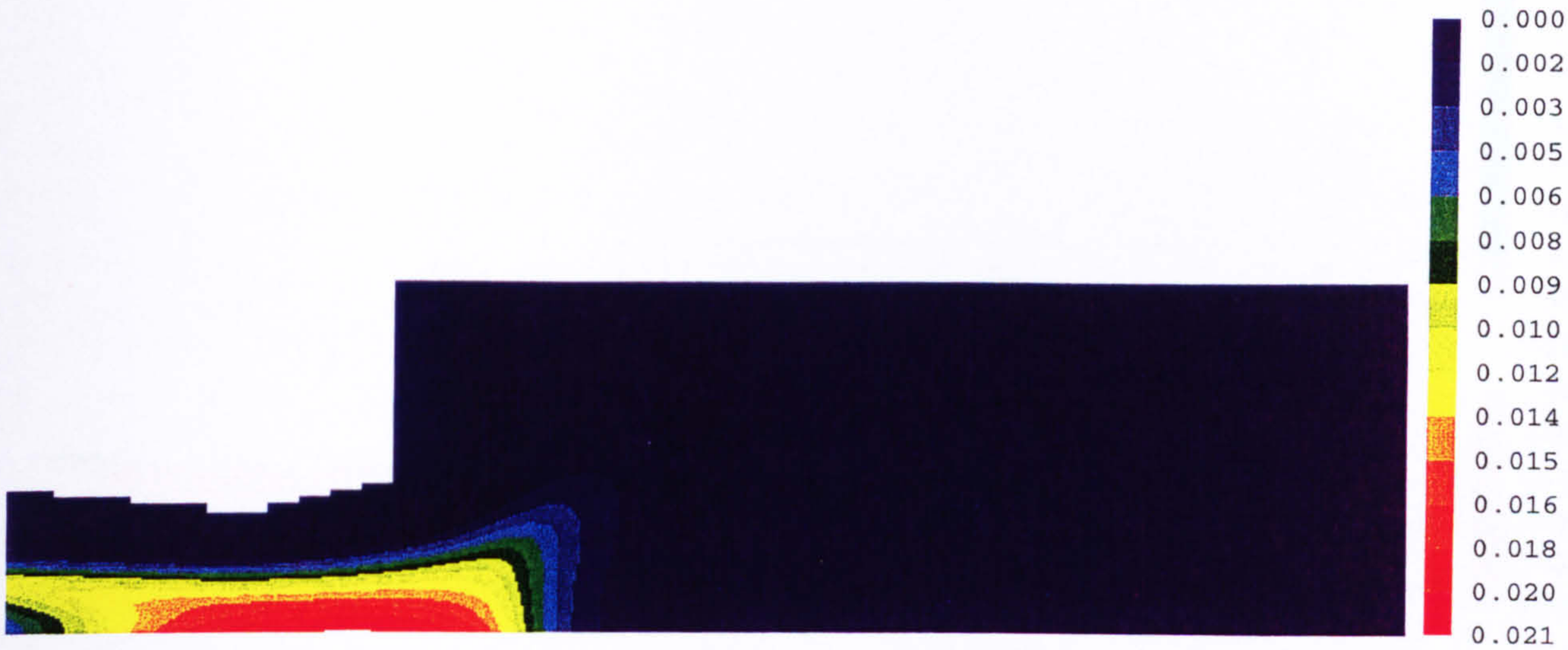

Figure 5.2.3.5 Variance of the Mixture Fraction for the original BML Crossing Frequency and k-ε Models

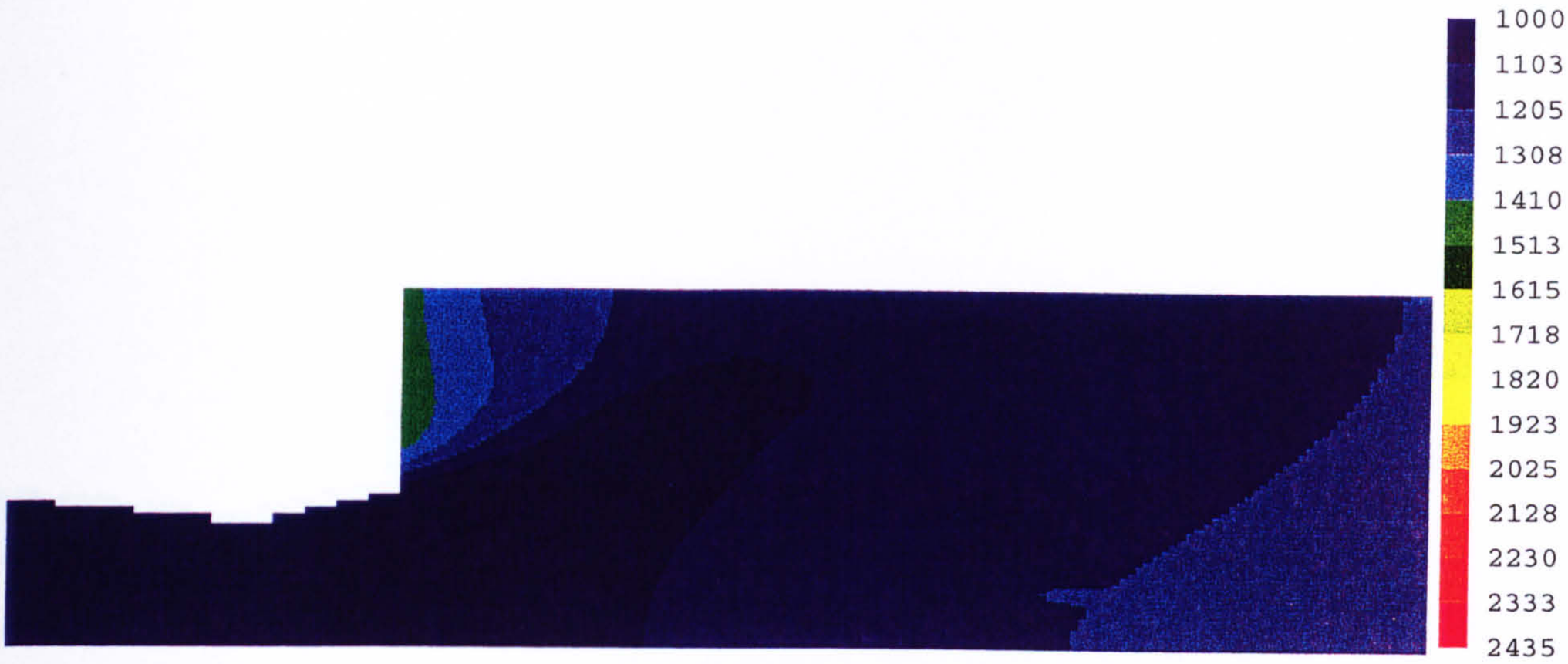

Figure 5.2.3.6 Mean Temperature (K) for the original BML Crossing Frequency and k-ε Models

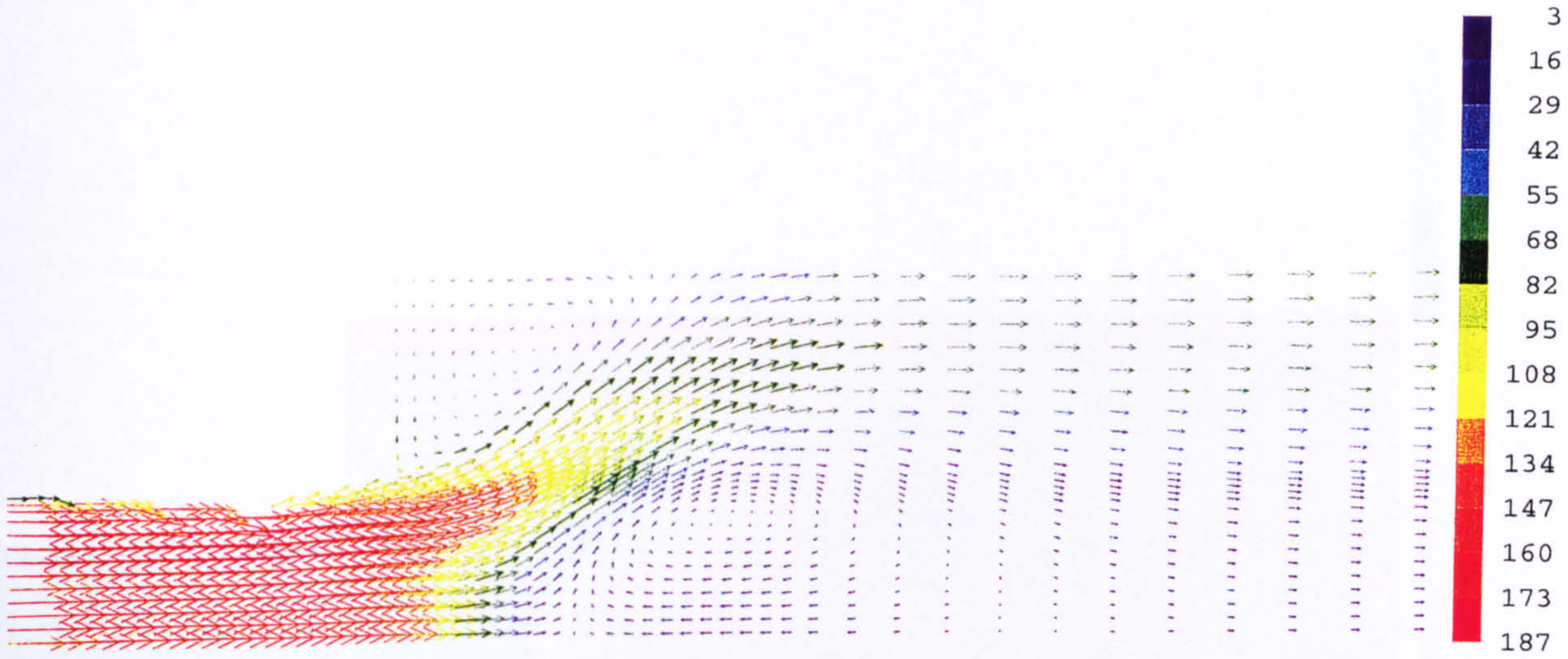

Figure 5.2.3.7 Velocity Vectors (m/s) for the calibrated BML Crossing Frequency and k-ε Models

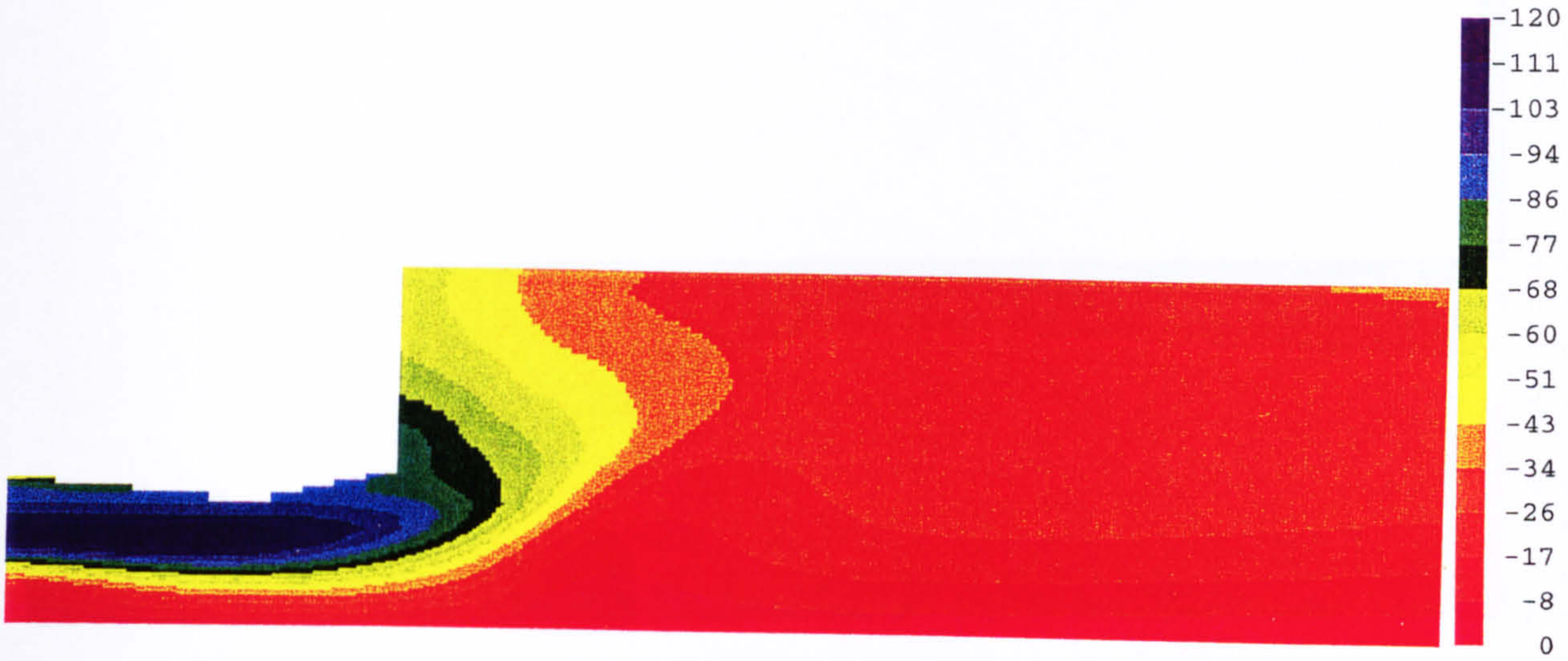

Figure 5.2.3.8 Tangential Velocity (m/s) for the calibrated BML Crossing Frequency and k-ε Models

Figure 5.2.3.9 Mean Reaction Progress Variable for the calibrated BML Crossing Frequency and k-ε Models

Figure 5.2.3.10 Mean Mixture Fraction for the calibrated BML Crossing Frequency and k-ε Models

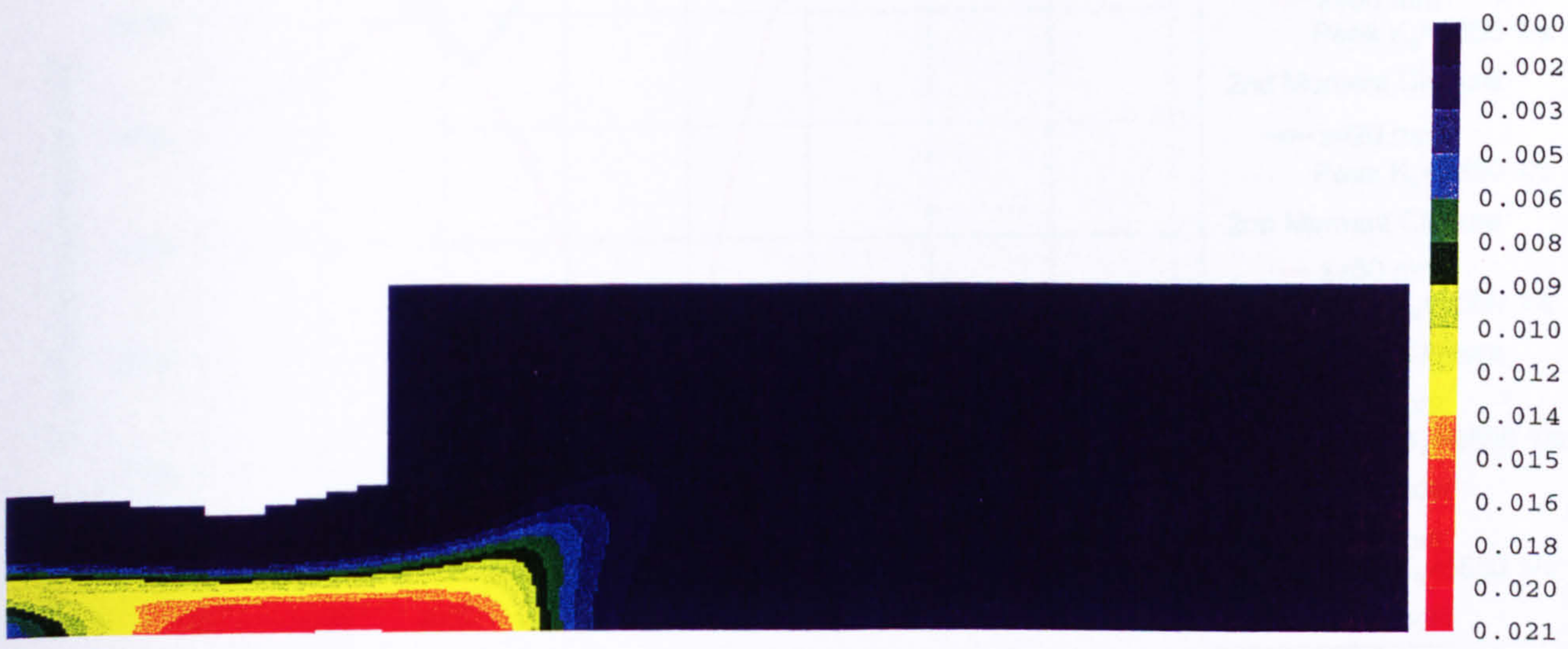

Figure 5.2.3.11 Variance of the Mixture Fraction for the calibrated BML Crossing Frequency and k-ε Models

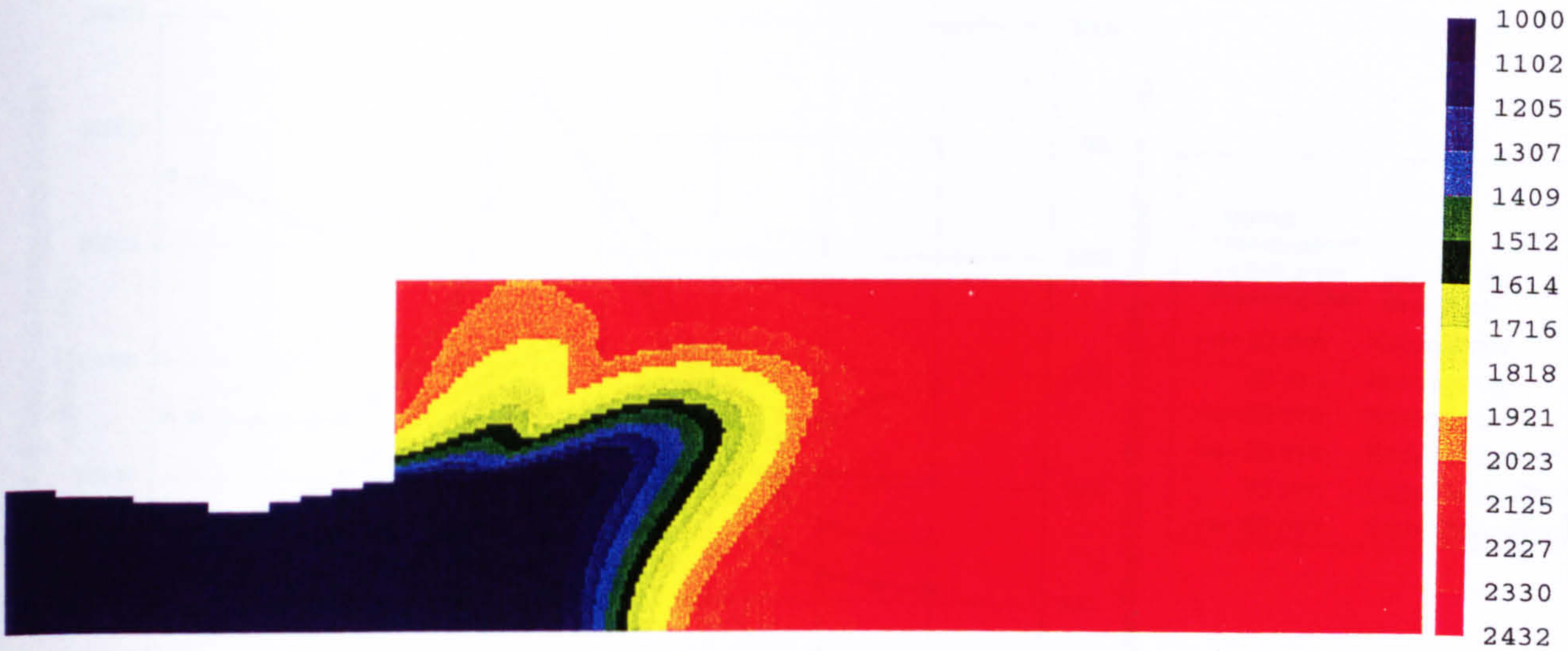

Figure 5.2.3.12 Mean Temperature (K) for the calibrated BML Crossing Frequency and k-ε Models

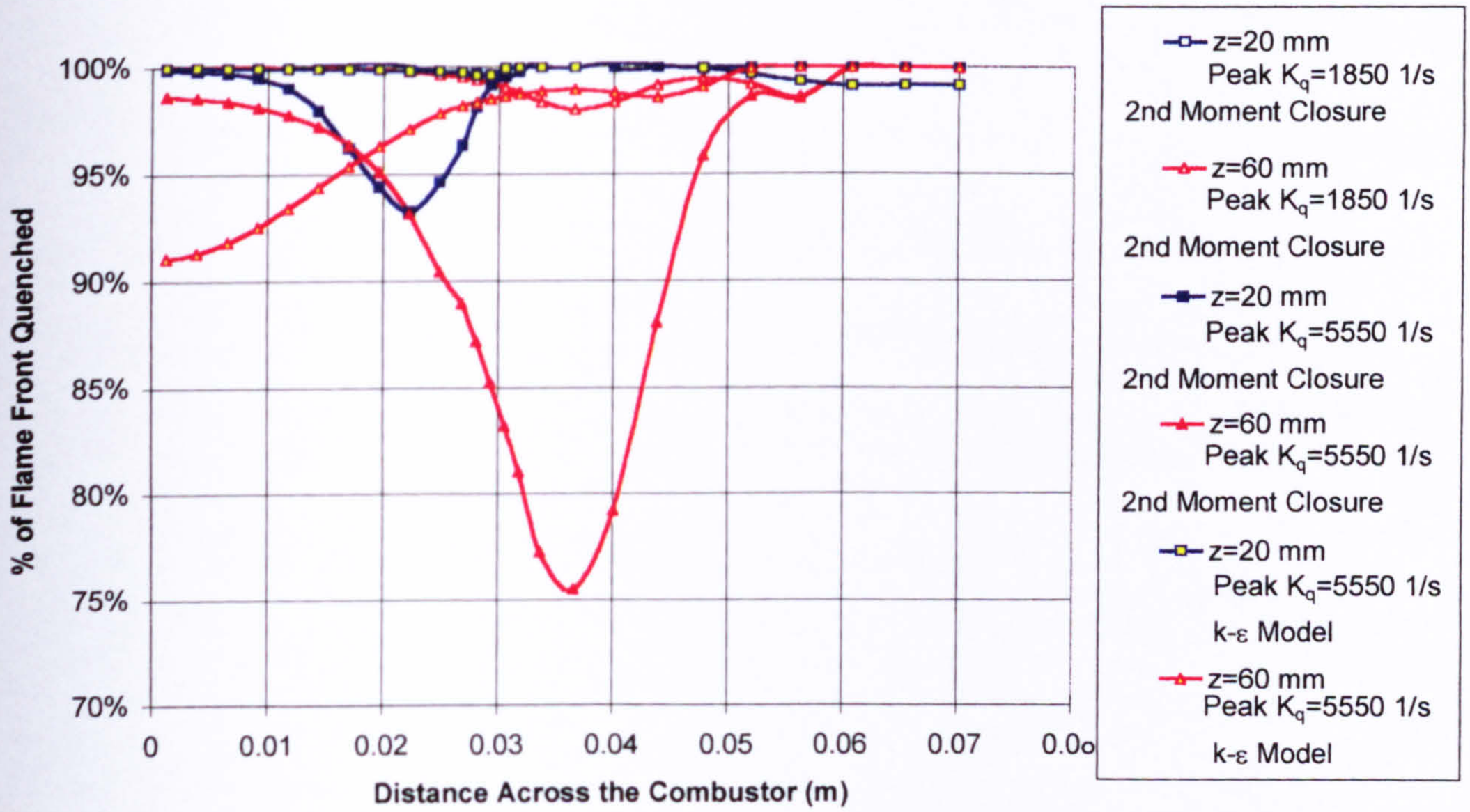

Figure 5.2.3.13 Percentage of Flame Front which is Quenched due to Straining (for BML Crossing Frequency Model where K_q is the strain rate where the flame front quenches)

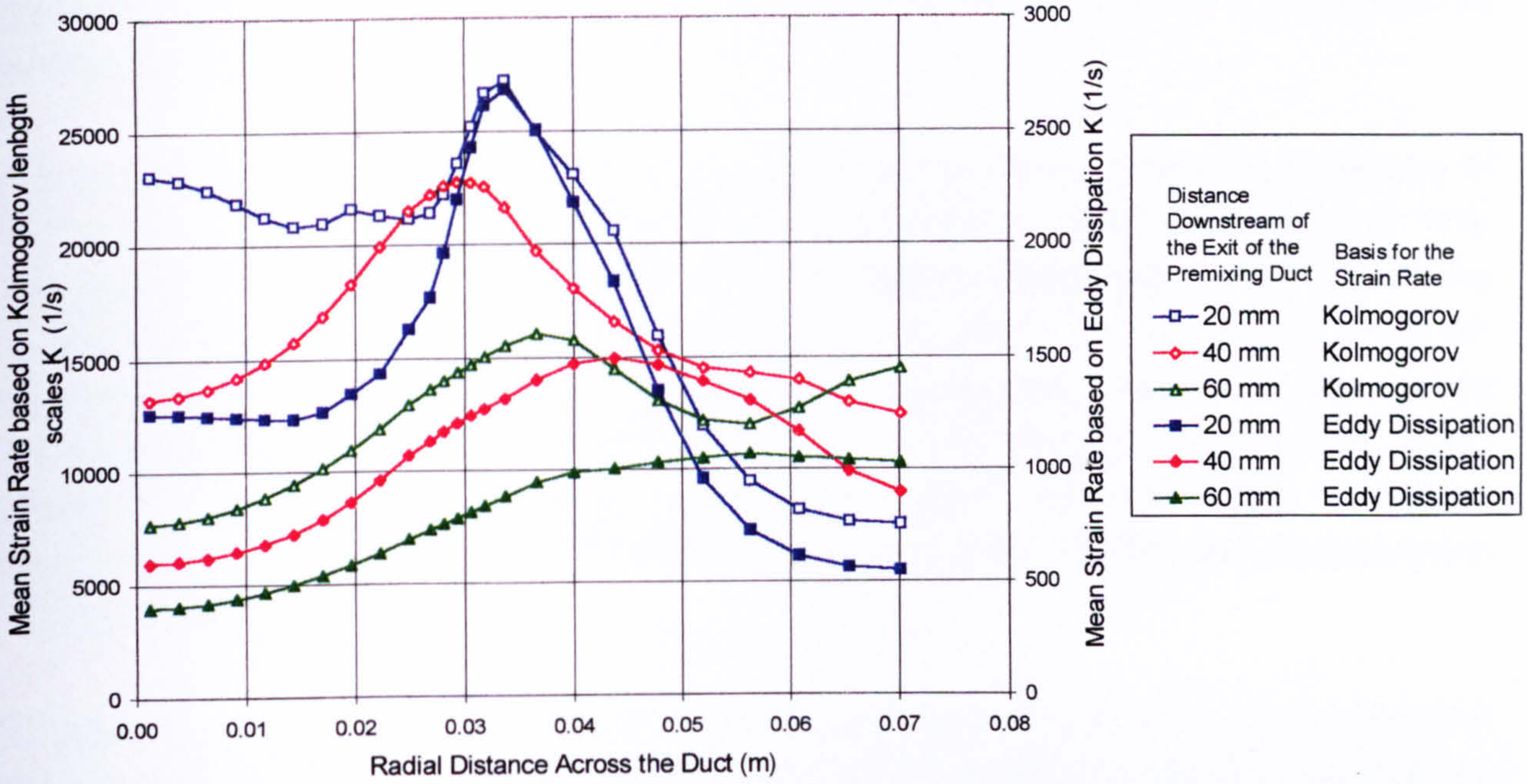

Figure 5.2.3.14 Radial Profiles of the Mean Strain Rate at various distances downstream of the exit of the premixing duct (k-ε Turbulence Model)

5.2.4 Second Moment Turbulence Model

Perhaps the largest difference between the calculations performed with the second moment turbulence model (RSTM) and the k-ε turbulence model are evidenced in the flow field itself.

One of the strangest features noted in the cold flow calculations was the existence of two recirculations within the vortex breakdown bubble. Instantaneous and time averaged LIF images (Harding, 1996) of the aromatics in the kerosene fuel within the combustor, downstream of the premixing duct, (Figures 5.2.8 and 5.2.9) show an unburnt region on the axis. This is similar to the predictions made with the second moment turbulence model for combusting flow. A representative plot of the mean reaction progress variable from calculations made with the Eddy Break-up combustion model (Figure 5.2.4.3) shows clearly this unburnt patch on the centreline of the combustor.

Figures 5.2.4.4 through 5.2.4.7 show radial profiles of the axial and tangential velocity at three points downstream of the exit of the premixing duct for both the k-ε and second moment closure calculations and for both cold and combusting calculations with the Eddy Break-up model. Both turbulence models predict an expansion of the recirculation in the upper corner of the combustor just after the exit of the premixing duct for the combusting calculation over the cold one. The flow nearer the axis accelerates, in accordance with mass conservation, which tends to push the point at which the vortex breakdown occurs further downstream. This appears to contradict the findings of Harding (1996), who reported that the existence of combustion brought the vortex breakdown closer to the exit of the premixing duct. As discussed earlier, however, the cold flow calculations indicate that the injection of the fuel increases the swirl strength and causes the vortex breakdown bubble to move upstream. This might account for the discrepancy between the calculations and Harding's (1996) findings, given that he did not operate the experiment cold with fuel injection for safety reasons. The combusting calculations also predict an increase in the tangential velocity over the cold flow calculations. This increase tends to be greater for the k-ε turbulence model than the second moment closure model and will diminish the tendency of the higher axial velocity to push the point of the vortex breakdown downstream. This in part explains why the vortex breakdown bubble of the k-ε turbulence model appears stronger, with higher velocities, than that of the second moment closure model.

Another feature of the flow field which is evident from the cold flow calculations is that the turbulence frequency, as defined by the ratio of the dissipation rate of the turbulence kinetic energy to the turbulence kinetic energy, is generally higher for the

second moment closure model. This can be seen in Figure 5.2.4.8. As all of the combustion models adopted here are effectively proportional to this frequency, this implies that the chemical source term will be stronger for the second moment closure model over the k-ε model. This is clearly illustrated by mean contours of the temperature for the Eddy Break-up model seen in Figures 5.2.5 and 5.2.6 for both the k-ε and second moment turbulence models respectively. This can also be seen in Figure 5.2.4.9, which shows contours of the chemical source term for the Eddy Break combustion model for both turbulence models.

Other features which affect the predicted heat release rate are counter gradient diffusion and flame front straining. Counter gradient diffusion influences all the mixing-controlled combustion models investigated while flame front straining is only addressed in the BML Crossing Frequency Model.

The second moment closure model, which does not introduce the gradient assumption for the scalar fluxes as does the k-ε model, allows for the prediction of counter gradient transport. This can be seen in the plot of the axial flux of the reaction progress variable, in Figure 5.2.4.10, 20 mm downstream of the exit of the premixing duct for the Eddy Break-up combustion model.

Comparisons were made of the mean strain rates predicted for the BML Crossing Frequency combustion model for both turbulence models. Figures 5.2.4.11 and 5.2.4.12 illustrate both the Kolmogorov length scale based strain rate (Equation 3-31) and the eddy dissipation based strain rate (ε/k) respectively. One prominent feature is that the first measure of strain rate for the k-ε turbulence model gives larger peaks, whereas the other rate gives larger peaks for the second moment closure model. This would indicate, since the eddy dissipation based strain rate is inversely dependent on the turbulence kinetic energy and the Kolmogorov length scale based strain rate is not, that the second moment closure model is predicting a lower level of turbulence kinetic energy than the k-ε turbulence model. This is verified by Figure 5.2.4.13. It also indicates that the length scale of the turbulence predicted by the second moment closure is much smaller than that of the k-ε model which is shown in Figure 5.2.4.14. Figure 5.2.3.13 illustrates the fraction of the flame front which is quenched for both turbulence models for the Kolmogorov length scale based strain rate. It is clear from this figure that the turbulence model has a strong influence on this parameter. Considering the case with a peak quenching strain rate of 5550 1/s, which is typical of a burnt-to-unburnt laminar flame experiment, at a distance of 60 mm from the exit of the premixing duct, the k-ε turbulence model predicts that a minimum of 90% of the flame front is quenched while the second moment model predicts a minimum of 75% of the flame front is quenched. For the case which we considered, with a peak quenching strain rate of

1850 1/s from an unburnt-to-unburnt laminar flame experiment, the difference is only a few percent. Therefore for this geometry this parameter can be strongly influenced by the choice of turbulence model if the quenching strain rate is high (i.e. based on an unburnt-to-burnt laminar flame configuration). For the case we considered the impact on the source term is limited, similar to that of the counter gradient diffusion.

Figure 5.2.4.3 Mean Reaction Progress Variable for the Eddy Break-up and Second Moment Models

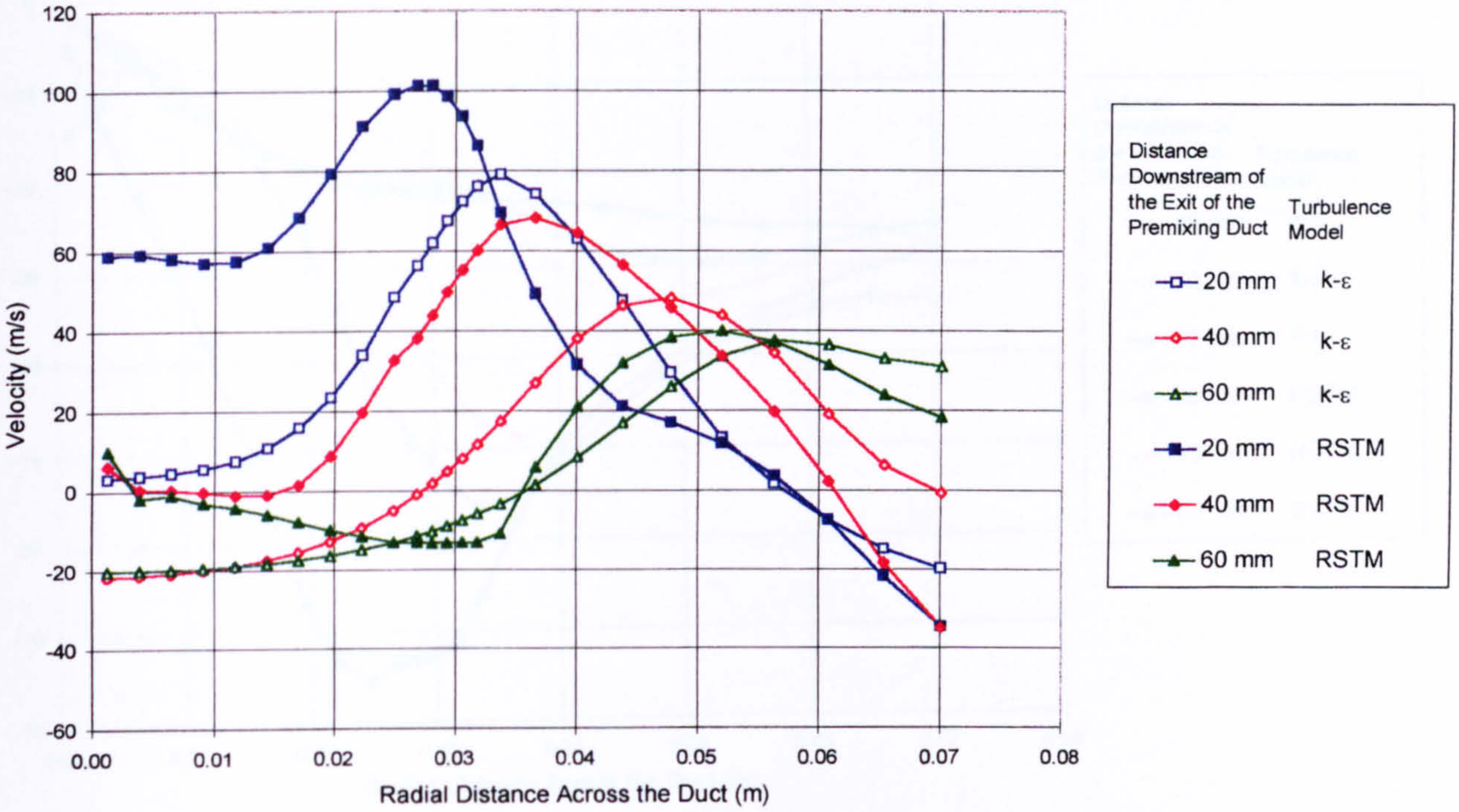

Figure 5.2.4.4 Radial Profiles of the Axial Velocity for the Isothermal Calculations

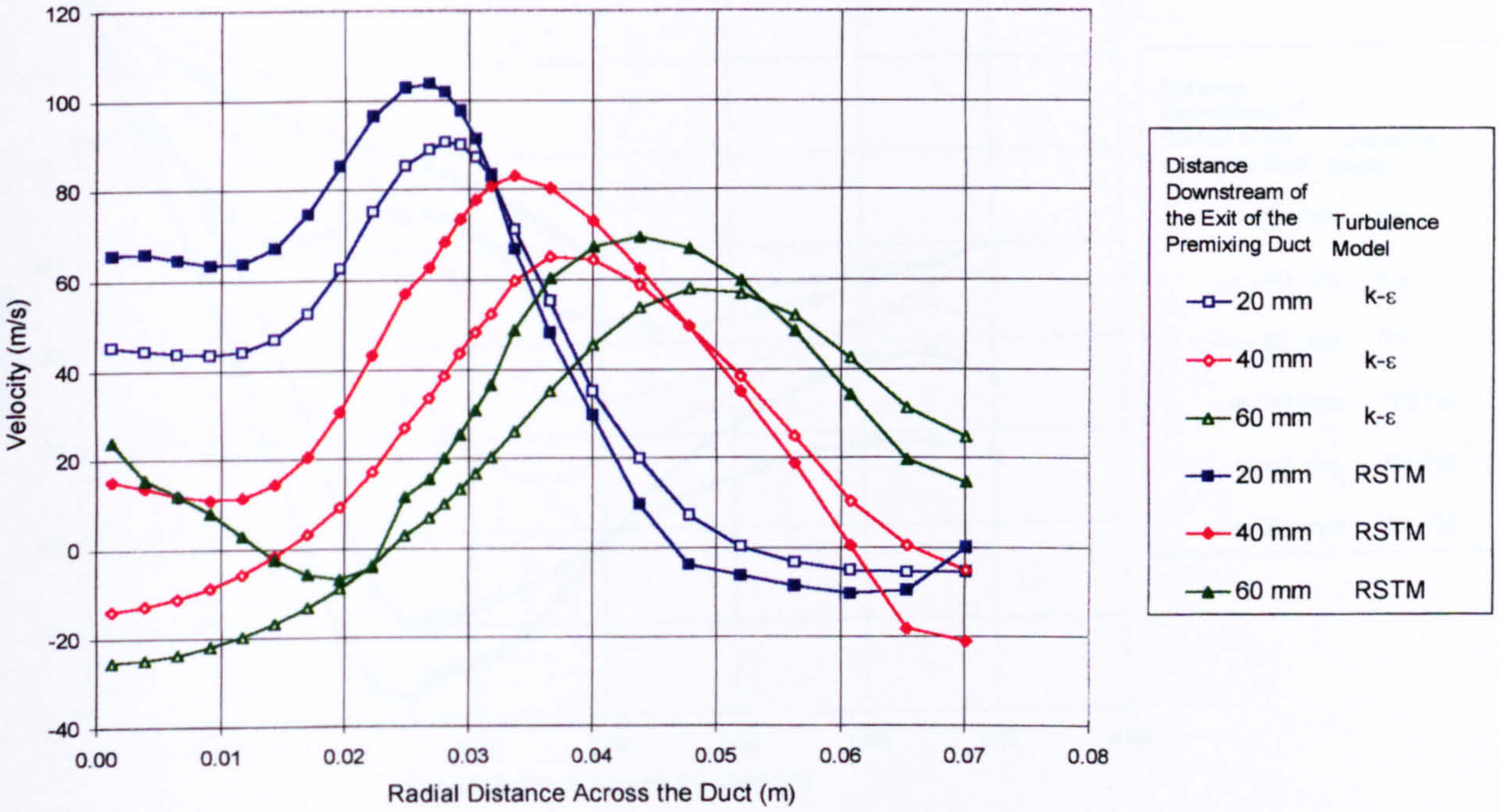

Figure 5.2.4.5 Radial Profiles of the Axial Velocity for the Eddy Break-up Model Calculations

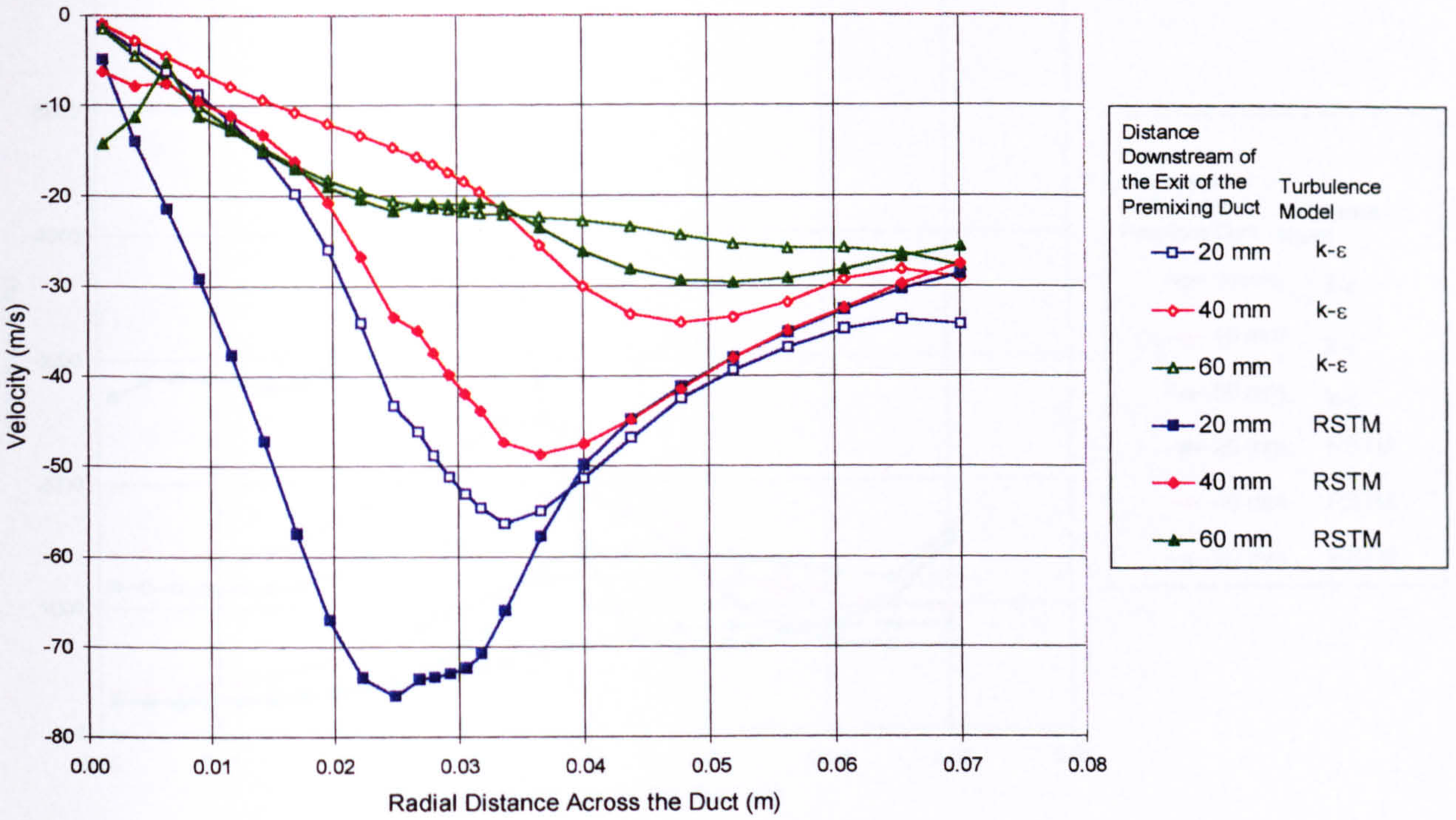

Figure 5.2.4.6 Radial Profiles of the Tangential Velocity for the Isothermal Calculations

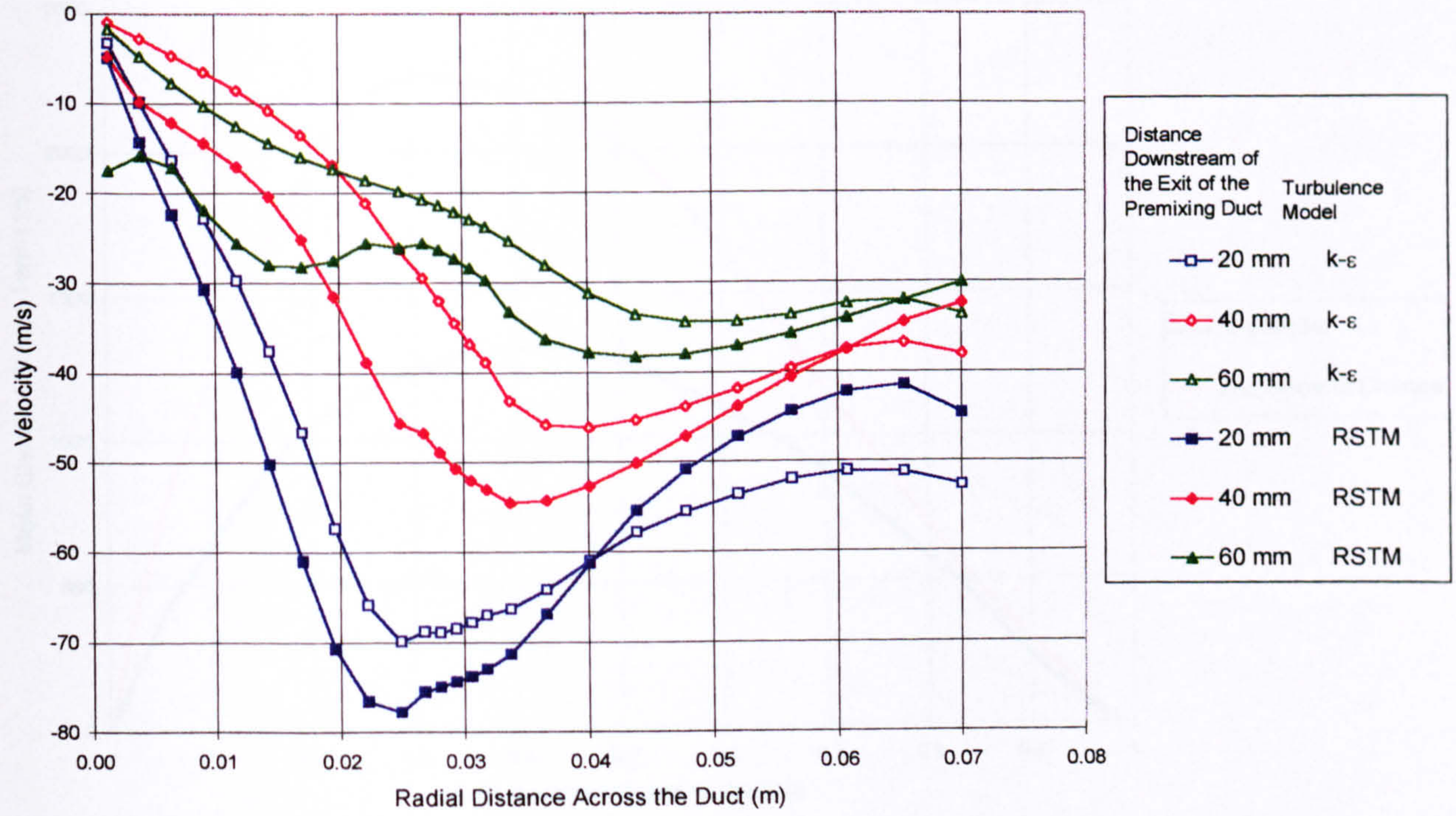

Figure 5.2.4.7 Radial Profiles of the Tangential Velocity for the Eddy Break-up Model Calculations

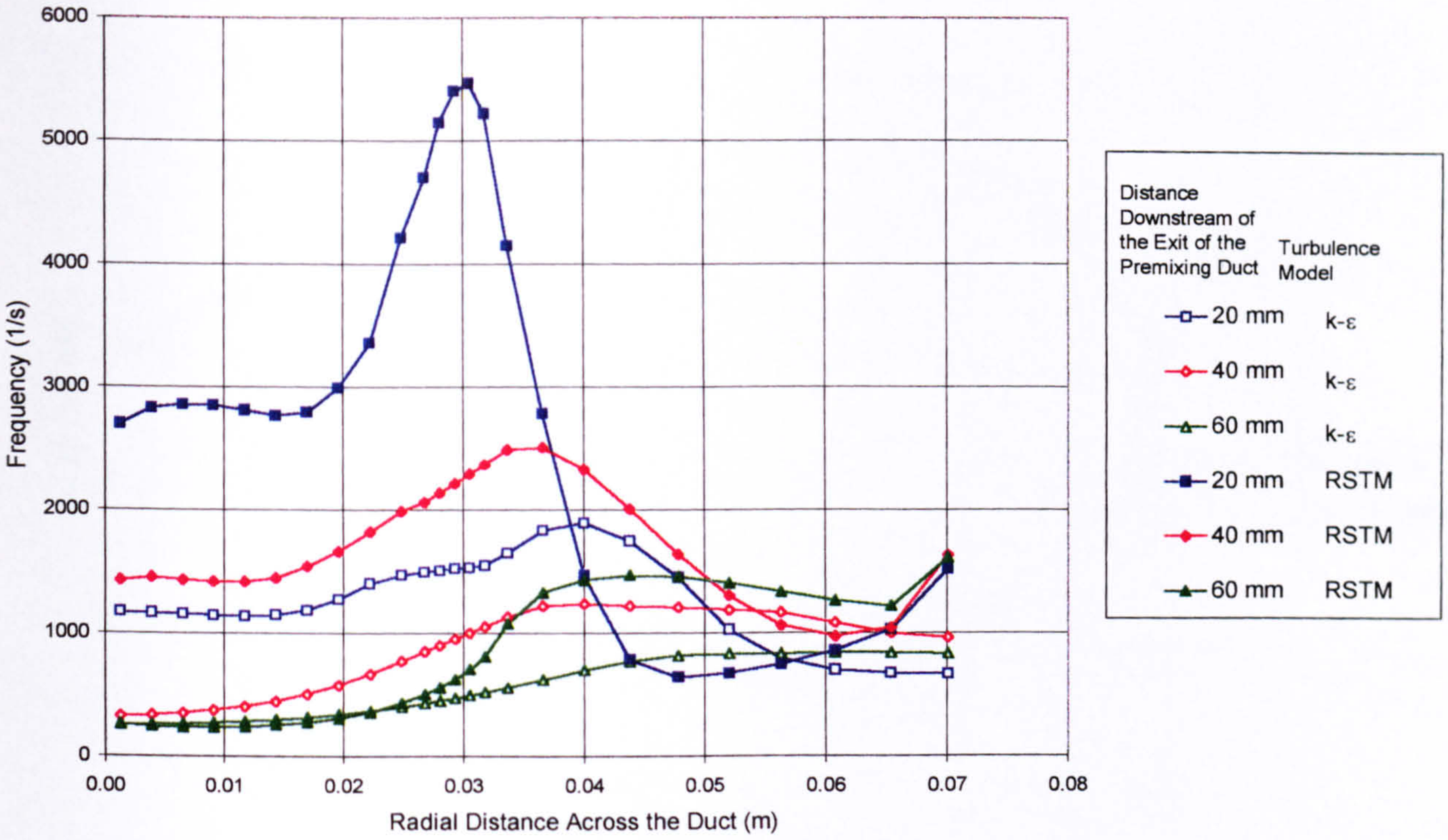

Figure 5.2.4.8 Radial Profiles of the Turbulence Frequency (ε/k) for the Isothermal Calculations

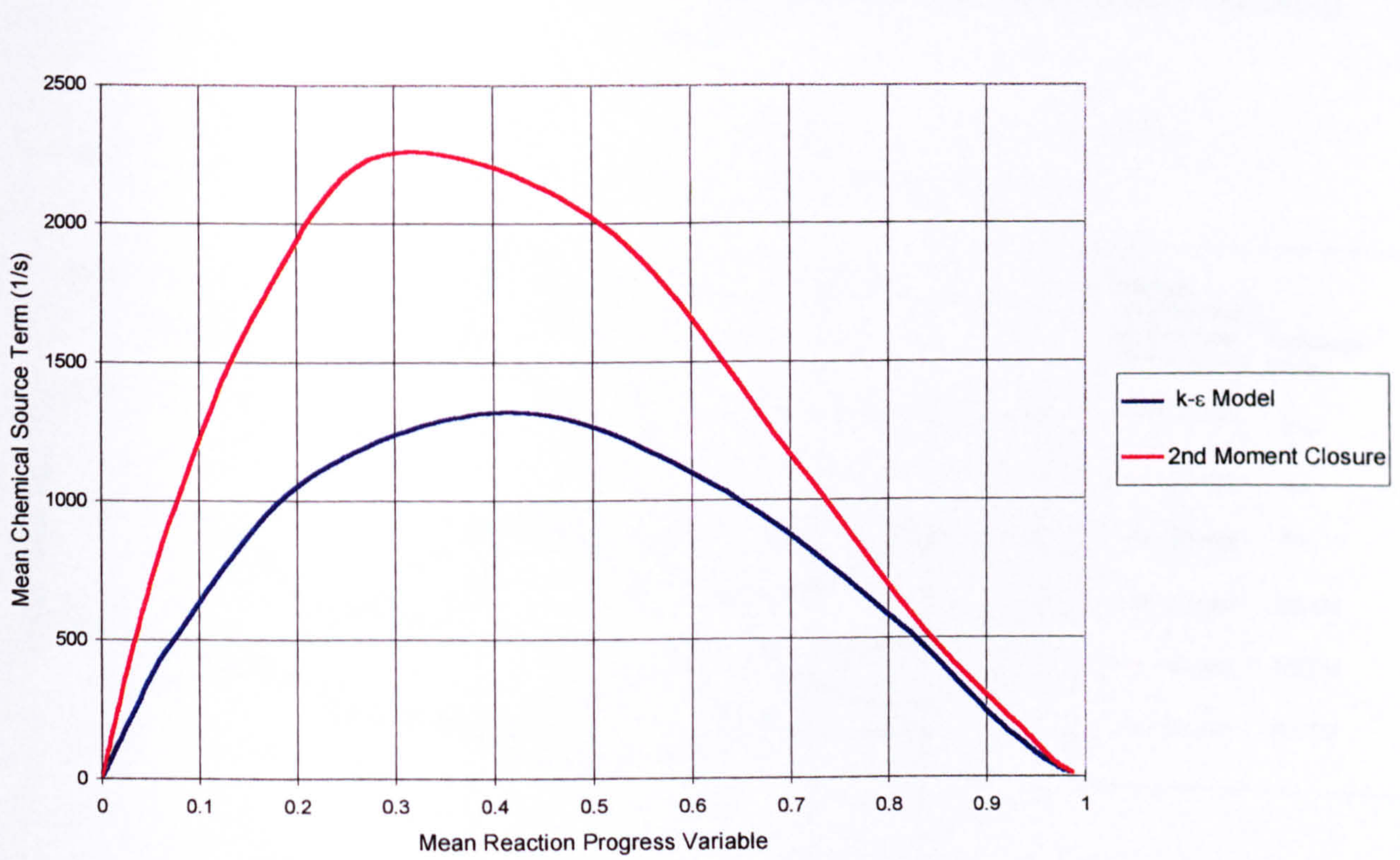

Figure 5.2.4.9 Mean Chemical Source Term for the Eddy Break-up Model (C_{ebu}=2.43) 20 mm downstream of the exit of the Premixing Duct

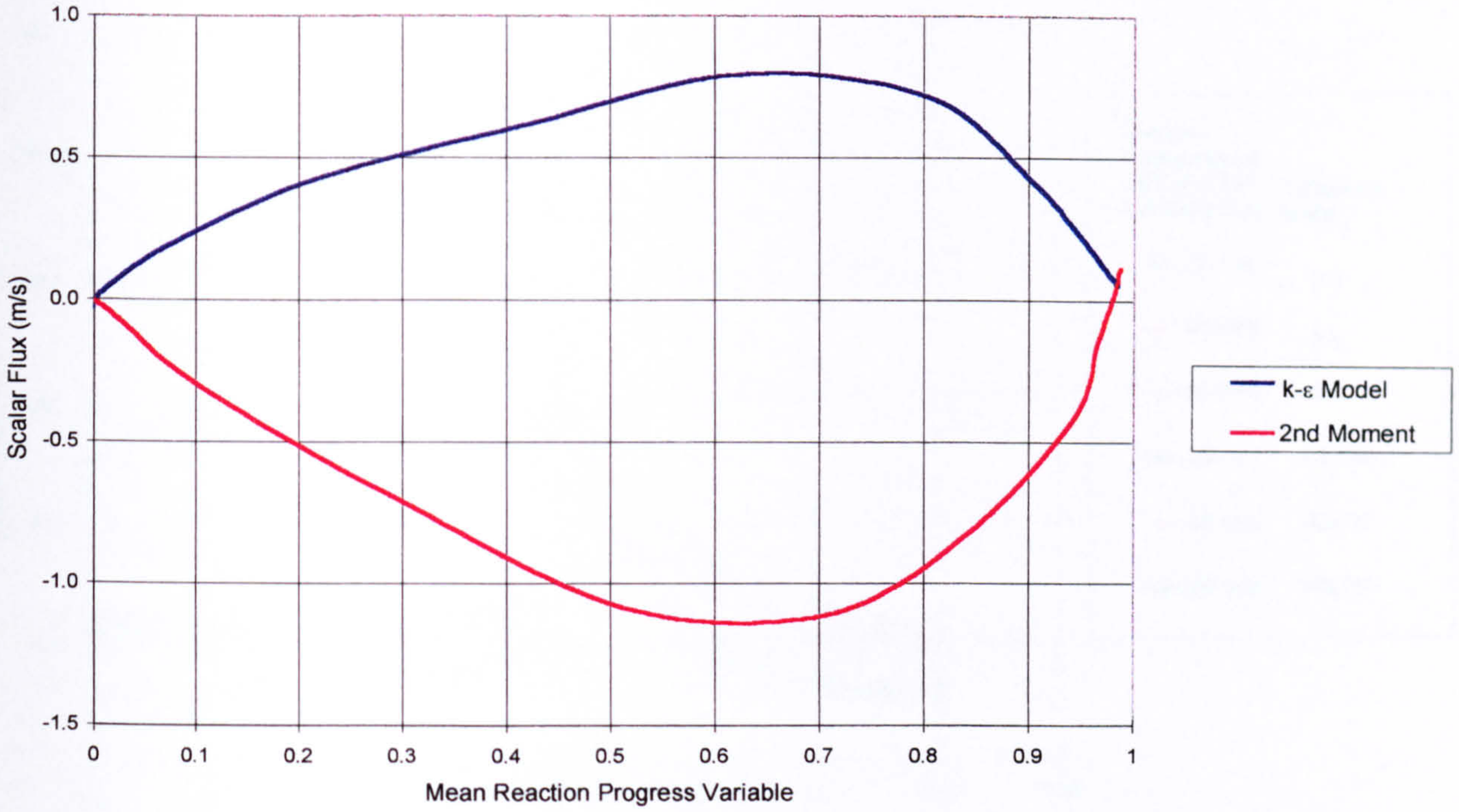

Figure 5.2.4.10 Axial-Reaction Progress Variable Scalar Flux ($\tilde{w''c''}$) for the Eddy Break-up Model (C_{ebu}=2.43) 20 mm downstream of the exit of the Premixing Duct

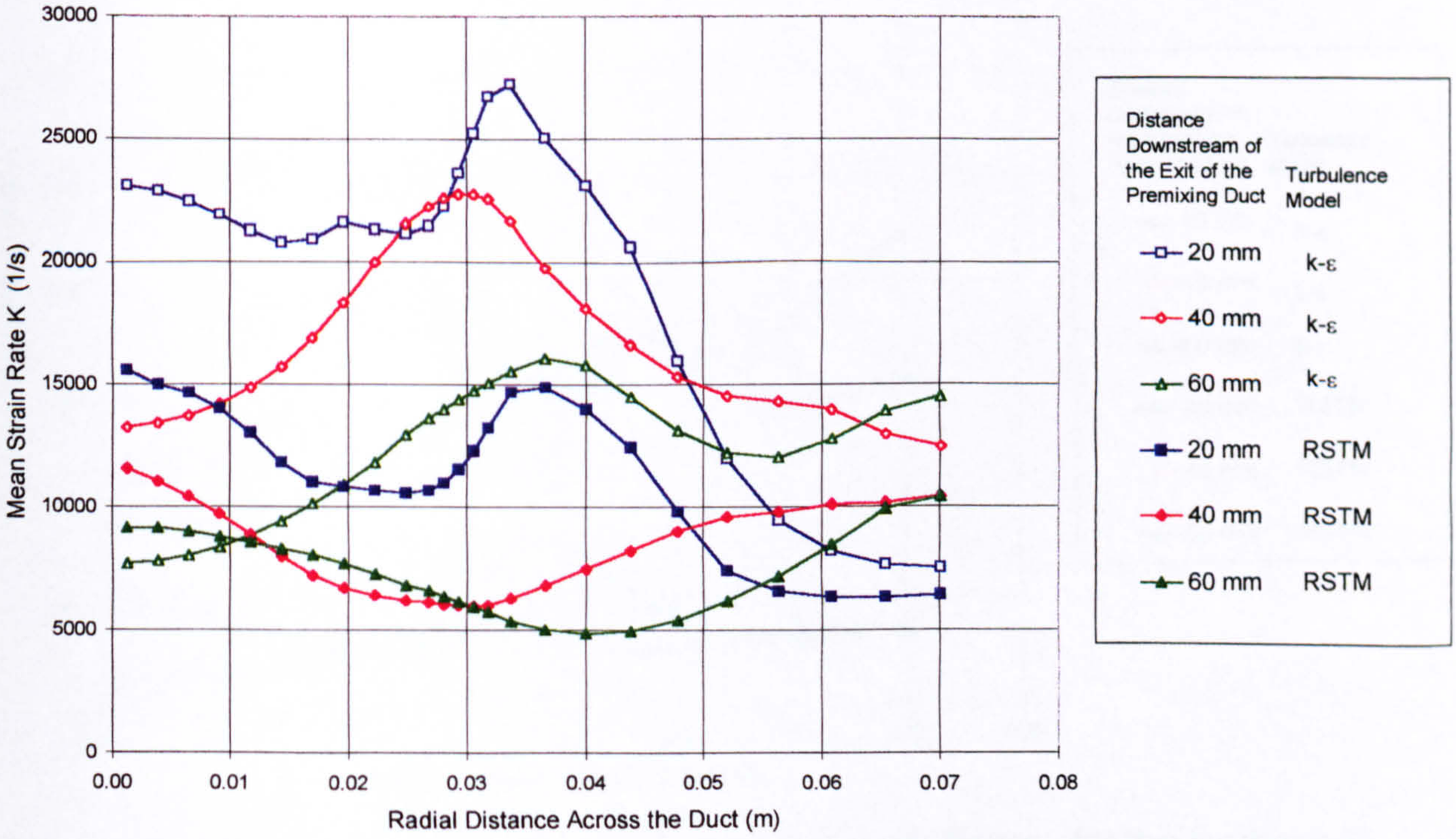

Figure 5.2.4.11 Radial Profiles of the Mean Strain Rate based on the Kolmogorov Length Scale for the BML Crossing Frequency Combustion Model

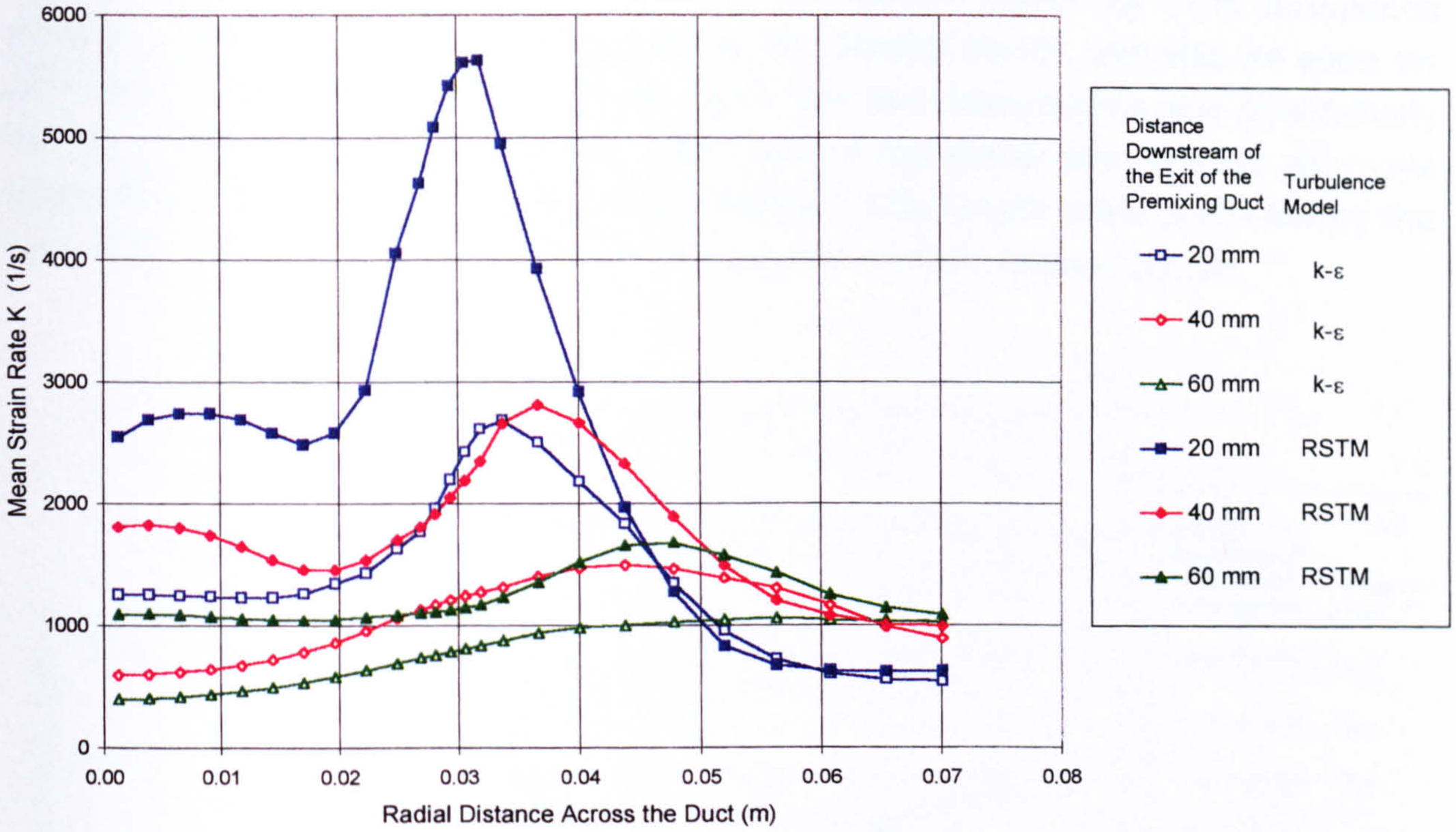

Figure 5.2.4.12 Radial Profiles of Mean Strain Rate based on the Eddy Dissipation Length Scale for the BML Crossing Frequency Combustion Model

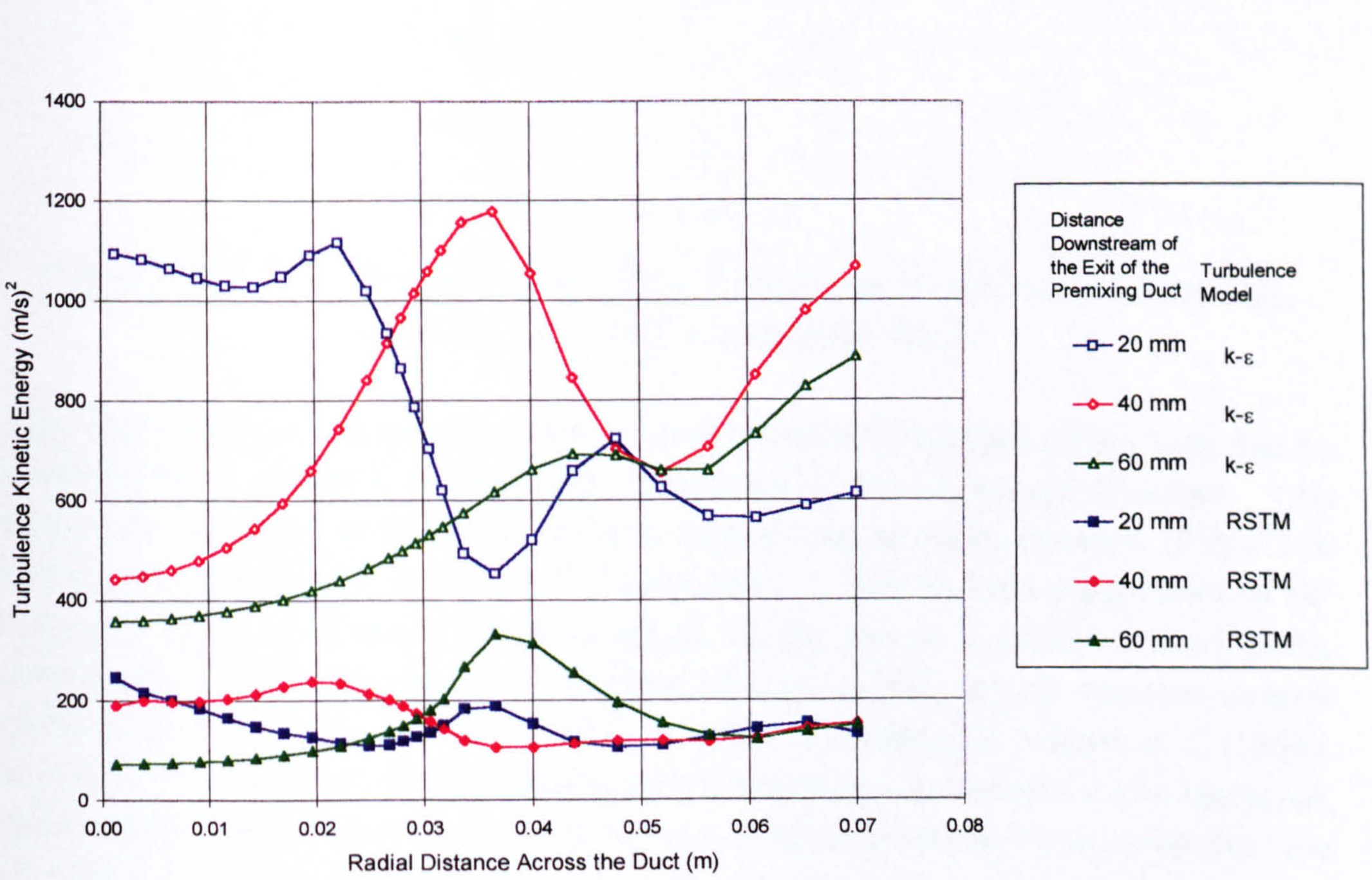

Figure 5.2.4.13 Radial Profiles of Turbulent Kinetic Energy for the Isothermal Calculations

A comparison of the turbulence length scale based on Equation (3-25) was also made with the BML Crossing Frequency combustion model for both turbulence models. This can be seen in Figure 5.2.4.14. Similar trends can also be seen for the other combustion models. Once again the two calculations are qualitatively similar. The length scale near the outer wall of the combustor falls as we move downstream, while near the axis it is increasing. The length scale predicted by the k-ε model is slightly larger than that of the second moment closure model.

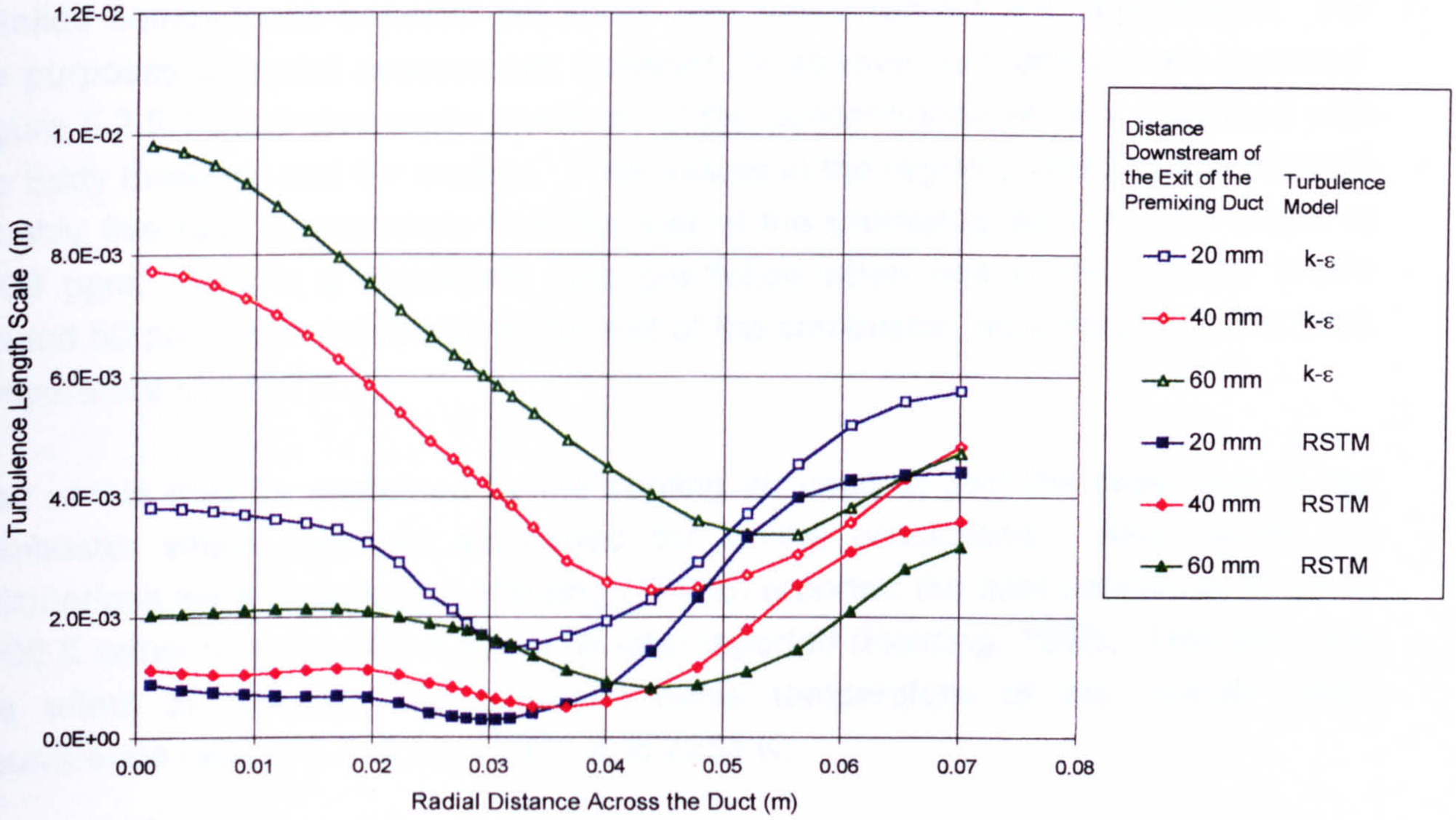

Figure 5.2.4.14 Radial Profiles of the Turbulence Length Scale for the BML Crossing Frequency Combustion Model

One major potential advantage of the second moment turbulence model over the k-ε model is that it should provide a better prediction of the underlying flow field. This cannot be assessed in the absence of a detailed set of measurements of the flow field for this experiment, however. It is interesting to note that the instantaneous LIF images (Figure 5.2.9) show unburnt regions on the axis in a similar fashion to the predictions of the mean reaction progress variable of the second moment closure model (Figure 5.2.4.3). Launder (1989), Hogg *et al* (1989) and Gibson *et al* (1986), based on a comparison of calculations with isothermal experiments in the literature, demonstrate that the second moment closure turbulence model fares better than the k-ε model in strongly swirling flows. The latter model was generally found to produce far too high levels of turbulent diffusion particularly in the radial direction.

5.2.5 NO_x Model

The rate of production of NO_x is a very strong function of temperature. The calculations were performed assuming adiabatic conditions and, as noted earlier, the flame temperature was substantially over-predicted relative to the measurements. Consequently, in the present study the mean concentration of NO_x was also significantly over predicted.

The experiment was poorly defined in respect of energy release and therefore detailed comparisons between prediction and measurement are unprofitable. For the purposes of model assessment, however, illustrative comparisons are reported. Figure 5.2.5.1 illustrates mean contours of the concentration of NO_x predicted with the Eddy Break-up and k-ε models. Peak values in the region plotted, which extends roughly five radii downstream from the exit of the premixing duct, rise to levels of 2500 ppm. This is a significant over prediction when one considers that levels around 50 ppm were measured at the exit of the combustor, accompanying the peak temperature of 1800 K.

Part of this may be explained by the cooling air used to cool the outer wall of the combustor which was not accounted for in the predictions. Also, when the calculations were undertaken, Harding (1996b) reported the inlet conditions to be at 1000 K rather than the 900 K which he later reported (Harding, 1996). This will have the effect of reducing the adiabatic flame temperature at the overall mean equivalence ratio of 0.712 from 2370 K to 2253 K.

An additional case was run with the Eddy Break-up and k-ε models to gauge the effect of reducing the flame temperature on the NO_x produced. The addition of the cooling air reduced the overall equivalence ratio from 0.712 to 0.638 which had the effect of reducing the adiabatic flame temperature from about 2370 K to 2280 K or a difference of about 3.8%. This is a similar order of magnitude to that caused by the difference in inlet temperature.

We recalculated the case with the Eddy Break-up and k-ε models reducing the adiabatic flame temperature by a factor of 3.8%. This had a quite dramatic effect on the concentration of NO_x predicted as is illustrated in Figure 5.2.5.2. Peak levels in the domain plotted dropped from around 2500 ppm to below 900 ppm. This is still an order of magnitude higher than the levels measured at the exit of the combustor, however it demonstrates the extreme sensitivity of the concentration of NO_x at these sorts of flame temperatures.

In general, the exaggerated NO_x predictions can be attributed to poorly specified boundary conditions. The inlet temperature was too high and cooling air was not accounted for. Additionally, radiation heat transfer was also not incorporated. A combination of these three factors may lower the computed flame temperature sufficiently to match the levels measured experimentally and account for the very low NO_x levels reported.

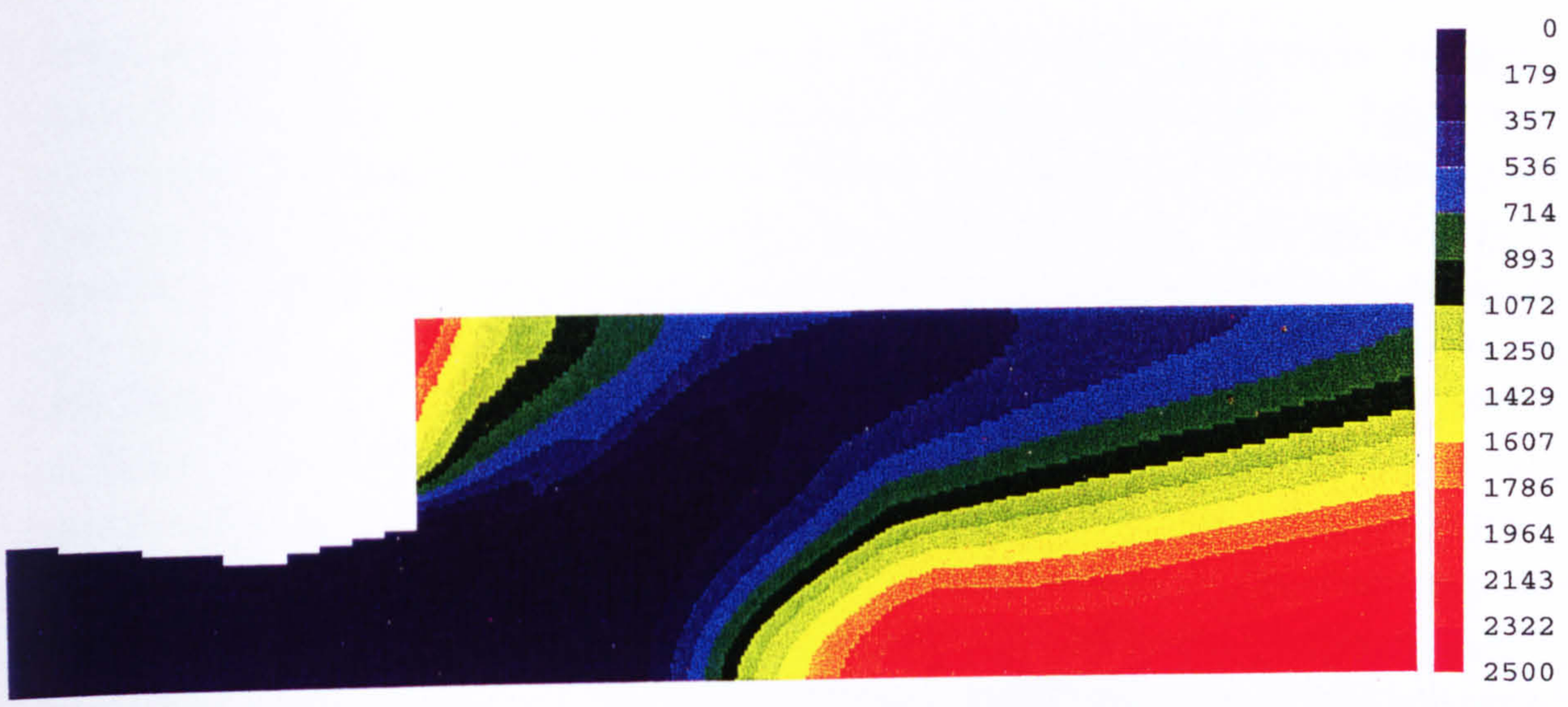

Figure 5.2.5.1 Contours of Mean NOx (ppm) for the Eddy Break-up and k-ε Models

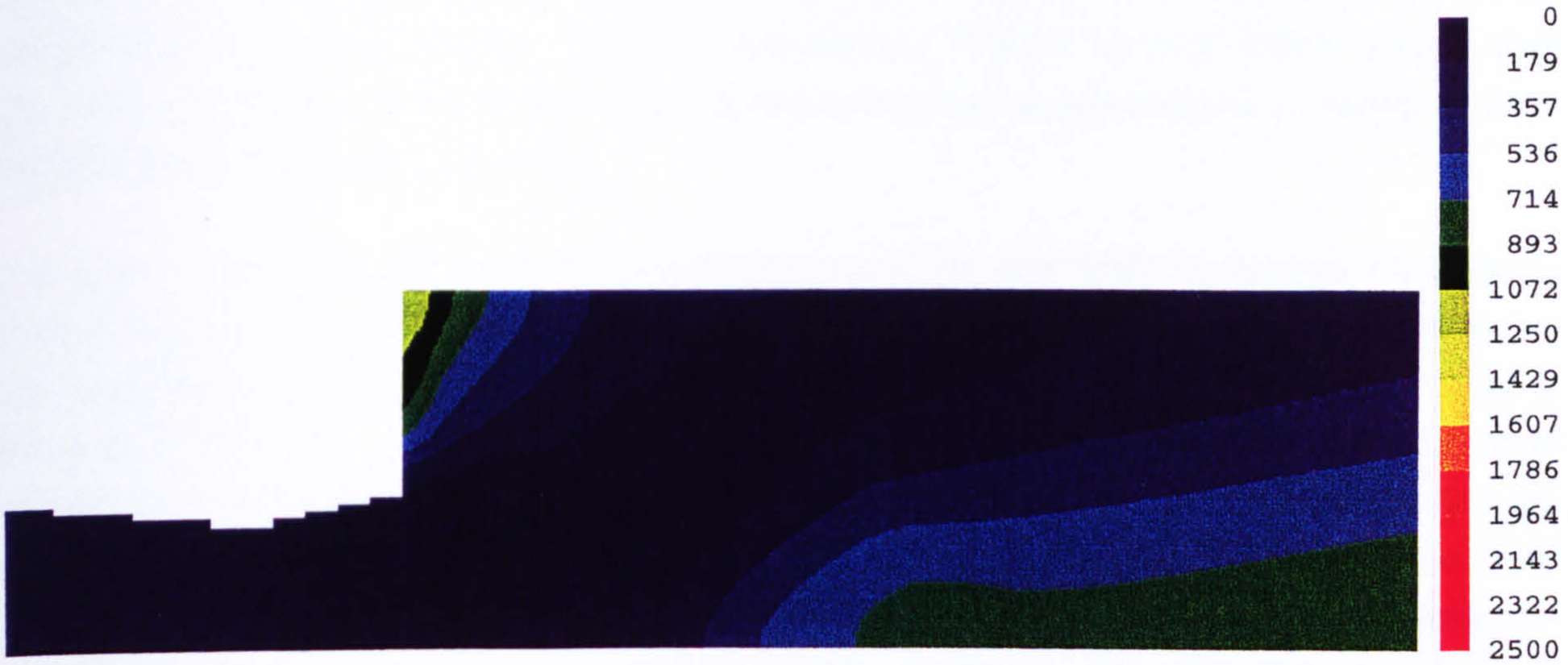

Figure 5.2.5.2 Contours of Mean NOx (ppm) for the Eddy Break-up and k-ε Models with a reduced adiabatic flame temperature

5.3 Discussion

The limited nature of the experimental data from this model LPP combustor has restricted the opportunity for validation of the several models investigated and of their CFD implementation but a number of important insights have emerged from the comparisons possible and simply from the predictions of the alternative models.

With some minor adjustment of parameters all three combustion models gave reasonably good predictions of the heat release distribution. Apart from the presumed pdf model, which, in the absence of a formal "cold" boundary, predicted ignition at the inlet boundary conditions due to the high inlet temperatures, the results from the other models were nearly identical. The additional consideration of strain effects, in the BML crossing frequency model, did not appear to have a significant influence on the shape and location of the flame front. These effects had a much larger influence on the strength of the source term itself, which required some calibration in order to give reasonable values. For the presumed pdf model the flame front shape and position were also very similar to the other two models, except that a small amount of combustion occurred within the premixing duct. This feature of the presumed pdf model makes it a possible simple model to predict self ignition. Thus despite the problems of predicting the flame spreading rate for the backward facing step and bluff-body geometries, these steady state models all worked plausibly for the experimental combustor.

Even though counter gradient diffusion was predicted by the second moment closure turbulence model, this was not a large factor in the prediction of the flame front position under the conditions investigated. The greatest influence of this more comprehensive turbulence model lay in its prediction of the Reynolds stresses, rather than the scalar fluxes. This is indicated by Figure 5.2.4.9, which shows that the chemical source term for the second moment closure predictions is nearly double that predicted with the k-ε model.

The high levels of flame front quenching found for the BML Crossing Frequency model may indicate that the choice of model for the strain rate is not a valid one for this flow field. With around 98% of the flame front quenched the flame front is very close to extinction. One would expect that the flame would be very unstable and might even blow off. This is not evident in the experiment where the lean limit was found at an air to fuel ratio of 40 (Harding, 1996), nearly double that of the test conditions. The adoption of a quenching strain rate based on the burnt-to-unburnt laminar flame experiment or a larger length scale to describe the flame front straining would both reduce the amount of flame front which is quenched.

The NOx model substantially overpredicted the measured levels of NOx within the combustor. This was primarily due to the incomplete specification of boundary

conditions and the assumption of adiabatic flow. However, the NOx predictions can be used to illustrate qualitatively where problem areas exist within the combustor flow field. It is interesting to note that, despite temperatures which are below the mean adiabatic flame temperature, when the influence of the inlet temperature is accounted for, the outer recirculation zone produced higher concentrations of NOx than the vortex breakdown bubble. This can be seen clearly in Figure 5.2.5.2. This stems from the fact that there is a fuel lean layer along the outer wall of the premixing duct. Since the fuel is mixing into this layer from the fuel rich layer next to it the variance of the mixture fraction is high and therefore, although the mean flame temperature is low, the NOx production which is an exponential function of instantaneous temperature is high. Overall, limited NOx is produced here compared to the complete flow, and most of the combustor outlet NOx is generated behind the flame front attached to the vortex breakdown bubble which is larger and has a longer residence time associated with it.

Generally speaking, the combustor generates more NOx than is desired. 50 ppm was measured by Harding (1996) at the exit of the combustor at atmospheric conditions and this design is being investigated for aircraft operation without water injection. Compared to other LPP combustors in the literature the mean equivalence ratio of the experiment is quite high, with a value of around 0.7. In fact, the mean equivalence ratio appears to be around the level where any lack of mixture homogeneity no longer has a large impact on the amount of NOx produced (Figure 2.1.1.2). Thus to reduce the amount of NOx it would be necessary to increase the amount of air through the burner, thereby reducing peak temperatures, by using convective, rather than film cooling, for the combustor liner. Also, it will be necessary to improve the mixture homogeneity across the premixing duct, especially towards the centre of the duct where there is a non-swirling jet of air without any fuel. A richer mixture in the centre of the premixing duct may also help to improve flame stability in relation to the vortex breakdown bubble, allowing for a reduction in the lean extinction limit of the burner.

From the second moment closure predictions of the vortex breakdown bubble, there is a complex pattern of counter rotating recirculations. This flow is not optimal for fuel air mixing, especially towards the centre of the burner as can be seen in Figure 5.3.1, which shows a contour plot of the mean mixture fraction. Essentially, the fuel lean central jet is entrained into the smaller recirculation near the burner axis, whilst the richer flow next to it enters the outer recirculation. Compared to the k-ε turbulence model predictions (Figure 5.2.7), which only identify one recirculation zone within the vortex breakdown bubble, the flow field takes much longer before the fuel is evenly distributed across the duct. This will mean that the variance of the mixture fraction and hence the NOx produced will be higher. This complicated recirculation pattern is probably being produced by the strong non-swirling jet along

the centreline. If the strength of this jet was reduced or eliminated then perhaps a single recirculation pattern might exist and a reduction in NOx might be found to occur.

Figure 5.3.1 Mean Mixture Fraction for the Eddy Break-up and Second Moment Closure Turbulence Models

The manner of fuel injection appears to have an influence on the strength of the vortex breakdown displacing it upstream relative to the case without fuel. This influence comes from two features. Firstly, the fuel is injected with a tangential component increasing the swirl strength of the flow. Secondly, in the case of the predictions, the fuel has a significant displacement effect, forcing the air approaching it to travel radially outwards. This will also have the effect of increasing the tangential velocity of the flow in order to conserve angular momentum. In the experiment, the fuel is a liquid spray injected through discrete holes, however, and so will not have exactly the same effect since air can pass more easily between the fuel sprays. However, some of the air will be entrained in the fuel sprays and momentum exchanged, and so to a certain extent the same effect will be felt. This view is reinforced up by the findings of Harding (1996) that the vortex breakdown bubble was closer to the exit of the premixing duct when the flow was combusting, compared to the case when the flow was not combusting without fuel flowing. Harding (1996) argued that the position of the vortex breakdown was influenced

mainly by the existence of combustion. However, the present calculations show that the position of the vortex breakdown actually shifts further downstream when combustion occurs rather than upstream (see for example Figures 5.1.25 and 5.2.1.1). This is due to the acceleration of the flow in the axial direction as it passes through the flame front which reduces the relative magnitude of the swirl of the flow and hence weakens the vortex breakdown.

5.4 Conclusions

All three models performed well in this LPP configuration. This demonstrates that these time averaged models of varying complexity are useful for flows which do not contain large transient coherent structures, such as that of this experimental combustor and most practical engine combustors designed today.

The Eddy Break-up model, which remains the most popular combustion model in use today, performed well, giving qualitatively plausible results using the same model constants as those applied to the backward facing step exercise. This is a relatively simple model which perhaps requires the most care in ensuring that appropriate constants are used when modelling a new geometry, given that there is little physical basis for the prescribed rate constant. However, the ease of use of this model makes it an attractive choice for design calculations made in conjunction with experiments when the distribution of heat release is reasonably well known and its effect on other aspects of the flow is of greater interest.

The BML crossing frequency model, as implemented here, appears to add little further information for this geometry. The effect of the strain rate in the flow appears to be relatively uniform everywhere. This is caused partly by the very low quenched strain rate which is predicted by the back-to-back laminar flamelet geometry and the very high alternative Kolmogorov length scale based strain rates which were predicted within the flow field. Predictions with a quenched strain rate based on an unburnt-to-burnt laminar flamelet geometry (Figure 5.2.3.13) would show a stronger influence from the strain rate in the flow. This model is still relatively simple and slightly more robust scientifically, compared to the Eddy Break-up model, since it introduces more physical arguments to underpin the rate constant, based on the established concept of burning velocity.

The Presumed pdf model predicted self ignition within the premixing duct due to the exceptionally high inlet air temperatures. Although, the degree of progress made within the premixing duct by the reaction is small, it does influence the initial development of the flame front between the two recirculation zones, cf. Figure 5.2.2.6. The reliability of this aspect of the model is questionable. This behaviour was not detected in the experiment which shows the flame front position much closer

to that predicted by the other two models. Part of this can be explained by the fairly arbitrary factor of 5 which was added to the source term to improve the predictions, in the context of the backward facing step. Clearly this "calibration" factor is too large for this geometry. The remaining discrepancy can be explained by the inlet temperature used for the predictions which was 100 C° higher than that measured in the experiment. On the other hand, it is not unexpected that there should be some reaction occurring within the premixing duct if one considers the spontaneous ignition temperature for propane which is about 766 K (cf. Glassman, 1987). Thus, this model is capturing a facet of the flow, which is missed by the other two. Again, it is more robust technically but, as a result, more complicated, making it less favourable from a routine computational perspective. In the case where the heat release distribution is of primary interest then this model is perhaps the best of the three and would benefit from more detailed experimental comparison.

The high levels of NOx from the burner can be reduced if the mean equivalence ratio is reduced. The fuel needs to be more evenly distributed across the duct, especially towards the central axis of the burner. The central non-swirling air jet should be reduced in strength or eliminated, in order to strengthen the vortex breakdown bubble and to secure a single recirculation. This should improve fuel air mixing and may even improve the stability of the flame by reducing the lean extinction limit.

The second moment closure model, for this geometry, had a stronger influence on the Reynolds stresses and hence the turbulent flow field than on the scalar fluxes. Counter gradient diffusion did not appear to substantially influence the gross flow features.

6 Conclusions

All three of the combustion models, after appropriate tuning, worked well for the LPP test combustor. This illustrates that such time averaged models are useful for flows which do not contain large transient coherent structures, such as that of this experiment and most practical engine combustors designed today. Despite being unable to capture the flame front spreading in the case of the backward facing step, these predictions also provided insight into the performance and implementation of the models.

The Eddy Break-up model, which assumes that the reaction rate is only mixing controlled, produced qualitatively plausible predictions for the LPP test combustor without the need to modify the model constants adopted for the sudden expansion experiment. This is a relatively simple model and requires the most care in ensuring that the appropriate model constants are chosen, given that there is little physical basis for the prescribed rate constant. However ease of use of this model makes it an attractive choice for design calculations made in conjunction with experiments when the distribution of heat release is reasonably well known and its effect on other aspects of the flow is of greater interest.

The BML crossing frequency model, as implemented here, appears to add little additional information for the LPP test combustor. This model accounts for the effects of chemistry through the burning velocity and the influence of flame front straining. The effect of the strain rate in the flow appears to be relatively uniform everywhere. This is caused partly by the very low quenched strain rate which is predicted by the back-to-back laminar flamelet geometry and the very high alternative Kolmogorov length scale based strain rates which were predicted within the flow field. The calculations predict that around 98% of the flame front is quenched up to 60 mm from the exit of the premixing duct. This value is quite high and indicates that the flame is very close to complete extinction. One would expect that the risk of blow off would be very large given these conditions. The experimental measurements of Harding (1996) indicate though that this is not the case. This raises the question over the validity of the basis for the strain rate model. An unburnt-to-burnt laminar flame geometry and a strain rate based on a larger length scale would both reduce the predicted flame front which is quenched. Predictions with a quenched strain rate based on an unburnt-to-burnt laminar flamelet geometry (Figure 5.2.3.13) would show a stronger influence from the strain rate in the flow. The inclusion of chemistry effects through the laminar burning velocity imply that this model is somewhat more robust in terms of varying conditions over the Eddy Break-up model.

The Presumed pdf model, which accounts for finite rate chemistry, offers perhaps the greatest information about the heat release rate of the three models for this configuration. This is because it does not require mixing to occur between the reactants and burnt product for ignition to occur. If the initial temperature is high enough the chemical source term will take on a non-zero value when the reaction progress variable is zero. It is also the slowest of the three models to converge since it required two transport equations and a numerical integration over the chemical source term to describe the heat release. This model tended to over predict the flame front spreading rate partly because of the non-zero reaction rate when c=0, but mainly because of the Arrhenius expression was calibrated in order to achieve a better agreement with the predictions of the backward facing step. A comparison of two presumed pdf functions was carried out for the backward facing step geometry. For these predictions the variance of the reaction progress variable was always found to be very high. Both the simple block pdf of Figure 2.3.3.2.1 and the β function pdf gave very similar shapes (Figure 4.1.2.32). Thus given the added complexity of numerically integrating the β function pdf the choice of the simple block pdf was a good one for this type of flow.

The second moment closure turbulence model produced the greatest difference from the k-ε turbulence model through its prediction of the flow field. Although points in the flow were found to have counter gradient diffusion this was not found to make a large difference in the global features of the flame front.

The NO_x model faired well for the earlier co-flowing flame predictions however seriously over predicted NO_x concentrations within the LPP test combustor. These poor predictions were mainly due to the poor boundary conditions adopted. The LPP test combustor was experimentally found to have relatively high NO_x at its exit. Results from the predictions offer several possible solutions for this. The equivalence ratio for the burner is quite high compared to that reported for practical LPP combustors. This could be improved by using convective cooling rather than film cooling for the combustor liner. All of the cooling air could then be diverted through the premixing duct. Fuel air mixing in the premixing duct also needs to be improved with more fuel added to the near axis region of the burner. Lean stability limits for the combustor could be improved by reducing or eliminating the central non-swirling air jet which would strengthen the vortex breakdown and secure a single recirculation.

7 Future Work

In terms of support for the further development of computational modelling of this sort of flow a more detailed set of experimental data is required from a practical LPP type combustor. Measurements of the velocity, turbulence intensity, mean and variance of the mixture fraction, mean and variance of the reaction progress variable and mean and variance of NO_x concentrations are all needed from within the combustor.

The Presumed pdf model has the ability to self ignite if the temperature and pressure are high enough such that the instantaneous chemical source term is not zero when the reaction progress variable is zero. This aspect of this model should be further investigated to see to what degree it can be used to predict flashback and/or autoignition.

For the BML Crossing Frequency model a further investigation as to the impact of the choice of the definition of the strain rate on the chemical source term should be carried out. Also an investigation into whether or not the parameter $|\sigma_y|$ which represents the mean crossing angle of the flame front to a unit line in space can be related to the turbulence intensity should be carried out. A comparison should also be made with flame sheet based models, where Σ is solved by a transport equation, to see if there is a significant improvement to counteract the increased complexity of these models in the context of a practical framework.

Further development is also required to correctly model the fuel injection. This requires a multiphase approach as the fuel is initially a liquid. This may also require the development of models for fuel droplets attaching to the walls of the burner and the re-atomisation of this liquid. This is particularly important for this type of burner as the fuel is sprayed towards splash plates which are used to prevent fuel from reaching the outer walls of the premixing duct.

As for tool development it would be extremely advantageous to produce or purchase some sort of general curvilinear grid generator for SOFIE as well as the incorporation of the second moment closure turbulence model. This would make SOFIE at least as flexible as PHOENICS and perhaps better given that SOFIE should be able to handle both a body fitted grid and blockages with the second moment closure model. Additionally SOFIE has the advantage of containing several higher order differencing schemes.

Consideration should also be made into looking at a transient computation of the backward facing step geometry. However, given that this work has shown that the flame front in the LPP combustor is not influenced by large scale vortex shedding as exists in the backward facing step geometry perhaps this latter configuration is not very relevant. This flow field is perhaps of more interest to people investigating afterburners or other bluff-body stabilised flames.

8 References

Abd Al-Masseeh, W.A., Bradley, D., Gaskell, P.H., Lau, A.K.C., **Turbulent Premixed, Swirling Combustion: Direct Stress, Strained Flamelet Modelling and Experimental Investigation**, 23rd Symposium (International) on Combustion, The Combustion Institute, pp. 825-833, 1990.

Abdel-Gayed, R.G., Bradley, D., Lung, F.K.-K., **Combustion Regimes and the Straining of Turbulent Premixed Flames**, Combustion and Flame, V. 76, pp. 213-218, 1989.

Abdel-Gayed, R.G., Bradley, D., Lau, A.K.C., **The Straining of Premixed Turbulent Flames**, 22nd Symposium (International) on Combustion, The Combustion Institute, pp. 731-738, 1988.

Abu-Orf, G.M., Cant, R.S., **Reaction Rate Modelling for Premixed Turbulent Methane-Air Flames**, Joint Meeting of the Portuguese, British, Spanish and Swedish Sections of the Combustion Institute, Funchal, Madeira, April 1-4, pp. 12.4.1-12.4.4, 1996.

Agarwal, R.K., **A Third Order Accurate Upwind Scheme for Navier Stokes Solutionsin Three Dimensions**, "Computers in Flow Prediction and Fluid Dynamics Experiments", ASME Winter Meeting, Washington D.C., pp. 73-82, 1981.

Ahmed, S.A., Nejad, A.S., **Premixed, Turbulent Combustion of Axisymmetric Sudden Expansion Flows**, International Journal of Heat and Fluid Flow, V. 13, N. 1, pp. 15-21, 1992.

Aksit, M., **A Stoichastic Model for Aircraft Gas Turbine Combustor Emissions**, Ph.D. Thesis, Cranfield University, 1995.

Al Dabbagh, N.A., Andrews, G.E., **Weak Extinction and Turbulent Burning Velocity for Grid Stabilized Premixed Flames**, Combustion and Flame, V. 55, pp. 31-52, 1984.

Allen, J.D., Combustion and Flame, V. 24, p. 133, 1975.

Alvarez, J., Jones, W.P., Seoud, R., **Prediction of Momentum and Scalar Fields in a Jet Cross-Flow using First and Second Order Turbulence Closures**, AGARD Symposium on Computational and Experimental Assessment of Jets in Cross Flow, Winchester, April 1993.

Anand, M.S., Pope, S.B., Mongia, H.C., **Pressure Algorithm for Elliptic Flow Calculations with the PDF Method**, Computational Fluid Dynamics Symposium on Aeropropulsion, NASA, Cleveland OH, pp. 347-362, 24-26 April 1990.

Anand, M.S., Pope, S.B., Mongia, H.C., **A PDF Method for Turbulent Recirculating Flows**, "Turbulent Reactive Flows: Lecture Notes in Engineering 40", Springer-Verlag, Berlin, pp. 672-693, 1989.

Anand, M.S., Gouldin, F.C., **Combustion Efficiency of a Premixed Continuous Flow Combustor**, Transactions of the ASME: Journal of Engineering for Gas Turbines and Power, V. 107, pp. 695-705, 1985.

Anderson, D.A., Tannehill, J.C., Pletcher, R.H., "Computational Fluid Mechanics and Heat Transfer", Hemisphere Publishing, 1984.

Anderson, D.N., **Emissions of Oxides of Nitrogen from an Experimental Premixed-Hydrogen Burner**, NASA TM X-3393, 1976.

Anderson, D.N., **Effect of Hydrogen Injection on Stability and Emissions of an Experimental, Premixed Prevaporized Propane Burner**, NASA TM X-3301, 1975a.

Anderson, D., **Effects of Equivalence Ratio and Dwell Time on Exhaust Emissions from an Experimental Premixing Prevaporizing Burner**, 20th Annual International Gas Turbine Conference, Houston, March 1975b.

Andrews, G.E., Bradley, D., Lwakabamba, S.B., Combustion and Flame, V. 24, p. 285, 1975.

Argueyrolles, B., Souhaite, P., Gauffie, S., Borghi, R., **Application of a "Presumed p.d.f." Model of Turbulent Combustion to Reciprocating Engines - Part 2**, International Conference on Supercomputer Applications in the Automotive Industry, Zürich, 7-8 October, 1986.

Autret, A., Grandotto, M., Dekeyser, I., **Finite Element Computation of a Turbulent Flow Over a Two-Dimensional Backward-Facing Step**, International Journal of Numerical Methods in Fluids, V. 8, p. 997, 1988.

Badami, G.N., Egerton, A., **The Determination of Burning Velocities of Slow Flames**, Proceedings of the Royal Society of London, Series A. Mathematical and Physical Sciences, V. 228, pp. 297-322, 1955.

Bahr, D.W., **Gas Turbine Engine Emission Abatement-Status and Needed Advancements**, Gas Turbine Combustor Design Problems, Proceedings of the Project Squid Workshop on Gas Turbine Combustion Design Problems, Purdue University, May 31-June 1, 1978.

Bahr, D.W., Gleason, C.C., **Experimental Clean Combustor Program, Phase I Final Report (General Electric Company GE-74AEG380)**, NASA CR-134737, 1975.

Bailly, P., Garréton, D., **On the numerical results of a combustion zone stabilized by a rectangular section cylinder obtained with Hades CFD code**, European Test for Combustion Modelling, 1st ETCM Workshop, Aussois, France, February 5-10, 1995

Ballal, D.R., **Further development of the three-region model of a premixed turbulent flame: I. Turbulent diffusion dominated region 2**, Proceedings of the Royal Society London, V. 368, pp. 267-282, 1979a

Ballal, D.R., **Further development of the three-region model of a premixed turbulent flame: II. Instability dominated region 1**, Proceedings of the Royal Society London, V. 368, pp. 283-293, 1979b

Ballal, D.R., **Further development of the three-region model of a premixed turbulent flame: III. Eddy entrainment, combustion in depth process of region 3**, Proceedings of the Royal Society London, V. 368, pp. 295-304, 1979c

Ballal, D.R., **The structure of a premixed turbulent flame**, Proceedings of the Royal Society London, V. 367, pp. 353-380, 1979d

Ballal, D.R., Lefebvre, A.H., Proceedings of the Royal Society London, V. 217, pp. 344, 1975

Batchelor, G.K., "An Introduction to Fluid Dynamics", Cambridge University Press, Cambridge, 1988.

Baulch, D.L., Drysdale, D.D., Duxburg, J., Grant, S.J., "Evaluated Kinetic Data for High Temperature Reactants", V. 3, Butterworths, London, 1976.

Baulch, D.L., Drysdale, D.D., Horne, D.G., Lloyd, A.C., "Evaluated Kinetic Data for High Temperature Reactants", V. 2, Butterworths, London, 1973.

Benim, A.C., Syed, K.J., **Laminar Flamelet Modelling of Turbulent Premixed Combustion**, to be published private communication, 1997.

Bhatia, R., Sirignano, W.A., **A One-Dimensional Model of Ramjet Combustion Instability**, AIAA-90-0271, 28th Aerospace Sciences Meeting, Reno, January 8-11, 1990.

Borghi, R., **Turbulent Combustion Modelling**, Progress in Energy and Combustion Science, V. 14, pp. 245-292, 1988.

Borghi, R., Argueyrolles, B., Gauffie, S., Souhaite, P., **Application of a "Presumed p.d.f." Model of Turbulent Combustion to Reciprocating Engines**, 21st Symposium (International) on Combustion, The Combustion Institute, 1986.

Borghi, R., in "Recent Advances in the Aerospace Sciences", Plenum Press, New York, 1985.

Borghi, R., Dutoya, D., **On the scales of the fluctuations in turbulent combustion**, 17th Symposium (International) on Combustion, The Combustion Institute, pp. 235-244, 1978.

Borghi, R., Moreau, P., **Turbulent Combustion in a Premixed Flow**, Acta Astronautica, V. 4, pp.321-341, 1977.

Borghi, R., Moreau, P., Bonniot, C., **Theoretical Predictions of a High Velocity, Premixed, Turbulent Flame**, ONERA T.P. n° 1977-66, 1977b.

Borris, J.P., Brook, D.L., **Solution of the Continuity Equation by the Method of Flux Corrected Transport**, Journal of Computational Physics, V. 16, pp. 85-129, 1976.

Borris, J.P., Brook, D.L., **Flux Corrected Transport I: SHASTA, A Fluid Transport Algorithm that Works**, Journal of Computational Physics, V. 11, pp. 38-69, 1973.

Bosque Fernández, M.A., **Effects of Percentage of Blockage and Flameholder Downstream Counterbores on Lean Combustion Limits of Premixed, Prevaporized Propane-Air Mixture**, NASA TP-2227, 1983.

Boudier, P., Henriot, S., Poinsot, T., Baritaud, T., 24th Symposium (International) on Combustion, The Combustion Institute, pp. 503-510, 1992.

Boussinesq, J., **Essai Sur La Théorie Des Eaux Courantes**, Mem. Présentés Acad. Sci., V. 23, p.46, 1877.

Bradley, D., Gaskell, P.H., Gu, X.J., **Application of a Reynolds Stress, Stretched Flamelet, Mathematical Model to Computations of Turbulent Burning Velocities and Comparison with Experiments**, Combustion and Flame, V. 96, pp. 221-248, 1994.

Bradley, D., Gaskell, P.H., Lau, A.K.C., **A Mixedness-Reactedness Flamelet Model for Turbulent Diffusion Flames**, 23rd Symposium (International) on Combustion, The Combustion Institute, pp. 685-692, 1990.

Bradley, D., Lau, A.K.C., **The mathematical modelling of premixed turbulent combustion**, Pure and Applied Chemistry, V. 62, N. 5, pp. 803-814, 1990.

Bray, K.N.C., Champion, M., Libby, P.A., **Extinction of Premixed Flames in Turbulent Counterflowing Streams with Unequal Enthalpies**, Combustion and Flame, V. 107, pp. 53-64, 1996.

Bray, K.N.C., Champion, M., Libby, P.A., **Premixed Flames in Stagnating Turbulence: Part I. The General Formulation for Counterflowing Streams and Gradient Models for Turbulent Transport**, Combustion and Flame, V. 84, pp. 391-410, 1991.

Bray, K.N.C., **Studies of the Turbulent Burning Velocity**, Cambridge University Report CUED/A-THERMO/TR.32, February 1990.

Bray, K.N.C., Champion, M., Libby, P.A., **The Interaction Between Turbulence and Chemistry in Premixed Turbulent Flames**, "Turbulent Reactive Flows (Lecture Notes in Engineering 40)", Springer-Verlag, Heidelberg, pp. 541-563, 1989.

Bray, K.N.C., Libby, P.A., **Passage Times and Flamelet Crossing Frequencies in Premixed Turbulent Combustion**, Combustion Science and Technology, V. 47, pp. 253-274, 1986.

Bray, K.N.C., Libby, P.A., Moss, J.B., **Unified Modeling Approach for Premixed Turbulent Combustion - Part I: General Formulation**, Combustion and Flame, V. 61, pp. 87-102, 1985.

Bray, K.N.C, Libby, P.A., Moss, J.B., **Flamelet Crossing Frequencies and Mean Reaction Rates in Premixed Turbulent Combustion**, Combustion Science and Technology, V. 41, pp. 143-172, 1984a.

Bray, K.N.C., Libby, P.A., Moss, J.B., **Scalar Length Scale Variations in Premixed Turbulent Flames**, 20th Symposium (International) on Combustion, The Combustion Institute, pp. 421-427, 1984b.

Bray, K.N.C., Moss, J.B., Libby, P.A., **Turbulent Transport in Premixed Flames**, "Convective Transport and Instability Phenomena", Braun Verlag, Karlsruhe, pp. 389-423, 1982.

Bray, K.N.C., Libby, P.A., Masuya, G., Moss, J.B., **Turbulence Production in Premixed Turbulent Flames**, Combustion Science and Technology, V. 25, pp. 127-140, 1981.

Bray, K.N.C., Moss, J.B., **A Unified Statistical Model of the Premixed Turbulent Flame**, AASU Report No. 335, University of Southampton, Department of Aeronautics and Astronautics, November, 1974.

Buchheim, R., **Influences on Exhaust Emissions from Automotive Gas Turbines (Volkswagen)**, ASME Paper 78-GT-85, 1978.

Burbank, **Low Emission Combustor Technology Task 5: Selection of Pollution Reduction Methods**, MTU München Technical Report MTUM-B92ET-0038, August 4, 1992.

Candel, S., Veyante, D., Lacas, F., Maistret, E., Darabiha, N., Poinsot, T., in "Recent Advances in Combustion Modeling", World Scientific, Singapore, 1990.

Cant, R.S., Pope, S.B., Bray, K.N.C., **Modelling of Flamelet Surface-to-Volume Ratio in Turbulent Premixed Combustion**, 23rd Symposium (International) on Combustion, The Combustion Institute, pp. 809-815, 1990.

Cant, R.S., Rogg, B., Bray, K.N.C., **On Laminar Flamelet Modelling of the Mean Reaction Rate in a Premixed Turbulent Flame**, Cambridge University Report CUED/A-THERMO/TR25, January 1989.

Cant, R.S., Bray, K.N.C., **Strained Laminar Flamelet Calculations of Premixed Turbulent Combustion in a Closed Vessel**, 22nd Symposium (International) on Combustion, The Combustion Institute, pp. 791-799, 1988.

Cernansky, N.P., AIAA Paper No. 76-139, 14th Aerospace Sciences Meeting, Washington, January, 1976.

Cernansky, N.P., Sawyer, R.F., **NO and NO_2 Formation in a Turbulent Hydrocarbon/Air Diffusion Flame**, 15th Symposium (International) on Combustion, The Combustion Institute, pp. 1039-1050, 1975.

CHAM, private communication, 1998.

Chakravarthy, S.R., Osher, S., **High Resolution Application of the OSHER Upwind Scheme for the Euler Equations**, AIAA Paper No. 83-1943, 1983.

Chapman, M., **FRAM Nonlinear Damping Algorithm for the Continuity Equation**, Journal of Computational Physics, V. 44, pp. 84-103, 1981.

Cheng, W.K., Diringer, J.A., SAE Technical Paper 910268, 1991a.

Cheng, W.K., Lai, M.C., Chue, W.K., 29th Aerospace Sciences Meeting, AIAA 91-0414, 1991b.

Chieng, C. C., Launder, B. E., **On the Calculation of Turbulent Heat Transport Downstream from an abrupt Pipe Expansion**, Numerical Heat Transfer, V. 3, p. 189, 1980.

Choi, C.R., Huh, K.Y., **Development of a Coherent Flamelet Model for a Spark-Ignited Turbulent Premixed Flame in a Closed Vessel**, Combustion and Flame, V. 114, pp. 336-348, 1998.

Chomiak, J., Nisbet, J.R., **Modeling Variable Density Effects in Turbulent Flames - Some Basic Considerations**, Combustion and Flame, V. 102, N. 3, pp. 371-386, 1995.

Coats, C.M., **Comment on "Review of Flashback Reported in Prevaporizing/Premixing Combustors"**, Combustion and Flame, V. 37, pp. 331-333, 1980.

Collin, K.-H., **Brite/Euram Task 4.7: Low Emission Combustor Technology (BMW Rolls-Royce GmbH)**, Technical Report ET-TR 036/92-OU, Oberursel, July 16, 1992.

Cooper, L.P., **Analysis of Effect of Flameholder Characteristics on Lean, Premixed, Partially Vaporized Fuel-Air Mixture Quality and Nitrogen Oxides Emissions**, NASA TP-1842, 1981.

Cooper, L.P., **Effect of Degree of Fuel Vaporization Upon Emissions for a Premixed Partially Vaporized Combustion System**, NASA TP-1582, 1980.

Corr, R.A., Malte, P.C., Marinor, N.M., **Evaluation of NO_x Mechanisms for Lean Premixed Combustion**, Journal of Engineering for Gas Turbines and Power, V. 114, p. 425, 1992.

Correa, S.M., Hu, I.Z., Tolpadi, A.K., **Combustion Technology for Low-Emissions Gas-Turbines: Some Recent Modeling Results**, Journal of Energy Resources Technology, V. 118, pp. 201-208, 1996.

Correa, S.M., **A Direct Comparison of Pair-Exchange and IEM Models in Premixed Combustion**, Combustion and Flame, V. 103, pp. 194-206, 1995.

Correa, S.M., Gulati, A., **Measurements and Modeling of a Bluff Body Stabalized Flame**, Combustion and Flame, V.89, pp. 195-213, 1992.

Correa, S.M., **Lean Premixed Combustion for Gas-Turbines: Review and Required Research (General Electric)**, Fossil Fuel Combustion, PD-V. 33, pp. 1-9, ASME, 1991.

Darabiha, N., Candel, S.M., Giovangigli, V., Smooke, M.D., **Extinction of Strained Premixed Propane-air Flames with Complex Chemistry**, Combustion Science and Technology, V. 60, pp. 267-285, 1988.

Darwish, M.S., Moukalled, F.H., **Normalized Variable and Space Formulation Methodology for High-Resolution Schemes**, Numerical Heat Transfer, Part B, V. 26, pp. 79-96, 1994.

Darwish, M.S., **A New High-Resolution Scheme Based on the Normalized Variable Formulation**, Numerical Heat Transfer, Part B, V. 24, pp. 353-371, 1993.

De Soete, G.G., **Overall Reaction Rates of NO and N_2 Formation From Fuel Nitrogen**, 15th Symposium (International) on Combustion, The Combustion Institute, pp. 1093-1102, 1974.

Dixon-Lewis, G., David, T., Gaskell, P.H., Fukutani, S., Jinno, H., Miller, J.A., Kee, R.J., Smooke, M.D., Peters, N., Effelsberg, E., Warnatz, J., Behrendt, F., **Calculation of the Structure and Extinction Limit of a Methane-Air Counterflow Diffusion Flame in the Forward Stagnation Region of a Porous Cylinder**, 20th Symposium (International) on Combustion, The Combustion Institute, pp. 1893-1904, 1984.

Djavdan, E., Darabiha, N., Giovangigli, V., Candel, S.M., **Strained Propane-Air Flames With Detailed and Reduced Kinetic Schemes**, Combustion Science and Technology, V. 76, pp. 287-309, 1991.

Drake, M.C., Correa, S.M., Pitz, R.W., Shyy, W., Fenimore, C.P., **Superequilibrium and Thermal Nitric Oxide Formation in Turbulent Diffusion Flames**, Combustion and Flame, V. 69, pp. 347-365, 1987.

Duclos, J.M., Veynante, D., Poinsot, T., **A Comparison of Flamelet Models for Premixed Turbulent Combustion**, Combustion and Flame, V. 95, pp. 101-117, 1993.

Duerr, R.A., Lyons, V.J., **Effect of Flameholder Pressure Drop on Emissions and Performance of Premixed-Prevaporized Combustors**, NASA TP-2131, 1983.

Dupont, V., Pourkashanian, M., Williams, A., **Modelling of Process Heaters Fired by Natural Gas**, Journal of the Institute of Energy, pp. 20-28, 1993a.

Dupont, V., Pourkashanian, M., Williams, A., **Prediction of Prompt NOx in Hydrocarbon Air Flames**, private communication, 1993b.

Duterque, J., Avezard, N., Borghi, R., **Further Results on Nitrogen Oxides Production in Combustion Zones**, Combustion Science and Technology, V. 25, pp. 85-95, 1981.

Eaton, J.K., Johnston, J.P., **A Review of Research on Subsonic Turbulent Flow Reattachment**, AIAA Journal, V. 19, N. 9, pp. 1093-1100, 1981.

Egerton, A., Thabet, S.K., **Flame Propagation: The Measurement of Burning Velocities of Slow Flames and the Determination of Limits of Combustion**, Proceedings of the Royal Society of London Series A. Mathematical and Physical Sciences, V. 211, pp. 445-471, 1952.

Eswaran, V., Pope, S.B., **Direct Numerical Simulations of the turbulent mixing of a passive scalar**, Physics of Fluids, V. 31, n. 3, pp. 506-520, 1988.

Favre, A., **Statistical Equations of Turbulent Gases**, Problems of Hydrodynamics and Continuum Mechanics, SIAM, Philadelphia, 1969.

Favre, A., **Equations des gaz turbulents compressibles**, J. Mechanique, V. 4, p. 361, 1965.

Fenimore, C.P., **The Ratio NO_2/NO in Fuel-Lean Flames**, Combustion and Flame, V. 25, pp. 85-90, 1975.

Fenimore, C.P., **Formation of Nitric Oxide in Premixed Hydrocarbon Flames**, 13th Symposium (International) on Combustion, The Combustion Institute, pp. 373-380, 1971.

Fiorentino, A.J., Greene, W., Kim, J.C., Mularz, E.J., **Variable Geometry, Lean, Premixed, Prevaporized Fuel Combustor Conceptual Design Study (Pratt & Whitney Aircraft)**, ASME Paper 80-GT-16, Journal of Engineering for Power, V. 102, pp. 896-902, 1980.

Fromm, E.A., **A Method for Reducing Dispersion in Convective Difference Schemes**, Journal of Computational Physics, V. 3, pp. 176-189, 1968.

Fureby, C., Lundgren, E., Möller, S.I., **Simulations of Bluff Body Stabilized Flames**, First European Test for Combustion Modelling (E.T.C.M.) Workshop, Aussois, France, February 5-10, 1995.

Ganji, A.T., Sawyer, R.F., **Turbulence, Combustion, Pollutant, and Stability Characterization of a Premixed, Step Combustor**, NASA CR-3230, January, 1980.

Gardner, R.M., **Pollution from Aircraft**, "Colloquium on Pollution of land, sea and air: an overview for Engineers", IEE Digest No. 1995/165, pp. 13/1-13/4, 10 October, 1995.

Gaskell, P.H., Lau, A.K.C., **Curvature Compensated Convective Transport: SMART, a New Boundedness Preserving Transport Algorithm**, Int. J. Numer. Meth. Fluids, V. 8, pp. 617-641, 1988.

Giovangigli, V., Smooke, M.D., **Extinction of Strained Premixed Laminar Flames with Complex Chemistry**, Combustion Science and Technology, V. 53, pp. 23-49, 1987a.

Giovangigli, V., Smooke, M.D., **Calculation of Extinction Limits for Premixed Laminar Flames in a Stagnation Point Flow**, Journal of Computational Physics, V. 68, pp. 327-345, 1987b.

Giovannini, A., **Dynamics of Cold and Reacting Flows on Backward Facing Step Geometry**, "Turbulent Reactive Flows: Lecture Notes in Engineering 40", Springer-Verlag, Berlin, pp. 694-714, 1989.

Girimaji, S.S., **Assumed β-pdf Model for Turbulent Mixing: Validation and Extension to Multiple Scalar Mixing**, Combustion Science and Technology, V. 78, pp. 177-196, 1991.

Glassman, I., "Combustion: Second Edition", Academic Press Inc., Toronto, 1987.

Gleason, C.C., Bahr, D.W., **Experimental Clean Combustor Program Phase III Final Report (General Electric Company)**, NASA CR-135384, 1979.

Gleason, C.C., Rogers, D.W., Bahr, D.W., **Experimental Clean Combustor Program, Phase II Final Report (General Electric Company R76AEG422)**, NASA CR-134971, 1976a.

Gleason, C.C., Bahr, D.W., **Experimental Clean Combustor Program Alternate Fuels Addendum Phase II Final Report (General Electric Company)**, NASA CR-134972, 1976b.

Gouldin, F.C., Bray, K.N.C., Chen, J.-Y., **Chemical Closure Model for Fractal Flamelets**, Combustion and Flame, V. 77, pp. 241-259, 1989.

Gouldin, F.C., **A Fractal Description of Flamelets**, "Turbulent Reactive Flows (Lecture Notes in Engineering 40)", Springer-Verlag, Heidelberg, pp. 278-306, 1989.

Gouldin, F.C., **An Application of Fractals to Modeling Premixed Turbulent Flames**, Combustion and Flame, V. 68, pp. 249-266, 1987.

Gordon, S., McBride, B.J., **Computer Program for Calculation of Complex Chemical Equilibrium Compositions, Rocket Performance, Incident and Reflected Shocks, and Chapman-Jouguet Detonations**, NASA SP-273, 1971.

Goyal, A., Ekstedt, E.E., Szaniszlo, A.J., **NASA Advanced Low Emissions Combustor Program (General Electric Company)**, ASME Paper 83-JPGC-GT-10, ASME and IEEE, Joint Power Generation Conference, Indianapolis, Sept. 25-29, 1983.

Grouset, D., Esposito, E., Candel, S., **Model of the Recirculating Flow in a Premixed Combustor**, 7th International Colloquim on Gasdynamics of Explosions and Reactive Systems, Gottingen, August 20-24, 1979.

Gülder, O.L., **Laminar Burning Velocities of Methanol, Isooctane and Isooctane/Methanol Blends**, Combustion Science and Technology, V. 33, pp. 179-192, 1983.

Han, T., Humphrey, J.A.C., Launder, B.E., **A Comparison of Hybrid and Quadratic-Upstream Differencing in High Reynolds Number Elliptic Flows**, Comput. Methods Appl. Mech. Eng., V. 29, pp. 81-95, 1981.

Harding, S.C., **Investigation into Mixing and Combustion in an Optical, Lean, Premixed, Prevaporised Combustor**, Ph.D. Thesis, Cranfield University, 1996.

Harding, S.C., private communication, Cranfield University, 1996b.

Harlow, F.H., Nakayama, P.I., **Transport of Turbulence Energy Decay Rate**, Los Alamos Scientific Laboratory Report LA-3854, 1968.

Hayase, T., Humphrey, J.A.C., Greif, R., **A Consistently Formulated QUICK Scheme for Fast and Stable Convergence Using Finite-volume Iterative Calculation Procedures**, Journal of Computational Physics, V. 98, pp. 108-118, 1992.

Hayhurst, A.N., Vince, I.M., **Nitric Oxide Formation from N_2 in Flames: The Importance of "Prompt" NO**, Progress in Energy and Combustion Science, V. 6, pp. 35-51, 1980.

Haynes, B.S., Wagner, H.G.G., **Soot Formation**, Progress in Energy and Combustion Science, V. 7, n. 4, pp. 229-274, 1981.

Heitor, M.V., Taylor, A.M.K.P., Whitelaw, J.H., **Simultaneous velocity and temperature measurments in a premixed flame**, Experiments in Fluids, V. 3, pp. 323-339, 1985.

Hillemanns, R., Lenze, B., **Determination of Time-Mean Flow and Turbulence Properties within Strongly Swirling Jets and Flames using Laser Doppler Anemometry**, 4th International Symposium on Application of Laser Anemometry to Fluid Mechanics, Lisboa, 1988.

Hirsch, C., "Numerical Computation of Internal and External Flows: Volume 2: Computational Methods for Inviscid and Viscous Flows", John Wiley and Sons, Chichester, 1990.

Hirsch, C., "Numerical Computation of Internal and External Flows: Volume 1: Fundamentals of Numerical Discretization", John Wiley and Sons, Chichester, 1988.

Hopf, E., **Statistical hydromechanics and functional calculus**, Journal of Ration. Mech. Analysis, V. 1, pp. 87-123, 1952.

Hori, M., **Experimental Study of Nitrogen Dioxide Formation in Combustion Systems**, 21st Symposium (International) on Combustion, The Combustion Institute, pp. 1181-1188, 1986.

Howe, N.M., Shipman, C.W., Vranos, A., **Turbulent Mass Transfer and Rates of Combustion in Confined Turbulent Flames**, 9th Symposium (International) on Combustion, The Combustion Institute, pp. 36-47, 1963.

Hsiao, C.C., Oppenheim, A.K., Ghoniem, A.F., Chorin, A.J., **Numerical Simulation of a Turbulent Flame Stabilized Behind a Rearward-Facing Step**, 20th Symposium (International) on Combustion, The Combustion Institute, pp. 495-504, 1984.

Hsu, A.T., Anand, M.S., Razdan, M.K., **Calculation of a Premixed Swirl Combustor using the pdf Method**, ASME 97-GT-334, International Gas Turbine and Aeroengine Congress and Exhibition, Orlando, June 2-5, 1997.

Iljima, T., Takeno, T., **Effects of Temperature and Pressure on Burning Velocity**, Combustion and Flame, V. 65, pp. 35-43, 1986.

Jang, D.S., Jetli, R., Acharya, S., **Comparison of the PISO, SIMPLER and SIMPLEC algorithms for the treatment of the pressure-velocity coupling in steady flow problems**, Numerical Heat Transfer, V. 10, pp. 209-228, 1986.

Janicka, J., Kollmann, W., **A Two-Variables Formalism for the Treatment of Chemical Reactions in Turbulent H_2-Air Diffusion Flames**, 17th Symposium (International) on Combustion, The Combustion Institute, pp. 421-430, 1978.

Janssen, G., Lamers, A., Jansen, J, **A Numerical Parameter Study for a Turbulent Backward Facing Step Problem**, CHAM: The PHOENICS Journal of Computational Fluid Dynamics and Its Applications, V. 6, N. 2, 1993.

Johnson, G.M., Smith, M.Y., Mulcahy, M.R.F., **The Presence of NO_2 in Premixed Flames**, 17th Symposium (International) on Combustion, The Combustion Institute, pp. 647-660, 1979.

Jones, R.E., **Gas Turbine Engine Emissions-Problems Progress and Future**, Progress in Energy and Combustion Science, V. 4, pp. 73-113, 1978.

Jones, W.P., Whitelaw, J.H., **Calculation Methods for Reacting Turbulent Flows: A Review**, Combustion and Flames, V. 48, pp. 1-26, 1982.

Jones, W.P., **Models for Turbulent Flows with Variable Density and Combustion**, Prediction Methods for Turbulent Flows, von Karman Institute for Fluid Dynamics Lecture Series 1979-2, January 15-19, 1979.

Jones, W.P., Pridden, C.H., **Predictions of the Flow Field and Local Gas Composition in Gas Turbine Combustors**, 17th Symposium (International) on Combustion, 1978.

Jones, W.P., Launder, B.E., **The Prediction of Laminarization with a Two-Equation Model of Turbulence**, International Journal of Heat and Mass Transfer, V. 15, pp. 301-314, 1972.

Katsuki, M., Mizutani, Y., Yasuda, T., Kurosawa, Y., Kobayashi, K., Takahashi, T., **Local Fine Flame Structure and its Influence on Mixing Processes in Turbulent Premixed Flames**, Combustion and Flame, V. 82, pp. 93-105, 1990.

Katsuki, M., Mizutani, Y., Yasuda, T., Kurosawa, Y., Kobayashi, K., Takahashi, T., **The Effect of Initial Conditions on the Propagation of a Premixed Flame in a Mixing Layer**, Combustion and Flame, V. 74, pp. 9-18, 1988.

Kee, R.J., Miller, J.A., Evans, G.H., Dixon-Lewis, G., **A Computational Model of the Structure and Extinction of Strained, Opposed Flow, Premixed Methane-Air Flames**, 22nd Symposium (International) on Combustion, The Combustion Institute, pp. 1479-1494, 1988.

Kerstein, A.R., Ashurst, W., Williams, F.A., **Field equation for interface propagation in an unsteady homogeneous flow field**, Physical Review A, V. 37, pp. 2728-2731, 1988.

Kido, H., Huang, S., Nakashima, K., **A Premixed Turbulent Flame Structure Model Having Reactant Islands and Fractal Flame Surfaces**, JSME Paper No. 90-0627A, JSME International Journal, Series II, V. 34, N. 4, pp. 509-519, 1991.

Kilham, J.K., Kirmani, N., **The Effect of Turbulence on Premixed Flame Noise**, 17th Symposium (International) on Combustion, The Combustion Institute, pp. 327-336, 1978.

Konnov, A.A., **Detailed reaction mechanism for small hydrocarbons combustion. Release 0.3**, http://homepages.vub.ac.be/~akonnov/, 1997.

Kovsznay, K.S.G., Jet Propul., V. 24, p. 482, 1956.

Kuo, K.K., "Principles of Combustion", John Wiley and Sons, Chichester, 1986.

Kwon, S., Tseng, L.-K., Faeth, G.M., **Laminar Burning Velocities and Transition to Unstable Flames in $H_2/O_2/N_2$ and $C_3H_8/O_2/N_2$ Mixtures**, Combustion and Flame, V. 90, pp.230-246, 1992.

Lai, M.C., Chue, T.H., Cheng, W.K., Spring Meeting Technical Program, The Combustion Institute, 1991.

Lasher, W.C., Taulbee, D.B., **On the computation of turbulent backstep flow**, International Journal of Heat and Fluid Flow, V. 13, N. 1, pp. 30-40, 1992.

Launder, B.E., **Second-moment closure: present ... and future?**, International Journal of Heat and Fluid Flow, V. 10, N. 4, pp. 282-300, 1989.

Launder, B.E., Reece, G.J., Rodi, W., **Progress in the development of a Reynolds-stress turbulence closure**, Journal of Fluid Mechanics, V. 68, N. 3, pp. 537-566, 1975.

Launder, B.E., **On the effects of a gravitational field on the turbulent transport of heat and momentum**, Journal of Fluid Mechanics, V. 67, N. 3, pp. 569-581, 1975.

Launder, B.E., Spalding, D.B., **The Numerical Computation of Turbulent Flows**, Comput. Methods Appl. Mech. Eng., V. 3, pp. 269-289, 1974.

Launder, B.E., Spalding, D.B., "Lectures in Mathematical Models of Turbulence", Academic Press, London, 1972.

Laurendeau, N.M., **Fast Nitrogen Dioxide Reactions: Significance during NO Decomposition and NO_2 Formation**, Combustion Science and Technology, V. 11, pp. 89-96, 1975.

Lavoie, G.A., Heywood, J.B., Keck, J.C., **Experimental and Theoretical Study of Nitric Oxide Formation in Internal Combustion Engines**, Combustion Science and Technology, V. 1, pp. 313-326, 1970.

Law, C.K., **Dynamics of Stretched Flames**, 22nd Symposium (International) on Combustion, pp. 1381-1402, 1988.

Law, C.K., Zhu, D.L., Yu, G., **Propagation and Extinction of Stretched Premixed Flames**, 21st Symposium (International) on Combustion, pp. 1419-1426, 1986.

Lefebvre, A.H., "Gas Turbine Combustion", McGraw-Hill Book Company, London, 1983.

Lefebvre, A.H., **Lean Premixed/Prevaporized Combustion**, NASA CP-2016, 1977.

Lefebvre, A.H., **Pollution Control in Continuous Combustion Engines**, 15th Symposium (International) on Combustion, The Combustion Institute, pp. 1169-1180, 1974.

Leonard, B.P., **Simple High-Accuracy Resolution Program for Convective Modelling of Discontinuities**, Int. J. Numer. Meth. Eng., V. 8, pp. 1291-1318, 1988.

Leonard, B.P., **A Survey of Finite Differences with Upwinding for Numerical Modelling of the Incompressible Convection Diffusion Equation**, "Computational Techniques in Transient and Turbulent Flow", Pineridge Press, Swansea, V. 2, pp. 1-35, 1981.

Leonard, B.P., **A Stable and Accurate Convective Modelling Procedure on Quadratic Upstream Interpolation**, Comput. Methods Appl. Mech. Eng., V. 19, pp. 59-98, 1979.

Leung, S.W., Strand, M., Sawyer, R.F., Koshland, C.P., **The Formation and Destruction of Nitrogen Dioxide**, Proc. Joint Conf. Western States Jap. Sect. Combust. Inst., pp. 11-13, 1987.

Lewis, K.J., Moss, J.B., **Time-Resolved Scalar Measurements in a Confined Turbulent Premixed Flame**, 17th Symposium (International) on Combustion, The Combustion Institute, pp. 267-277, 1978.

Libby, P.A., **Theory of Normal Premixed Turbulent Flames Revisited**, Progress in Energy and Combustion Science, V. 11, pp. 83-96, 1985.

Libby, P.A., Bray, K.N.C., **Countergradient Diffusion in Premixed Turbulent Flames**, AIAA Journal, V. 19, N. 2, pp. 205-213, 1981.

Libby, P.A., **A Non-Gradient Theory for Premixed Turbulent Flames**, "Mechanics Today", V. 5, pp. 215-232, Pergamon Press, Oxford, 1980.

Libby, P.A., Bray, K.N.C., **Implications of the Laminar Flamelet Model in Premixed Turbulent Combustion**, Combustion and Flame, V. 39, pp. 33-41, 1980.

Libby, P.A., Bray, K.N.C., Moss, J.B., **Effects of Finite Reaction Rate and Molecular Transport in Premixed Turbulent Combustion**, Combustion and Flame, V. 34, pp. 285-301, 1979.

Lin, H., Chieng, C.C., **Characteristic-Based Flux Limiters of an Essentially Third-Order Flux-Splitting Method for Hyperbolic Conservation Laws**, Int. J. Numer. Meth. Fluids, V. 13, pp. 287-307, 1991.

Lindstedt, Vaos, First European Test for Combustion Modelling (E.T.C.M.) Workshop, Aussois, France, February 5-10, 1995.

Lockwood, F.C., Naguib, A.S., **The Prediction of the Fluctuations in the Porperties of Free Round-Jet, Turbulent, Diffusion Flames**, Combustion and Flame, V. 24, pp. 109-124, 1975.

Lundgren, T.S., **Model equation for nonhomogeneous turbulence**, Phys. Fluids, V. 12, n. 3, pp. 485-499, 1969.

Lutz, A.E., Kee, R.J., Miller, J.A., **SENKIN: A Fortran Program for Predicting Homogeneous Gas Phase Chemical Kinetics with Sensitivity Analysis**, SAND87-8248, 1996.

Lyons, V.J., **Effect of Fuel-Air-Ratio Nonuniformity on Emissions of Nitrogen Oxides**, NASA TP-1798, 1981.

Magnussen, B.F., Hjertager, B.H., **On Mathematical Modeling of Turbulent Combustion with Special Emphasis on Soot Formation and Combustion**, 16th Symposium (International) on Combustion, The Combustion Institute, pp.719-729, 1976.

Maistret, E., Darabiha, E., Poinsot, T., Veyante, D., Lacas, F., Candel, S., Esposito, E., 3rd International Conference on Numerical Combustion, pp. 177-188, 1989.

Malin, M.R., Younis, B.A., **Calculation of turbulent buoyant plumes with a Reynolds stress and heat flux transport closure**, International Journal of Heat and Mass Transfer, V. 33, N. 10, pp. 2247-2264, 1990.

Malte, P.C., Pratt, D.T., **The Role of Energy-Releasing Kinetics in NO_x Formation: Fuel-Lean, Jet Stirred CO-Air Combustion**, Combustion Science and Technology, V. 9, pp. 221-231, 1974.

Mantel, T., Borghi, R., **A New Model of Premixed Wrinkled Flame Propagation Based on a Scalar Dissipation Equation**, Combustion and Flame, V. 96, pp. 443-457, 1994.

Mantel, T., Borghi, R., 13th ICDERS, p. 167, 1991.

Marble, F.E., Broadwell, J.E., Report No. TRW-9-PU, 1977.

Marek, C.J., Papathakos, L.C., Verbulecz, P.W., **Preliminary Studies of Autoignition and Flashback in a Premixing-Prevaporizing Flame Tube Using Jet-A Fuel at Lean Equivalence Ratios**, NASA TM X-3526, 1977.

Marek, C.J., Papathakos, L.C., **Exhaust Emissions from a Premixing, Prevaporizing Flame Tube using Liquid Jet A Fuel**, NASA TM X-3383, 1976.

Mårtensson, H., Eriksson, L.-E., Albråten, P.J., **Numerical Simulations of Unsteady Wakeflow**, 10th International Symposium on Air Breathing Engines, Nottingham, UK, pp. 983-992, September 1991.

Mason, H.B., Spalding, D.B., **Prediction of Reaction-Rates in Turbulent Premixed Boundary-Layer Flows**, Combustion Institute European Symposium 1973, University of Sheffield, September 16-21, 1973.

McLean, W.J., 17th Symposium (International) on Combustion, The Combustion Institute, pp. 659-660, 1979.

Merryman, E.L., Levy, A., **Nitrogen Oxide Formation in Flames: The Roles of NO_2 and Fuel Nitrogen**, 15th Symposium (International) on Combustion, The Combustion Institute, pp. 1073-1083, 1975.

Metghalchi, M., Keck, J.C., **Laminar Burning Velocity of Propane-Air Mixtures at High Temperatures and Pressure**, Combustion and Flame, V. 38, pp. 143-154, 1980.

Miller, J.A., Bowman, C.T., **Mechanism and Modeling of Nitrogen Chemistry in Combustion**, Progress in Energy and Combustion Science, V. 15, pp. 287-338, 1989.

Moreau, P., Borghi, R., **Experimental and Theoretical Studies of Nitrogen Oxides Production in a Turbulent Premixed Flame**, ONERA T.P. n° 1980-1, 1980.

Moreau, P., **Turbulent Flame Development in a High Velocity Premixed Flow**, ONERA T.P. n° 1977-5, 1977.

Moreau, P., Boutier, A., **Laser Velocimeter Measurements in a Turbulent Flame,** ONERA T.P. n° 1976-126, 1976.

Moreau, P., **Inflammation et Développement de la Combustion Turbulente dans un Mélange Homogène Air-Méthane**, ONERA T.P. n° 1388, 1974.

Mosier, S.A., Roberts, R., **Low-Power Turbopropulsion Combustor Exhaust Emissions: Volume III Analysis (Pratt & Whitney Aircraft)**, AFAPL-TR-73-36-VOL-3, Air Force Aero Propulsion Laboratory, 1974a.

Mosier, S.A., Roberts, R., **Low-Power Turbopropulsion Combustor Exhaust Emissions: Volume II Demonstration and Total Emission Analysis and Prediction (Pratt & Whitney Aircraft)**, AFAPL-TR-73-36-VOL-2, Air Force Aero Propulsion Laboratory, 1974b.

Mosier, S.A., Roberts, R., **Low-Power Turbopropulsion Combustor Exhaust Emissions: Volume I Theoretical Formulation and Design Assessment (Pratt & Whitney Aircraft)**, AFAPL-TR-73-36-VOL-1, Air Force Aero Propulsion Laboratory, 1973.

Moss, J.B., **Simultaneous Measurements of Concentration and Velocity in an Open Premixed Turbulent Flame**, Combustion Science and Technology, V. 22, pp. 119-129,1980.

Moss, J.B., Bray, K.N.C., **A Statistical Model of NO Formation in Pre-Mixed Turbulent Flames**, Deuxieme Symposium Europeen sur la Combustion, The Combustion Institute, Orléans, France, pp. 315-320, 1-5 September, 1975.

Mularz, E.J., **Lean, Premixed, Prevaporized Combustion for Aircraft Gas Turbine Engines**, NASA TM-79148, 1979.

Mularz, E.J., Gleason, C.C., Dodds, W.J., **Combustor Concepts for Aircraft Gas Turbine Low-Power Emissions Reduction**, Journal of Energy, V. 3, N. 1, pp. 55-61, 1979.

Nagey, T.F., Mykolenko, P., Naylor, M.E., Verkamp, F.J., **The Low Emission Gas Turbine Car - What Does the Future Hold?**, ASME Paper 73-GT-49, 1973.

Négishi, N., **Lean Premixture Combustion on a Coaxial Burner**, 19th Symposium (International) on Combustion, The Combustion Institute, pp. 441-447, 1982.

Nein, A.G., Mellor, A.M., **Flashback in Prevaporizing/Premixing Combustion Systems**, ASME 83-GT-94, 28th ASME International Gas Turbine Conference and Exhibit, Phoenix, March 27-31, 1983.

Nisbet, J.R., Chomiak, J., **Modeling of Flame Generated Turbulence and Buoyant Scalar Fluxes in High Speed Turbulent Premixed Flames**, private communication, 1994.

Nisbet, J.R., Chomiak, J., **Modeling of Flame-Generated Turbulence and Buoyant Scalar Fluxes in Diffusion Flames Subject to Pressure Gradients**, 9th Symposium on Turbulent Shear Flows, V. 3, pp. 25:5:1-25:5:6, 1993a.

Nisbet, J.R., Chomiak, J., **Non-Equilibrium Effects in Non-Premixed High Intensity Turbulent Flames with Radiation**, 5th (International) Symposium on Refined Flow Modeling and Turbulence Measurments, 1993b.

Nisbet, J., Davidson, L., Olsson, E., **Analysis of Two Fast-Chemsitry Combustion Models and Turbulence Modeling in Variable Density Flow**, Computational Fluid Dynamics '92, V. 1, 1992.

O'Brien, E.E., **The probability density function approach to reacting turbulent flows**, "Turbulent Reacting Flows: Topics in Applied Physics 44", Springer-Verlag, Heidelberg, pp. 184-207, 1980.

Odgers, J., Halpin, J., Kretschmer, D., **Prediction of the Lower Limits of Combustion of Premixed Gases**, International Chemical Engineering, V. 29, N. 1, pp. 48-56, 1989.

Odgers, J., Kretschmer, D., Halpin, J., **Weak Limits of Premixed Gases**, Transactions of the ASME: Journal of Engineering for Gas Turbines and Power, V. 107, pp. 11-17, 1985.

Olovsson, S., **Combustion Calculations on a Premixed System with a Bluff Body Flameholder**, AIAA 92-3470, 1992.

Osher, S., **Riemann Solvers, the Entropy Condition and Difference Approximations**, SIAM J. Numer. Anals., V. 21, pp. 217-235, 1984.

Osher, S., Chakravarthy, S., **High Resolution Schemes and the Entropy Condition**, SIAM J. Numer. Anals., V. 21, pp. 955-984, 1984.

Parker, L.J., Sawyer, R.F., Ganji, A.R., **Measurement of Vortex Frequencies in a Lean, Premixed Precaporized Combustor**, Combustion Science and Technology, V. 20, pp. 235-241, 1979.

Peric, M., **A Finite Volume Method for the Prediction of Three Dimensional Fluid Flow in Complex Ducts**, Ph.D. Thesis, Imperial College, London, 1985.

Peters, N., **Fifteen Lectures on Laminar and Turbulent Combustion**, RWTH Aachen, Ercoftac Summer School, September 14-28, 1992.

Peters, N., **The Premixed Turbulent Flame in the Limit of a Large Activation Energy**, Journal of Non-Equilibrium Thermodynamics, V. 7, pp.25-38, 1982.

Philipp, M., Hoffmann, S., Habisreuther, P., Lenze, B., Eickhoff, H., **Experimental and Numerical Study concerning Stabilzation of Strongly Swirling Premixed and Nonpremixed Flames**, 24th Symposium (International) on Combustion, The Combustion Institute, pp. 361-368, 1992.

Picart, A., Borghi, R., Chollet, J.P., **Numerical Simulation of Turbulent Reactive Flows**, Computers and Fluids, V. 16, N. 4, pp. 475-484, 1988.

Pitz, R.W., Daily, J.W., **Combustion in a Turbulent Mixing Layer Formed at a Rearward-Facing Step**, AIAA Journal, V. 21, N. 11, pp. 1565-1570, 1983.

Pitz, R.W., Daily, J.W., **An Experimental Study of Combustion: The Turbulent Structure of a Reacting Shear Layer Formed at a Rearward-Facing Step**, NASA CR-165427, August, 1981.

Plee, S.L., Mellor, A.M., **Reply to Comments by C.M. Coats on "Review of Flashback Reported in Prevaporizing/Premixing Combustors"**, Combustion and Flame, V. 37, pp. 335-336, 1980.

Plee, S.L., Mellor, A.M., **Flame Stabilization in Simplified Prevaporizing, Partially Vaporizing, and Conventional Gas Turbine Combustors**, Journal of Energy, V. 2, N. 5, pp. 346-353, 1978a.

Plee, S.L., Mellor, A.M., **Review of Flashback Reported in Prevaporizing/Premixing Combustors**, Combustion and Flame, V. 32, pp. 193-203, 1978b.

Polifke, W., Döbbeling, K., Sattelmayer, T., Nicol, D.G., Malte, P.C., **A NO_x Prediction Scheme for Lean-Premixed Gas Turbine Combustion Based on Detailed Chemical Kinetics**, Journal for Gas Turbines and Power, V. 118, pp. 765-772, 1996.

Polifke, W., Döbbeling, K., Sattelmayer, T., **A Computational Model for Lean-Premixed, Highly Turbulent Combustion**, CIMAC 21st International Congress on Combustion Engines, Interlaken, 1995.

Pollard, A., Siu, A.L.W., **The Calculation of Some Laminar Flows Using Various Discretization Schemes**, Comput. Methods Appl. Mech. Eng., V. 35, pp. 293-313, 1982.

Pope, S.B., International Journal of Engineering Science, V. 26, p. 445, 1988.

Pope, S.B., **PDF Methods for Turbulent Reactive Flows**, Progress in Energy and Combustion Science, V. 11, pp. 119-192, 1985.

Pope, S.B., **Transport equations for the joint probability density function of velocity and scalars in turbulent flow**, Physics of Fluids, V. 24, N. 4, pp. 588-596, 1981a.

Pope, S.B., **A Monte Carlo Method for the PDF Equations of Turbulent Reactive Flow**, Combustion Science and Technology, V. 25, pp. 159-174, 1981b.

Pope, S.B., **The statistical theory of turbulent flames**, Phil. Transactions of the Royal Society London, V. A291, pp. 529-568, 1979.

Price, T., Probert, D., **Environmental Impacts of Air Traffic**, Applied Energy, V. 50, N. 2, pp. 133-162, 1995.

Proctor II, C.L., Mellor, A.M., **Numerical Examination of a Tube- and Disk-Type Combustor Configuration**, AIAA Journal, V. 25, N. 5, pp. 762-765, 1987a.

Proctor II, C.L., Mellor, A.M., **Experimental Examination of a Prevaporized Premixed Combustor**, AIAA Journal, V. 25, N. 4, pp. 573-577, 1987b.

Proctor, M.P., Anderson, D.N., T'ien, J.S., **Flame Flashback in a Premixed Dump Combustor**, AIAA-85-0145, AIAA 23rd Aerospace Sciences Meeting, Reno, January 14-17, 1985.

Pronchick, S.W., Kline, S.J., **An Experimental Investigation of the Structure of Turbulent Reattaching Flow Behind a Backward-Facing Step**, Report MD-42, Stanford University, Stanford, California, 1983.

Raju, M.S., Sirignano, W.A., **Multicomponent Spray Computations in a Modified Centrebody Combustor**, AIAA-88-0638, AIAA 26th Aerospace Sciences Meeting, Reno, January 11-14, 1988.

Roberts, R., Fiorentino, A., Greene, W., **Experimental Clean Combustor Program Phase III (Pratt & Whitney Aircraft PWA-5493)**, NASA CR-135253, 1977.

Roberts, R., Peduzzi, A., Vitti, G.E., **Experimental Clean Combustor Program Phase II (Pratt & Whitney Aircraft PWA-5370)**, NASA CR-134970, 1976.

Roffe, G., Venkataramani, K.S., **Experimental Study of the Effect of Cycle Pressure on Lean Combustion Emissions**, NASA CR-3032, 1978.

Roffe, G., Ferri, A., **Effect of Premixing Quality on Oxides of Nitrogen in Gas Turbine Combustors**, NASA CR-2657, 1976.

Roffe, G., **Effect of Inlet Temperature and Pressure on Emissions from a Premixing Gas Turbine Primary Zone Combustor**, NASA CR-2740, 1976.

Roffe, G., Ferri, A., **Prevaporization and Premixing to Obtain Low Oxides of Nitrogen in Gas Turbine Combustors**, NASA CR-2495, 1975.

Rogg, B., **Response and Flamelet Structure of Stretched Premixed Methane-Air Flames**, Combustion and Flame, V. 73, pp. 45-65, 1988.

Rogg, B., Behrendt, F., Warnatz, J., **Turbulent Non-Premixed Combustion in Partially Premixed Diffusion Flamelets with Detailed Chemistry**, 21st Symposium (International) on Combustion, The Combustion Institute, pp. 1533-1541, 1986.

Ross, P.T., Williams, J.R., Anderson, D.N., **Combustor Development for Automotive Gas Turbines (Detroit Diesel Allison)**, Journal of Energy, V. 7, N. 5, pp. 429-435, 1983.

Rubini, P., private communication, 1993.

Sano, T., **NO_2 Formation in the Mixing Region of Hot Burned Gas with Cool Air - Effect of Surrounding Air**, Combustion Science and Technology, V. 43, pp. 259-269, 1985.

Sano, T., **NO_2 Formation in the Mixing Region of Hot Burned Gas with Cool Air**, Combustion Science and Technology, V. 38, pp. 129-144, 1984.

Sano, T., **NO_2 Formation in Laminar Flames**, Combustion Science and Technology, V. 29, pp. 261-275, 1982.

Sasaki, M., Kumakura, H., Suzuki, D., **Low NO_x Combustor for Automotive Ceramic Gas Turbine - Conceptual Design (Nissan Motor Co.)**, ASME Paper 91-GT-369, International Gas Turbine and Aeroengine Congress and Exposition, Orlando, June 3-6, 1991.

Sattelmayer, T., Felchlin, M.P., Haumann, J., Hellat, J., Styner, D., **Second-Generation Low-Emission Combustor for ABB Gas Turbines: Burner Development and Tests at Atmospheric Pressure**, ASME Paper 90-GT-162, Journal of Engineering for Gas Turbines and Power, V. 114, pp. 118-125, 1992.

Schefer, R.W., Sawyer, R.F., **Lean Premixed Recirculating Flow Combustion for Control of Oxides of Nitrogen**, 16th Symposium (International) on Combustion, The Combustion Institute, pp. 119-134, 1977.

Scholte, T.G., Vaags, P.B., **The Burning Velocity of Hydrogen-Air Mixtures and Mixtures of Some Hydrocarbons with Air**, Combustion and Flame, V. 3, pp. 495-501, 1959.

Shah, P., Glynn, D.R., Malin, M.R., **Use of a Flame Front Model for Numerical Prediction of Combustion in a Spark-Ignition Engine**, The PHOENICS Journal of Computational Fluid Dynamics and Its Applications, V. 3, N. 3, 1990.

Sharifi, M., Stokes, M., Foss, D., **Roles of CFD and Testing in Developing Ultra Low NOx Combustors**, ASME Paper 95-CTP-17, 1995.

Shepherd, I.G., Moss, J.B., Bray, K.N.C., **Turbulent Transport in a Confined Premixed Flame**, 19th Symposium (International) on Combustion, The Combustion Institute, pp. 423-431, 1982.

Shepherd, I.G., Moss, J.B., **Measurements of Conditioned Velocities in a Turbulent Premixed Flame**, AIAA 81-0181, AIAA 19th Aerospace Sciences Meeting, St. Louis, 12-15 January, 1981.

Sjunnesson, A., Nelsson, C., Max, E., **LDA Measurements of Velocities and Turbulence in a Bluff Body Stabilized Flame**, 4th International Conference on Laser Anemometry - Advances and Applications, ASME, Cleveland, August 1991a.

Sjunnesson, A., Olovsson, S., Sjöblom, B., **Validation Rig - A Tool for Flame Studies**, 10th International Symposium on Air Breathing Engines, Nottingham, UK, pp. 385-393, September 1991b.

Smith, K.O., Angello, L.C., Kurzynske, F.R., **Preliminary Development of an Ultra-Low NO_x Gas Turbine Combustor**, Proceedings of the 1986 International Gas Research Conference, Toronto, pp. 1031-1043, September 8-11, 1987.

Sotheran, A., Pearce, D.E., Overton, D.L., **Some Practical Aspects of Staged Premixed, Low Emissions Combustion (Rolls-Royce, Bristol)**, ASME Paper 84-GT-88, Journal of Engineering for Gas Turbines and Power, V. 107, N. 1, pp. 2-9, 1985.

Spalding, D.B., **A General Purpose Computer Program for Multi-Dimensional One- and Two-Phase Flow**, Mathematics and Computers in Simulation, V. 23, pp. 267-276, 1981.

Spalding, D.B., **Mathematical modelling of Fluid-Mechanics, Heat Transfer and Chemical-Reaction processes: a lecture course**, Imperial College CFDU Report HTS/80/1, 1980.

Spalding, D.B., **A Novel Finite-difference Formulation for Differential Expressions Involving Both First and Second Derivatives**, International Journal of Numerical Methods for Engineering, V. 4, p. 551, 1972.

Stahl, G. Warnatz, J., Rogg, B., **Simulation of Stretched Premixed CH_4 - Air and C_3H_8 - Air Flames with Detailed Chemistry**, CUED/A-THERMO/TR20, Cambridge University, January, 1988.

Stull, F.D., Craig, R.R., Hajnacki, J.T., **Dump Combustor Parametric Investigations**, Fluid Mechanics of Combustion, ASME, pp. 135-154, 1974.

Stwalley, R.M., Lefebvre, A.H., **Characteristics of Dune-Shape Flameholders**, AIAA-87-2106, AIAA/SAE/ASME/ASEE 23rd Joint Propulsion Conference, San Diego, June 29-July 2, 1987a.

Stwalley, R.M., Lefebvre, A.H., **Flame Stabilization Using Large Flameholders of Irregular Shape**, AIAA-87-0469, AIAA 25th Aerospace Sciences Meeting, Reno, January 12-15, 1987b.

Syed, S.A., Chiappetta, L.M., Gosman, A.D., **Error Reduction Program: Final Report**, NASA-CR-174776, 1985.

Thomas, L.H., **Elliptic Problems in Linear Difference Equations over a Network**, Watson Sci. Computer Laboratory Report, Columbia University, New York, 1949.

Tien, J.H., Matalon, M., **On the Burning Velocity of Stretched Flames**, Combustion and Flame, V. 84, pp. 238-248, 1991.

Tolpadi, A.K., Correa, S.M., Burrus, D.L., Mongia, H.C., **Monte Carlo probability density function method for gas turbine combustor flowfield predictions**, Journal of Propulsion and Power, V. 13, N. 2, pp. 218-225, 1997.

Tolpadi, A.K., Hu, I.Z., Correa, S.M., Burrus, D.L., **Coupled Lagrangian Monte Carlo pdf-CFD Computation of Gas Turbine Combustor Flowfields with Finite-Rate Chemistry**, ASME Paper 96-GT-205, 1996.

Tseng, L.-K., Ismail, M.,A., Faeth, G.M., **Laminar Burning Velocities and Markstein Numbers of Hydrocarbon/Air Flames**, Combustion and Flame, V. 95, pp. 410-426, 1993.

Turan, A., Van Doormaal, J.P., **Improved Numerical Methods for Turbulent Viscous Recirculating Flows**, NASA-CR-180852, 1988.

Van Leer, B., **Towards the Ultimate Conservative Difference Scheme V. A Second Order Sequel to Gadunov's Method**, Journal of Computational Physics, V. 23, pp. 101-136, 1977.

Van Leer, B., **Towards the Ultimate Conservative Difference Scheme II. Monotonicity and Conservation Combined in a Second-order Scheme**, Journal of Computational Physics, V. 14, pp. 361-370, 1974.

Van Leer, B., **Towards the Ultimate Conservative Difference Scheme I. The Quest of Monotonicity**, "Lecture Notes in Physics", Springer-Verlag, Berlin, V. 18, pp. 163-168, 1973.

Veyante, D., Lacas, F., Candel, S., Proceedings of the Marble Symposium, pp. 237-256, 1988.

Verkamp, F.J., Verdouw, A.J., Tomlinson, J.G., **Impact of Emission Regulations on Future Gas Turbine Engine Combustors**, AIAA Paper 73-1277, AIAA/SAE 9th Propulsion Conference, AIAA, Las Vegas, November 5-7, 1973.

Versteeg, H.K., Malalasekera, W., "An Introduction to Computational Fluid Dynamics: The Finite Volume Method", Longman, Harlow, 1995.

Wade, W.R., Shen, P.I., Owens, C.W., McLean, A.F., **Low Emissions Combustion for the Regenerative Gas Turbine: Part 1 - Theoretical and Design Considerations (Ford)**, ASME Paper 73-GT-11, 1973.

Warnatz, J., **The Mechanism of High Temperature Combustion of Propane and Butane**, Combustion Science and Technology, V. 34, pp. 177-200, 1983.

Wendt, J.O.L., Ekmann, J.M., **Effect of Fuel Sulfur Species on Nitrogen Oxide Emissions from Premixed Flames**, Combustion and Flame, V. 25, pp. 355-360, 1975.

Westbrook, C.K., Dryer, F.L., **Chemical Kinetic Modelling of Hydrocarbon Combustion**, Progress in Energy and Combustion Science, V. 10, pp. 1-57, 1984.

White, D.J., Roberts, P.B., Compton, W.A., **Low Emission Variable Area Combustor for Vehicular Gas Turbines (Solar)**, ASME Paper 73-GT-19, 1973.

Wierzba, I., Kar, K., **Flame Flashback within Turbulent Streams of Lean Homogeneous Fuel Mixtures and Air**, Transactions of the ASME: Journal of Energy Resources Technology, V. 114, N. 2, pp. 142-145, 1992.

Williams, F.A., **Structure of Flamelets in Turbulent Reacting Flows and Influence of Combustion on Turbulence Fields**, "Turbulent Reactive Flows (Lecture Notes in Engineering 40)", Springer-Verlag, Heidelberg, pp. 195-212, 1989.

Williams, F.A., "Combustion Theory: Fundamental Theory of Chemically Reacting Flow Systems 2nd Ed.", Benjamin/Cummings Publishing Co., Menlo Park, 1985.

Williams, F.A., Combustion and Flame, V. 26, p. 269, 1976.

Wirth, M., Peters, N., **Turbulent Premixed Combustion: A Flamelet Formulation and Spectral Analysis in Theory and IC-Engine Experiments**, 24th Symposium (International) on Combustion, The Combustion Institute, pp. 493-501, 1992.

Wu, A.S., Bray K.N.C., **A Coherent Flame Model of Premixed Turbulent Combustion in a Counterflow Geometry**, CUED/A-THERMO/TR.60, Cambridge University, 1993.

Yakhot, V., Orszag, S.A., Thangam, S., Gatski, T.B., Speziale, C.G., **Development of turbulence models for shear flows by a double expansion technique**, Phys. Fluids, V. A 4, n. 7, pp. 1510-1520, 1992.

Yakhot, V., **Renormalization Group for Modelling of Turbulent Flows and Turbulent Combustion**, AIAA 91-0218, 1991.

Yoshida, A., Tsuji, H., **Characteristic Scale of Wrinkles in Turbulent Premixed Flames**, 19th Symposium (International) on Combustion, The Combustion Institute, pp. 403-411, 1982.

Yoshida, A., Günther, R., **Temperature and Ionization Measurements in Turbulent Premixed Flames**, AIAA 18th Aerospace Sciences Meeting, Pasadena, January 1980.

Yoshida, A., Günther, R., 18th Japanese Symposium on Combustion, p. 128, 1980b.

Zalesak, S.T., **Fully Multidimensional Flux-Corrected Transport Algorithms for Fluids**, Journal of Computational Physics, V. 31, pp. 335-362, 1979.

Zhu, J., **A Low-diffusive and Oscillation-free Convective Scheme**, Commun. Appl. Numer. Methods, V. 7, p. 225, 1991.

Zhu, J., Rodi, W., **A Low Dispersion and Bounded Convection Scheme**, Comp. Meth. Appl. Mech. Eng., V. 92, pp. 87-96, 1991.

Zhu, J., Leschziner, M.A., **A Local Oscillation-Damping Algorithm for Higher Order Convection Schemes**, Comp. Methods Appl. Mech. Eng., V. 67, pp. 355-366, 1988.

Zimont, V., Polifke, W., Bettelini, M., Weisenstein, W., **An Efficient Computational Model for Premixed Turbulent Combustion at High Reynolds Numbers based on a Turbulent Flame Speed Closure**, ASME GT Expo, Orlando, 1997.

Appendix A LPP Test Combustor Layout

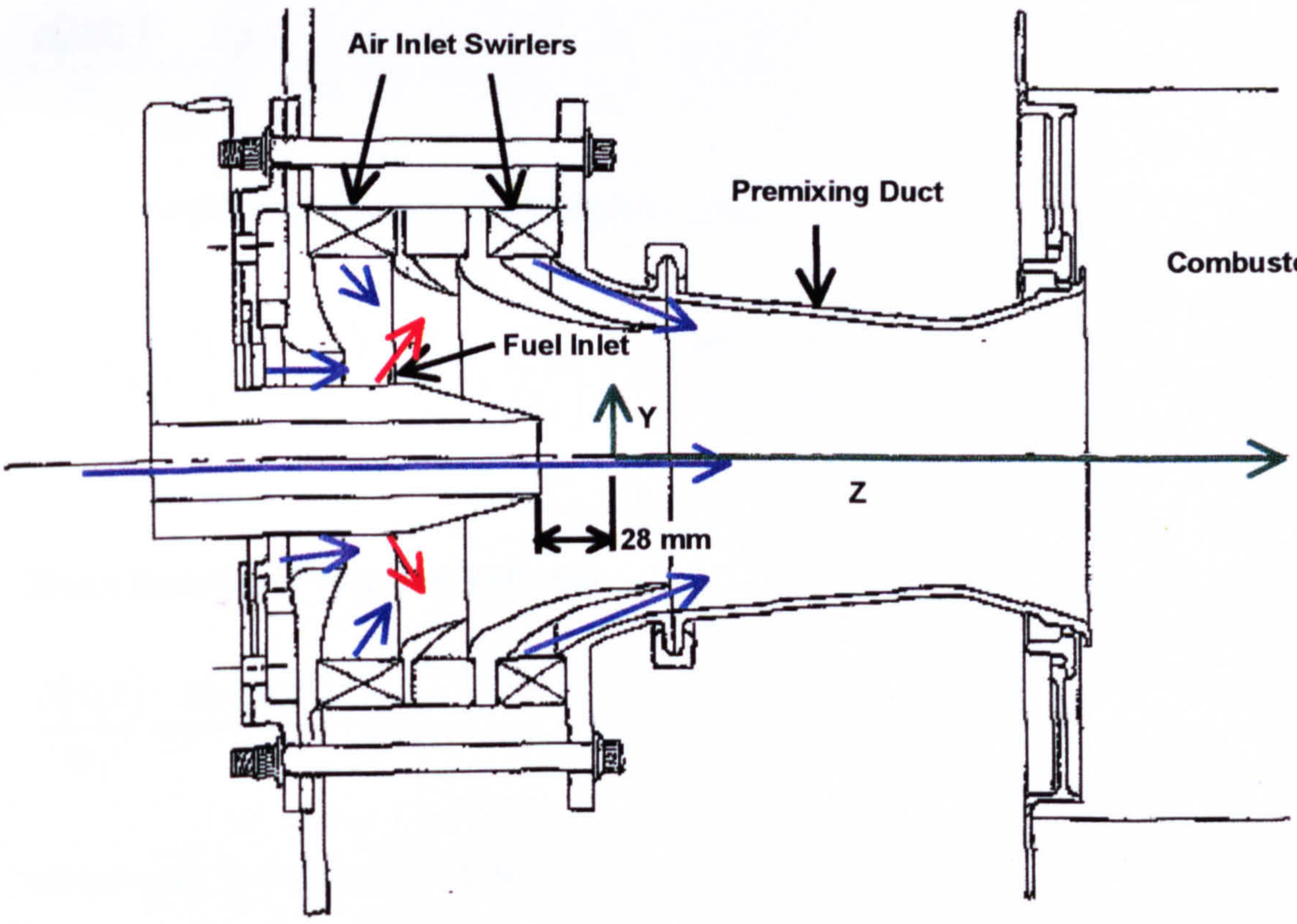

Appendix B Governing Equations for Steady State Flow

Continuity

$$\frac{\partial(\bar{\rho}\tilde{u}_j)}{\partial x_j} = 0$$

Momentum

$$\frac{\partial(\bar{\rho}\tilde{u}_i\tilde{u}_j)}{\partial x_j} = -\frac{\partial \bar{p}}{\partial x_i} + \frac{\partial}{\partial x_j}\left(\bar{\tau}_{ij} - \overline{\rho u_i'' u_j''}\right)$$

where, neglecting viscosity fluctuations, $\bar{\tau}_{ij}$ is:

$$\bar{\tau}_{ij} = \mu\left[\left(\frac{\partial \tilde{u}_i}{\partial x_j} + \frac{\partial \tilde{u}_j}{\partial x_i}\right) - \frac{2}{3}\delta_{ij}\frac{\partial \tilde{u}_k}{\partial x_k}\right] + \mu\left[\left(\frac{\partial \overline{u_i''}}{\partial x_j} + \frac{\partial \overline{u_j''}}{\partial x_i}\right) - \frac{2}{3}\delta_{ij}\frac{\partial \overline{u_k''}}{\partial x_k}\right]$$

Mean Reaction Progress Variable

$$\frac{\partial(\bar{\rho}\tilde{u}_j\tilde{c})}{\partial x_j} = \frac{\partial\left(-\overline{\rho u_j'' c''}\right)}{\partial x_j} + \overline{\rho w_c}$$

where $\overline{\rho w_c}$ is defined in Table B.1

Variance of the Reaction Progress Variable

$$\frac{\partial \bar{\rho}\tilde{u}_j \widetilde{c''^2}}{\partial x_j} = \frac{\partial(-\overline{\rho u_j'' c''^2})}{\partial x_j} - 2\overline{\rho u_j'' c''}\frac{\partial \tilde{c}}{\partial x_j} - 2\overline{\rho \mathcal{D}\frac{\partial c''}{\partial x_j}\frac{\partial c''}{\partial x_j}} + 2\overline{\rho c'' w_c}$$

where $2\overline{\rho \mathcal{D}\frac{\partial c''}{\partial x_j}\frac{\partial c''}{\partial x_j}} = 2\bar{\rho}\tilde{\varepsilon}_c = \frac{\bar{\rho}}{2}\frac{\widetilde{c''^2}}{\tau_{ex}}$, $\frac{1}{\tau_{ex}} = 4\frac{\varepsilon}{k}$ and $\overline{\rho c'' w_c}$ is defined in Table B.1

	Eddy Break-up Model	Presumed pdf Model	BML Crossing Frequency Model
$\overline{\rho w_c}$	$\bar{\rho} C_{ebu} \frac{\varepsilon}{k} \tilde{c}(1-\tilde{c})$	$\bar{\rho} \int_0^1 \int_0^1 w_c(c,f) \tilde{P}(c) \tilde{P}(f) dc df$	$\frac{\rho_R}{\overline{\sigma_y}} \frac{g \bar{c}(1-\bar{c})}{\hat{L}_y} \int_0^1 \int_0^\infty S_L(f,K) \tilde{P}(f) \tilde{P}(K) dK df$
$\overline{\rho c'' w_c}$		$\bar{\rho} \int_0^1 \int_0^1 (c-\tilde{c}) w_c(c,f) \tilde{P}(c) \tilde{P}(f) dc df$	

where $\tilde{P}(c)$ is defined in Figure 2.3.3.2.1, $\tilde{P}(f)$ is defined by Equation (2-43), $\tilde{P}(K)$ is defined by Equation (3-31), $w_c(c,f)$ is defined by Equation (3-13) and $S_L(f,K)$ is defined in Section 3.3

Table B.1 Combustion Model Chemical Source Terms

Mean Mixture Fraction

$$\frac{\partial\left(\bar{\rho}\tilde{u}_j \tilde{f}\right)}{\partial x_j} = \frac{\partial\left(-\overline{\rho u_j'' f''}\right)}{\partial x_j}$$

Variance of the Mixture Fraction

$$\frac{\partial \bar{\rho}\tilde{u}_j \widetilde{f''^2}}{\partial x_j} = \frac{\partial(-\overline{\rho u_j'' f''^2})}{\partial x_j} - 2\overline{\rho u_j'' f''} \frac{\partial \tilde{f}}{\partial x_j} - 2\overline{\rho \mathcal{D} \frac{\partial f''}{\partial x_j} \frac{\partial f''}{\partial x_j}}$$

where $2\overline{\rho \mathcal{D} \frac{\partial f''}{\partial x_j} \frac{\partial f''}{\partial x_j}} = 2\bar{\rho}\tilde{\varepsilon}_f = \frac{\bar{\rho}}{2} \frac{\widetilde{f''^2}}{\tau_{ex}}$ and $\frac{1}{\tau_{ex}} = 4\frac{\varepsilon}{k}$

Density

$$\frac{\bar{\rho}}{\rho_r} = \int_0^1 \left(\frac{1}{1+\tau\tilde{c}}\right) \tilde{P}(f) df$$

where $\tau = \frac{T_p}{T_r} - 1$ and the subscripts p and r represent the product and reactant states respectively.

Turbulence Closure: k-ε model

Reynolds Stresses

$$-\overline{\rho u_i'' u_j''} = \mu_T\left(\frac{\partial \tilde{u}_i}{\partial x_j}+\frac{\partial \tilde{u}_j}{\partial x_i}\right)-\frac{2}{3}\delta_{ij}\left(\mu_T\frac{\partial \tilde{u}_k}{\partial x_k}+\bar{\rho}k\right)$$

where $\mu_T = c'\rho k^{1/2}\ell = \dfrac{\rho C_\mu k^2}{\varepsilon}$

Scalar Fluxes

$$-\overline{\rho u_i'' c''} = \frac{\mu_T}{Sc_T}\frac{\partial \tilde{c}}{\partial x_i}$$

where Sc_T=1.0

Turbulence Kinetic Energy

$$\frac{\partial(\bar{\rho}\tilde{u}_j k)}{\partial x_j} = \frac{\partial}{\partial x_j}\left(\frac{\mu_T}{\sigma_k}\frac{\partial k}{\partial x_j}\right)-\overline{\rho u_i'' u_j''}\frac{\partial \tilde{u}_i}{\partial x_j}-\frac{\mu_T}{\bar{\rho}^2}\frac{\partial \bar{\rho}}{\partial x_i}\frac{\partial \bar{P}}{\partial x_i}-\varepsilon\bar{\rho}$$

Dissipation Rate of the Turbulence Kinetic Energy

$$\frac{\partial(\bar{\rho}\tilde{u}_j \varepsilon)}{\partial x_j} = \frac{\partial}{\partial x_j}\left(\frac{\mu_T}{\sigma_\varepsilon}\frac{\partial \varepsilon}{\partial x_j}\right)-C_1\frac{\varepsilon}{k}\left(\overline{\rho u_i'' u_j''}\frac{\partial \tilde{u}_i}{\partial x_j}+\frac{\mu_T}{\bar{\rho}^2}\frac{\partial \bar{\rho}}{\partial x_i}\frac{\partial \bar{P}}{\partial x_i}\right)-C_2\frac{\varepsilon^2}{k}\bar{\rho}$$

where C_μ=0.09, C_1=1.44, C_2=1.92, σ_k=1.0 and σ_ε=1.3

Turbulence Closure: Second Moment Closure Model

Reynolds Stresses

$$\bar{\rho}\tilde{u}_k\frac{\partial \widetilde{\overline{u_i'' u_j''}}}{\partial x_k} = -\frac{\partial J_{ijk}}{\partial x_k}+P_{ij}+\Pi_{ij}-\left(\overline{u_i''}\frac{\partial \bar{p}}{\partial x_j}+\overline{u_j''}\frac{\partial \bar{p}}{\partial x_i}\right)-\frac{2}{3}\delta_{ij}\bar{\rho}\varepsilon$$

where

$$\frac{\partial J_{ijk}}{\partial x_k} = -\frac{\partial}{\partial x_k}\left(C_s \bar{\rho}\frac{k}{\varepsilon}\widetilde{u_k'' u_l''}\frac{\partial \widetilde{u_i'' u_j''}}{\partial x_l}\right)$$

$$P_{ij} = -\bar{\rho}\left(\widetilde{u_k'' u_i''}\frac{\partial \tilde{u}_j}{\partial x_k} + \widetilde{u_k'' u_j''}\frac{\partial \tilde{u}_i}{\partial x_k}\right)$$

$$\Pi_{ij} = -C_1\bar{\rho}\frac{\varepsilon}{k}\left(\widetilde{u_i'' u_j''} - \frac{2}{3}\delta_{ij}k\right) - C_2\left(P_{ij} - \frac{1}{3}\delta_{ij}P_{kk}\right)$$

$$\overline{u''} = \frac{\overline{\tau\rho u'' c''}}{\rho_r}$$

C_s=0.22, C_1=1.8 and C_2=0.6

Scalar Fluxes: Reaction Progress Variable

$$\bar{\rho}\tilde{u}_k\frac{\partial \widetilde{u_i'' c''}}{\partial x_k} = -\frac{\partial J_{ik}}{\partial x_k} + P_{ic} + \Pi_{ic} - \overline{c''}\frac{\partial p}{\partial x_i} + \overline{u_i'' w}$$

where

$$\frac{\partial J_{ik}}{\partial x_k} = -\frac{\partial}{\partial x_k}\left(C_{st}\bar{\rho}\frac{k}{\varepsilon}\widetilde{u_k'' u_l''}\frac{\partial \widetilde{u_i'' c''}}{\partial x_l}\right)$$

$$P_{ic} = -\bar{\rho}\left(\widetilde{u_k'' c''}\frac{\partial \tilde{u}_i}{\partial x_k} + \widetilde{u_k'' u_i''}\frac{\partial \tilde{c}}{\partial x_k}\right)$$

$$\Pi_{ic} = \overline{p'\frac{\partial c''}{\partial x_i}} = -C_{1T}\bar{\rho}\frac{\tilde{\varepsilon}}{\tilde{k}}\widetilde{u_i'' c''} + C_{2T}\bar{\rho}\widetilde{u_k'' c''}\frac{\partial \tilde{u}_i}{\partial x_k}$$

$$\overline{c''} = \frac{\bar{\rho}}{\rho_r}\int_0^1\int_0^1 (1+\tau c)(c-\tilde{c})\tilde{P}(c)\tilde{P}(f)\,df\,dc$$